ZooKeys 1139: 1–32 (2023)
doi: 10.3897/zookeys.1139.81641
https://zookeys.pensoft.net

RESEARCH ARTICLE

A peer-reviewed open-access journal
ZooKeys
Launched to accelerate biodiversity research

Tadpoles of four sympatric megophryinid frogs (Anura, Megophryidae, Megophryinae) from Mangshan in southern China

Tianyu Qian[1,2], Yonghui Li[3], Jun Chen[3], Pipeng Li[2], Daode Yang[1]

1 *Institute of Wildlife Conservation, Central South University of Forestry and Technology, Changsha 410004, China* **2** *Institute of Herpetology, Shenyang Normal University, Shenyang 110034, China* **3** *Administration Bureau of Hunan Mangshan National Nature Reserve, Chenzhou 423000, Hunan, China*

Corresponding author: Daode Yang (csfuyydd@126.com)

Academic editor: Annemarie Ohler | Received 30 March 2022 | Accepted 17 December 2022 | Published 9 January 2023

https://zoobank.org/DCAED79B-A881-4720-A549-DA889EE6C9DA

Citation: Qian T, Li Y, Chen J, Li P, Yang D (2023) Tadpoles of four sympatric megophryinid frogs (Anura, Megophryidae, Megophryinae) from Mangshan in southern China. ZooKeys 1139: 1–32. https://doi.org/10.3897/zookeys.1139.81641

Abstract

Sympatric distribution and potentially long larval development time make the assignment of tadpoles confusing in Asian-horned frogs of the subfamily Megophryinae. In this study, we used molecular data to identify four syntopic megophryinid tadpoles from Mangshan on the border between Hunan and Guangdong provinces in southern China: *Brachytarsophrys popei*, *Boulenophrys shimentaina*, *Bo.* cf. *ombrophila*, and *Bo. nanlingensis*. A detailed re-description of the *Br. popei* tadpoles is provided as well as the first descriptions of three *Boulenophrys* tadpoles based on external morphology and coloration. An effort is attempted to distinguish these tadpoles by coloration patterns: the dorsal pattern, ventral pattern, and pattern on tail are useful for field identification of these tadpoles. However, the variation of color pattern could sometimes make species delineation difficult. Researchers are encouraged to document coloration in life with photographs and the collection of tadpoles of different development stages and sizes advocated in order to better understand how color may change during larval development.

Keywords

Amphibian, integrative taxonomy, larvae, *Megophrys*, Nanling Mountains

Introduction

The Asian Horned Frogs in the subfamily Megophryinae Bonaparte, 1850 belong to seven genera and 129 recognized species with wide distributed in Asia, ranging from India and Bhutan to China and south to the Sundas and the Philippines (Frost 2022). Tadpoles of Megophryinae are characterized by a funnel-like oral disc, which allows them to feed beneath the water surface or anchor to a substrate for keeping safe during floods or other threats; this mouthpart specialization had intrigued scientists for almost a century (Hora 1928; Pope 1931; Liu 1950; Huang et al. 1991; Zeng 2021).

Seven monophyletic clades were found within Megophryinae based on molecular analysis (Mahony et al. 2017), previously regarded as seven subgenera of *Megophrys* sensu lato: *Atympanophrys* Tian & Hu, 1983; *Boulenophrys* Fei, Ye and Jiang in Fei & Ye, 2016 (under the name *Panophrys* Rao & Yang, 1997); *Brachytarsophrys* Tian & Hu, 1983; *Megophrys* Kuhl & Van Hasselt, 1822; *Ophryophryne* Boulenger, 1903; *Pelobatrachus* Beddard, 1908; and *Xenophrys* Günther, 1864. Recent taxonomic studies have elevated the seven subgenera to the level of genera (Li et al. 2020; Lyu et al. 2021; Qi et al. 2021). However, the morphological differences remain insufficient for clear delineation of these genera. A recent review of the genus *Brachytarsophrys* by Li et al. (2020) regarded the tadpole ventral pattern as a diagnostic character for species identification. Subsequently, Tapley et al. (2020a) tentatively suggested the presence of "white longitudinal stripe on the ventrolateral surface of the head and body" in tadpoles as a diagnostic character for *Brachytarsophrys*. However, there are no known larval characters that differentiate the remaining megophryinid genera from one another. The external morphology, including oral disc, as well as internal buccal features are highly conserved in all species in this subfamily (Huang et al. 1991; Grosjean 2003). The coloration in life, although rarely described, is considered useful for species identification since Leong and Chou (1998) and has attracted more and more attention (Oberhummer et al. 2014; Poyarkov et al. 2017; Tapley et al. 2017, 2020a, 2020b; Li et al. 2018; Munir et al. 2019; Liu et al. 2020; Shi et al. 2020a, 2020b, 2021; Wu et al. 2020). However, compared to the rate of new megophryinid frog species descriptions, tadpole descriptions remain scarce or are very brief, resulting in insufficient diagnostic characters for comparison and/or field recognition.

Before molecular analysis was widely used in megophryinid taxonomic studies, tadpoles were assigned to species based on their association with post-metamorphic/adult specimens collected from the same site, e.g., *Boulenophrys jinggangensis* (Wang in Wang et al. 2012), *Xenophrys mangshanensis* (Fei & Ye in Fei et al. 1990), tadpoles described by Fei and Ye (2016) and *Xenophrys longipes* (Boulenger, 1886), tadpoles described by Leong and Chou (1998). Notably, many megophryinid species are reported to be in sympatry, including sister species (e.g., Wang et al. 2014, 2019; Chen et al. 2017; Poyarkov et al. 2017; Liu et al. 2018; Mahony et al. 2018, 2020; Shi et al. 2020a; Tapley et al. 2018, 2020b, 2021). Some megophryinid tadpoles are suspected of having long larval development periods of over one year (Grosjean 2003; Tapley et al. 2020a). Consequently, cf. tadpoles collected from the same site with adult frogs may not necessarily belong to the same species. Thus, the description of tadpoles without molecular data has become suspicious if there are any other megophyinid species discovered in sympatry.

Mangshan, a part of Nanling Mountains, is located on the border between Hunan and Guangdong provinces in southern China. The first megophryinid record from this area was a tadpole with a funnel-like oral disc collected at the mountain top of Guangdong/Hunan border (Mell 1922), which was identified as "*Megalophrys boettgeri*" (currently *Boulenophrys boettgeri*). This record has been shown to be erroneous as no adult *B. boettgeri* frogs were found in this area (Shen 1983; Shen et al. 2014), and the horned frogs collected in Mangshan were identified as "*Megophrys kuatunensis*" (currently *Bo. kuatunensis*), "*Megophrys brachykolos*" (currently *Bo. brachykolos*), and *Brachytarsophrys carinense* in "*Fauna Hunan, Amphibia*" (Shen et al. 2014). Subsequently, this "*Brachytarsophrys carinense*" population was described as a new species *Brachytarsophrys popei* Wang, Yang & Zhao in Zhao et al. (2014), while the identity of the two *Boulenophrys* frogs, that were both previously regarded as widespread (e.g., Fei et al. 2009; Fei and Ye 2016) was questioned after molecular analysis based on large-scale sampling (Tapley et al. 2017; Liu et al. 2018; Gao et al. 2022).

In this study, we collected tadpoles bearing funnel-like oral disc from Mangshan. Using DNA barcoding, we confirmed that this collection of syntopic tadpoles was composed of four species: *Brachytarsophrys popei*, *Boulenophrys nanlingensis* (Lyu, Wang, Liu & Wang in Wang et al. 2019), *Bo. shimentaina* (Lyu, Liu & Wang in Lyu et al. 2020), and *Bo.* cf. *ombrophila* (Messenger & Dahn in Messenger et al. 2019). Based on the examination of external morphology and coloration in life, we re-described the tadpoles of *Br. popei* and provided the first description of the three *Boulenophrys* tadpoles.

Materials and methods

Samples

All tadpoles were collected from Mangshan, Yizhang, Hunan Province, China during field surveys in June, July, and November 2021. Specimens were photographed in life in a transparent acrylic box before being euthanized with buffered tricaine methanesulfonate (MS-222) and then fixed with 10% formalin for storage. Tissue samples (tail fin/muscle) were preserved in 95% ethanol for molecular analysis. Specimens were deposited at the Institute of Wildlife Conservation, Central South University of Forestry and Technology (**CSUFT**), Changsha, China.

Molecular analysis

Segments of the 16S ribosomal RNA gene (16S) were used for species identification. Primer sequences (L3975 and H4551) from Simon et al. (1994) were used for PCR amplification in 50 μl reaction volumes under the following conditions: 98 °C for 2 min; followed by 30 cycles of 98 °C for 10 sec, 55 °C for 10 sec, and 72 °C for 10 sec, with a final extension step at 72 °C for 5 min. PCR purification and sequencing were performed by Biomarker Technologies Co. (Beijing, China). The new sequences were then searched on BLAST (**NCBI**) to verify their approximate identity. The

identification of GenBank accession numbers were retrieved from the BLAST result and manually verified by checking the original references. Uncorrected *p*–distance between the new sequences and sequences from the BLAST result was calculated using MEGA 6 (Tamura et al. 2013). Before calculating uncorrected *p*–distances, sequences were aligned using the MUSCLE algorithm with default parameters (Edgar 2004) and trimmed with gaps partially deleted in MEGA 6.

Morphology

Image J 1.53k software (Schneider et al. 2012) was used to measure the tadpoles from photographs of preserved specimens taken next to a scale (10 mm length). The staging follows Gosner (1960), and the terminology for external morphology follows Altig and McDiarmid (1999). Measurements and morphometric abbreviations follow Oberhummer et al. (2014). Definitions of abbreviations are as follows:

BH body height, maximal body height at trunk;
BL body length from snout to the point where the axis of the tail myotomes meets the body wall;
BS body end to the center of spiracle;
BW maximal body width;
ED eye diameter;
ES eye–snout distance;
IND the internarial distance measured from center to center;
IOD the interorbital distance measured from center to center;
MTH maximal tail height;
LFH lower fin height at MTH;
UFH upper fin height at MTH;
NE distance from the center of naris to the center of the eye;
ODW oral disc width;
SN distance from the center of naris to snout;
SS distance from snout to the center of spiracle;
TTL total length;
TAL tail length = TTL – BL;
TMH tail muscle height at the body-tail junction, where ventral line of musculature meets trunk contour;
TMW tail muscle width at the same level as TMH.

For the measurement of oral disc width (ODW) in preserved specimens, we expanded the oral disc by anchoring it to a glass (as shown in Fig. 3D).

We compared the tadpoles with their congeneric tadpoles described in the literature where molecular data has been used to confirm species identity: *Br. popei*, tadpoles described by Zhao et al. (2014) and Li et al. (2020); *Br. feae* (Boulenger, 1886), *Br. orientalis* Li, Lyu, Wang & Wang in Li et al. 2020, and *Br. chuannanensis* Fei, Ye &

Huang in Fei and Ye 2001, tadpoles described by Li et al. (2020); *Br. intermedia* (Smith, 1921), tadpoles described by Tapley et al. (2020a); *Bo. lini* (Wang & Yang in Wang et al. 2014); *Bo. fansipanensis* (Tapley, Cutajar, Mahony, Nguyen, Dau, Luong, Le, Nguyen, Nguyen, Portway, Luong & Rowley, 2018), *Bo. hoanglienensis* (Tapley, Cutajar, Mahony, Nguyen, Dau, Luong, Le, Nguyen, Nguyen, Portway, Luong & Rowley, 2018), and *Bo. jingdongensis* (Fei & Ye in Fei et al. 1983), tadpoles described by Tapley et al (2020b); *Bo. baishanzuensis* (Wu, Li, Liu, Wang & Wu, 2020); *Bo. lushuiensis* (Shi, Li, Zhu, Jiang, Jiang & Wang, 2021); *Bo. rubrimera* (Tapley, Cutajar, Mahony, Chung, Dau, Nguyen, Luong & Rowley, 2017); *Bo. jiangi* (Liu, Li, Wei, Xu, Cheng, Wang & Wu, 2020); and *Bo. leishanensis* (Li, Xu, Liu, Jiang, Wei & Wang, 2018). We further summarized the morphological characteristics of all megophryinid tadpoles that were identified based on molecular data as described in the literature: *Atympanophrys gigantica* (Liu, Hu & Yang, 1960), tadpoles described by Tapley et al. (2020b); *Ophryophryne elfina* Poyarkov, Duong, Orlov, Gogoleva, Vassilieva, Nguyen, Nguyen, Nguyen, Che & Mahony, 2017; *Pelobatrachus kalimantanensis* (Munir, Hamidy, Matsui, Iskandar, Sidik & Shimada, 2019); *Xenophrys medogensis* (Fei, Ye & Huang, 1983), *X.* cf. *pachyproctus* (Huang in Huang and Fei 1981), and *X. yeae* (Shi, Zhang, Xie, Jiang, Liu, Ding, Luan & Wang, 2020), tadpoles described by Shi et al. (2020a); *X. maosonensis* (Bourret, 1937), tadpoles described by Tapley et al. (2020b); *X. serchhipii* Mathew & Sen, 2007, tadpoles described by Raj et al. (2022); *X. lekaguli* (Stuart, Chuaynkern, Chan-ard & Inger, 2006); "*X. katabhako*" Deuti, Grosjean, Nicolas, Vasudevan & Ohler, 2017 (synonymized to *X. monticola* Günther, 1864 by Mahony et al. 2018); *X. periosa* (Mahony, Kamei, Teeling & Biju, 2018), tadpoles described by Shi et al. (2020b); and "*Megophrys*" *dringi* Inger, Stuebing & Tan, 1995, tadpoles described by Oberhummer et al. (2014).

Results

Tadpole identification

Two tadpoles were identified as *Brachytarsophrys popei* based on an uncorrected *p*–distance of 0.0–0.7% from the samples in the type series from Hunan, Guangdong, and Jiangxi Provinces (GenBank accession numbers: KM504251–KM504258). Three tadpoles from the same collection site and bearing the same characteristics as the above two tadpoles but without molecular data were also assigned to *Br. popei*. The collection site of these tadpoles is only ~ 5 km from the collection site of paratype SYS a00589 (GenBank accession number: KM504051) in the adjacent Nanling Nature Reserve, Guangdong Province.

A total of 14 tadpoles was identified as *Boulenophrys nanlingensis*, which exhibited an uncorrected *p*–distance of 0.0–0.4% from the holotype SYS a001964 (GenBank accession number: MH406646) collected ~ 10 km in the adjacent Nanling Nature Reserve, Guangdong Province.

Five tadpoles were identified as *Boulenophrys shimentaina*, which exhibited an uncorrected *p*–distance of 1.2% from the type series (GenBank accession numbers: MH406655–MH406656, and 787–788) collected from Shimentai Nature Reserve, Guangdong Province, China ~ 70 km to the south of Mangshan. This genetic distance is smaller than the interspecies *p*–distance in the subfamily Megophryinae used to identify tadpoles (1.4% in *Br. intermedia*, Tapley et al. 2020a).

Four tadpoles showed an uncorrected *p*–distance of 1.8–2.1% from the type series of *Bo. ombrophila* (GenBank accession numbers: KX856397–KX856404) collected from Wuyishan, Fujian Province, China ~ 500 km to the northeast of Mangshan. This genetic distance almost equals to the threshold (2.0% in 16S gene, proposed by Chen et al. 2017) for a potential new species in this subfamily. However, the other two populations of *Bo. ombrophila* suspected by Messenger et al. (2019) from Jiulianshan, Jiangxi Province (*Megophrys* sp 8 in Liu et al. 2018) and Renhua County, Guangdong Province (*M.* sp 9 in Liu et al. 2018) were closer to our samples both in the geographical distance of collection sites and genetic distances based on 16S gene. The Jiulianshan population of *Bo. ombrophila* (GenBank accession numbers: MH406836–MH406840) collected from ~ 160 km to the east of Mangshan showed an uncorrected *p*–distance of 1.6–1.8% from our samples. The Renhua population of *Bo. ombrophila* (GenBank accession numbers: MH406650–MH406653, and MH406834) collected from ~ 70 km to the east of Mangshan showed an uncorrected *p*–distance of 1.4–1.6% from our samples. Further examination of adult frogs revealed morphometric differences between the Mangshan population and the type series from Wuyishan, Fujian. However, the morphometric and morphological data were unavailable for the Jiulianshan population and Renhua Population. Thus, we currently identified the Mangshan population as *Bo.* cf. *ombrophila*.

Morphological description

All examined specimens exhibited a funnel-like oral disc corresponding to the tadpole description of "*Megophrys minor*" by Liu (1950): "The mouth is terminal, with a large funnel that has two long lateral wings, a short ventral wing and a comparatively narrow convex flap above. The tips of the lateral and ventral wings are bluntly pointed." Detailed tadpole descriptions are given below.

Brachytarsophrys popei

Fig. 1

Remark. The following description is based on five tadpoles at Stages 26–27 ($N = 2$) and 36–37 ($N = 3$). Body ratio ranges represent all specimens. Raw measurements are given in Table 1.

Specimens examined. CSUFT T10115 (Stage 37, Field voucher: MT05; GenBank accession number: ON209276), CSUFT T10117 (Stage 37; Field voucher: MT07; GenBank accession number: ON209284), and CSUFT T10119 (Stage 36;

Figure 1. *Brachytarsophrys popei* tadpoles in life **A–C** tadpole CSUFT T10117 (Stage 37) lateral view, dorsal view, and ventral view **D** ventral pattern of tadpole CSUFT T10119 (Stage 36) **E** ventral pattern of tadpole CSUFT T10945 (Stage 26); and **F** oral disc of tadpole CSUFT T10117 (Stage 37). **D** and **E** share the same scale bar with **A–C**.

Field voucher: MT09; not sequenced), collected on 30 May 2021 from Tiantaishan (24.972277°N, 112.963394°E, ca. 1280 m a.s.l.), Mangshan, Hunan Province, China; and CSUFT T10944 (Stage 27, Field voucher: MT1104; not sequenced), and CSUFT T10945 (Stage 26; Field voucher: MT1105; not sequenced), collected on 16 November 2021 from the same site as the first specimens.

External morphology. The body is oval, robust, and flattened above (BW/BL 53.3–55.7% at Stages 26–27, $N = 2$; and 53.6–55.2% at Stages 36–37, $N = 3$); the head is wider than the trunk; the eyes are located dorsolaterally, the pupils are round; the nares are oval, opening laterally, closer to the eye than to the tip of the snout (NE/SN 68.8–73.3% at Stages 26–27, $N = 2$; and 73.7–83.3% at Stages 36–37, $N = 3$); the internarial distance

Table 1. Morphometric data of the tadpole specimens used in this study. For abbreviations, see Materials and Methods. "*" indicates specimens with broken tails, and "\" indicates "no data".

Species	Voucher No.	Stage	TTL	BL	TAL	BH	SS	BS	ED	TMH	MTH	UFH	LFH	IOD	IND	NE	SN	ES	TMW	BW	ODW
Brachytarsophrys popei	CSUFT T10944	27	31.8	9.0	22.8	4.2	5.0	4.2	1.2	3.0	5.4	1.7	1.9	3.8	2.5	1.1	1.6	2.7	2.7	4.8	5.4
	CSUFT T10945	26	27.9	7.9	20.0	3.9	4.9	3.4	1.2	2.9	5.2	1.4	1.6	3.8	2.6	1.1	1.5	2.6	2.5	4.4	5.9
	CSUFT T10115	37	35.0	10.5	24.5	4.7	6.1	4.5	1.4	3.1	6.4	2.1	2.0	4.6	2.8	1.4	1.9	3.3	2.9	5.8	7.4
	CSUFT T10117	37	37.3	11.0	26.3	5.0	6.3	4.7	1.5	2.9	5.8	1.9	1.9	4.7	2.8	1.5	2.0	3.4	2.9	5.9	7.8
	CSUFT T10119	36	36.9	10.9	26.0	5.0	6.3	4.9	1.4	3.2	6.3	2.1	2.1	4.7	3.0	1.5	1.8	3.2	3.1	5.9	7.6
Boulenophrys shimentaina	CSUFT T10156	25	28.5	7.3	21.2	3.1	3.9	3.8	0.8	2.3	4.4	1.2	1.1	3.1	2.2	1.0	1.4	2.3	2.4	4.0	5.2
	CSUFT T10277	26	28.6	8.0	20.6	3.8	4.6	3.5	1.0	2.5	4.5	1.3	1.3	3.4	2.4	1.0	1.6	2.6	2.4	4.4	6.3
	CSUFT T10279*	25	\	8.3	\	3.7	4.7	3.9	1.0	2.6	\	\	\	3.4	2.3	1.0	1.5	2.4	2.5	4.3	6.6
	CSUFT T10285	27	28.5	8.1	20.4	3.7	4.7	3.6	1.0	2.8	5.6	1.5	1.5	3.4	2.3	1.0	1.5	2.4	2.4	4.4	5.7
	CSUFT T10283	28	27.0	8.0	19.0	3.5	4.4	3.7	0.9	2.6	4.8	1.3	1.2	3.2	2.3	0.9	1.4	2.3	2.2	4.1	6.0
Boulenophrys nanlingensis	CSUFT T10144	25	18.7	5.4	13.3	2.3	3.2	2.5	0.7	1.7	2.7	0.7	0.8	2.3	1.6	0.7	1.0	1.7	1.5	2.8	3.8
	CSUFT T10986	35	40.1	10.8	29.3	5.4	6.4	4.5	1.6	3.7	7.3	1.7	1.6	4.7	3.2	1.5	2.4	3.7	3.6	5.7	7.8
	CSUFT T10969	34	34.4	8.8	25.6	4.0	5.6	4.2	1.3	3.0	5.5	1.4	1.3	3.9	2.7	1.1	1.9	3.0	2.8	4.8	5.6
	CSUFT T10261	25	25.1	6.7	18.4	3.1	4.2	2.7	0.8	1.8	4.0	1.2	1.2	2.7	1.9	0.8	1.2	2.0	1.5	3.8	5.4
	CSUFT T10262	25	27.2	6.5	20.7	2.8	4.0	2.8	1.0	1.9	4.2	1.2	1.2	2.9	1.9	0.9	1.2	2.1	1.7	3.6	5.2
	CSUFT T10273	28	35.7	9.4	26.3	4.4	5.4	4.3	1.1	3.2	5.9	1.5	1.5	4.0	2.8	1.0	1.8	2.9	3.0	5.0	7.9
	CSUFT T10991	27	39.1	10.3	28.8	4.4	6.0	4.4	1.3	3.1	6.7	2.0	1.8	4.0	2.8	1.2	1.9	3.1	2.8	5.3	7.6
	CSUFT T10284	25	18.9	5.3	13.6	2.6	3.3	2.2	0.8	1.7	3.4	1.0	0.9	2.6	1.6	0.8	1.0	1.8	1.6	3.2	4.1
	CSUFT T10302*	25	\	7.3	\	3.3	4.0	3.3	0.9	2.4	\	\	\	3.0	2.0	0.9	1.3	2.2	2.1	4.0.	6.0
	CSUFT T10303	25	26.2	6.8	19.4	3.3	3.9	3.1	0.8	2.3	4.0	1.3	1.2	2.9	1.9	0.9	1.3	2.2	2.0	3.9	4.9
	CSUFT T10377	27	28.1	8.2	19.9	3.5	4.9	3.4	1.0	2.3	5.3	1.5	1.5	3.4	2.3	0.9	1.6	2.4	2.0	4.4	6.8
	CSUFT T10378	28	26.9	8.2	18.7	3.4	5.0	3.2	1.2	2.4	5.2	1.3	1.4	3.4	2.2	0.9	1.4	2.3	2.2	4.2	5.9
	CSUFT T10376	27	24.8	7.0	17.8	3.5	4.1	3.1	1.0	2.1	4.8	1.4	1.4	3.1	2.1	0.9	1.3	2.1	2.0	4.0	5.7
	CSUFT T10379	29	27.8	7.7	20.1	3.5	4.5	3.1	1.2	2.5	5.0	1.3	1.4	3.1	2.2	1.0	1.4	2.3	1.9	4.0	5.7
Boulenophrys cf. *ombrophila*	CSUFT T10270	36	33.7	10.0	23.7	4.5	5.6	4.6	1.4	2.9	6.0	1.4	1.6	4.2	2.8	1.4	1.7	3.0	2.9	5.1	8.3
	CSUFT T10272	27	33.1	8.9	24.2	4.1	5.3	4.2	1.2	3.0	6.0	1.4	1.4	3.8	2.5	1.1	1.7	2.8	2.8	4.8	7.8
	CSUFT T10288	26	30.4	8.4	22.0	3.9	4.8	3.8	1.1	2.7	5.9	1.6	1.4	3.6	2.4	1.1	1.5	2.6	2.6	4.6	7.2
	CSUFT T10992	25	20.9	5.1	15.8	2.1	2.8	2.0	0.5	1.6	3.0	0.8	0.8	2.2	1.5	0.6	1.0	1.7	1.3	2.7	3.9

is smaller than the interorbital distance (IND/IOD 65.8–68.4% at Stages 26–27, $N = 2$; and 59.6–63.8% at Stages 36–37, $N = 3$); the rims of nares are raised from the body wall and directed posterolaterally; the spiracle is sinistral and low on the left flank; the spiracle tube is short, protruding posterodorsally, free from the body at the tip, and opening posterolaterally (SS/BL 55.6–62.0% at Stages 26–27, $N = 2$; and 57.3–58.1% at Stages 36–37, $N = 3$); the anal tube opens medially, unattached to the ventral fin; the dorsal fin arises behind the body-tail junction while the ventral fin is connected to the trunk; the tail muscle is massive, taller than tail fins before reaching the maximum tail height (TMH/MTH 55.6–55.8% at Stages 26–27, $N = 2$; and 48.4–50.8% at Stages 36–37, $N = 3$), and the tail tip is bluntly pointed, the tail length accounts for 71.7% (at Stages 26–27, $N = 2$) and 70.5–70.5% (at Stages 36–37, $N = 3$) of the total length; the mouth is terminal and the oral disc is funnel-like (BW/ODW 74.6–88.9% at Stages 26–27, $N = 2$; and 75.6–78.4% at Stages 36–37, $N = 3$); three and four rows of short oval submarginal papillae can be observed on the upper lip and lower lip, respectively; keratodonts are absent; the upper jaw sheath is brush-like, exhibiting a small median notch, while the lower jaw sheath is thin, sickle-shaped, weakly keratinized, and finely serrated.

Coloration. In life, the background color of the head and trunk is dark brown; the dorsal pattern is pale brown interspersed with dark brown chromocytes, extending to above the horizontal level of the spiracle on the trunk from a lateral perspective; the dorsal surface of the anterior part of the tail is pale brown marbled with dark brown speckles; neuromasts are distinctly visible on the head, trunk and tail; the region between the anterior edges of the eyes and the median point of the upper lip is pigmented with a dark brown V-shaped pattern; the narial rims are pale brown; the oral disc is golden-pigmented, with a translucent edge; the submarginal papillae on lips are dark brown-pigmented. Laterally, the tail is pale brown-pigmented; dense goldish spots are located at the anterior part of the lateral surface of tail muscle, becoming smaller and at the middle, then disappearing posteriorly; three distinct dark brown stripes extended from the body-tail junction, and horizontally positioned at the anterior part of the tail; the upper and lower stripes end before reaching the maximum tail height, while the middle stripe is about half the length of the others; the upper and middle stripes are incomplete; the anterior part of the upper fin is opaque, marbled with goldish pigmentation and brown speckles; the anterior part of the ventral fin, as well as the anal tube are semi-translucent with dense large golden spots; the rest of the fins are semi-translucent, and exhibit sparse dark brown speckles interspersed with small goldish dots. The ventral surface of the body is rather dark; the belly is dark purplish covered with dense white spots; two longitudinal stripes, positioned ventrolaterally, extending from the snout to the vertical edge of the eyes posteriorly, and sometimes appear to broken; a transverse bar is positioned at the head-trunk junction of the vertical edge of the anterior spiracle and is always interrupted at the middle; the spiracle region and the corresponding region on the other side of the body, are covered with a short white stripe, that starts from the head-body connection, and terminated before reaching the region of the spiracle tube opening; regions without white pigmentation have less melanocytes; the gills and gut coils are indistinctly visible through the ventral skin. The eye sclera is silver with black dots; the iris periphery is wide and black; the iris is golden sprinkled with black dots; and the spiracle is translucent without pigmentation. In tadpoles at Stages 36–37, the hindlimbs are semi-transparent, and the outer aspect of the legs exhibits brown pigmentation interspersed with goldish chromocytes.

In preserved specimens, the tail stripes are still prominent; an incomplete V-shaped pigmentation pattern is still visible; the ventral pattern is translucent milky white; the golden pigmentation wanes on the oral disc; and the hindlimb bones are visible in ventral view in Stage 36–37 tadpoles.

Comparisons. Tadpoles of *Br. popei* differ significantly from the three syntopic *Boulenophrys* tadpoles described below by the unique pattern of two longitudinal white ventrolateal stripes on head, a transverse white bar on chest, and distinct large spots on belly (vs. absence of stripes and bars, and smaller spots/speckles on belly).

The differences in ventral pattern between four *Brachytarsophrys* tadpoles were compared by Li et al. (2020) and summarized in Table 2. The tadpole of *Br. popei* (Stage 29, $N = 1$) illustrated in their paper (also in Zhao et al. 2014, but marked as

Table 2. Comparison of color pattern among tadpoles of the subfamily Megophryinae which were identified based on molecular data. "*" indicates characteristics not mentioned in the text but were illustrated in the figure, and "\" indicates "no data".

Species	Stage	Neuromasts visibility	Intestine visibility	Dorsum pattern	Pattern on tail	Ventral pattern	References
Atympanophrys							
A. gigantica	35, *N* = 5	visible	visible	uniform dark brown	pale yellowish brown without speckles	translucent dark grey and speckled with white	Tapley et al. 2020b
Brachytarsophrys							
Br. popei	26–27, and 36–37, *N* = 5	distinct	indistinct	uniform dark brown	small dots and longtitudinal stripes	ventrolateral stripes on head and body, incomplete transverse bar on chest, dense large spots on belly	This study
	26–29, *N* = 14	\	\	\	three dark longitudinal stripes	two longitudinal white stripes along the sides of body, a completed transverse bar on chest, belly mottled with dense white speckles	Zhao et al. 2014
Br. intermedia	32, 36, and 39, *N* = 4	pale brown	not visible	pale brown with a darker brown medial saddle	speckled with dark brown, and longitudinal stripes	ventrolateral stripes on head and body, small spots on chest and belly	Tapley et al. 2020a
Br. chuannanensis	38, *N* = 1	\	\	\	distinct dark longtitudinal stripes*	wide ventrolateral stripes on head*; wide transverse bar on chest; and several spots on belly*	Li et al. 2020
Br. orientalis	36, *N* = 1	\	\	brown	three short dark longitudinal stripes	two short, longitudinal white stripes on sides of ventral surface of head and body; absence of transversal white stripe on chest; belly mottled with dense white speckles	Li et al. 2020
Br. feae	44, *N* = 1	\	\	\	\	transeverse bar on chest; several several transeverse stripes on belly	Li et al. 2020
Boulenophrys							
Bo. shimentaina	25–28, *N* = 5	distinct	visible	brown with dark brown reticulation	pigmented with dense dark brown markings posteriorly	milky white ventrolateral spots on chest, dense indistinct small milky white speckles on belly	This study
Bo. cf. *ombrophila*	25, *N* = 1 (TTL 20.9 mm)	indistinct	distinct	pale brown, scattered with dense dark melanocytes	pigmented orange and dark brown speckles	belly covered with dense melanocytes	This study
	26–27, and 36, *N* = 3 (TTL 30.4–33.1 mm)	distinct	indistinct	brown pattern along mid-vertical line	several large brown spots along tail muscle	gold-pigmented white ventrolateral spots on chest, dense white speckles on belly	This study
Bo. nanlingensis	25, *N* = 2 (TTL 18.7–18.9 mm)	distinct	distinct	yellowish with pale orangish blotches, or brown with whitish patterns	many brown speckles	gold-pigmented white ventrolateral spots on chest, sparse white speckles on belly	This study
	25, *N* = 3 (TTL 25.1–27.2 mm)	distinct	distinct	pale brown with dark brown pigmentation	many brown speckles	gold-pigmented white ventrolateral spots on chest, sparse white speckles on belly	This study
	27–29, *N* = 4, TTL 24.8–28.1 mm)	distinct	distinct	bi-colored dorsum of pale brown anteriorly and dark brown posteriorly	many brown speckles	gold-pigmented white ventrolateral spots on chest, sparse white speckles on belly	This study
	27–28, and 34–35, *N* = 4, (TTL 35.7–44.4 mm)	distinct	distinct	uniform brownish	many brown speckles	gold-pigmented white ventrolateral spots on chest, sparse white speckles or dense large spots on belly	This study
Bo. fansipanensis	25, *N* = 2	obvious	visible	brown with dark brown speckles	small spots and dark brown speckles	a translucent grey brown and speckled with metallic blue and flecked with dark brown	This study

Species	Stage	Neuromasts visibility	Intestine visibility	Dorsum pattern	Pattern on tail	Ventral pattern	References
Bo. jingdongensis	25, *N* = 1	indistinct	visible	dark brown with cream blotches, bordered by orange flecks	many dark brown speckles	grey brown and speckled with metallic blue	Tapley et al. 2020b
Bo. hoanglienensis	26, *N* = 1	distinct	visible	dark brown with reddish brown blotches and reticulated blackish brown	many dark brown speckles	speckled with metallic grey blue flecks	Tapley et al. 2020b
Bo. rubrimera	37, *N* = 1	obvious	\	brown with darker speckles	pale yellowish brown with speckles	speckled white and brown	Tapley et al. 2017
Bo. baishanzuensis	31, *N* = 1	\	\	brownish black	small white and black spots	\	Wu et al. 2020
Bo. lushuiensis	26–27, 32, and 36, *N* = 5	\	visible	brown without distinct patterns	pale brown with dozens of small dark brown patches	scattered with silver tiny patches	Shi et al. 2021
Bo. leishanensis	25–26, *N* = 6	visible*	\	yellow-brown	pale colored on fins, and small black spots on tail muscle	dense small white speckles*	Li et al. 2018
Bo. jiangi	26, *N* = 2	\	\	yellow-brown	few dark spots on posterior tail muscle*	\	Liu et al. 2020
Ophryophryne							
O. elfina	25, *N* = 5	visible	not visible	uniform brownish red or brownish orange	few round blackish spots on tail	pale brownish orange, intestine	Poyarkov et al. 2017
Pelobatrachus							
P. kalimantanensis	30, and 36, *N* = 2	visible*	not visible*	conspicuous dark brown and gold or orange brown pigmentation	marbled with dark brown pigmentation, edges of fins with golden iridophores	belly milky-white pigmented, pale stripe below spiracle extends laterally to half of abdomen*	Munir et al. 2019
	45, *N* = 1	invisible*	not visible*	dark brown without orange gold pigmentation	dark brown	dark brown marbled pattern	Munir et al. 2019
Xenophrys							
X. medogensis (low-elevation)	35, and 38, *N* = 2	\	\	pale yellow-brown	mottled with pale colored patches	without white patches	Shi et al. 2020a
X. medogensis (high-elevation)	27, *N* = 1	\	\	deep brown with copper pigmentation	brown, scattered with tiny white pigment spots, no dark brown patches on tail	semitransparent brown, covered with small white pigments	Shi et al. 2020a
X. cf. *pachyproctus*	25, *N* = 1	\	\	yellow-brown with two golden spots on dorsalateral mid body	\	\	Shi et al. 2020a
X. yeae	28–29, and 31–35, *N* = 9	\	\	brown with dense copper pigments	above lower fin mottled with copper patches	semi-transparent	Shi et al. 2020a
X. maosonensis	25, *N* = 2	obvious	visible	brown with dark brown speckles posteriorly	few dark brown speckles	speckled with metallic grey blue	Tapley et al. 2020b
X. lekaguli	25, 37–38, and 42, *N* = 6	\	\	pale gray (in preservative)	proximal half of caudal muscle with two or three irregular dark streaks, fins distinctly pigmented only in distal portions (in preservative)	small black spots (in preservative)	Stuart et al. 2006
X. serchhipii	32, 34, and 36–38, *N* = 11	\	visible	dark brown (in preservative)	translucent and grey (in preservative)	dark brown, fins are opaque and speckled (in preservative)	Raj et al. 2022
X. monticola	25, *N* = 5	\	\	grey olive-green with irregular melanophores (in preservative)	densely arranged melanophores (in preservative)	immaculate, slightly translucent with some rare spots of melanophores (in preservative)	Deuti et al. 2017

Species	Stage	Neuromasts visibility	Intestine visibility	Dorsum pattern	Pattern on tail	Ventral pattern	References
X. periosa	27, *N* = 1	\	\	greyish brown	dense small speckles	translucent greyish brown	Shi et al. 2020b
	34, *N* = 1	\	\	greyish brown	large spots alongside anterior 2/3 of tail muscle	translucent greyish brown	Shi et al. 2020b
Incertae sedis with Megophryinae							
"*Megophrys*" *dringi*	25, *N* = 4	\	visible	conspicuous pattern of intense dark brown and gold pigmentation	pigmented dark brown, interspersed with pale golden iridophores	milky translucent with a few irregularly shaped golden spots	Oberhummer et al. 2014

Stage 27), which was collected ~ 200 km north of Mangshan has a complete transverse white ventral bar. In contrast, our tadpoles (Stages 26–27, *N* = 2; and Stages 36–37, *N* = 3) consistently exhibit an interrupted white transverse ventral bar. This difference may be due to geographic variation or insufficient sample size. However, the presence of a transverse bar on chest could distinguish *Br. popei* tadpoles from *Br. orientalis* and *Br. intermedia* (vs. absent in both). In addition, the width of the transverse bar is markedly smaller than that in *Br. chuannanensis* (see Li et al. 2020: fig. 5E, F). Furthermore, compared with *Br. intermedia*, the tadpoles of *Br. popei* have a distinctly smaller size at Stage 36 (TTL 36.9 mm vs. 48.7 mm). Zhao et al. (2014) illustrated a metamorph of *Br. feae* at Stage 44 with several short stripes on belly (vs. spots or speckles in *Br. popei*, *Br. orientalis*, and *Br. chuannanensis*). We believe this pattern should be confirmed using more specimens at an earlier developmental stage in case this is a transitional form during metamorphosis. Further comparisons between *Br. popei* tadpoles and all megophryinid tadpoles that were identified using molecular data are shown in Tables 2 and 3.

Ecology notes. All tadpoles were collected from an artificial roadside drainage ditch (Fig. 5C) at night while feeding beneath the water surface. Upstream of the ditch is a narrow, slow-moving stream with many rocks covered by moss. The ditch was rocky with a sandy substrate. The maximum depth of this ditch was ~ 0.5 m. Branches of plants from the mountain side of the road extended over this ditch, however, sunlight did reach the water surface at certain times of the day. Tadpoles were observed in a still water stretch behind big rocks, or a small dam formed by submerged leaf litter. Three tadpoles at Stages 36–37 were collected on 30 May 2021 at 22:30 h, together with tadpoles of *Bo. shimentaina* and *Bo. nanlingensis* with an ambient air temperature of ~ 20 °C. Two tadpoles at Stages 2627 were collected on 16 November 2021 at 19:30 h with an ambient temperature of ~ 13 °C. Tadpoles were considered nocturnal because we did not encounter any tadpoles during the day. Male *Br. popei* frogs began their calling activities under rock crevices in this ditch in late July. Zhao et al. (2014) reported that the breeding season of *Br. popei* is July to September, and that their tadpoles (Stages 26–29) were collected in April and December. This indicates that the development of these tadpoles may be very prolonged, and it is likely that they can over winter. Interestingly, it is unknown why no tadpoles were collected during the breeding season both in this study and in Zhao et al. (2014).

Table 3. Comparison of morphological characteristics among tadpoles of the subfamily Megophryinae, which was identified based on molecular data. "*" indicates characteristics not mentioned in the text but were illustrated in the figure, and "\" indicates "no data".

Species	Stage	*N*	TTL	BL	TAL/TTL	BW/ODW (expanded)	Mouthpart shape	Narial rim	Tail tip	References
Atympanophrys										
A. gigantica	35	5	50.7 (42.6–54.9)	16.9 (15.7–18.0)	66.6 (63.2–68.4)	62.6, *N* = 1	hastate	serrated and raised	broadly rounded	Tapley et al. 2020b
Brachytarsophrys										
Br. popei	26–27	2	36.4±1.2 (35.0–37.3)	8.5±0.8 (7.9–9.0)	71.7(–)	81.7±10.1 (74.6–88.9)	bi-triangular	raised	bluntly pointed	This study
	36–37	3	36.4±1.2 (35.0–37.3)	10.8±0.3 (10.5–11.0)	70.3±0.3 (70.0–70.5)	77.2±1.4 (75.6–78.4)	bi-triangular	raised	bluntly pointed	This study
	26–27	12	\	\	\	\	\	\	bluntly pointed	Zhao et al. 2014
	29	2	\	\	\	\	\	\	bluntly pointed	Zhao et al. 2014
Br. intermedia	32	2	45.0±4.7 (41.7–48.3)	14.0±2.2 (12.4–15.5)	69.7±1.7 (67.9–70.3)	\	bi-triangular	raised	pointed	Tapley et al. 2020a
	36	1	48.7	15.0	69.2	50.6	bi-triangular	raised	pointed	Tapley et al. 2020a
	39	1	55.1	16.3	70.4	\	bi-triangular	raised	pointed	Tapley et al. 2020a
Br. orientalis	36	1	33.9	12.3	69.2	\	\	\	pointed	Li et al. 2020
Boulenophrys										
Bo. fansipanensis	25	2	30.8 (26.5–35.0)	9.1 (7.4–10.8)	69.1–72.1	64.8, *N* = 1	bi-triangular	serrated and raised	pointed	Tapley et al. 2020b
Bo. jingdongensis	25	1	27.9	8.9	68.1	80.4, *N* = 1	bi-triangular	serrated and raised	rounded	Tapley et al. 2020b
Bo. hoanglienensis	26	1	26.5	7.1	73.2	79.3, *N* = 1	bi-triangular	serrated and raised	pointed	Tapley et al. 2020b
Bo. shimentaina	25–27	4	28.5±0.1 (28.5–28.6)	7.9±0.4 (7.3–8.3)	72.7±1.5 (71.6–74.4)	72.3±5.8 (65.2–77.2)	bi-triangular	serrated and raised	bluntly pointed	This study
	28	1	27	8	70.4	68.3	bi-triangular	serrated and raised	bluntly pointed	This study
Bo. cf. *ombrophila*	25	1	20.9	5.1	75.6	69.2	bi-triangular	serrated and raised	bluntly rounded	This study
	26–27	2	31.8±1.9 (30.4–33.1)	8.7±0.4 (8.4–8.9)	72.7±0.5 (72.4–73.1)	62.7±1.7 (61.5–63.9)	bi-triangular	serrated and raised	sharply pointed	This study
	36	1	33.7	10.0	70.3	61.4	bi-triangular	serrated and raised	sharply pointed	This study
Bo. nanlingensis	25–27	9	26.0±6.4 (18.7–39.1)	7.1±1.5 (5.3–10.3)	72.8±1.8 (70.8–76.1)	71.4±4.9 (64.7–79.6)	bi-triangular	serrated and raised	pointed	This study
	28–29	3	30.1±4.8 (26.9–35.7)	8.4±0.9 (7.7–9.4)	71.8±2.1 (69.5–73.7)	68.2±4.2 (63.3–71.2)	bi-triangular	serrated and raised	pointed	This study
	34	1	34.4	8.8	74.4	85.7	bi-triangular	serrated and raised	pointed	This study
	35	1	40.1	10.8	73.1	73.1	bi-triangular	serrated and raised	pointed	This study
Bo. lushuiensis	26–27	3	27.8±4.0 (23.1–30.3)	8.0±1.1 (6.8–8.8)	70.2±1.9 (68.0–71.3)	66.8±11.0 (56.1–78.0)	\	\	\	Shi et al. 2021
	32	1	42.7	12.1	71.9	57.9	bi-triangular*	\	rounded*	Shi et al. 2021
	36	1	41.1	11.3	72.5	58.4	\	\	\	Shi et al. 2021
Bo. rubrimera	37	1	33.3	10.5	68.5	\	\	\	rounded	Tapley et al. 2017
Bo. baishanzuensis	31	1	22.7	\	64.8	\	bi-triangular*	\	pointed	Wu et al. 2020
Bo. leishanensis	25–27	6	29.7±2.3 (27.0–33.0)	\	64.2±2.1 (61.5–66.7)	\	\	\	pointed	Li et al. 2018
Bo. jiangi	26	2	25.5–26.0	\	65.5–70.4	\	bi-triangular*	\	pointed	Liu et al. 2020
Bo. lini	28	not provided	\	\	\	\	\	raised	pointed	Wang et al. 2014
	31–34	not provided	\	\	\	\	\	raised	pointed	Wang et al. 2014

Species	Stage	*N*	TTL	BL	TAL/TTL	BW/ODW (expanded)	Mouthpart shape	Narial rim	Tail tip	References
Ophryophryne										
O. elfina	25	5	28.4±1.3 (27.4–30.2)	8.6±0.1 (8.4–8.7)	\	\	bi-triangular*	"nares tubular"	bluntly rounded	Poyarkov et al. 2017
Pelobatrachus										
P. kalimantanensis	30	1	38.9	11.2	71.2	\	\	\	blunt	Munir et al. 2019
	36	1	47.0	12.9	72.6	\	\	\	blunt	Munir et al. 2019
	45	1	31.2	13.5	56.7	\	\	\	\	Munir et al. 2019
Xenophrys										
X. yeae	28–29	4	34.3±0.4 (33.9–34.8)	10.6±0.3 (10.2–11.0)	69.0±1.2 (67.3–69.9)	70.6±6.1 (64.8–78.0)	\	\	\	Shi et al. 2020a
	31–34	4	34.9±1.1 (33.7–35.8)	11.0±0.5 (10.4–11.4)	68.4±0.5 (68.0–69.1)	78.6±13.7 (66.2–92.9)	\	\	\	Shi et al. 2020a
	35	1	38.4	10.9	71.6	66.2	\	\	rounded*	Shi et al. 2020a
X. cf. *pachyproctus*	25	1	19.1	6.1	68.1	63.3	\	\	bluntly pointed*	Shi et al. 2020a
X. medogensis (high-elevation)	27	1	33.7	9.5	71.5	98.1	\	\	pointed*	Shi et al. 2020a
X. medogensis (low-middle elevation)	35	1	42.7	13.3	68.9	85.2	\	\	pointed*	Shi et al. 2020a
	38	1	43.6	13.2	69.5	83.1	\	\	\	Shi et al. 2020a
X. maosonensis	25	2	35.5 (34.4–36.6)	8.8 (8.1–9.5)	76.5–77.9	73.2	bi-triangular	raised	narrowly rounded	Tapley et al. 2020b
X. lekaguli	25	2	\	9.0–10.4	\	\	\	not raised	rounded	Stuart et al. 2006
	37	2	\	12.1–12.9	\	\	\	not raised	rounded	Stuart et al. 2006
	38	1	\	13.8	\	\	\	not raised	rounded	Stuart et al. 2006
	42	1	\	14.2	\	\	\	not raised	rounded	Stuart et al. 2006
X. serchhipii	32	1	28.6	10	65.0	\	\	\	\	Raj et al. 2022
	34	4	29.9±1.40	10.2±0.30	\	\	\	\	\	Raj et al. 2022
	36	4	29.3±0.47	11.3±0.11	72, *N* = 1	\	\	"an elevated projection"	pointed	Raj et al. 2022
	37	1	28.9	11.9	58.8	\	\	\	\	Raj et al. 2022
	38	1	35.6	13.0	63.5	\	\	\	\	Raj et al. 2022
X. monticola	25	7	24.7±2.7 (21.1–28.1), *N* = 5	6.9±0.9 (5.9–8.2)	70–71, *N* = 4	\	\	"waves"	finely rounded	Deuti et al. 2017
X. periosa	27	3	30.4±1.5 (29.0–32.0)	8.9±0.1 (8.4–9.5)	70.7±0.4 (70.3–71.0)	60.3±3.6 (58.2–64.5)	bi-triangular*	\	bluntly pointed	Shi et al. 2020b
	34	3	47.3±4.4 (42.7–51.4)	12.8±0.9 (12.1–13.8)	72.9±1.1 (71.7–73.9)	75.8±5.9 (69.9–81.6)	bi-triangular*	\	bluntly pointed	Shi et al. 2020b
Incertae sedis with Megophryinae										
"*Megophrys*" *dringi*	25	4	32.28±6.05 (23.23–37.63)	9.11±1.89 (6.74–11.35)	71±2 (69–73)	\	\	raised and projected	pointed*	Oberhummer et al. 2014

Boulenophrys shimentaina

Fig. 2

Remark. The following description is based on five tadpoles at Stages 25–28 (*N* = 5). Body ratio ranges represent all specimens. Raw measurements are given in Table 1.

Specimens examined. CSUFT T10156 (Stage 25; Field voucher: MT06; GenBank accession number: ON209270) collected on 30 May 2021 from Tiantaishan (24.972277°N, 112.963394°E, ca. 1280 m a.s.l.), Mangshan, Hunan Province, China;

and CSUFT T10277 (Stage 26, Field voucher: MT707; GenBank accession number ON209281), CSUFT T10279 (Stage 26; Field voucher: MT709; GenBank accession number: ON209264), CSUFT T10283 (Stage 28, Field voucher: MT713; GenBank accession number: ON209261); and CSUFT T10285 (Stage 27; Field voucher: MT715; GenBank accession number: ON209272) collected on 14 July 2021 from Xiangsikeng (24.937705°N, 112.990257°E, ca. 1530 m, a.s.l.), Mangshan, Hunan Province, China.

External morphology. The body is oval and flattened above (BW/BL 51.3–55.0%, *N* = 5); the eyes are located dorsolaterally, and the pupils are round; the nares are oval, open laterally, closer to the eye than to the tip of the snout (NE/SN 62.5–71.4%, IND/IOD 67.6–71.9%, *N* = 5); the rims of nares are serrated, slightly raised from the body wall; the spiracle is sinistral, low on the left flank; the spiracle tube is short, free from the body at the tip and opens laterally (SS/BL 53.4–58.0%, *N* = 5); the anal tube opens medially, unattached to the ventral fin; the dorsal fin arises behind the body-tail junction while the ventral fin is connected to the trunk; the tail muscle is massive, taller than tail fins before reaching the 2/3 part of the tail length (TMH/MTH 50.0–55.6%, *N* = 5); the tail tip is bluntly pointed, the tail length accounts for 69.5–76.1% (*N* = 4) of the total length; the mouth is terminal and the oral disc is funnel-like (BW/ODW 65.2–77.2%, *N* = 5); four rows of oval submarginal papillae are visible on the upper lip, and five rows of oval submarginal papillae on the lower lip; keratodonts are absent; the upper jaw sheath is comb-like, exhibiting a small median notch; the lower jaw sheath is thin and sickle-shaped, weakly keratinized, and finely serrated.

Coloration. The following description is based on a tadpole at Stage 27 (CSUFT T10285). In life, the background color of the body and tail is semi-transparent dark brown; the dorsum is pigmented pale brown which extends to the dorsal surface of anterior tail and gradually becomes golden; a distinct circled marking is present at the center of dorsum, forming a saddle with the background dark brownish coloration; the middle of the saddle is pigmented pale brown; and the neuromasts are distinctly visible. Laterally, the dorsal pattern extends to the region above the horizontal level of the spiracle on the trunk, and covers the whole lateral surface of head; the lateral surface of tail is pigmented brown; the tail and fins are covered with irregularly shaped pale golden spots, interspersed with dense dark brown speckles; the fins are semi-transparent; the anterior part of the dorsal fin is marbled with golden and dark brown speckles; the junction of the anterior half of the dorsal fin and the caudal muscle is pigmented dark brown, forming an incomplete line; the anterior part of the ventral fin and the anal tube exhibit minimal dark brown pigmentation; the posterior part of tail and fins are pigmented with dense dark brown markings. The ventral body is semi-translucent grey, pigmented with dark brown chromocytes, and is covered with dense small, indistinct milky-white speckles; the gills and gut coils are visible through the ventral skin; two large, milky-white spots are present on each side of the ventrolateral surface of head-body connection and are followed by a cluster of smaller spots. The oral disc is translucent milky white; the lateral and middle wings are covered with orangish

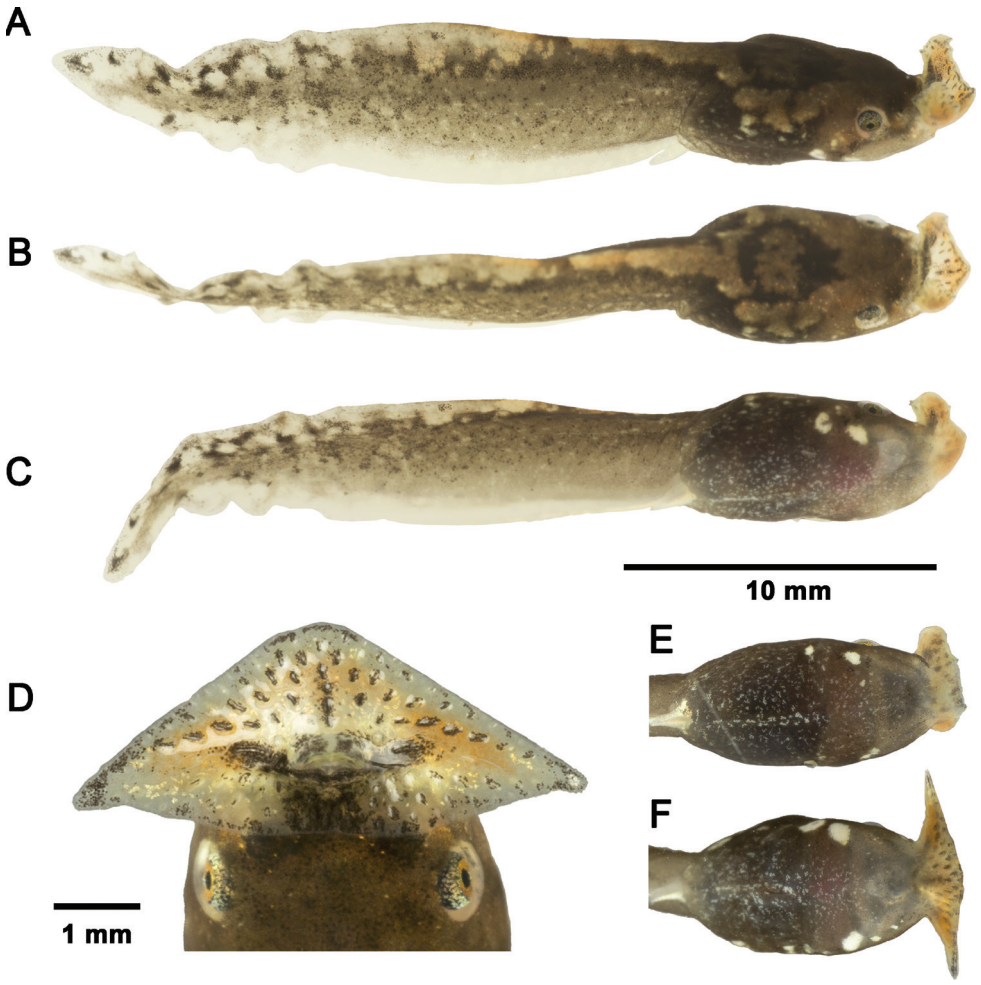

Figure 2. *Boulenophrys shimentaina* tadpoles **A–C** freshly dead tadpole CSUFT T10285 (Stage 27) lateral view, dorsal view, and ventral view **D** oral disc of tadpole CSUFT T10283 (Stage 28) in life **E** ventral pattern of tadpole CSUFT T10277 (Stage 26) in life; and **F** ventral pattern of CSUFT T10283 (Stage 28) in life. **E** and **F** share the same scale bar with **A–C**.

pigmentation; the tips of the wings and the middle of the upper lip exhibit dark brown pigmentation; the submarginal papillae on lips are dark brown, and the narial rims are pigmented beige. The eye sclera is silver with black dots; the iris is orange sprinkled with black dots; and the spiracle is translucent without pigmentation.

Variation of coloration in life. The other four tadpole specimens match most of the descriptions above. However, the dorsum pattern of a saddle is not clearly visible in CSUFT T10156 and the dorsum is almost uniform pale brown in CSUFT T10177. The ventrolateral spots on head-body connection are very large in CSUFT T10283 (Stage 28, Fig. 2F), but smaller in CSUFT T10277 (Stage 26, Fig. 2E).

In preserved specimens, the pale brown pigmentation on the dorsal surfaces of the body and tail are still visible; the golden and orangish pigmentation fade to milky white; the white spots on each side of the ventrolateral surface of head-body connection become translucent; there is no orange pigmentation on the mouthparts, and prominent black pigmentation can be observed on the tail.

Comparisons. The two distinct, conspicuous ventrolateral spots on ventrolateral surface of head-body connection could distinguish the tadpoles of *Bo. shimentaina* from most *Boulenophrys* tadpoles, including *Bo. fansipanensis*, which have a single spot visible on each side, and *Bo. rubrimera*, *Bo. hoanglienensis*, *Bo. jingdongensis*, *Bo. leishanensis*, *Bo. jiangi*, and *Bo. lushuiensis* with no ventrolateral spots; the ventral pattern of indistinct, small speckles on belly could distinguish *Bo. shimentaina* tadpoles from *Bo. lini*, which have dense large speckles (see Wang et al. 2014: fig. 5F). Furthermore, the tadpoles of *Bo. shimentaina* differs from *Bo. lushuiensis* by having a silver sclera with black dots (vs. black with golden pigments); and from *Bo. baishanzuensis* by having a pale brown pattern on dorsum (vs. uniformly brownish black).

Tadpoles of *Bo. shimentaina* could be distinguished from the syntopic *Boulenophrys* tadpoles in Mangshan (see below for the descriptions) by having a dark brown background coloration of body and tail (vs. pale brown in *Bo.* cf. *ombrophila* and *Bo. nanlingensis*), and a tail pattern of dense dark brown markings posteriorly (vs. several large brown spots along tail muscle in *Bo.* cf. *ombrophila*; and many brown speckles in *Bo. nanlingensis*). Further comparisons between *Bo. shimentaina* tadpoles and all megophryinid tadpoles identified based on molecular data are shown in Tables 2, 3.

Ecology notes. A single tadpole at Stage 25 was collected on 30 May 2021, together with the tadpoles of *Bo. nanlingensis* and *Br. popei* from the road ditch (Fig. 5C) that was mentioned above in the *Br. popei* section. Four tadpoles at Stages 25–28 were collected together with tadpoles of *Bo. nanlingensis* and *Bo.* cf. *ombrophila* from a rocky, slow-flowing narrow stream (Fig. 5B) on 14 July 2021 at 23:20 h while nearby adult males were calling. As this stream is located near the mountain top, it is narrow and slow. There were low trees and bamboo on both sides of the stream, and many fallen logs lay across the stream with a rocky stream bed. This site was used by many species as a breeding site including *Bo. nanlingensis*, *Bo. shimentaina*, *Br. popei*, *Leptobrachella mangshanensis* (Hou, Zhang, Hu, Li, Shi, Chen, Mo & Wang, 2018), and *Quasipaa exilispinosa* (Liu & Hu, 1975). The tadpoles of *Bo. shimentaina* found in this stream were observed at night in an area with sandy substrate near the stream bank or in still water behind a small dam formed by submerged leaf litter. Sunlight could reach the surface of these areas at certain times during the day. While feeding beneath the water surface, the tadpoles rely on submerged leaf litter or rocks (Fig. 5A). Once disturbed, they hid quickly under the submerged leaf litter and emerged from the leaf litter after several seconds. In the still water area where these tadpoles were found, we also encountered many *Q. exilispinosa* tadpoles on the stream substrate, and a subadult newts, *Pachytriton xanthospilos* Wu, Wang & Hanken, 2012, hiding under submerged leaf litter. Male *Bo. shimentaina* frogs were observed calling from late June to August in Mangshan, and it was suggested that the breeding season of *Bo. shimentaina* is from

April to August in Shimentai Nature Reserve, Guangdong Province (Lyu et al. 2020). It is not clear if tadpoles complete metamorphosis within a single year, and we didn't collect any tadpoles of more advanced developmental stages.

Boulenophrys cf. *ombrophila*

Fig. 3

Remark. The following description is based on four tadpoles at Stages 25–27 (N = 3) and Stage 36 (N = 1). Body ratio ranges represent all specimens except where specified. Raw measurements are given in Table 1.

Specimens examined. CSUFT T10992 (Stage 25; field voucher: MT02; GenBank accession number: ON209283) collected on 3 June 2021; and CSUFT T10281 (Stage 26; field voucher: MT718; GenBank accession number: ON209275), CSUFT 10270 (Stage 36, field voucher: MT710; GenBank accession number: ON209267), and CSUFT T10272 (Stage 27, field voucher: MT712; GenBank accession number: ON209269) collected on 14 July 2021. All specimens were collected from Xiangsikeng (24.937705°N, 112.990257°E, ca. 1530 m, a.s.l.), Mangshan, Hunan Province, China.

External morphology. The body is flattened and oval (BW/BL 52.9–54.8% at Stages 25–27, N = 3; and 51.0% at Stage 36, N = 1); the eyes are located dorsolaterally, the pupils are round; the nares are oval, opening laterally, closer to the eye than to the tip of the snout (NE/SN 60.0–73.3% at Stages 25–27, N = 3; and 82.4% at Stage 36, N = 1); the internarial distance is smaller than interorbital distance (IND/IOD 65.8–68.2% at Stages 25–27, N = 3; and 66.7% at Stage 36, N = 1); the rims of nares are serrated, slightly raised from the body wall; the spiracle is sinistral, low on the left flank, and opens posterolaterally; the spiracle tube protrudes posteriorly, free from the body at the tip (SS/BL 54.9–59.6% at Stages 25–27, N = 3; and 56.0% at Stage 36, N = 1); the anal tube opens medially, unattached to the ventral fin; the dorsal fin arises behind the body-tail junction while the ventral fin is connected to the trunk; the tail muscle is massive, taller than tail fins until reaching 2/3 of the tail length (TMH/MTH 45.8–53.3% at Stages 25–27, N = 3; and 48.3% at Stage 36, N = 1); the tail tip is usually sharply pointed (bluntly rounded in one small-sized specimen CSUFT T10992, Stage 25, TTL 20.9 mm); the tail length accounts for 72.4–75.6% of the total length at Stages 25–27 (N = 3), and 70.3% at Stage 36 (N = 1); the mouth is terminal and the oral disc is funnel-like (BW/ODW 61.5–69.2% at Stages 25–27, N = 3; and 61.4% at Stage 36, N = 1); three and four rows of short oval submarginal papillae are present on the upper and lower lips, respectively; keratodonts are absent; the upper jaw sheath is comb-like, exhibiting a small median notch, whereas the lower jaw sheath is thin and sickle-shaped, weakly keratinized, and finely serrated.

Coloration. The following description is based on a tadpole at Stage 27 (CSUFT T10272, Fig. 3A–C). In life, the background color of the body and tail is semi-transparent beige; the dorsal surface of the body is covered by a pale brown pattern that extends

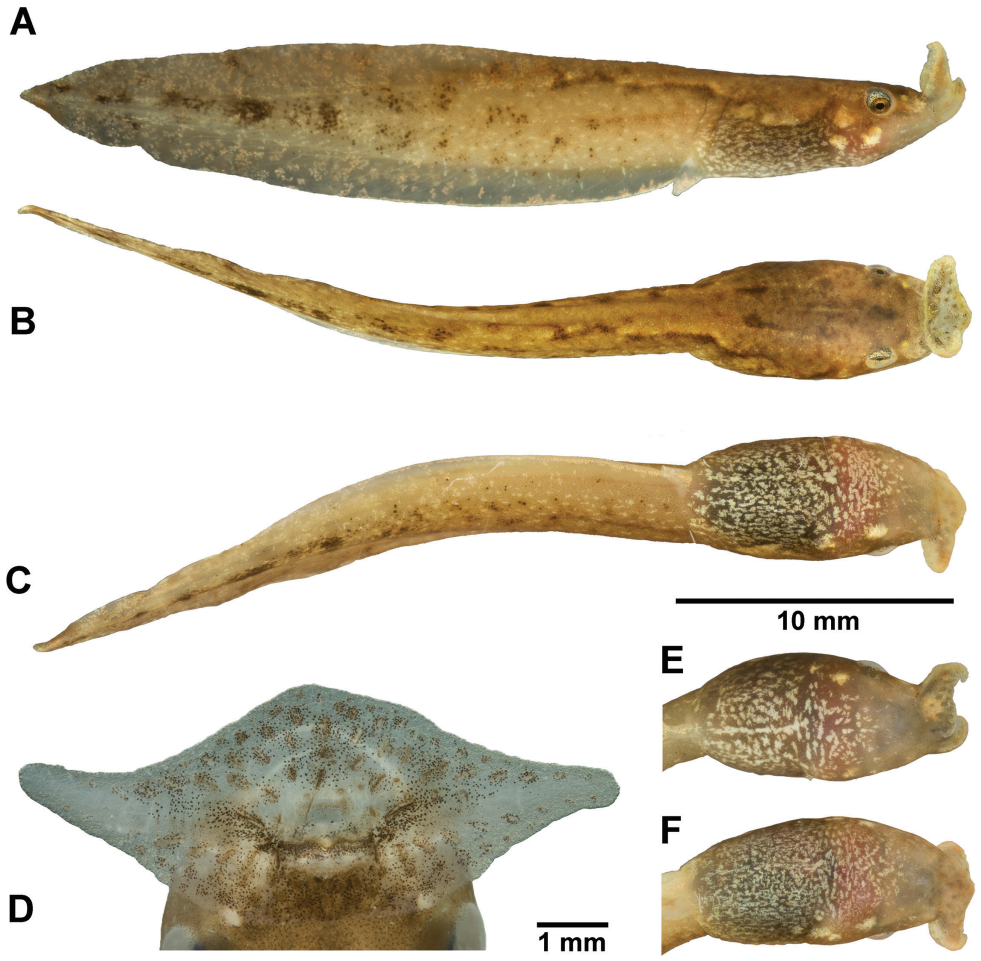

Figure 3. *Boulenophrys* cf. *ombrophila* tadpoles **A–C** tadpole CSUFT T10272 (Stage 27) lateral view, dorsal view, and ventral view in life **D** oral disc of tadpole CSUFT T10270 (Stage 36) in preservative **E** ventral pattern of tadpole CSUFT T10281 (Stage 26) in life; and **F** ventral pattern of tadpole CSUFT T10270 (Stage 36) in life. **E** and **F** share the same scale bar with **A–C**.

to the dorsal surface of the anterior part of the tail; a dark spot is present between the eyes and followed by a short beige vertical line on the anterior dorsum; the neuromasts are distinctly visible; and sparse dark brown markings alongside the vertical line and the dorsolateral neuromasts. Laterally, the dorsal pattern extends to above the horizontal level of the spiracle; three large, whitish, and golden pigmented spots are present behind the eyes on each side of the lower part of head-body connection, two of them are visible from the ventral view; the lateral surface of the tail and fins is covered by irregularly shaped pale golden spots, interspersed with whitish chromocytes which form short lines, and brown chromocytes which gather into large spots along the tail muscle at the posterior part of the tail; the fins are semi-transparent; the anterior part of the dorsal fin

is marbled with golden and dark brown speckles; the anterior part of the ventral fin and the anal tube exhibit minimal brown pigmentation whereas the rest of fins that exhibits sparse dark brown speckles. The ventral body skin is translucent beige, covered by dense milky white speckles; the gills and gut coils are indistinctly visible through the ventral skin. The oral disc is translucent beige; the lateral and middle wings are covered by orange pigmentation; the submarginal papillae on lips are dark brown; the narial rims are yellow; the eye sclera is silver with black dots; the iris is bright orange sprinkled with black dots; the spiracle is translucent, with scattered golden pigmentation.

Variation of coloration in life. Among the remaining three specimens examined, two tadpoles at Stages 26 and 36 match most of the coloration pattern of the description for CSUFT T10272 above (see Fig. 3E, F for ventral patterns). However, the dark spot between the eyes is not present in both; the vertical line is more distinct in CSUFT T10281, which extends from the middle of the eyes to the body-tail connection; and the vertical line in CSUFT T10270 is a bit longer than CSUFT T10272, which extend to the posterior dorsum. In the Stage 36 tadpole (CSUFT T10270), the hindlimbs are semi-transparent, and the legs are covered externally by brown chromocytes. A small-sized tadpole at Stage 25 (CSUFT T10992, TTL 20.9 mm) exhibited a significantly different coloration from other three tadpoles of larger body size (Stages 26–27, and 36; TTL 30.4–33.7 mm): the dorsal pattern is pale brown, with scattered dense dark melanocytes, especially at the vertebral line region; an inconspicuous orange V-shaped pattern between the anterior edges of the eyes and the median point of the upper lip; two orangish spots at the posterior edge of the eyes; the orangish pigmentation is also diffuse on the dorsal aspect of the body and tail; the ventral skin is almost clear, translucent milky, with sparse goldish speckles on the edge of the belly; the belly is covered with dense melanocytes, however, gut coils clearly visible through these melanocytes.

In preserved specimens, a fading of the dorsal pattern is observed; the golden spots on the lateral surfaces of the tail are not visible; the large spots on the anterior corner of the spiracle and gills become translucent, and the orange pigmentation on the lips disappears.

Comparisons. The tadpoles of *Bo.* cf. *ombrophila* differ from the syntopic tadpoles of *Bo. shimentaina* by the semi-translucent beige background coloration of body and tail (vs. dark brown), a ventral pattern of dense milky white speckles on belly (vs. indistinct small speckles), and the pattern on tail of large spots along tail muscle (vs. dense markings posteriorly); from *Bo. nanlingensis* (see below for tadpole description) by the ventral pattern of dense whitish speckles (vs. sparse speckles), and the pattern on tail of several large spots (vs. many speckles).

Compared to other described *Boulenophrys* tadpoles where species identification is supported with molecular data, the tadpoles of *Bo.* cf. *ombrophila* differs by the ventral pattern of dense whitish speckles (vs. relatively sparse metallic blue speckles in *Bo. fansipanensis*; sparse whitish speckles in *Bo. jingdongensis*; sparse metallic grey blue speckles in *Bo. hoanglieneneis*; and scattered with silver tiny patches in *Bo. lushuiensis*), and the tail pattern of several large spots along tail muscle (vs. few dark brown speckles in *Bo. fansipanensis*; absence of large spots in *Bo. jingdongensis*; many dark brown speckles in *Bo. hoanglienensis*; small black spots in *Bo. baishanzuensis*; few dark spots on

posterior tail muscle in *Bo. jiangi*; small black spots on tail muscle in *Bo. leishanensis*; and dozens of small dark brown patches in *Bo. lushuiensis*). Further comparisons between *Bo.* cf. *ombrophila* tadpoles and all megophryinid tadpoles that were identified based on molecular data are shown in Tables 2, 3.

Ecology notes. One observed breeding site of *Bo.* cf. *ombrophila* was a relatively broad wetland crossed by a small shallow creek. Several water sources from the gentle slope of the bamboo forest fed this creek and made the entire area very wet. This breeding site was muddy, covered with leaf litter and fallen logs. The creek was narrow and slow flowing with maximum depth of 0.2 m. Some fallen logs blocked the creek and created still water areas. Only male *Bo.* cf. *ombrophila* and *Q. exilispinosa* were observed calling in this site during our visits from May to August, and in November. The potential predator of these frogs, an aquatic snake *Opisthotropis cheni* Zhao, 1999 which was observed once, in July, in this creek. A single small-sized tadpole specimen (CSUFT T10992, TTL 20.9 mm) at Stage 25 was collected from this site while the male frogs were heard calling before a heavy rainstorm on 3 June 2021 at 19:30 h at dusk. Three tadpoles were collected from the rocky area (Fig. 5B, mentioned above in the *Bo. shimentaina* section) 20 m downstream of this creek together with tadpoles of *Bo. shimentaina* and *Bo. nanlingensis*. Interestingly, male *Bo.* cf. *ombrophila* frogs were not observed calling in the rocky area, and the other two species did not breed in this wetland. This indicates a different microhabitat preference between these congeneric species. The breeding season of *Bo.* cf. *ombrophila* ends in mid-July in Mangshan. It is not clear if tadpoles will complete metamorphosis during the year.

Boulenophrys nanlingensis

Fig. 4

Remark. The following description is based on 14 tadpoles at Stages 25–29 (N = 12), and 34–35 (N = 2). Body ratio ranges represent all specimens except where specified. Raw measurements are given in Table 1.

Specimens examined. CSUFT T10144 (Stage 25; field voucher: MT04; GenBank accession number: ON209279) collected on 30 May 2021; and CSUFT T10302 (Stage 25, field voucher: MT722; GenBank accession number: ON209280), and CSUFT T10303 (Stage 25, field voucher MT723; GenBank accession number: ON209277) collected on 19 July 2021 from Tiantaishan (24.972277°N, 112.963394°E, ca. 1280 m a.s.l.); CSUFT T10261 (Stage 25; field voucher: MT701; GenBank accession number: ON209263), CSUFT T10262 (Stage 25; field voucher: MT702; GenBank accession number: ON209268), CSUFT T10273 (Stage 28, field voucher: MT703, GenBank accession number: ON209278), CSUFT T10991 (Stage 27; field voucher: MT711; GenBank accession number: ON209265), and CSUFT T10284 (Stage 25, field voucher: MT714; GenBank accession number: ON209271) collected on 14 July 2021; and CSUFT T10986 (Stage 35, field voucher: MT1106; GenBank accession number: ON209285) and CSUFT T10969 (Stage 34, field voucher: MT1109;

GenBank accession number: ON209274) collected on 19 November, 2021 from Xiangsikeng (24.937705°N, 112.990257°E, ca. 1530 m, a.s.l.); and CSUFT T10376 (Stage 27, field voucher: MT756; GenBank accession number: ON209273), CSUFT T10377 (Stage 27, field voucher: MT757; GenBank accession number: ON209262), CSUFT T10378 (Stage 28, field voucher: MT758; GenBank accession number: ON209282), and CSUFT T10379 (Stage 29, field voucher: MT769; GenBank accession number: ON209266) collected on 28 July 2021 from Guizizhai (24.952750°N, 112.960470°E, ca. 1210 m a.s.l.), Mangshan, Hunan Province, China.

External morphology. The body is elongated, oval, and flattened above (BW/BL 51.2–60.4% at Stages 25–29, N = 11; and 52.8–54.5% at Stages 34–35, N = 2); the eyes are located dorsolaterally, and the pupils are round; the nares are oval, closer to the eye than to the tip of the snout (NE/SN 55.6–80.0% at Stages 25–29, N = 12; and 57.9–62.5% at Stages 34–35, N = 2); the internarial distance is smaller than interorbital distance (IND/IOD 61.5–71.0% at Stages 25–29, N = 12; and 68.1–69.2% at Stages 34–35, N = 2); the nares open laterally; the rims of nares are serrated, slightly raised from the body wall; the spiracle is sinistral, low on the left flank, and opens posteriorly; the spiracle tube is short and slightly protrudes posteriorly (SS/BL 54.8–62.7% at Stages 25–29, N = 12; and 59.3–63.6% at Stages 34–35, N = 2). The anal tube opens medially and is unattached to the ventral fin; the dorsal fin arises behind the body-tail junction, and the ventral fin is connected to the trunk. The tail muscle is massive, deeper than tail fins before reaching the maximum tail height (TMH/MTH 43.4–63.0% at Stages 25–29, N = 11; and 50.7–54.5% at Stages 34–35, N = 2); the tail tip is pointed, the tail length accounts for 69.5–76.1% (at Stages 25–29, N = 11) and 73.1–74.4% (at Stages 34–35, N = 2) of the total length; the mouth is terminal and the oral disc is funnel-like (BW/ODW 63.3–79.6% at Stages 25–29, N = 12; and 73.1–85.7% at Stages 34–35, N = 2); four and five rows of short oval submarginal papillae can be observed on the upper and lower lips, respectively; keratodonts are absent; the upper jaw sheath is comb-like, exhibiting a weak median notch; the lower jaw sheath is thin and sickle-shaped, weakly keratinized, and finely serrated.

Coloration. The following description is based on a tadpole at Stage 25 (CSUFT T10303, Fig. 4A–C). In life, the background color of the body and tail are semi-transparent grey; the dorsal surface of the body is covered by a pale brown pattern that extends to the dorsal surface of the anterior part of the tail; roughly symmetrical dark brown pigmentation can be observed on the dorsal body; and the neuromasts are distinctly visible. Laterally, the dorsal pattern extends to above the horizontal level of the spiracle; the lateral surface of the tail is pigmented brown, interspersed with pale golden spots and irregular dark brown speckles; the fins are semi-transparent and scattered with pale golden spots; the anterior part of the dorsal fin is marbled with golden and dark brown speckles, with the dark brown speckles forming an incomplete line; the anterior part of the ventral fin and the anal tube, lacks brown pigmentation but with sparse golden speckles. The ventral surface of the body is semi-transparent grey; the gills appear pink through the ventral skin; two large gold-pigmented white spots are present at ventrolateral head-body connection; the gut coils are distinctly visible

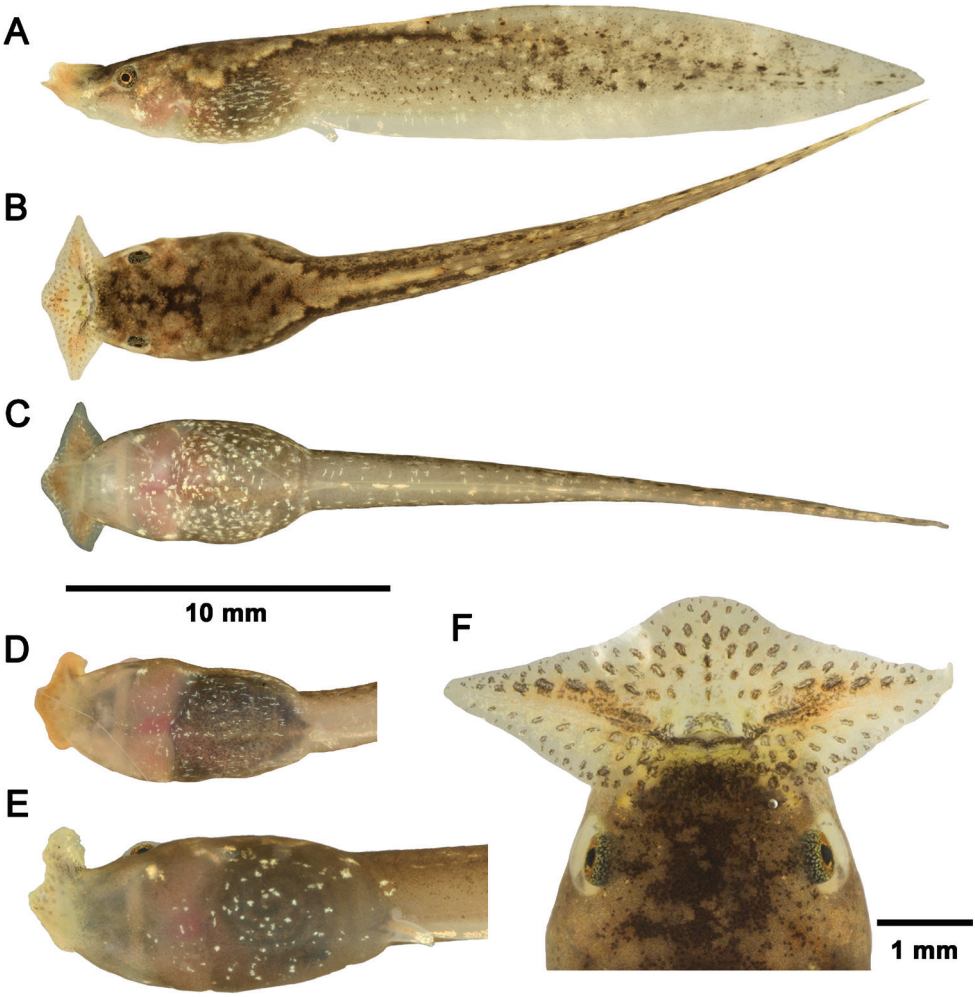

Figure 4. *Boulenophrys nanlingensis* tadpoles in life **A–C** tadpole CSUFT T10303 (Stage 25) lateral view, dorsal view, and ventral view **D** ventral pattern of tadpole CSUFT T10262 (Stage 25) **E** ventral pattern of tadpole CSUFT T10273 (Stage 28); and **F** oral disc of tadpole CSUFT T10261 (Stage 25). **D** and **E** share the same scale bar with **A–C**.

through the ventral skin, the belly is scattered with small whitish speckles; the oral disc is translucent beige; the lateral and middle wings are covered by orangish pigmentation; the submarginal papillae on lips are dark brown; the narial rims are beige; the eye sclera is silver with black dots; the iris is copper-colored sprinkled with black dots, comparable to the iris coloration in adults; and the spiracle is translucent.

Variation of coloration in life. The dorsal pattern coloration in tadpoles of *Bo. nanlingensis* is subject to significant variation both in same stages and between stages. At Stage 25, a small-sized tadpole (CSUFT T10144, TTL 18.7 mm) exhibits a yellowish dorsum with pale orange blotches, and dark brown pigmentation present

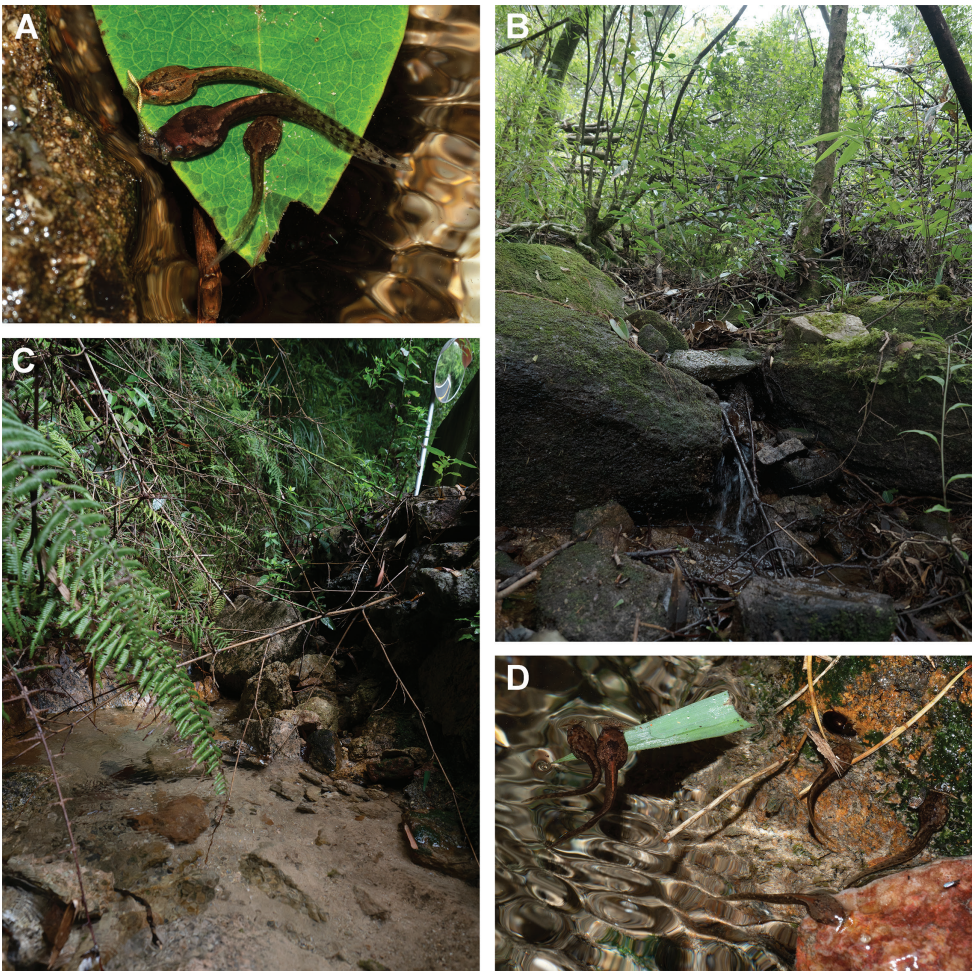

Figure 5. Megophryinid tadpoles and their habitats in Mangshan, Hunan Province, China (**A**) Non-collected *Bo. shimentaina* tadpole (middle) feeding together with two unrecognized tadpoles in its habitat (**B**); and tadpole habitat (**C**) of a mixed-species assemblage beside a forest road, with unrecognized tadpoles feeding together (**D**).

posteriorly; another small tadpole (CSUFT T10284, TTL 18.9 mm) displays a brown dorsum with whitish patterns on the dorsolateral surfaces of the trunk and these extend to the tip of the tail. The coloration of the medium-sized tadpoles at Stage 25 (CSUFT T10261, TTL 25.1 mm; and CSUFT T10262, TTL 27.2 mm) and a broken-tailed individual at Stage 25 (CSUFT T10302) correspond to the dorsal pattern of CSUFT T10303 described above. However, the shape and coverage of dark brown markings varies between individuals. At later Stages 27–29, three medium-sized tadpoles (CSUFT 10377, Stage 27, TTL 28.1 mm; CSUFT T10376, Stage 27, TTL 24.8 mm; and CSUFT 10378, Stage 28, TTL 26.9 mm) exhibit a bi-colored

dorsum, which is anteriorly pale brown and posteriorly inconspicuous dark brown. Tadpoles with relatively larger size at both early Stages 27–28 and advanced Stages 34–35 (CSUFT T10273, Stage 28, TTL 35.7 mm; CSUFT T10991, Stage 27, TTL 39.1 mm; CSUFT T10986, Stage 35, TTL 40.1 mm; and CSUFT T10969, Stage 34, TTL 34.4 mm) exhibit a uniform brownish dorsum coloration with almost invisible markings. Two tadpoles, CSUFT T10144 (Stage 25, TTL 18.7 mm) and CSUFT T10379 (Stage 29, TTL 27.8 mm) exhibit pale yellowish dorsum with orange pigmentation, which are indistinguishable from the small-sized *Bo.* cf. *ombrophila* tadpole (CSUFT T10992, TTL 20.9 mm). A tadpole at Stage 27 (CSUFT T10376, TTL 24.8 mm) with a mid-vertical line on dorsum is similar with that of larger *Bo.* cf. *ombrophila* tadpoles (Stages 26–27, and 36; TTL 30.4–33.7 mm). However, they were not collected form the same site as *Bo.* cf. *ombrophila* tadpoles. A large-sized tadpole at Stage 35 (CSUFT 10986, TTL 40.1 mm) showed a ventral pattern of large spots on belly that was different with other specimens. For tadpoles at Stages 34–35 (CSUFT T10969, and CSUFT T10986), the hindlimbs are semi-transparent, the outer aspect of the legs is pigmented yellow and interspersed with brown chromocytes on top.

In preserved specimens, a fading of the dorsal pattern is observed; the tail is translucent with sparse dark-brown pigmentation; the orange pigmentation on lips is no longer visible; the whitish speckle on the ventral surface and the nares are translucent.

Comparisons. The variation of dorsum pattern makes the tadpoles of *Bo. nanlingensis* are sometimes confused with the syntopic tadpoles of *Bo.* cf. *ombrophila*. Usually, the ventral pattern of sparse speckles (vs. dense speckles) and the tail pattern of many small speckles (vs. large spots) could distinguish them. An exception is the small-sized tadpole CSUFT 10144 (Stage 25, TTL 18.7 mm), which bears almost the same pattern as a small-sized *Bo.* cf. *ombrophila* tadpole CSUFT T10992 (Stage 25, TTL 20.9 mm). The tadpoles of *Bo. nanlingensis* differ from the syntopic *Bo. shimentaina* tadpoles by the pale brownish background coloration of the body and tail (vs. dark brown), the ventral pattern of sparse speckles (vs. dense small speckles), and the tail pattern of small dots (vs. large speckles).

Compared to other described *Boulenophrys* tadpoles where species identification is supported by molecular data, the tadpoles of *Bo. nanlingensis* differs by the presence of ventrolateral spots on each side of head-body connection (vs. absent in *Bo. jingdongensis*, *Bo. hoanglienensis*, *Bo. leishanensis*, and *Bo. lushuiensis*); the tail pattern of many brown speckles (vs. small spots on tail muscle in *Bo. leishanensis*; few dark spots on posterior tail muscle in *Bo. jiangi*; and small white and black dots in *Bo. baishanzuensis*). Further comparisons between *Bo. nanlingensis* tadpoles and all megophryinid tadpoles that were identified based on molecular data are shown in Tables 2, 3.

Ecology notes. Tadpoles of *Bo. nanlingensis* were discovered in all collection sites during our field surveys in 2021, which perhaps implies that this species has larger population size, or it might exhibit less microhabitat specificity. Besides the three sites mentioned above, four *Bo. nanlingensis* tadpoles were collected from a relatively wide stream (3–5 m wide), with a maximum depth of 0.5 m. An adult male was observed calling under rocks near the stream bank with its feet standing in shallow water on 28 July 2021.

The male calling activities of *Bo. nanlingensis*, which began in late July, had increased during our visit in November in Mangshan. It seems the newborn larva would have to over-winter. Thus, we suspected the tadpoles of early Stages 25–29 collected in May and July were born in the previous year. Two tadpoles at advanced Stages 34–35 were collected on the 19th of November. Considering tadpoles in late stages develop relatively fast (Grosjean, 2003; TQ, personal observation). It was likely these advanced tadpoles would finish metamorphosis in cold season at the beginning of the next year. However, this assumption needs further confirmation because the cold weather and scarce food in winter may not be suitable for the survival of froglets.

Discussion

In this study, we attempted to identify sympatric megophryinid tadpoles using external morphology and color patterns, especially ventral patterns. However, our sample size was small. Tadpoles of *Bo. shimentaina* and *Bo.* cf. *ombrophila* bearing stable and distinct ventral pattern were collected from a single site. It is not clear if the color pattern may differ between sites. In *Bo. nanlingensis*, the color pattern varied between different body size ranges rather than stages or collection sites. This provides new insight into that the coloration pattern perhaps should be classified by body size ranges in megophyinid tadpoles, and not only development stages. Diagnostic larval characters for delineating megophryid genera are still insufficient except for the ventrolateral pattern in *Brachytarsophrys*. However, there are characters shared within genera, such as the rim of nares is "tubular" in *Ophryophryne elfina* (Poyarkov et al. 2017), and *O. microstoma* Boulenger, 1903 (tadpoles described by Grosjean, 2003 without molecular data), but this rim is "serrated" in *Boulenophrys* tadpoles, described both in this study and in Tapley et al. (2020b); or the oral disc is "hastate shaped" in *Atympanophrys gigantica* (Tapley et al. 2020b), which has not been reported in other genera.

We failed to find any *Xenophrys mangshanensis* adult or larva during our field surveys, despite Mangshan being its type locality. However, it was reported to be in sympatry with *Bo. nanlingensis* and *Br. popei* in Guangdong Province (Wang et al. 2019). As earlier mentioned under the ecology notes for *Boulenophrys* cf. *ombrophila*, sometimes larvae maybe washed downstream where adult frogs are not thought to be present. Therefore, if megophryinid species occur in sympatry with others, the tadpole identification without molecular data should be re-considered. Perhaps, the tadpole specimens previously described as *X. mangshanensis*, for example, by Fei and Ye (2016) should be re-examined after molecular identification.

The presence of *Bo. kuatunensis* and *Bo. brachykolos* in Mangshan was not confirmed in this study, which agrees with the conjecture proposed by Liu et al. (2018) and Tapley et al. (2017) that both species are restricted to their type localities. However, taxonomic revisions need adequate field surveys and detailed examination of museum specimens (Qi et al. 2021). This study provides an example of using tadpole identification to document the presence of species where adults may not always be visible.

This proved particularly useful here as the tadpoles of megophryinid frogs at this site appear to be relatively slow to develop, and they could always be found outside the breeding season.

Acknowledgements

We would like to thank Yuanlingbo Shang and Yao Luo for help collecting specimens; Guoxing Deng for assistance during field surveys. We thank Chaosheng Mu for the help in collecting literature. TQ thanks Zhengyan Zhou for the guidance in tadpole photography, and Yu Zhang for the help in tadpole staging. We are sincerely grateful to Annemarie Ohler, Benjamin Tapley, and an anonymous reviewer for their helpful comments and suggestions.

This work was supported by the project for Endangered Wildlife Protection of Hunan Forestry Bureau of China (No. HNYB-202201), the National Natural Science Foundation of China (No. 31472021), and the project for Endangered Wildlife Investigation, Supervision and Industry Regulation of the National Forestry and Grassland Bureau of China (No. 2021072-HN-001).

References

Altig R, McDiarmid RW (1999) Body plan. Development and morphology. In: McDiarmid RW, Altig R (Eds) Tadpoles. The biology of anuran larvae. The University of Chicago Press, Chicago/London, 24–51.

Beddard FE (1908) Contributions to the knowledge of the anatomy of the batrachian family Pelobatidae. Proceedings of the Zoological Society of London 1907: 871–911. https://doi.org/10.1111/j.1469-7998.1907.tb06963.x

Bonaparte CLJL (1850) Conspectus Systematum Herpetologiae et Amphibiologiae. Editio altera reformata [Lugduni Batavorum], Brill EJ, Leiden, 1 pp.

Boulenger GA (1886) Description of a new frog of the genus *Megalophrys*. Proceedings of the Zoological Society of London 1885: 850. [pl. LV.] https://doi.org/10.1111/j.1096-3642.1885.tb02927.x

Boulenger GA (1903) Descriptions of three new batrachians from Tonkin. Annals & Magazine of Natural History 7(12): 186–188. https://doi.org/10.1080/00222930308678835

Bourret R (1937) Notes herpétologiques sur l'Indochine française. XIV. Les batraciens de la collection du Laboratoire des Sciences Naturelles de l'Université. Descriptions de quinze espèces ou variétés nouvelles. Annexe au Bulletin Général de l'Instruction Publique 4: 5–56.

Chen JM, Zhou WW, Poyarkov Jr NA, Stuart BL, Brown RM, Lathrop A, Wang YY, Yuan ZY, Jiang K, Hou M, Chen HM, Suwannapoom C, Nguyen SN, Duong TV, Papenfuss TJ, Murphy RW, Zhang YP, Che J (2017) A novel multilocus phylogenetic estimation reveals unrecognized diversity in Asian horned toads, genus *Megophrys* sensu lato

(Anura: Megophryidae). Molecular Phylogenetics and Evolution 106: 28–43. https://doi.org/10.1016/j.ympev.2016.09.004

Deuti K, Grosjean S, Nicolas V, Vasudevan KV, Ohler A (2017) Nomenclatural puzzle in early *Xenophrys nomina* (Anura, Megophryidae) solved with description of two new species from India (Darjeeling hills and Sikkim). Alytes 34: 20–48.

Edgar RC (2004) MUSCLE: Multiple sequence alignment with high accuracy and high throughput. Nucleic Acids Research 32(5): 1792–1797. https://doi.org/10.1093/nar/gkh340

Fei L, Ye CY (2001) The colour handbook of the amphibians of Sichuan. Chinese Forestry Publishing House, Beijing, 263 pp.

Fei L, Ye CY (2016) Amphibians of China (I). Science Press, Beijing, 1040 pp.

Fei L, Ye CY, Huang YZ (1983) Two new subspecies of *Megophrys omeimontis* Liu from China (Amphibia, Pelobatidae). Acta Herpetologica Sinica 2(2): 49–52. [New Series]

Fei L, Ye CY, Huang YZ (1990) Key to Chinese Amphibia. Chongqing Branch, Science and Technology Literature Press, Chongqing, 364 pp.

Fei L, Hu SQ, Ye CY, Huang YZ (2009) Fauna Sinica. Amphibia. Volume 2. Anura. Science Press, Beijing, 957 pp. [In Chinese]

Frost DR (2022) Amphibian Species of the World: an Online Reference. Version 6.1. Electronic Database. American Museum of Natural History, New York. https://amphibiansoftheworld.amnh.org/index.php [Accessed: 22 Nov 2022]

Gao ZW, Qian TY, Jiang JP, Hou DJ, Deng XJ, Yang DD (2022) Species diversity and distribution of amphibians and reptiles in Hunan Province, China. Biodiversity Science 30(2): 21290. [In Chinese with English abstract] https://doi.org/10.17520/biods.2021290

Gosner KL (1960) A simplified table for staging anuran embryos and larvae with notes on identification. Herpetologica 16(3): 183–190.

Grosjean S (2003) A redescription of the external and buccopharyngeal morphology of the tadpole of *Ophryophryne microstoma* Boulenger, 1903 (Megophryidae). Alytes 21(1–2): 45–58.

Günther ACLG (1864) The Reptiles of British India. Robert Hardwicke, London, 452 pp. [pl. i–xxvii.] https://doi.org/10.5962/bhl.title.5012

Hora SL (1928) Further observations on the oral apparatus of the tadpoles of the genus *Megalophrys*. Records of the Indian Museum 30: 139–146. [A Journal of Indian Zoology] https://doi.org/10.26515/rzsi/v30/i1/1928/163205

Hou YM, Zhang MF, Hu F, Li SY, Shi SC, Chen J, Mo XY, Wang B (2018) A new species of the genus *Leptolalax* (Anura, Megophryidae) from Hunan, China. Zootaxa 4444(3): 247–266. https://doi.org/10.11646/zootaxa.4444.3.2

Huang YZ, Fei L (1981) Two new species of amphibians from Xizang. Acta Zootaxonomica Sinica 6(2): 211–215.

Huang Y, Fei L, Ye C (1991) Studies on internal oral structures of tadpoles of Chinese Pelobatidae. Acta Biologica Plateau Sinica 10: 71–99. [In Chinese with English abstract]

Inger RF, Stuebing RB, Tan FL (1995) New species and new records of anurans from Borneo. The Raffles Bulletin of Zoology 43(1): 115–131.

Kuhl H, Van Hasselt JC (1822) Aus einem Schreiben von Dr. Kuhl und Dr. van Hasselt auf Java, an Th. Van Swinderen zu Groningen. Isis von Oken 1822(4): 472–476.

Leong TM, Chou LM (1998) Larval identity of the montane horned frog, *Megophrys longipes* (Boulenger) (Amphibia: Anura: Megophryidae). The Raffles Bulletin of Zoology 46(2): 471–475.

Li SZ, Xu N, Liu J, Jiang JP, Wei G, Wang B (2018) A new species of the Asian toad genus *Megophrys* sensu lato (Amphibia: Anura: Megophryidae) from Guizhou Province, China. Asian Herpetological Research 9(4): 224–239. https://doi.org/10.16373/j.cnki.ahr.180072

Li Y, Zhang DD, Lyu ZT, Wang J, Li YL, Liu ZY, Chen HH, Rao DQ, Jin ZF, Zhang CY, Wang YY (2020) Review of the genus *Brachytarsophrys* (Anura: Megophryidae), with revalidation of *Brachytarsophrys platyparietus* and description of a new species from China. Zoological Research 41(2): 105–122. https://doi.org/10.24272/j.issn.2095-8137.2020.033

Liu CC (1950) Amphibians of western China. Fieldiana: Zoology Memoirs 2: 1–400. [pl. 1–10.] https://doi.org/10.5962/bhl.part.4737

Liu CC, Hu SC (1975) Report on three new species of Amphibia from Fujian Province. Acta Zoologica Sinica 21(3): 265–271. [福建省两栖动物的三新种] [pl. I.]

Liu CC, Hu SC, Yang FH (1960) Amphibia of Yunnan collected in 1958. Acta Zoologica Sinica 12(2): 149–174. [pl. I–IV.]

Liu ZY, Chen GL, Zhu TQ, Zeng ZC, Lyu ZT, Wang J, Messenger K, Greenberg AJ, Guo ZX, Yang ZH, Shi SH, Wang YY (2018) Prevalence of cryptic species in morphologically uniform taxa – Fast speciation and evolutionary radiation in Asian frogs. Molecular Phylogenetics and Evolution 127: 723–731. https://doi.org/10.1016/j.ympev.2018.06.020

Liu J, Li SZ, Wei G, Xu N, Cheng YL, Wang B, Wu J (2020) A new species of the Asian toad genus *Megophrys sensu lato* (Anura: Megophryidae) from Guizhou Province, China. Asian Herpetological Research 11(1): 1–18. http://doi.org/10.16373/j.cnki.ahr.190041

Lyu ZT, Li YQ, Zeng ZC, Zhao J, Liu ZY, Guo GX, Wang YY (2020) Four new species of Asian horned toads (Anura, Megophryidae, *Megophrys*) from southern China. ZooKeys 942: 105–140. https://doi.org/10.3897/zookeys.942.47983

Lyu ZT, Zeng ZC, Wang J, Liu ZY, Huang YQ, Li WZ, Wang YY (2021) Four new species of *Panophrys* (Anura, Megophryidae) from eastern China, with discussion on the recognition of *Panophrys* as a distinct genus. Zootaxa 4927(1): 9–40. https://doi.org/10.11646/zootaxa.4927.1.2

Mahony S, Foley NM, Biju SD, Teeling EC (2017) Evolutionary history of the Asian Horned Frogs (Megophryinae): Integrative approaches to timetree dating in the absence of a fossil record. Molecular Biology and Evolution 34(3): 744–771. https://doi.org/10.1093/molbev/msw267

Mahony S, Kamei RG, Teeling EC, Biju SD (2018) Cryptic diversity within the *Megophrys major* species group (Amphibia: Megophryidae) of the Asian Horned Frogs: Phylogenetic perspectives and a taxonomic revision of South Asian taxa, with descriptions of four new species. Zootaxa 4523(1): 1–96. https://doi.org/10.11646/zootaxa.4523.1.1

Mahony S, Kamei RG, Teeling EC, Biju SD (2020) Taxonomic review of the Asian Horned Frogs (Amphibia: *Megophrys* Kuhl & Van Hasselt) of Northeast India and Bangladesh previously misidentified as *M. parva* (Boulenger), with descriptions of three new species. Journal of Natural History 54(1–4): 1–76. https://doi.org/10.1080/00222933.2020.1736679

Mathew R, Sen N (2007) Description of two new species of *Xenophrys* (Amphibia: Anura: Megophryidae) from north-east India. Cobra 1(2): 18–28.

Mell R (1922) Beiträge zur Fauna Sinica. Archiv für Naturgeschichte 88: 1–146.

Messenger KR, Dahn HA, Liang Y, Xie P, Wang Y, Lu C (2019) A new species of the genus *Megophrys* Günther, 1864 (Amphibia: Anura: Megophryidae) from Mount Wuyi, China. Zootaxa 4554(2): 561–583. https://doi.org/10.11646/zootaxa.4554.2.9

Munir M, Hamidy A, Matsui M, Iskandar DT, Sidik I, Shimada T (2019) A new species of *Megophrys* Kuhl & Van Hasselt (Amphibia: Megophryidae) from Borneo allied to *M. nasuta* (Schlegel, 1858). Zootaxa 4679(1): 1–24. https://doi.org/10.11646/zootaxa.4679.1.1

Oberhummer E, Barten C, Schweizer M, Das I, Haas A (2014) Description of the tadpoles of three rare species of megophryid frogs (Amphibia: Anura: Megophryidae) from Gunung Mulu, Sarawak, Malaysis. Zootaxa 3835(1): 59–79. https://doi.org/10.11646/zootaxa.3835.1.3

Pope CH (1931) Notes on amphibians from Fukien, Hainan, and other parts of China. Bulletin of the American Museum of Natural History 61(8): 397–611.

Poyarkov Jr NA, Duong TV, Orlov NL, Gogoleva SS, Vassilieva AB, Nguyen LT, Nguyen VDH, Nguyen SN, Che J, Mahony S (2017) Molecular, morphological and acoustic assessment of the genus *Ophryophryne* (Anura, Megophryidae) from Langbian Plateau, southern Vietnam, with description of a new species. ZooKeys 672: 49–120. https://doi.org/10.3897/zookeys.672.10624

Qi S, Lyu ZT, Wang J, Mo YM, Zeng ZC, Zeng YJ, Dai KY, Li YQ, Grismer LL, Wang YY (2021) Three new species of the genus *Boulenophrys* (Anura, Megophryidae) from southern China. Zootaxa 5072(5): 401–438. https://doi.org/10.11646/zootaxa.5072.5.1

Raj P, Dutta SK, Lalremsanga HT (2022) Larval descriptions of *Rhacophorus bipunctatus* and *Xenophrys serchhipii* from northeast India. Zootaxa 5092(4): 493–500. https://doi.org/10.11646/zootaxa.5092.4.9

Schneider CA, Rasband WS, Eliceiri KW (2012) NIH Image to ImageJ: 25 years of image analysis. Nature Methods 9(7): 671–675. https://doi.org/10.1038/nmeth.2089

Shen YH [沈猷慧] (1983) Amphibian survey and fauna analysis in Hunan Province. Acta Herpetolocica Sinica 2(1): 49–58. [湖南省两栖动物调查及区系分析] [In Chinese]

Shen YH, Yang DD, Mo XY, Li HH, Chen D (2014) Fauna Hunan, Amphibia. Hunan Science and Technology Press, Changsha, 390 pp. [In Chinese]

Shi SC, Zhang MH, Xie F, Jiang JP, Liu WL, Ding L, Luan L, Wang B (2020a) Multiple data revealed two new species of the Asian horned toad *Megophrys* Kuhl & Van Hasselt, 1822 (Anura, Megophryidae) from the eastern corner of the Himalayas. ZooKeys 977: 101–161. https://doi.org/10.3897/zookeys.977.55693

Shi SC, Wang B, Zhu WB, Fu L, Jiang W, Li DH, Jiang JP (2020b) *Megophrys periosa* (Mahony, Kamei, Teeling, and Biju 2018) was first recorded in Yunan Province, China with description of its tadpole. Chinese Journal of Zoology 55(6): 730–740. [In Chinese with English abstract]

Shi SC, Li DH, Zhu WB, Jiang W, Jiang JP, Wang B (2021) Description of a new toad of *Megophrys* Kuhl & Van Hasselt, 1822 (Amphibia: Anura: Megophryidae) from western Yunnan Province, China. Zootaxa 4942(3): 351–381. https://doi.org/10.11646/zootaxa.4942.3.3

Simon C, Frati F, Beckenbach A, Crespi B, Liu H, Flook P (1994) Evolution, weighting, and phylogenetic utility of mitochondrial gene sequences and a compilation of conserved

polymerase chain reaction primers. Annals of the Entomological Society of America 87(6): 651–701. https://doi.org/10.1093/aesa/87.6.651

Stuart BL, Chuaynkern Y, Chan-ard T, Inger RF (2006) Three new species of frogs and a new tadpole from eastern Thailand. Fieldiana. Zoology 111: 1–19. https://doi.org/10.3158/0015-0754(2006)187[1:TNSOFA]2.0.CO;2

Tamura K, Stecher G, Peterson D, Filipski A, Kumar S (2013) MEGA6: Molecular evolutionary genetics analysis, version 6.0. Molecular Biology and Evolution 30(12): 2725–2729. https://doi.org/10.1093/molbev/mst197

Tapley B, Cutajar T, Mahony S, Nguyen CT, Dau VQ, Nguyen TT, Luong HV, Rowley JJL (2017) The Vietnamese population of *Megophrys kuatunensis* (Amphibia: Megophryidae) represents a new species of Asian horned frog from Vietnam and southern China. Zootaxa 4344(3): 465–492. https://doi.org/10.11646/zootaxa.4344.3.3

Tapley B, Cutajar T, Mahony S, Nguyen CT, Dau VQ, Luong AM, Le DT, Nguyen TT, Nguyen TQ, Portway C, Luong HV, Rowley JJL (2018) Two new and potentially highly threatened *Megophrys* Horned frogs (Amphibia: Megophryidae) from Indochina' s highest mountains. Zootaxa 4508(3): 301–333. https://doi.org/10.11646/zootaxa.4508.3.1

Tapley B, Nguyen LT, Le MV (2020a) A description of the tadpole of *Megophrys* "*Brachytarsophrys*" *intermedia* (Smith, 1921). Zootaxa 4845(1): 26–34. https://doi.org/10.11646/zootaxa.4845.1.2

Tapley B, Nguyen LT, Cutajar T, Nguyen CT, Portway C, Luong HV, Rowley JJL (2020b) The tadpoles of five *Megophrys* Horned frogs (Amphibia: Megophryidae) from the Hoang Lien Range, Vietnam. Zootaxa 4845(1): 35–52. https://doi.org/10.11646/zootaxa.4845.1.3

Tapley B, Cutajar T, Nguyen LT, Portway C, Mahony S, Nguyen CT, Harding L, Luong HV, Rowley JJL (2021) A new potentially Endangered species of *Megophrys* (Amphibia: Megophryidae) from Mount Ky Quan San, north-west Vietnam. Journal of Natural History 54(39–40): 2543–2575. https://doi.org/10.1080/00222933.2020.1856952

Tian WS, Hu QX (1983) Taxonomic study on genus *Megophrys*, with descriptions of two new genera. Acta Herpetologica Sinica 2(2): 41–48. [New Series]

Wang YY, Zhang TD, Zhao J, Sung YH, Yang JH, Pang H, Zhang Z (2012) Description of a new species of the genus *Xenophrys* Günther, 1864 (Amphibia: Anura: Megophryidae) from Mount Jinggang, China, based on molecular and morphological data. Zootaxa 3546(1): 53–67. https://doi.org/10.11646/zootaxa.3546.1.4

Wang YY, Zhao J, Yang JH, Zhou ZX, Chen GL, Liu Y (2014) Morphology, molecular genetics, and bioacoustics support two new sympatric *Xenophrys* toads (Amphibia: Anura: Megophryidae) in southeast China. PLoS ONE 9(4): e93075. https://doi.org/10.1371/journal.pone.0093075

Wang J, Lyu ZT, Liu ZY, Liao CK, Zeng ZC, Zhao J, Li YL, Wang YY (2019) Description of six new species of the subgenus *Panophrys* within the genus *Megophrys* (Anura, Megophryidae) from southeastern China based on molecular and morphological data. ZooKeys 851: 113–164. https://doi.org/10.3897/zookeys.851.29107

Wu YK, Wang YZ, Hanken J (2012) New species of *Pachytriton* (Caudata: Salamandridae) from the Nanling Mountain Range, southeastern China. Zootaxa 3388(1): 1–16. https://doi.org/10.11646/zootaxa.3388.1.1

Wu YQ, Li SZ, Liu W, Wang B, Wu J (2020) Description of a new horned toad of *Megophrys* Kuhl & Van Hasselt, 1822 (Amphibia, Megophryidae) from Zhejiang Province, China. ZooKeys 1005: 73–102. https://doi.org/10.3897/zookeys.1005.58629

Zeng Y (2021) Suction anchoring with an umbelliform oral disc by the surface-feeding tadpole of *Brachytarsophrys chuannanensis* Fei et al., 2001. Herpetology Notes 14: 557–561.

Zhao EM (1999) Diagnoses of a new frog and a new snake from China. Sichuan Journal of Zoology 18(3): Front cover II.

Zhao J, Yang JH, Chen GL, Chen CQ, Wang YY (2014) Description of a new species of the genus *Brachytarsophrys* Tian and Hu, 1983 (Amphibia: Anura: Megophryidae) from Southern China based on molecular and morphological data. Asian Herpetological Research 5(3): 150–160. https://doi.org/10.3724/SP.J.1245.2014.00150

ZooKeys 1139: 33–69 (2023)
doi: 10.3897/zookeys.1139.96639
https://zookeys.pensoft.net

RESEARCH ARTICLE

A peer-reviewed open-access journal
ZooKeys
Launched to accelerate biodiversity research

Four new species of cave-adapted pseudoscorpions (Pseudoscorpiones, Pseudotyrannochthoniidae) from Guizhou, China

Zhizhong Gao[1], Yanmeng Hou[2], Feng Zhang[2]

1 *Department of Biology, Xinzhou Teachers University, Xinzhou, Shanxi 034000, China* **2** *The Key Laboratory of Zoological Systematics and Application, Institute of Life Science and Green Development, College of Life Sciences, Hebei University, Baoding, Hebei 071002, China*

Corresponding author: Feng Zhang (dudu06042001@163.com)

Academic editor: J. Christophoryová | Received 23 October 2022 | Accepted 16 December 2022 | Published 9 January 2023

https://zoobank.org/0A828EAE-0A7E-4EF6-9086-9572E8F15E21

Citation: Gao Z, Hou Y, Zhang F (2023) Four new species of cave-adapted pseudoscorpions (Pseudoscorpiones, Pseudotyrannochthoniidae) from Guizhou, China. ZooKeys 1139: 33–69. https://doi.org/10.3897/zookeys.1139.96639

Abstract

Four new troglomorphic pseudotyrannochthoniid pseudoscorpion species collected from karst caves in Guizhou Province are described with detailed diagnoses and illustrations: *Allochthonius bainiensis* **sp. nov.** from Liangfeng Cave (Xishui County), *Allochthonius pandus* **sp. nov.** from Daozuo Cave (Xishui County), *Allochthonius xinqiaoensis* **sp. nov.** from Sanjie Cave (Fenggang County), and *Spelaeochthonius wulibeiensis* **sp. nov.** from Wulibei Cave (Weining County). *Spelaeochthonius wulibeiensis* **sp. nov.** represents the first record of the genus in China. The diagnostic features of these four new cave-adapted (troglomorphic) species are presented and discussed, as well as compared with closely related species. The data on their distribution, habitat and ecology of the species are also given.

Keywords

Allochthonius, *Spelaeochthonius*, taxonomy, troglomorphic

Introduction

The genus *Allochthonius* Chamberlin, 1929, belonging to the family Pseudotyrannochthoniidae Beier, 1932, mainly distributed in Asia, lately included two subgenera, *Allochthonius* Chamberlin, 1929 and *Urochthonius* Morikawa, 1954. The subgenus *Urochthonius* has been recently synonymized with *Allochthonius* (Harvey and Harms

2022; WPC 2022). Up to now, the genus *Allochthonius* contains a total of 30 species (nine species from China), and of these 30 species, only nine species have no eyes. Of these nine blind species, only *A. brevitus* Hu & Zhang, 2012 comes from China and it is an epigean species, while the other eight species were found in caves in Japan (Morikawa 1956; Hu and Zhang 2011, 2012; Zhang and Zhang 2014; Gao et al. 2016; Schwarze et al. 2021; Viana and Ferreira 2021; WPC 2022).

The genus *Spelaeochthonius* Morikawa, 1954, belonging to the family Pseudotyrannochthoniidae, was erected by Morikawa (1954). All nine species from this genus (six species from Japan and three species from Korea) were found in caves and are completely eyeless and highly troglomorphic. In general, *Spelaeochthonius* species can be distinguished from other genera in the family by the number of carapaceal setae; the number, shape, and arrangement of the coxal spines, and the shape of the intercoxal tubercle; see Morikawa (1956) and You et al. (2022) for details. *Spelaeochthonius wulibeiensis* sp. nov. represents the first record of the genus in China, even though it is not characterized by the typical distally pinnate or serrate coxal spines.

Southwest China is one of China's seven physical geographical regions, including Sichuan, Guizhou and Yunnan Province, Chongqing Municipality, and Xizang Autonomous Region (Tibet). It is also the main distribution area of karst landforms, covering an area of 426,240 km^2 (Zhang et al. 2001). Guizhou, located in the hinterland of southwest China, is the province with the most widely distributed karst landforms (10.91×10^4 km^2, accounting for 61.92% of the total land area of the province) and contains tens of thousands of karst caves that host a large amount of unique and undescribed fauna (Lin 2001). Among the at least 742 cave-dwelling species identified in China, nearly 20% of them are found in Guizhou (Latella 2019). One of the representative groups of cave-dwelling arthropods is subterranean-adapted pseudoscorpions. They are usually eyeless and have a hypopigmented body cuticle and elongated body appendages. To date, 54 cave-dwelling pseudoscorpion species from four families (Atemnidae, Chernetidae, Chthoniidae, Neobisiidae) have been described from China (Schawaller 1995; Mahnert 2003, 2009; Mahnert and Li 2016; Gao et al. 2017, 2018, 2020; Li et al. 2017, 2019; Feng et al. 2019, 2020; Zhang et al. 2020; Li and Wang 2021; Hou et al. 2022a, b; Li 2022; Xu et al. 2022), including 12 species from Guizhou. No cavernicolous pseudotyrannochthoniid species have been reported from China yet.

In this study, four new pseudotyrannochthoniid species are presented with detailed diagnoses, descriptions, and illustrations, all of which were collected from caves in Guizhou over the past few years.

Materials and methods

As none of these caves in the present study were subject to previous studies or exploration efforts, cave maps are not available. Information on the length of the cave, their temperature and humidity, and the height and width of the cave entrance are provided by using a temperature and humidity meter (LUGE L92-1) and a rangefinder (LEICA X3).

The specimens examined for this study are preserved in 75% alcohol and deposited in the Museum of Hebei University (**MHBU**) (Baoding, China) and the Museum of Southwest University (**MSWU**) (Chongqing, China). Photographs, drawings and measurements were taken using a Leica M205A stereo-microscope equipped with a Leica DFC550 camera and the Inkscape software (Ver. 1.0.2.0). Detailed examination was carried out with an Olympus BX53 general optical microscope. Distribution map was made using ArcGIS 10.6 (Fig. 1). All images were edited and formatted using Adobe Photoshop 2022.

Terminology and measurements follow Chamberlin (1931) with some minor modifications to the terminology of trichobothria (Harvey 1992; Judson 2007) and chelicera (Judson 2007). The chela and legs are measured in lateral view and others are taken in dorsal view. All measurements are given in mm unless noted otherwise. Proportions and measurements of chelicerae, carapace and pedipalps correspond to length/breadth, and those of legs to length/depth. For abbreviations of trichobothria, see Chamberlin (1931).

Taxonomy

Family Pseudotyrannochthoniidae Beier, 1932

Genus *Allochthonius* Chamberlin, 1929

Type species. *Chthonius opticus* Ellingsen, 1907, by original designation.

***Allochthonius bainiensis* sp. nov.**
https://zoobank.org/F80B7B0C-B722-4DD8-8170-2A945BD4698A
Figs 1B, 2–6
Chinese name 白坭异伪蝎

Type material. *Holotype*: China • ♀; Guizhou Province, Xishui County, Donghuang Town, Baini Village, Liangfeng Cave; 28°17.72'N, 106°16.80'E; 1308 m a.s.l., 24 Jul. 2022; Yanmeng Hou, Lu Zhang, Jianzhou Sun and Wenlong Fan leg.; under a stone in the deep zone; Ps.-MHBU-HBUARA#2022-478 (Figs 1B, 2).

Diagnosis (♀). The new species can be recognized by the following combination of characters: carapace without eyes or eyespots, posterior margin with two setae, chaetotaxy of carapace: 4–4–2–2–2, 14; cheliceral palm with four setae only; rallum with nine blades (each with fine pinnate, the basal-most blade shorter than the others); coxa I with six coxal spines (tridentate blades, each blade with a central fan-shaped spine terminally) on a tubercle; pedipalps slender, femur 9.07, chela 5.41× longer than broad, both chelal fingers with a row of teeth (fixed chelal finger with 19 teeth; movable chelal finger with 17 teeth), slightly retrorse and pointed.

Figure 1. Study area with indication of cave locations representing the type localities. Each color represents an administrative region (red: Guizhou Province; purple: Weining County; green: Xishui County; blue: Fenggang County) **A** Wulibei Cave (*Spelaeochthonius wulibeiensis* sp. nov.) **B** Liangfeng Cave (*Allochthonius bainiensis* sp. nov.) **C** Daozuo Cave (*A. pandus* sp. nov.) **D** Sanjie Cave (*A. xinqiaoensis* sp. nov.).

Etymology. Named after the village of Baini, near the type locality.

Description. Adult female (male unknown) (Figs 3–6). ***Color*** (Figs 3, 4): generally pale yellow, chelicerae, pedipalps and tergites slightly darker, soft parts pale. ***Cephalothorax*** (Figs 4B, D, 5A, C): carapace subquadrate, 0.87× longer than broad, gently narrowed posteriorly; surface smooth, without furrows but with six lyrifissures and the posterior part with squamous sculpturing; no traces of eyes; epistomal process

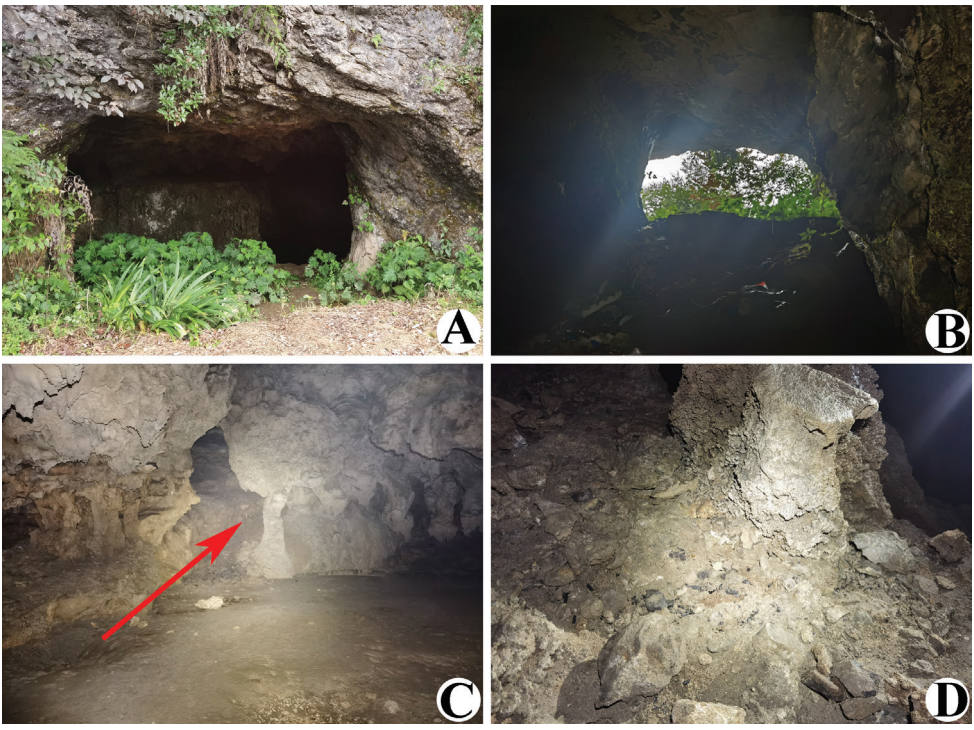

Figure 2. Liangfeng Cave, type locality of *Allochthonius bainiensis* sp. nov. **A** entrance **B** inside the cave entrance **C, D** area where *A. bainiensis* sp. nov. specimen was collected (red arrow).

absent, space between median setae slightly recurved; with 14 setae arranged 4: 4: 2: 2: 2, preocular setae absent, most setae heavy, long and gently curved. Chaetotaxy of coxae: P 3, I 4, II 5, III 5, IV 5–6; manducatory process with two acuminate distal setae, anterior seta less than 1/2 length of medial seta; coxal spines present on coxa I only, consisting of a tubercle expanded terminally into a characteristic "spray" or "fan" of six elevated processes which extend apically, subequal in length (Figs 4D, 5C); bisetose intercoxal tubercle present between coxae III and IV (Fig. 4D). ***Chelicera*** (Figs 4C, 5B, E): large, approximately as long as carapace, 2.37× longer than broad; four setae present on hand, all setae acuminate, ventrobasal seta shorter than others; movable finger with a medial seta; exterior condylar lyrifissure and exterior lyrifissure exist, palm with two extra setae (close to sub-basal seta). Cheliceral palm with moderate hispid granulation on both ventral and dorsal sides. Both fingers well provided with teeth, fixed finger with 14 acute teeth, distal one largest, plus five small basal teeth, 19 in total; movable finger with 21 retrorse contiguous teeth of equal length; galea absent. Serrula exterior with 18 blades and serrula interior with 12 blades. Rallum in two rows and composed of nine blades with fine pinnate, of which the basal-most blade shorter than the others (Fig. 5E). ***Pedipalp*** (Figs 4A, 5D, 6A, B): long and slender, trochanter 1.68, femur 9.07, patella 3.06, chela 5.41, hand 2.29× longer than broad;

Figure 3. *Allochthonius bainiensis* sp. nov., holotype female, habitus (dorsal view). Scale bar: 0.50 mm.

femur 2.62× longer than patella; movable chelal finger 1.44× longer than hand and 0.61× longer than chela. Setae generally long and acuminate; two distal lyrifissures present on patella (Fig. 5D). Chelal palm robust and slightly constricted towards fingers. Fixed chelal finger and hand with eight trichobothria, movable chelal finger with four trichobothria, *ib*, *isb*, *eb*, *esb*, and *ist* clustered at the base of fixed finger, *ist* slightly distal

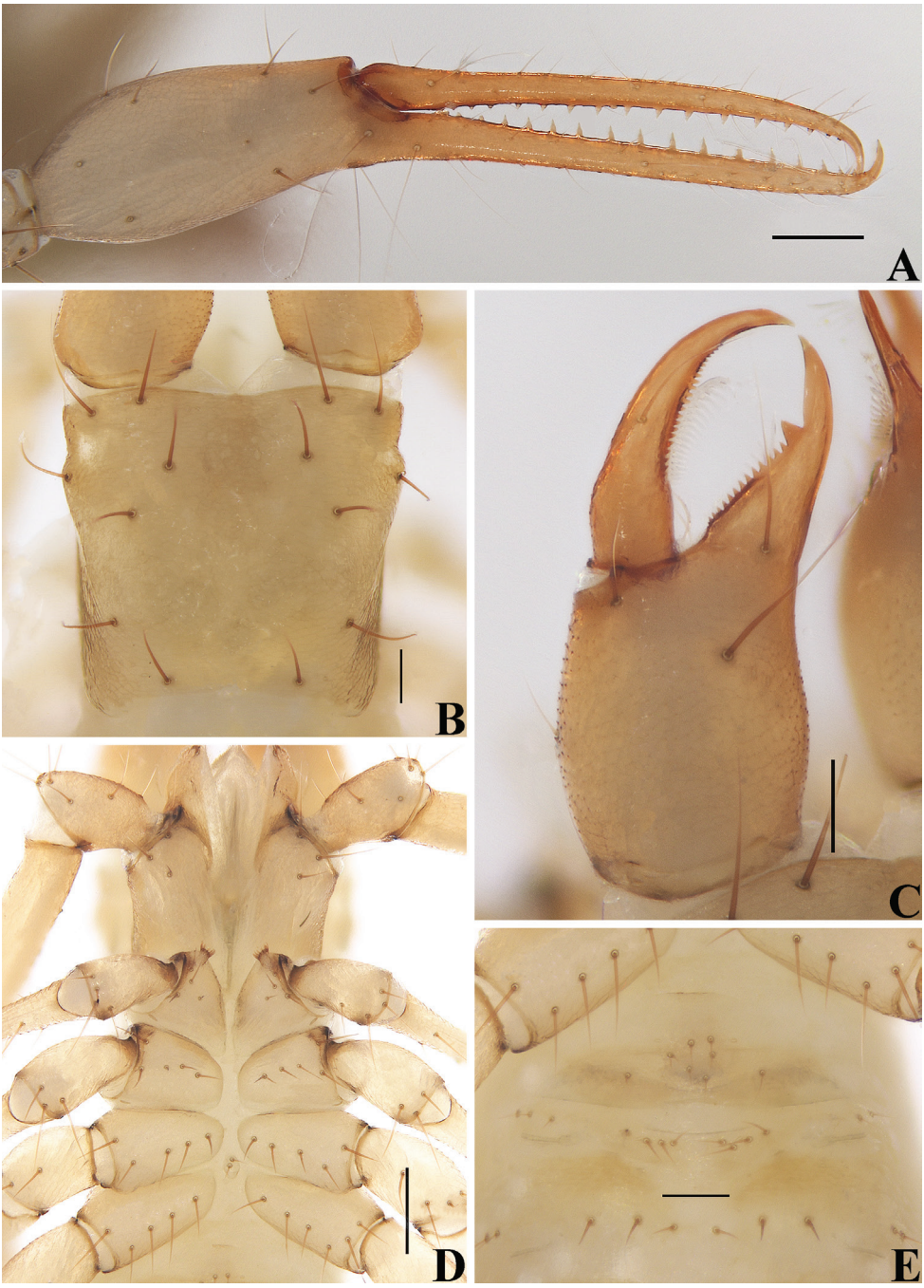

Figure 4. *Allochthonius bainiensis* sp. nov., holotype female **A** left chela (lateral view) **B** carapace (dorsal view) **C** left chelicera (dorsal view) **D** coxae (ventral view) **E** female genital area (ventral view). Scale bars: 0.20 mm (**A, D**); 0.10 mm (**B, C, E**).

to *esb*; *it* slightly distal to *est*, situated subdistally; *et* situated subdistally, very close to chelal teeth; *dx* situated distal to *et*, near the tip of fixed finger; *sb* situated closer to *b* than to *st* (Fig. 6A). Microsetae (chemosensory setae) absent on hand and both palpal fingers. Sensilla absent. Both chelal fingers with a row of teeth, homodentate, spaced regularly along the margin, larger and well-spaced teeth present in the middle of the row, becoming smaller and closer distally and proximally: fixed chelal finger with 19 teeth, slightly retrorse and pointed; movable chelal finger with 17 teeth (slightly smaller than teeth on fixed chelal finger) and a tubercle between the ninth and tenth teeth (Fig. 6A). Chelal fingers slightly curved in dorsal view (Fig. 6B). ***Opisthosoma*:** generally typical, pleural membrane finely granulated. Tergites and sternites undivided; setae uniseriate and acuminate. Tergal chaetotaxy I–XII: 2: 4: 4: 6: 6: 7: 7: 6: 7: 5: TT: 0; tergites IX and X each with an unpaired median seta. Sternal chaetotaxy IV–XII: 10: 11: 11: 11: 11: 9: 8: 0: 2. Anterior genital operculum with eight setae plus 14 setae on posterior margin, with a pair of lyrifissures present anterolateral and posteriolateral to genital opening, respectively (Fig. 4E). ***Legs*** (Fig. 6C, D): generally typical, long, and slender. Fine granulation present on anterodorsal faces of femur IV and patella IV. Femur of leg I 1.77× longer than patella and with one lyrifissure at the base of femur; tarsus 2.55× longer than tibia. Femoropatella of leg IV 4.86× longer than deep and with one lyrifissure at the base of femur; tibia 6.17× longer than deep; with basal tactile setae on both tarsal segments: basitarsus 4.22× longer than deep (TS = 0.24), telotarsus 12.43× longer than deep and 2.29× longer than basitarsus (TS = 0.31). Setae of leg I (trochanter to tibia) 2: 10: 9: 12, setae of leg IV (trochanter to basitarsus) 3: 3: 7: 15: 17. Arolium slightly shorter than the claws, not divided; claws simple. ***Dimensions of female holotype*** (length/breadth or, in the case of the legs, length/depth in mm): body length 2.72. Pedipalps: trochanter 0.32/0.19, femur 1.36/0.15, patella 0.52/0.17, chela 1.84/0.34, hand 0.78/0.34, movable finger length 1.12. Chelicera 0.64/0.27, movable finger length 0.34. Carapace 0.55/0.63. Leg I: trochanter 0.24/0.18, femur 0.76/0.11, patella 0.43/0.10, tibia 0.33/0.07, tarsus 0.84/0.07. Leg IV: trochanter 0.34/0.18, femoropatella 1.02/0.21, tibia 0.74/0.12, basitarsus 0.38/0.09, telotarsus 0.87/0.07.

Remarks. *Allochthonius bainiensis* sp. nov. is similar to *A. pandus* sp. nov. and *A. xinqiaoensis* sp. nov. in having the same number of setae on the carapace (14) and chelicera (6), while differs in the absence of a pair of curved chelal fingers (dorsal view) and the presence of lower number of teeth on chelal fingers (19 vs. 31–33 or 23 teeth on the fixed chelal finger and 17 vs. 26–28 or 23 teeth on the movable chelal finger).

Allochthonius bainiensis sp. nov. differs from *A. brevitus* and *A. yoshizawai* Viana & Ferreira, 2021 in the number of setae on the anterior of the carapace (4 vs. 6) and the cheliceral hand (5 vs. 6), and the number of rallum blades (9 vs. 11).

Allochthonius bainiensis sp. nov. can be distinguished from *A. ishikawai* Morikawa, 1954 and all *A. ishikawai* subspecies by the number of setae on the carapace (14 vs. 16 or more), the presence of lower number of rallum blades (9 vs. 10) and larger body size (2.72 vs. 2.38 mm, which is the longest body length of all *A. ishikawai* subspecies, for example, female of *A. ishikawai uyamadensis*, Morikawa, 1954).

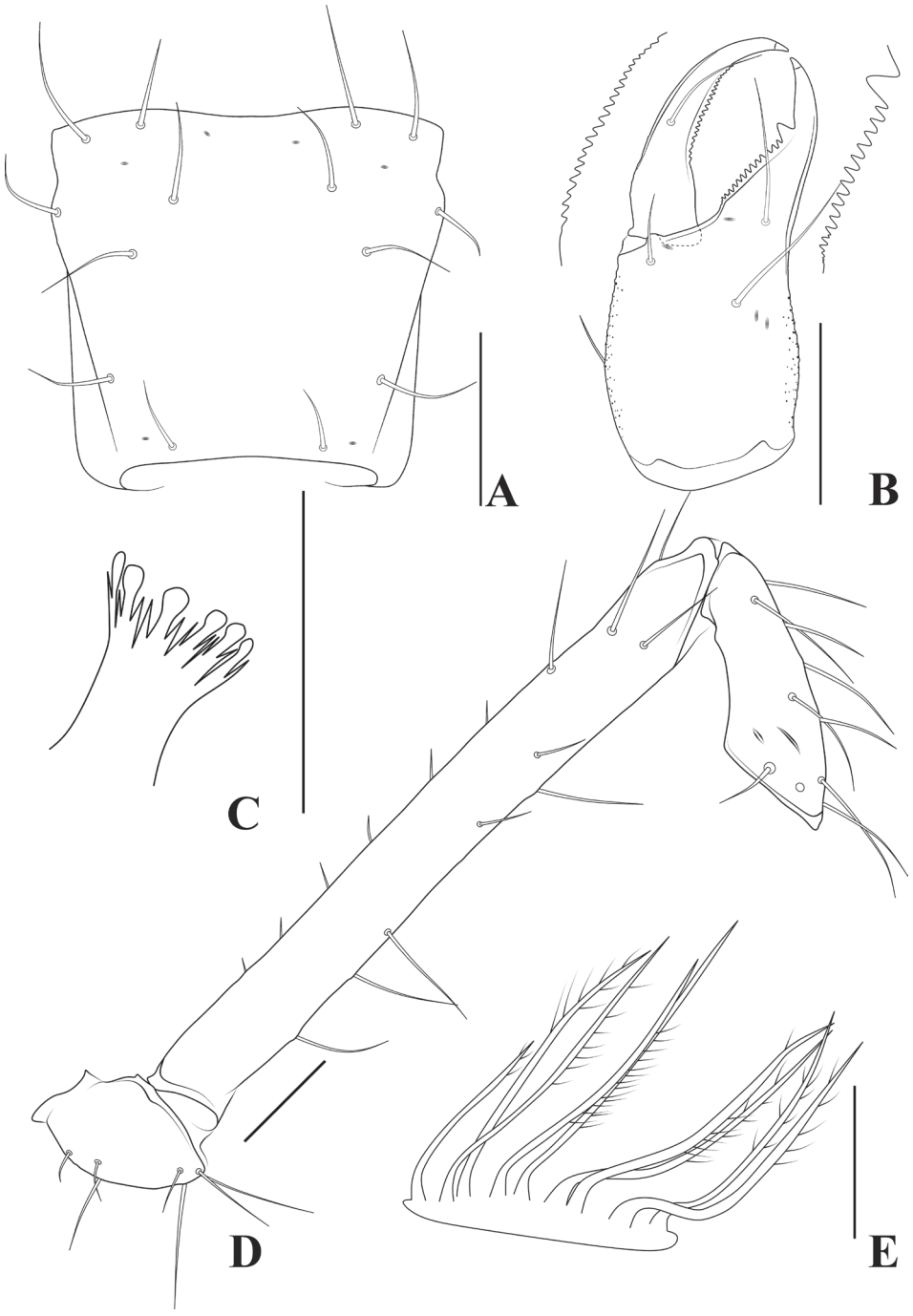

Figure 5. *Allochthonius bainiensis* sp. nov., holotype female **A** carapace (dorsal view) **B** left chelicera (dorsal view), with details of teeth **C** coxal spines on coxae I (ventral view) **D** left pedipalp (minus chela, dorsal view) **E** rallum. Scale bars: 0.20 mm (**A, B, D**); 0.10 mm (**C, E**).

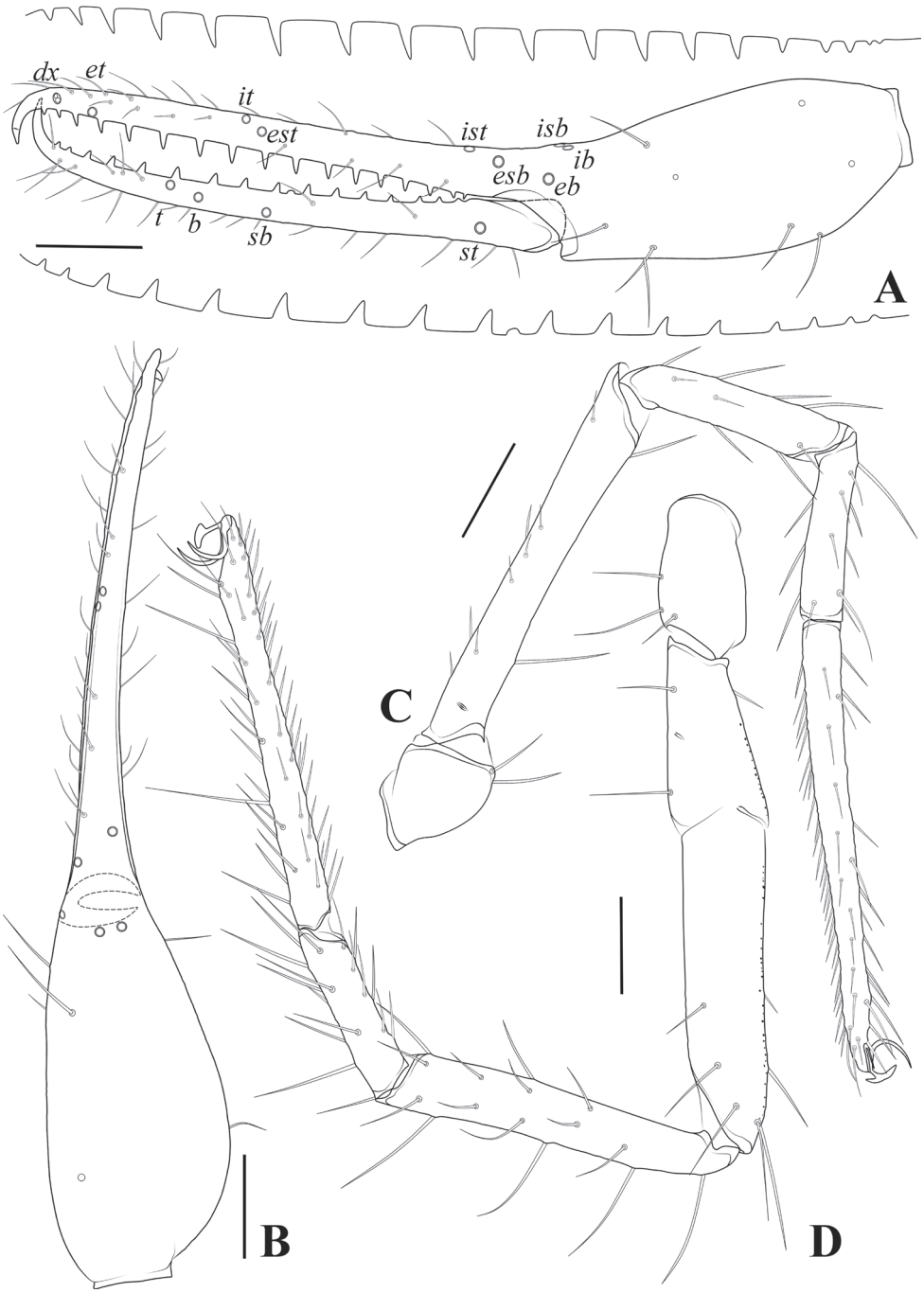

Figure 6. *Allochthonius bainiensis* sp. nov., holotype female **A** left chela (lateral view), with details of teeth and trichobothrial pattern **B** left chela (dorsal view) **C** leg I (lateral view) **D** leg IV (lateral view). Scale bars: 0.20 mm.

Allochthonius bainiensis sp. nov. can be distinguished from the other species of *Allochthonius* by the absence of any traces of eyes (Morikawa 1954, 1956, 1960; Hu and Zhang 2012; Viana and Ferreira 2021; WPC 2022).

Distribution and habitat. This species is only known from the type locality, Liangfeng Cave (Figs 1B, 2), which is located near a road, 0.6 km southeast of Baini Village (Xishui County). This limestone cave has a medium-sized rectangular entrance (~ 3 m high and 5 m wide) with a large horizontally extending interior space. The interior of the cave is mainly divided into three tunnels, the left tunnel extends ~ 200 m, the middle tunnel extends ~ 500 m, and the right tunnel communicates with the middle tunnel, ~ 100 m in length. Human disturbance in the entrance zone is serious, but the deep zone remains pristine. The specimen was collected under a stone near the wall in the deepest part of the middle tunnel. This space is completely dark, with constant temperature and humidity (temperature ~ 9 °C, humidity ~ 90%).

***Allochthonius pandus* sp. nov.**

https://zoobank.org/50DA34BD-CAD3-4A28-AFD6-28078FBF21E1

Figs 1C, 7–12

Chinese name 弯指异伪蝎

Type material. ***Holotype*:** China • ♂; Guizhou Province, Xishui County, Xianyuan Town, Jinshan Village, Daozuo Cave; 28°18.04'N, 106°41.70'E; 1606 m a.s.l.; 24 Jul. 2022; Yanmeng Hou, Lu Zhang, Jianzhou Sun and Wenlong Fan leg.; under a stone in the deep zone; Ps.-MHBU-HBUARA#2022-47701 (Figs 1C, 7A–E). ***Paratypes*:** • 1♂; the same location as the holotype; 28 Aug. 2020; Zegang Feng, Hongru Xu and Yanmeng Hou leg.; Ps.-MHBU-GZXS-20-24 • 2♀; the same data as the holotype; Ps.-MSWU-HBUARA#2022-47702-HBUARA#2022-47703.

Diagnosis (♂♀). The new species can be recognized by the following combination of characters: cheliceral palm with five setae; coxa I with four coxal spines (tridentate blades, each blade with a central fan-shaped spine terminally) on a tubercle; pedipalps slender, femur 9.07–10.15 (♂), 8.50–8.60 (♀), chela 7.00–7.52 (♂), 6.64–7.15 (♀) × longer than broad, both chelal fingers with a row of teeth (fixed chelal finger with 31 or 33 teeth; movable chelal finger with 26 or 28 teeth), slightly retrorse and pointed; chela fingers markedly curved in dorsal view.

Etymology. The specific name is derived from the Latin word *pandus* (curved) and refers to the character of the curved chelal fingers.

Description. Adult males (Figs 7F, 8A, 9, 10A, B, 11, 12). ***Color*** (Figs 7F, 8A, 9, 10A, B): generally pale yellow, chelicerae, pedipalps and tergites slightly darker, soft parts pale. ***Cephalothorax*** (Figs 9B, 10A, 11A, C): carapace inverted trapezoid, 0.91–0.93× longer than broad, gently narrowed posteriorly; surface smooth, without furrows but with six lyrifissures and the posterior part with squamous sculpturing; no traces of eyes; epistomal process absent, space between median setae slightly recurved;

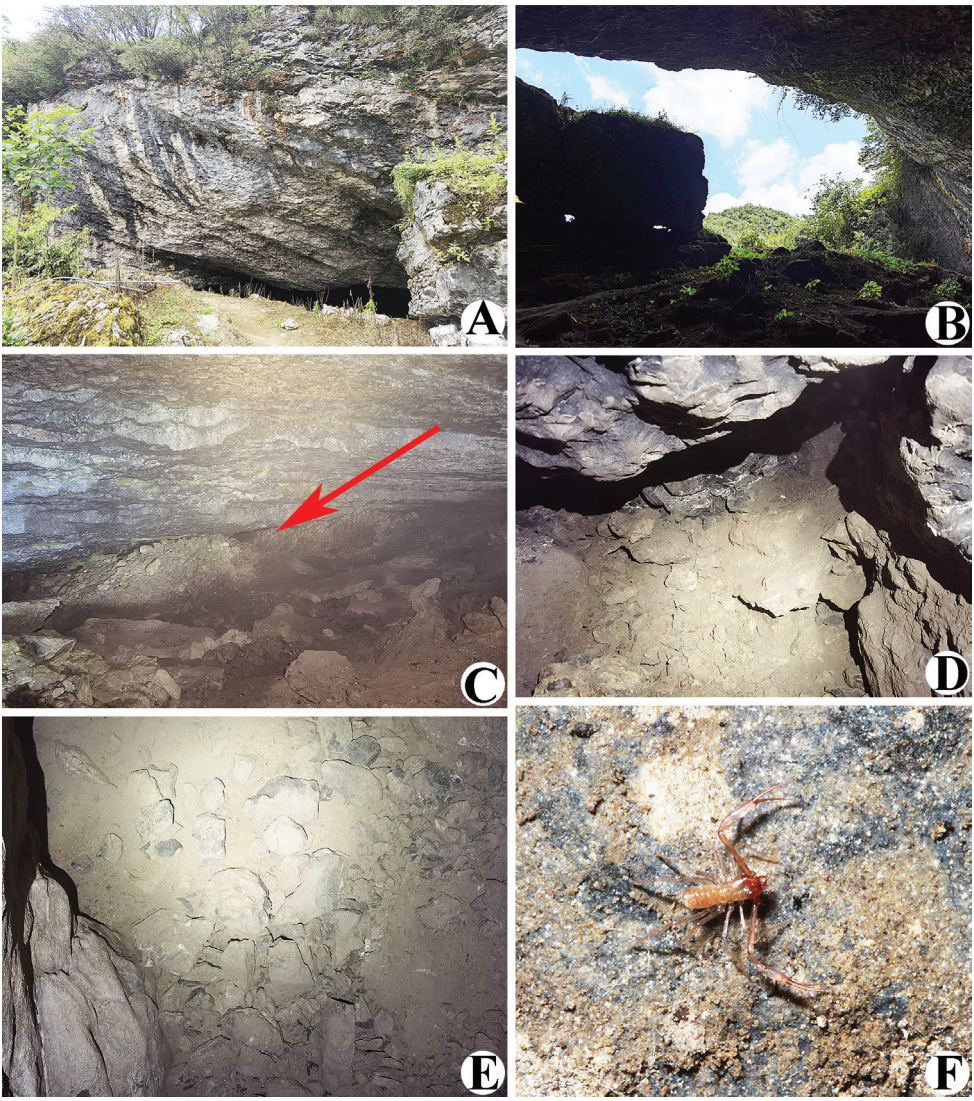

Figure 7. Daozuo Cave, type locality of *Allochthonius pandus* sp. nov. **A** entrance **B** inside the cave entrance **C** narrow tunnel to the deepest part of the cave (red arrow) **D, E** areas where *A. pandus* sp. nov. specimens were collected **F** live male of *A. pandus* sp. nov. in its natural environment.

with 14 setae arranged 4: 4: 2: 2: 2, preocular setae absent, most setae heavy, long, and gently curved. Chaetotaxy of coxae: P 3, I 4, II 4–6, III 5, IV 5; manducatory process with two acuminate distal setae, anterior seta less than 1/3 length of medial seta; coxal spines present on coxa I only, consisting of a tubercle expanded terminally into a characteristic "spray" or "fan" of four elevated processes which extend apically, subequal in length (Figs 10A, 11C); bisetose intercoxal tubercle present between coxae III and IV (Fig. 10A). ***Chelicera*** (Figs 9C, 11B, E): large, approximately as long as carapace,

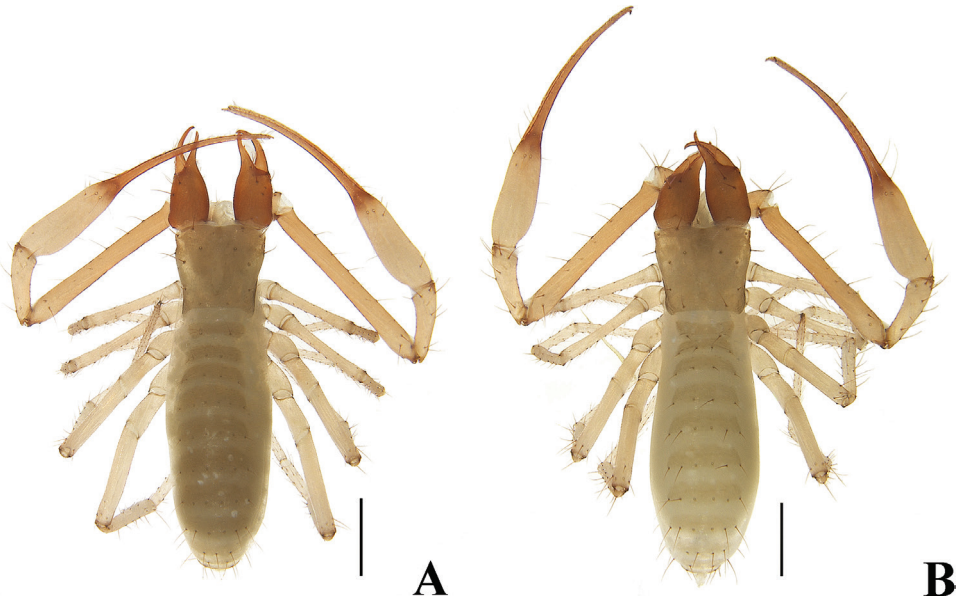

Figure 8. *Allochthonius pandus* sp. nov. **A** holotype male, habitus (dorsal view) **B** paratype female, habitus (dorsal view). Scale bars: 0.50 mm.

2.56–2.60× longer than broad; five setae and two lyrifissures (exterior condylar lyrifissure and exterior lyrifissure) present on hand, all setae acuminate, ventrobasal seta shorter than others; movable finger with a medial seta. Cheliceral palm with moderate hispid granulation on both ventral and dorsal sides. Both fingers well provided with teeth, fixed finger with ten acute teeth, distal one largest; movable finger with 15 or 16 retrorse contiguous teeth of equal length, plus four or five vestigial, rounded, and contiguous basal teeth, 19–21 in total; galea absent. Serrula exterior with 19 or 20 blades and serrula interior with 10 or 11 blades. Rallum in two rows and composed of nine blades with fine pinnate, of which the basal-most blade shorter than the others (Fig. 11E). ***Pedipalp*** (Figs 9A, 11D, 12A, B): long and slender, trochanter 1.65–1.67, femur 9.07–10.15, patella 3.47–3.57, chela 7.00–7.52, hand 2.60–2.96× longer than broad; femur 2.44–2.64× longer than patella; movable chelal finger 1.59–1.72× longer than hand and 0.62–0.64× longer than chela. Setae generally long and acuminate; one distal lyrifissure present on patella (Fig. 11D). Chelal palm slightly constricted towards fingers. Fixed chelal finger and hand with eight trichobothria, movable chelal finger with four trichobothria, *ib*, *isb*, *eb*, *esb*, and *ist* clustered at the base of fixed finger, *esb* slightly distal to *ist*; *it* slightly distal to *est*, situated subdistally; *et* situated subdistally, very close to chelal teeth; *dx* situated distal to *et*, near the tip of fixed finger; *sb* situated closer to *b* than to *st* (Fig. 12A). Microsetae (chemosensory setae) absent on hand and both palpal fingers. Sensilla absent. Both chelal fingers with a row of teeth, homodentate, spaced regularly along the margin, larger and well-spaced teeth present in the middle of the row, becoming smaller and closer distally and proximally:

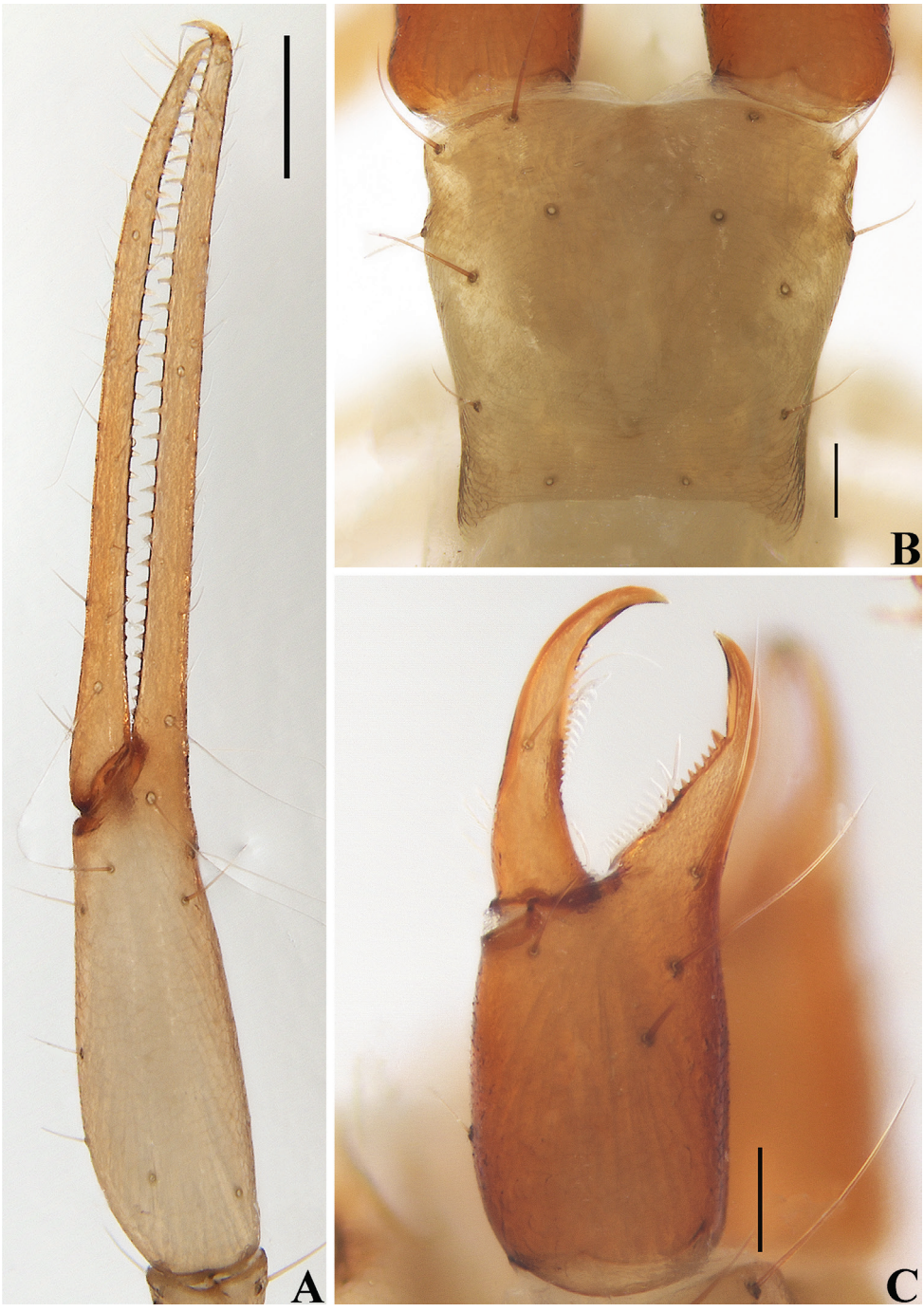

Figure 9. *Allochthonius pandus* sp. nov., holotype male **A** left chela (lateral view) **B** carapace (dorsal view) **C** left chelicera (dorsal view). Scale bars: 0.20 mm (**A**); 0.10 mm (**B, C**).

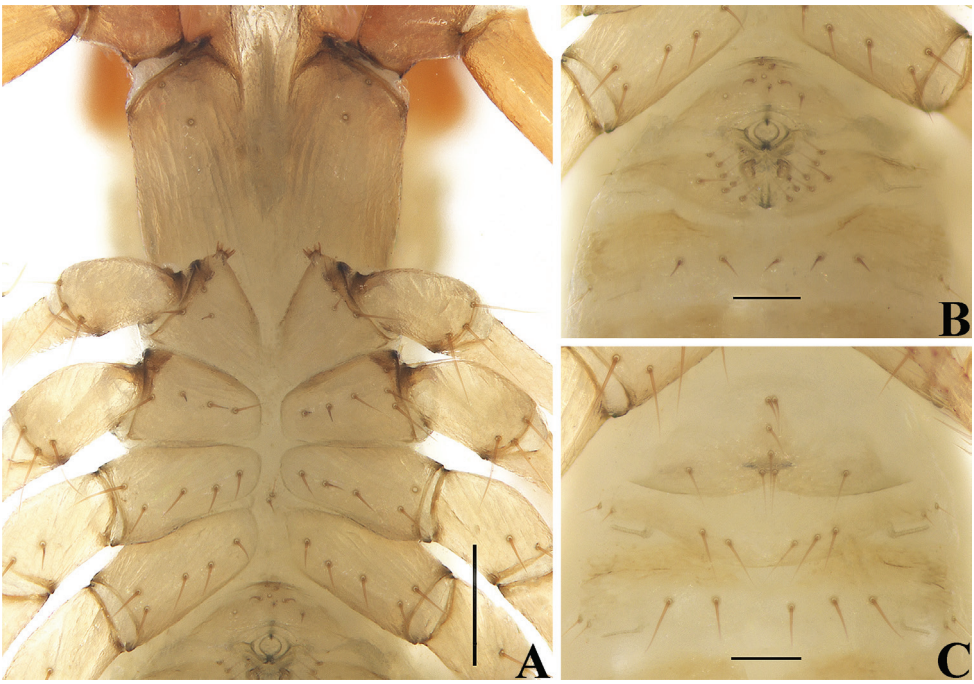

Figure 10. *Allochthonius pandus* sp. nov., holotype male (**A, B**), paratype female (**C**) **A** coxae (ventral view) **B** male genital area (ventral view) **C** female genital area (ventral view). Scale bars: 0.20 mm (**A**); 0.10 mm (**B, C**).

fixed chelal finger with 31 or 33 teeth, slightly retrorse and pointed; movable chelal finger with 24 or 25 teeth (slightly smaller than teeth on fixed chelal finger), plus two or three vestigial, rounded and contiguous basal teeth, 26–28 in total; a small tubercle between the fourteenth and fifteenth teeth present (Fig. 12A). Chelal fingers markedly curved in dorsal view (Fig. 12B). ***Opisthosoma*:** generally typical, pleural membrane finely granulated. Tergites and sternites undivided; setae uniseriate and acuminate. Tergal chaetotaxy I–XII: 2: 4–5: 4–5: 6: 6: 6: 6: 6: 3: 2: TT: 0, tergite IX with an unpaired median seta. Sternal chaetotaxy III–XII: 6–8: 9–10: 9–11: 9: 9–10: 9–10: 7–8: 5–6: 0: 2. Anterior genital operculum with eight setae, genital opening pit-like, with five or six marginal setae on each side, 18–19 in total, with a pair of lyrifissures present anterolateral and posteriolateral to genital opening, respectively (Fig. 10B). ***Legs*** (Fig. 12C, D): generally typical, long, and slender. Fine granulation present on anterodorsal faces of femur IV and patella IV. Femur of leg I 1.64–1.79× longer than patella and with one lyrifissure at the base of femur; tarsus 2.42–2.60× longer than tibia. Femoropatella of leg IV 5.00–5.17× longer than deep and with one lyrifissure at the base of femur; tibia 6.55–7.30× longer than deep; with a long tactile seta on both tarsal segments: basitarsus 4.00–4.86× longer than deep (TS = 0.21–0.25), telotarsus 13.50–14.50× longer than deep and 2.38–2.72× longer than basitarsus (TS = 0.22–0.25).

Setae of leg I (trochanter to tibia) 2–3: 9–11: 9–10: 12–13, setae of leg IV (trochanter to basitarsus) 2–3: 2: 4–5: 17–19: 10–11. Arolium slightly shorter than the claws, not divided; claws simple. ***Dimensions of adult males*** (length/breadth or, in the case of the legs, length/depth in mm): body length 1.97–2.23. Pedipalps: trochanter 0.28–0.30/0.17–0.18, femur 1.27–1.32/0.13–0.14, patella 0.50–0.52/0.14–0.15, chela 1.73–1.75/0.23–0.25, hand 0.65–0.68/0.23–0.25, movable chelal finger length 1.08–1.12. Chelicera 0.64–0.65/0.25, movable finger length 0.33–0.34. Carapace 0.53–0.54/0.58. Leg I: trochanter 0.20–0.21/0.15, femur 0.68–0.69/0.08–0.09, patella 0.38–0.42/0.08, tibia 0.30–0.31/0.05–0.06, tarsus 0.75–0.78/0.05–0.06. Leg IV: trochanter 0.29–0.30/0.16–0.17, femoropatella 0.93–0.95/0.18–0.19, tibia 0.72–0.73/0.10–0.11, basitarsus 0.32–0.34/0.07–0.08, telotarsus 0.81–0.87/0.06.

Adult females (Figs 8B, 10C). Mostly same as males, but a little larger; chaetotaxy of coxae: P 3, I 4, II 5, III 5, IV 5; tergal chaetotaxy I–XII: 2: 4: 4: 4–6: 6: 6: 6: 6: 4: 2: TT: 0; sternal chaetotaxy IV–XII: 9–10: 10–12: 9: 10–11: 10–12: 7–8: 6: 0: 2; anterior genital operculum with eight or nine setae, posterior margin with nine or ten marginal setae, 17–19 in total; leg IV with a long tactile seta on both tarsal segments: basitarsus 3.78× longer than deep (TS = 0.24), telotarsus 12.86–14.50× longer than deep and 2.56–2.65× longer than basitarsus (TS = 0.20–0.23). Body length 2.10–2.41. Pedipalps: trochanter 0.33/0.19–0.20 (1.65–1.74×), femur 1.36–1.38/0.16 (8.50–8.63×), patella 0.54–0.55/0.18–0.19 (2.89–3.00×), chela 1.86/0.26–0.28 (6.64–7.15×), hand 0.72–0.75/0.26–0.28 (2.68–2.77×), movable chelal finger length 1.16. Chelicera 0.73–0.76/0.26–0.28 (2.71–2.81×), movable finger length 0.39. Carapace 0.55–0.57/0.65 (0.85–0.88×). Leg I: trochanter 0.19/0.17 (1.12×), femur 0.70–0.75/0.10–0.11 (6.82–7.00×), patella 0.43–0.44/0.09 (4.78–4.89×), tibia 0.33–0.35/0.06 (5.50–5.83×), tarsus 0.79–0.84/0.06 (13.17–14.00×). Leg IV: trochanter 0.32–0.34/0.16–0.18 (1.89–2.00×), femoropatella 0.92–1.02/0.19–0.22 (4.64–4.84×), tibia 0.67–0.73/0.10–0.11 (6.64–6.70×), basitarsus 0.34/0.09 (3.78×), telotarsus 0.87–0.90/0.06–0.07 (12.86–14.50×).

Remarks. *Allochthonius pandus* sp. nov. is similar to *A. xinqiaoensis* sp. nov. in having a pair of distinctly curved chelal fingers and the same chaetotaxy of the carapace (4: 4: 2: 2: 2), but differs by the presence of lower number of blades of coxal spines (4 vs. 6), more rallum blades (9 vs. 8), more slender chela (chela 6.64–7.15 (♀) × vs. 5.44 (♀) × longer than broad), lower number of setae on the coxae (3: 4: 5: 5: 5 vs. 3: 6: 7–9: 5: 5) and more teeth on the chelal fingers (31–33 vs. 23 teeth on the fixed chelal finger and 26–28 vs. 23 teeth on the movable chelal finger); *Allochthonius pandus* sp. nov. can be distinguished from *A. bainiensis* sp. nov. by the presence of a pair of distinctly curved chelal fingers.

Allochthonius pandus sp. nov. differs from *A. brevitus* and *A. yoshizawai* in the number of setae on the anterior of the carapace (4 vs. 6), the cheliceral hand (5 vs. 6) and tergite II (4–5 vs. 6 or 2), and the number of rallum blades (9 vs. 11) and the presence of more slender pedipalps (e.g., palpal femur 9.07–10.15 (♂) × longer than broad in *A. pandus* sp. nov., while 4.33–4.73 (♂) and 6.50 (♂) × in *A. brevitus* and *A. yoshizawai*, respectively).

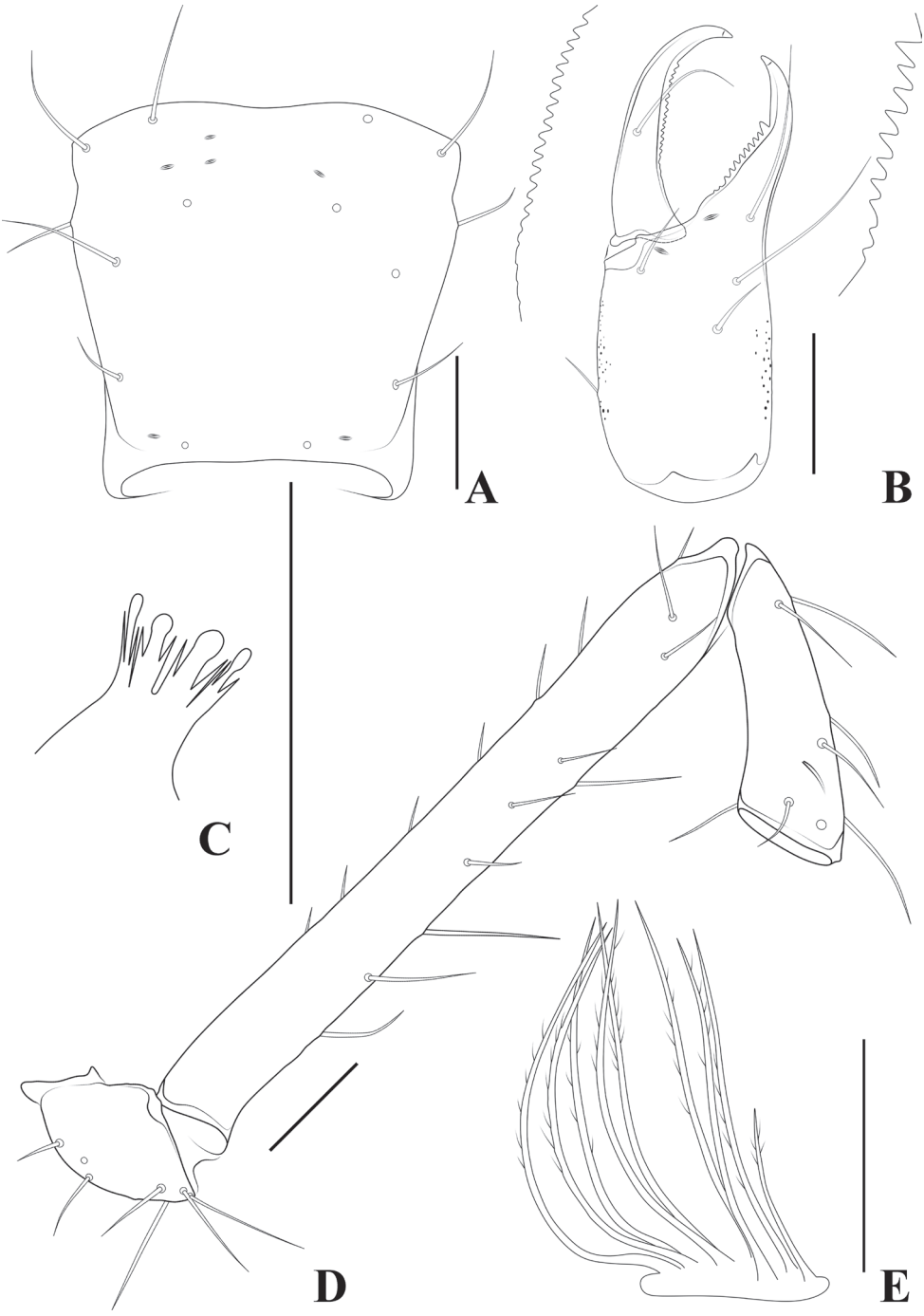

Figure 11. *Allochthonius pandus* sp. nov., holotype male **A** carapace (dorsal view) **B** left chelicera (dorsal view), with details of teeth **C** coxal spines on coxae I (ventral view) **D** left pedipalp (minus chela, dorsal view) **E** rallum. Scale bars: 0.20 mm (**A, B, D**); 0.10 mm (**C, E**).

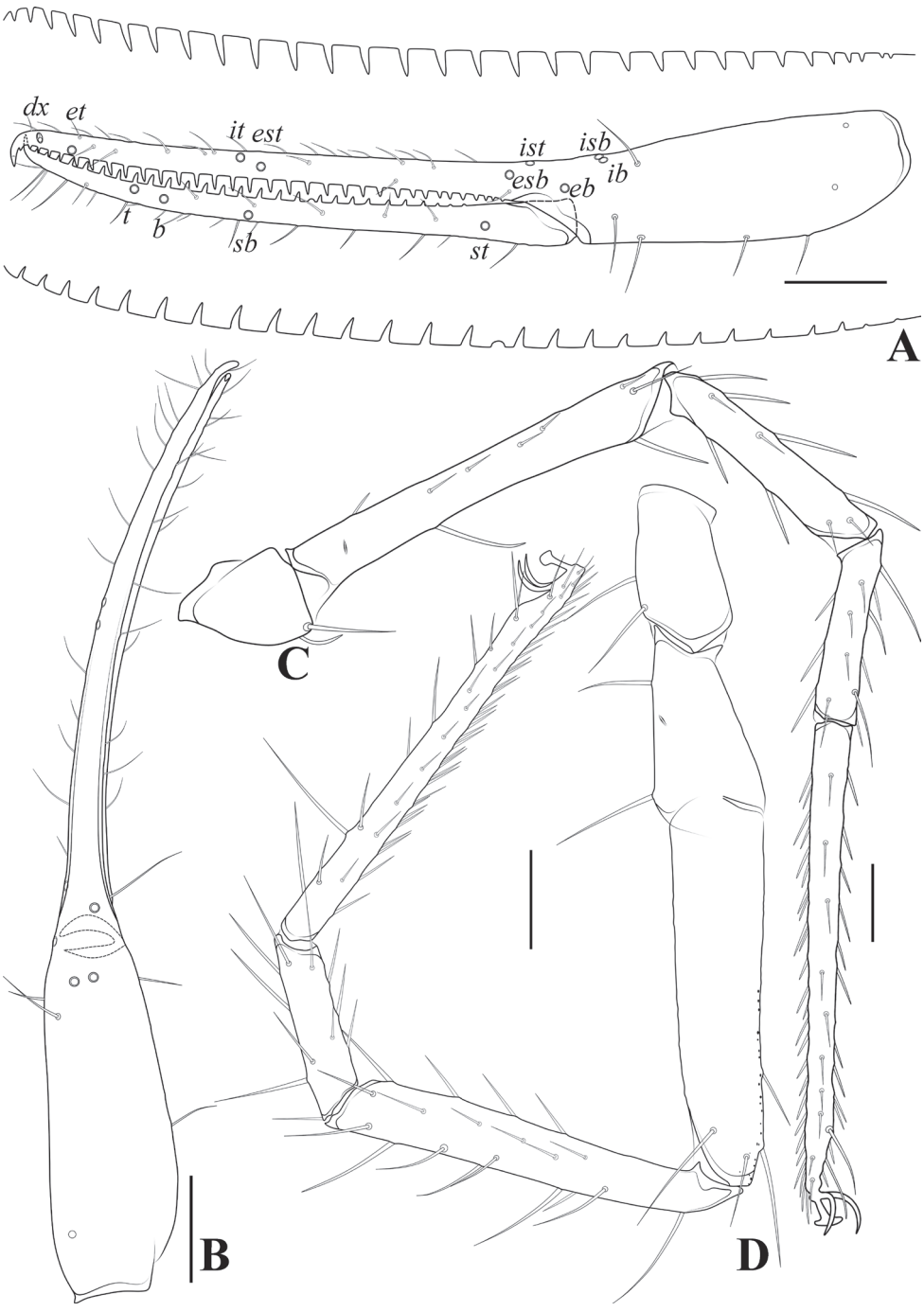

Figure 12. *Allochthonius pandus* sp. nov., holotype male **A** left chela (lateral view), with details of teeth and trichobothrial pattern **B** left chela (dorsal view) **C** leg I (lateral view) **D** leg IV (lateral view). Scale bars: 0.20 mm.

Allochthonius pandus sp. nov. can be distinguished from *A. ishikawai* and all *A. ishikawai* subspecies by the number of setae on the carapace (14 vs. 16 or more), the presence of lower number of rallum blades (9 vs. 10) and more teeth on both chelal fingers (26–28 vs. 11–17 teeth on the movable finger and 31–33 vs. 9–17 teeth on the fixed chelal finger).

Allochthonius pandus sp. nov. can be distinguished from the other species of *Allochthonius* by the absence of any traces of eyes (Morikawa 1954, 1956, 1960; Hu and Zhang 2012; Viana and Ferreira 2021; WPC 2022).

Distribution and habitat. This species is only known from the type locality, Daozuo Cave (Figs 1C, 7), which is located near a road, 1 km southwest of Jinshan Village (Xishui County) and is surrounded by rural and agricultural fields. This limestone cave has a large, rectangular entrance (~ 1 m high and 30 m wide) and a total length of ~ 300 m, only a narrow tunnel leads to the deepest part of the cave, which is a slightly wider, low-temperature, high-humidity, and completely lightless environment (temperature ~ 11 °C, humidity > 90%). All specimens were collected under stones in the deepest part of the cave.

***Allochthonius xinqiaoensis* sp. nov.**

https://zoobank.org/F4287D1F-ADBF-47DE-B878-E238375710CD

Figs 1D, 13–17

Chinese name 新桥异伪蝎

Type material. ***Holotype*:** China • ♀; Guizhou Province, Fenggang County, Heba Town, Xinqiao Village, Sanjie Cave; 27°54.23'N, 107°47.80'E; 828 m a.s.l.; 26 Jul. 2019; Zegang Feng, Zhaoyi Li and Chen Zhang leg.; under a stone in the deep zone; Ps.-MHBU-GZC190726 (Figs 1D, 13).

Diagnosis (♀). The new species can be recognized by the following combination of characters: each cheliceral finger with several small basal teeth between large teeth, most of which appear in pairs, the fingertips blunt, not sharp; rallum with eight blades (each with fine pinnate, the basal-most blade shorter than the others); pedipalps slender, femur 9.71, chela 5.44× longer than broad, both chelal fingers with a row of teeth (each chelal finger with 23 teeth), slightly retrorse and pointed.

Etymology. Named after the village of Xinqiao, near the type locality.

Description. Adult female (male unknown) (Figs 14–17). ***Color*** (Figs 14, 15): generally pale yellow, chelicerae, pedipalps and tergites slightly darker, soft parts pale. ***Cephalothorax*** (Figs 15B, D, 16A, C): carapace inverted trapezoid, 1.00× longer than broad, gently narrowed posteriorly; surface smooth, without furrows but with seven lyrifissures and the posterior part with squamous sculpturing; no traces of eyes; epistomal process absent, space between median setae slightly recurved; with 14 setae arranged 4: 4: 2: 2: 2, preocular setae absent, most setae heavy, long and gently curved. Chaetotaxy of coxae: P 3, I 6, II 7–9, III 5, IV 5; manducatory process with two acuminate distal setae, anterior seta less

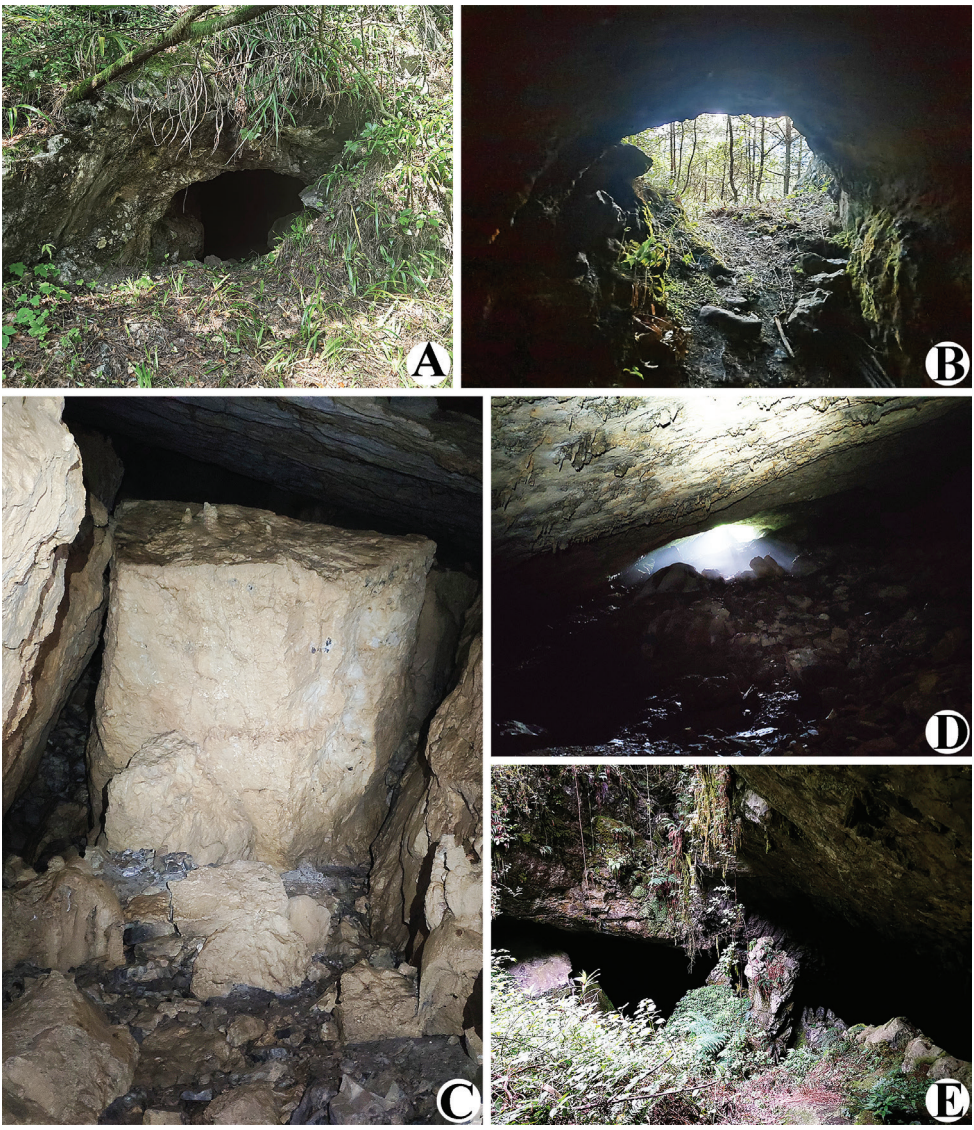

Figure 13. Sanjie Cave, type locality of *Allochthonius xinqiaoensis* sp. nov. **A** entrance **B** inside the cave entrance **C** area where *A. xinqiaoensis* sp. nov. specimen was collected **D, E** exit.

than 1/2 length of medial seta; coxal spines present on coxa I only, consisting of a tubercle expanded terminally into a characteristic "spray" or "fan" of six elevated processes which extend apically, subequal in length (Figs 15D, 16C); bisetose intercoxal tubercle present between coxae III and IV (Fig. 15D). ***Chelicera*** (Figs 15C, 16B, E): large, approximately as long as carapace, 2.38× longer than broad; five setae present on hand, all setae acuminate, ventrobasal seta shorter than others; movable finger with a medial seta; exterior condylar lyrifissure and exterior lyrifissure exist, palm with five extra (surrounding an accessory

Figure 14. *Allochthonius xinqiaoensis* sp. nov., holotype female, habitus (minus left chelicera, pedipalp, legs I and IV, dorsal view). Scale bar: 0.50 mm.

seta). Cheliceral palm with moderate hispid granulation on both ventral and dorsal sides. Both fingers well provided with teeth, fixed finger with nine acute teeth, distal one largest; movable finger with a slight bump apical tooth and 12 retrorse contiguous teeth of equal length, each finger with several small basal teeth between large teeth, most of which appear in pairs, four on movable finger and six on fixed finger; the fingertips blunt, not sharp; galea represented by a very slight bump on movable finger. Serrula exterior with 17 blades and serrula interior with ten blades. Rallum in two rows and composed of eight blades with fine pinnate, of which the basal-most blade shorter than the others (Fig. 16E). ***Pedipalp*** (Figs 15A, 16D, 17A, B): long and slender, trochanter 1.63, femur 9.71, patella 2.83, chela 5.44, hand 2.25× longer than broad; femur 2.67× longer than patella; movable chelal finger 1.44× longer than hand and 0.60× longer than chela. Setae generally long and acuminate; two distal lyrifissures present on patella, femur with one (Fig. 16D). Chelal palm robust

and slightly constricted towards fingers. Fixed chelal finger and hand with eight trichobothria, movable chelal finger with four trichobothria, *ib*, *isb*, *eb*, *esb*, and *ist* clustered at the base of fixed finger, *ist* slightly distal to *esb*; *it* slightly distal to *est*, situated subdistally; *et* situated subdistally, very close to chelal teeth; *dx* situated distal to *et*, near the tip of fixed finger; *sb* situated closer to *b* than to *st* (Fig. 17A). Microsetae (chemosensory setae) absent on hand and both palpal fingers. Sensilla absent. Both chelal fingers with a row of teeth, homodentate, spaced regularly along the margin, larger and well-spaced teeth present in the middle of the row, becoming smaller and closer distally and proximally: fixed chelal finger with 23 teeth, slightly retrorse and pointed; movable chelal finger with 23 teeth (slightly smaller than teeth on fixed chelal finger) and a tubercle between the eleventh and twelfth teeth (Fig. 17A). Chelal fingers markedly curved in dorsal view (Fig. 17B). ***Opisthosoma*:** generally typical, pleural membrane finely granulated. Tergites and sternites undivided; setae uniseriate and acuminate. Tergal chaetotaxy I–XII: 3: 4: 4: 6: 6: 6: 6: 7: 5: 4: TT: 0; tergites VIII and IX each with an unpaired median seta; a lyrifissure on each side of tergites I–IX. Sternal chaetotaxy IV–XII: 9: 12: 11: 12: 12: 9: 8: 0: 2. Anterior genital operculum with six setae plus 12 setae on posterior margin, with a pair of lyrifissures present anterolateral and posteriolateral to genital opening, respectively (Fig. 15E). ***Legs*** (Fig. 17C, D): generally typical, long, and slender. Fine granulation present on anterodorsal faces of femur IV and patella IV. Femur of leg I 1.61× longer than patella and with one lyrifissure at the base of femur; tarsus 2.24× longer than tibia. Femoropatella of leg IV 4.74× longer than deep and with one lyrifissure at the base of femur; tibia 6.58× longer than deep; with basal tactile setae on both tarsal segments: basitarsus 4.44× longer than deep (TS = 0.28), telotarsus 14.29× longer than deep and 2.50× longer than basitarsus (TS = 0.20). Setae of leg I (trochanter to tibia) 2: 12: 11: 19, setae of leg IV (trochanter to basitarsus) 3: 2: 6: 24: 14. Arolium slightly shorter than the claws, not divided; claws simple. ***Dimensions of female holotype*** (length/breadth or, in the case of the legs, length/depth in mm): body length 2.01. Pedipalps: trochanter 0.31/0.19, femur 1.36/0.14, patella 0.51/0.18, chela 1.74/0.32, hand 0.72/0.32, movable finger length 1.04. Chelicera 0.57/0.24, movable finger length 0.32. Carapace 0.55/0.55. Leg I: trochanter 0.22/0.17, femur 0.79/0.10, patella 0.49/0.09, tibia 0.38/0.07, tarsus 0.85/0.06. Leg IV: trochanter 0.34/0.19, femoropatella 1.09/0.23, tibia 0.79/0.12, basitarsus 0.40/0.09, telotarsus 1.00/0.07.

Remarks. *Allochthonius xinqiaoensis* sp. nov. is similar to *A. ishikawai shiragatakiensis* Morikawa, 1954 in having a pair of distinctly curved chelal fingers, but differs by the presence of lower number of rallum blades (8 vs. 10), larger body size (body length 2.01 vs. 1.75 mm) and more chelal fingers teeth (23 vs. 9 on the fixed chelal finger and 23 vs. 11 on the movable chelal finger).

Allochthonius xinqiaoensis sp. nov. can be distinguished from *A. pandus* sp. nov. by the presence of more blades of coxal spines (6 vs. 4), lower number of rallum blades (8 vs. 9), thicker chela (chela 5.44 (♀) × vs. 6.64–7.15 (♀) × longer than broad), more setae on the coxae (3: 6: 7–9: 5: 5 vs. 3: 4: 5: 5: 5) and lower number of teeth on the chelal fingers (23 vs. 31–33 teeth on the fixed chelal finger and 23 vs. 26–28 teeth on the movable chelal finger); *Allochthonius xinqiaoensis* sp. nov. can be distinguished from *A. bainiensis* sp. nov. by the presence a pair of distinctly curved chelal fingers.

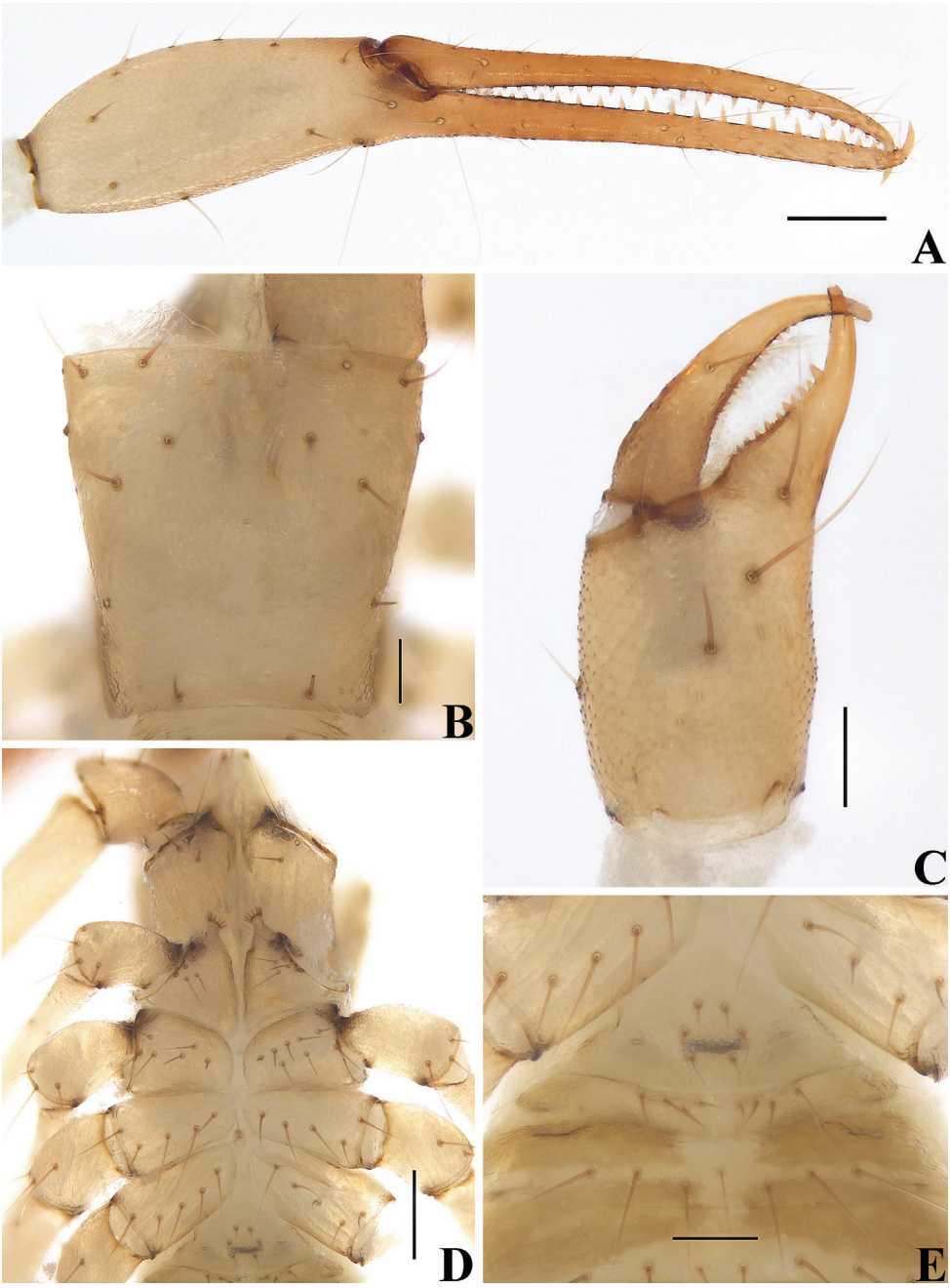

Figure 15. *Allochthonius xinqiaoensis* sp. nov., holotype female **A** left chela (lateral view) **B** carapace (dorsal view) **C** left chelicera (dorsal view) **D** coxae (ventral view) **E** female genital area (ventral view). Scale bars: 0.20 mm (**A, D**); 0.10 mm (**B, C, E**).

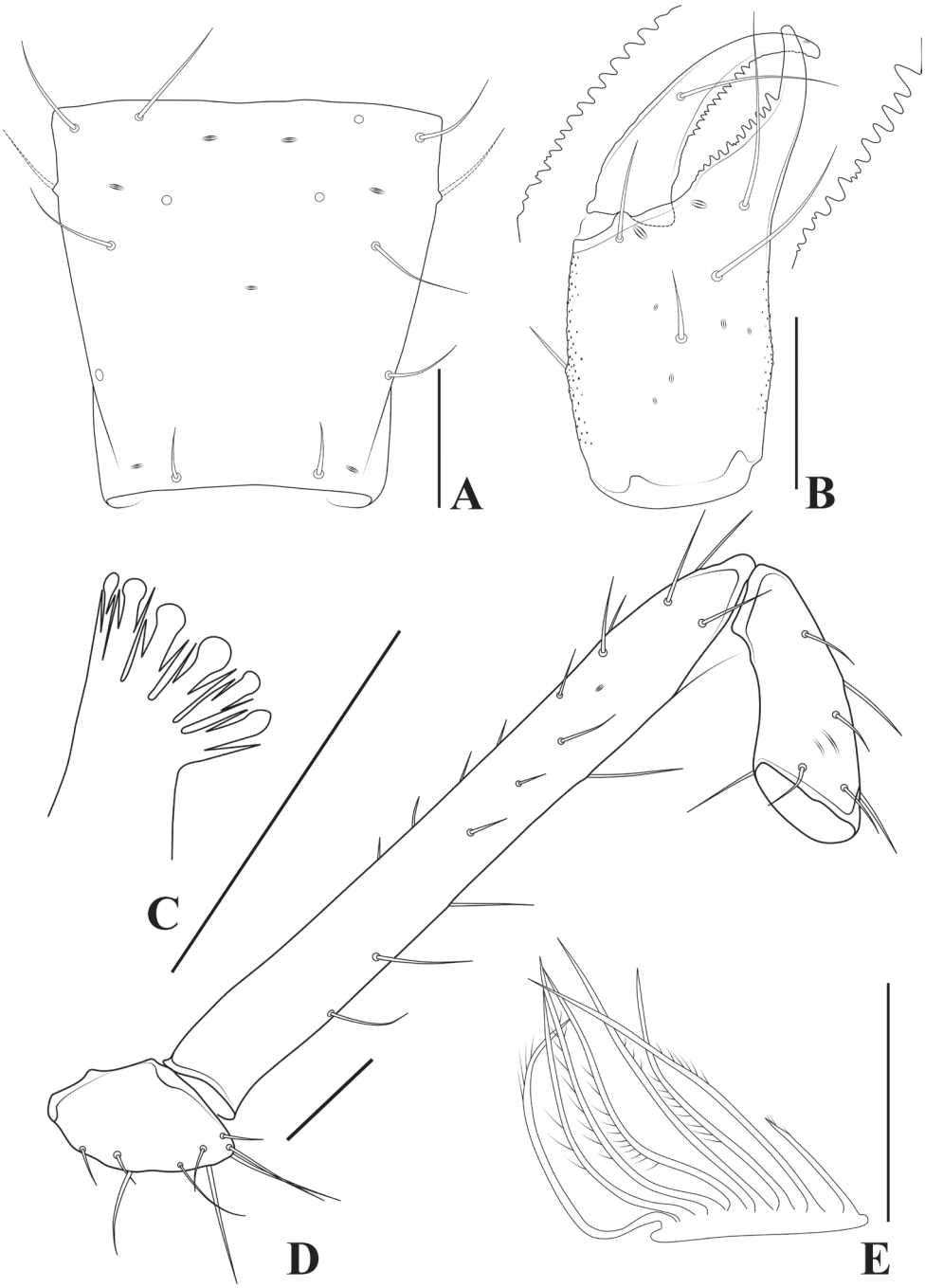

Figure 16. *Allochthonius xinqiaoensis* sp. nov., holotype female **A** carapace (dorsal view), two broken ocular row setae are shown as dashed lines **B** left chelicera (dorsal view), with details of teeth **C** coxal spines on coxae I (ventral view) **D** left pedipalp (minus chela, dorsal view) **E** rallum. Scale bars: 0.20 mm (**A, B, D**); 0.10 mm (**C, E**).

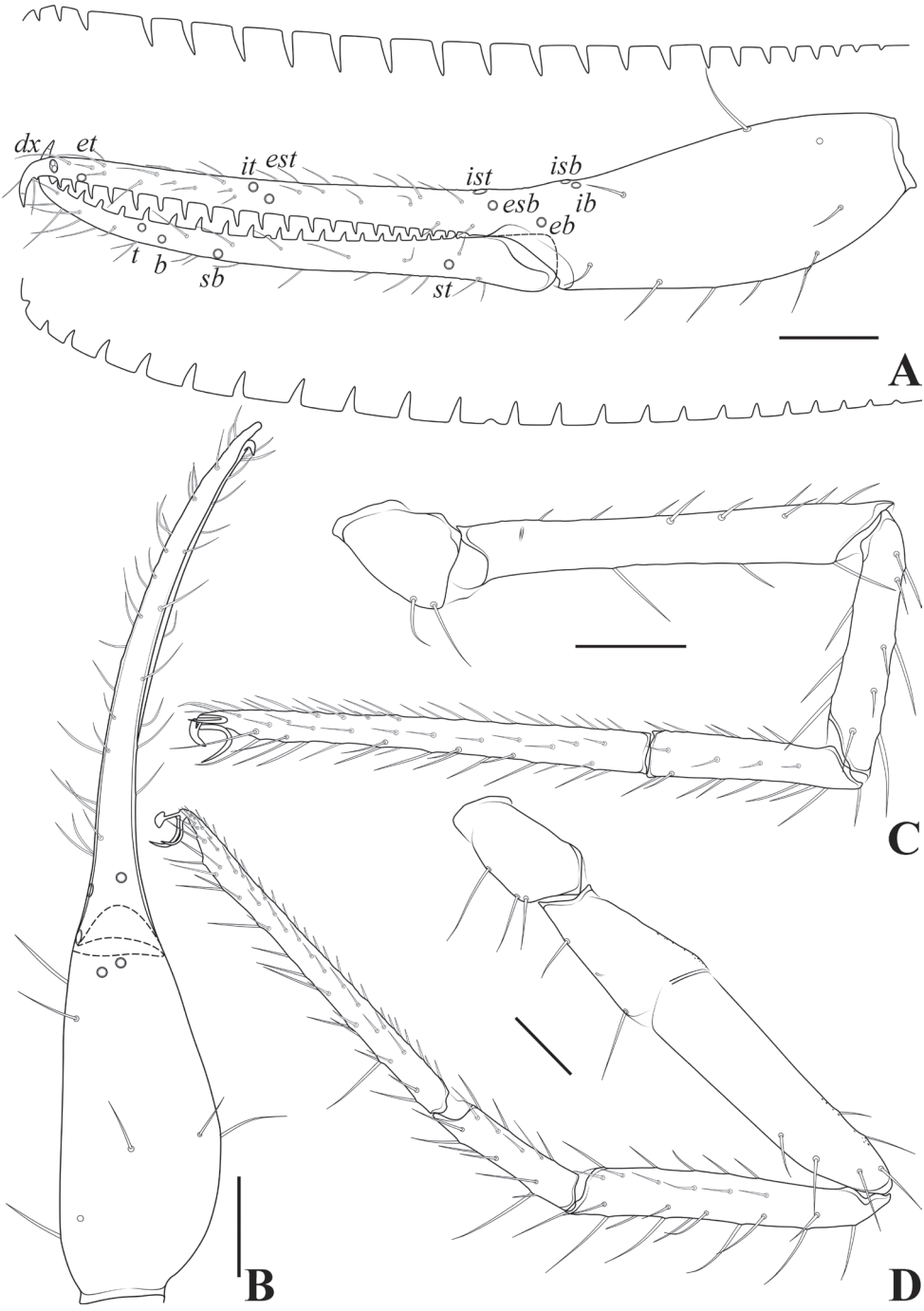

Figure 17. *Allochthonius xinqiaoensis* sp. nov., holotype female **A** left chela (lateral view), with details of teeth and trichobothrial pattern **B** left chela (dorsal view) **C** leg I (lateral view) **D** leg IV (lateral view). Scale bars: 0.20 mm.

Allochthonius xinqiaoensis sp. nov. differs from *A. brevitus* and *A. yoshizawai* in the number of setae on the anterior of the carapace (4 vs. 6) and the cheliceral hand (5 vs. 6), and the number of rallum blades (8 vs. 11).

Allochthonius xinqiaoensis sp. nov. can be distinguished from *A. ishikawai* and all the other *A. ishikawai* subspecies by the number of setae on the carapace (14 vs. 16 or more), the presence of lower number of rallum blades (8 vs. 10) and more teeth on both chelal fingers (23 vs. 11–17 teeth on the movable chelal finger and 23 vs. 9–17 teeth on the fixed chelal finger).

Allochthonius xinqiaoensis sp. nov. can be distinguished from the other species of *Allochthonius* by the absence of any traces of eyes (Morikawa 1954, 1956, 1960; Hu and Zhang 2012; Viana and Ferreira 2021; WPC 2022).

Distribution and habitat. This species is only known from the type locality, Sanjie Cave (Figs 1D, 13), which is located ~ 1.8 km northeast of Xinqiao Village (Fenggang County). This limestone cave has a small oval entrance (~ 1 m high and 2 m wide), ~ 200 meters in length, with a large, elongated exit at the end of the cave (~ 5 m high and 50 m wide). The interior entirety of the cave is large, inclined and extending downwards. The cave ground was covered with stones. The specimen was collected under a stone ~ 100 m from the cave entrance.

Genus *Spelaeochthonius* Morikawa, 1954

Type species. *Spelaeochthonius kubotai* Morikawa, 1954, by original designation.

Spelaeochthonius wulibeiensis sp. nov.

https://zoobank.org/296D1EC6-9D37-43A4-B971-6330674C6711
Figs 1A, 18–23
Chinese name 五里碑穴伪蝎

Type material. ***Holotype*:** China • ♂; Guizhou Province, Weining County, Yancang Town, Yangguan Village, Wulibei Cave; 26°53.82'N, 104°19.36'E; 2425 m a.s.l.; 07 Aug. 2019; Zegang Feng, Zhaoyi Li and Chen Zhang leg.; under a stone in the deep zone; Ps.-MHBU-GZC19080701 (Figs 1A, 18). ***Paratypes*:** • 2♂; the same data as the holotype; Ps.-MHBU-GZC19080702-GZC19080703 • 1♀; the same location as the holotype; 19 May. 2017, Zhisheng Zhang, Huiming Chen and Luyu Wang leg.; Ps.-MSWU-CZCH-17-06.

Diagnosis (♂♀). The new species can be recognized by the following combination of characters: surfaces mostly with fine reticulations; carapace without eyes or eyespots but eye region bulging and convex in dorsal view; anterior margin without protuberances; cheliceral palm with five setae; rallum with 11 blades (each with fine pinnate, the basal-most blade shorter than the others); coxal spines present on coxa I only, comprising a transverse, contiguous series of seven or eight tridentate blades, which

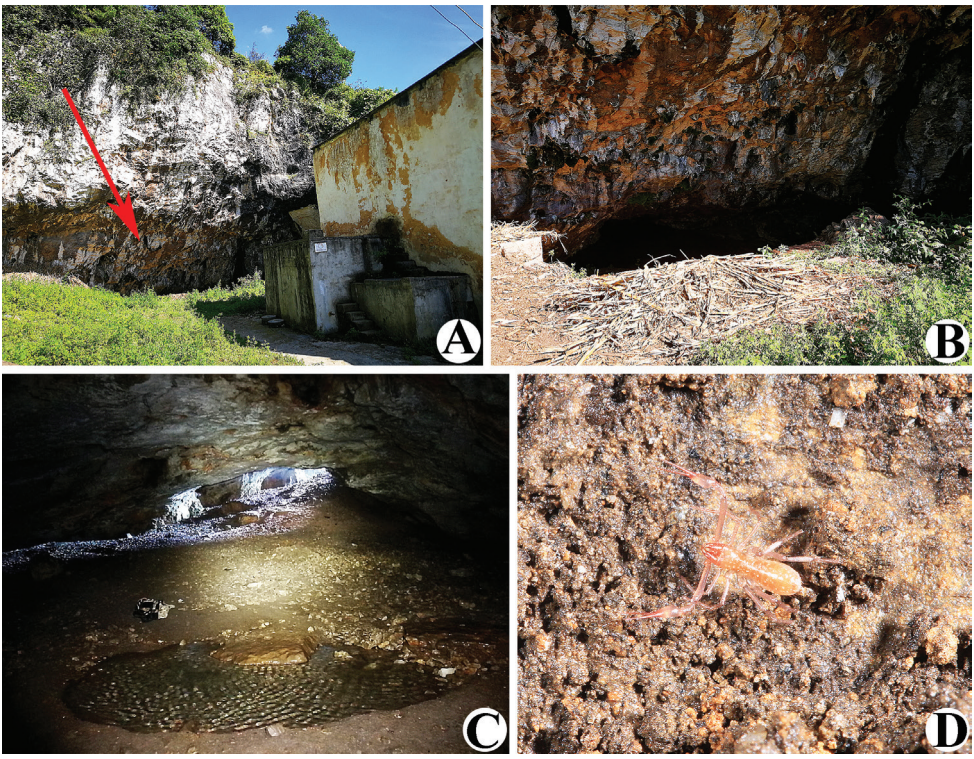

Figure 18. Wulibei Cave, type locality of *Spelaeochthonius wulibeiensis* sp. nov. **A** cave location (red arrow) **B** entrance **C** inside the cave entrance **D** live male of *S. wulibeiensis* sp. nov. in its natural environment.

arise from a lightly sclerotized or translucent hillock, the central ramus of each blade (except the basal two) sharply acumino-spatulate and extending beyond the lateral rami; pedipalps slender, femur 7.24 (♂), 6.40 (♀), chela 6.21–6.22 (♂), 5.68 (♀) × longer than broad, both chelal fingers with a row of teeth (fixed chelal finger with 22 or 24 teeth; movable chelal finger with 16–19 teeth), slightly retrorse and pointed; chela fingers straight in dorsal view.

Etymology. Named after the type locality, Wulibei Cave.

Description. Adult males (Figs 18D, 19A, 20, 21A, B, 22, 23). ***Color*** (Figs 18D, 19A, 20, 21A, B): generally pale yellow, chelicerae, pedipalps and tergites slightly darker, soft parts pale. ***Cephalothorax*** (Figs 20B, 21A, 22A, C): carapace subquadrate, 1.02–1.03× longer than broad, gently narrowed posteriorly; surface mostly with fine reticulations, without furrows but with seven or eight lyrifissures; no traces of eyes but eye region bulging and convex in dorsal view; epistome present and with some tiny spinules; with 16 setae arranged s4s: 4: 2: 2: 2, most setae heavy, long, and gently curved. Chaetotaxy of coxae: P 3, I 6–7, II 4–5, III 4, IV 4; manducatory process with two acuminate distal setae, anterior seta less than 1/2 length of medial seta; coxal spines present on coxa I only, comprising a transverse, contiguous series of seven or

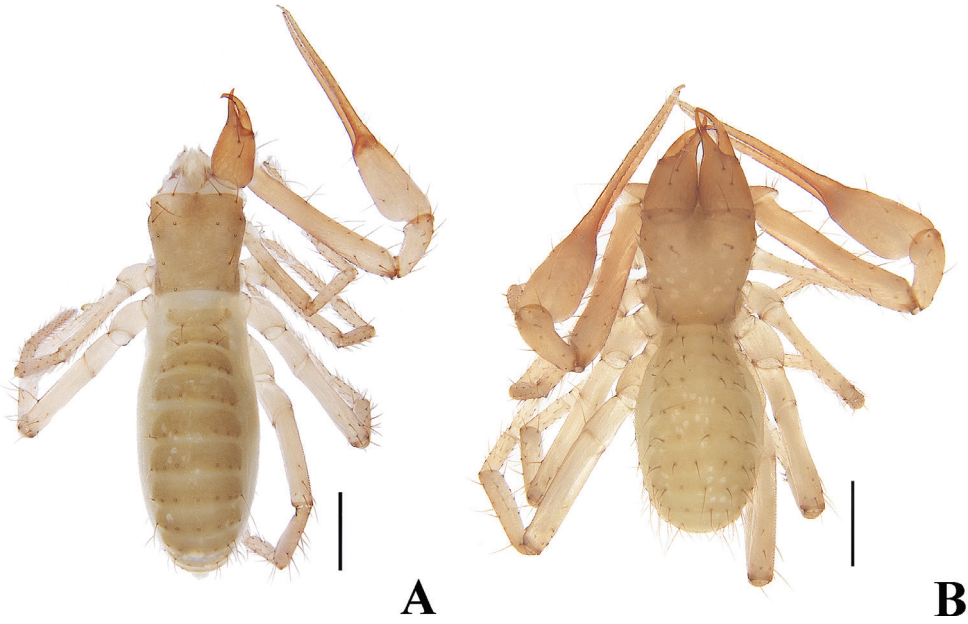

Figure 19. *Spelaeochthonius wulibeiensis* sp. nov. **A** holotype male, habitus (minus left chelicera, pedipalp, legs I and IV, dorsal view) **B** paratype female, habitus (dorsal view). Scale bars: 0.50 mm.

eight tridentate blades, which arise from a lightly sclerotized or translucent hillock, the central ramus of each blade (except the basal two) sharply acumino-spatulate and extending beyond the lateral rami (Figs 21A, 22C); bisetose intercoxal tubercle present between coxae III and IV, tear drop-shaped (Fig. 21A). ***Chelicera*** (Figs 20C, 22B, E): large, approximately as long as carapace, 2.37–2.41× longer than broad; five setae present on hand, movable finger with a medial seta, all setae acuminate, ventrobasal seta shorter than others; exterior condylar lyrifissure and exterior lyrifissure exist, palm with one extra (between sub-basal seta and an accessory seta). Cheliceral palm with moderate hispid granulation on both ventral and dorsal sides. Both fingers well provided with teeth, fixed finger with 13–15 acute teeth, distal one largest; movable finger with 12 retrorse contiguous teeth of equal length, plus three or four round proximal teeth, 15 or 16 in total; galea represented by a very slight bump on movable finger. Serrula exterior with 21 blades and serrula interior with 17–20 blades. Rallum in two rows and composed of 11 blades with fine pinnate, of which the basal-most blade shorter than the others (Fig. 22E). ***Pedipalp*** (Figs 20A, 22D, 23A, B): surfaces mostly with fine reticulations; long and slender, trochanter 1.78–2.00, femur 7.24, patella 2.44–2.47, chela 6.21–6.22, hand 2.26–2.36× longer than broad; femur 2.62–2.80× longer than patella; movable chelal finger 1.61–1.74× longer than hand and 0.61–0.63× longer than chela. Setae generally long and acuminate; one distal lyrifissure present on patella and femur, respectively (Fig. 22D). Chelal palm robust and slightly constricted

Figure 20. *Spelaeochthonius wulibeiensis* sp. nov., holotype male **A** left chela (lateral view) **B** carapace (dorsal view) **C** left chelicera (dorsal view). Scale bars: 0.20 mm (**A**); 0.10 mm (**B, C**).

towards fingers. Fixed chelal finger and hand with eight trichobothria, movable chelal finger with four trichobothria, *ib*, *isb*, *eb*, *esb*, and *ist* clustered at the base of fixed finger, *ist* slightly distal to *esb*, *esb* close to *ist* than to *eb*; *it* slightly distal to *est*, situated subdistally and forming a pair; *et* situated subdistally, very close to chelal teeth; *dx* situated distal to *et*, near the tip of fixed finger; *sb* distinctly closer to *b* than to *st* (Fig. 23A). Microsetae (chemosensory setae) absent on hand and both palpal fingers. Sensilla absent. Both chelal fingers with a row of teeth, homodentate, spaced regularly along the margin, larger and well-spaced teeth present in the middle of the row, becoming smaller and closer distally and proximally: fixed chelal finger with 22–24 teeth, slightly retrorse and pointed; movable chelal finger with 16–19 teeth (slightly smaller than teeth on fixed chelal finger); a small tubercle between the seventh and eighth teeth present (near trichobothrium *t*) (Fig. 23A). Chelal fingers straight in dorsal view (Fig. 23B). ***Opisthosoma*:** generally typical, ovate, pleural membrane finely granulated. Tergites and sternites undivided; setae uniseriate and acuminate. Tergal chaetotaxy I–XII: 2: 4: 6: 6: 6: 7–8: 8: 7: 6: 4: TT: 0, tergites VII–IX each with an unpaired median seta, one lyrifissure present on each side of tergites IV–IX. Sternal chaetotaxy III–XII: 6–9: 10–14: 13–14: 12: 12–13: 12–13: 10–11: 8–9: 0: 2, one lyrifissure present on each side of tergite III. Anterior genital operculum with 10–12 setae, genital opening pit-like, with seven marginal setae on each side, 24–26 in total, with a pair of lyrifissures present anterolateral and posteriolateral to genital opening, respectively (Fig. 21B). ***Legs*** (Fig. 23C, D): generally typical, long, and slender. Fine granulation present on anterodorsal faces of femur IV and patella IV. Femur of leg I 1.74× longer than patella and with one lyrifissure at the base of femur; tarsus 2.11–2.26× longer than tibia. Femoropatella of leg IV 3.70–3.88× longer than deep and with one lyrifissure at the base of femur; tibia 5.92–6.00× longer than deep; with a long tactile seta on both tarsal segments: basitarsus 4.00× longer than deep (TS = 0.22–0.28), telotarsus 11.13–12.43× longer than deep and 2.42–2.47× longer than basitarsus (TS = 0.26–0.27). Setae of leg I (trochanter to tibia) 1: 13: 12–15: 14–17, setae of leg IV (trochanter to basitarsus) 2: 2: 6: 16: 14. Arolium slightly shorter than the claws, not divided; claws simple. ***Dimensions of adult males*** (length/breadth or, in the case of the legs, length/depth in mm). Males: body length 2.50. Pedipalps: trochanter 0.32/0.16–0.18, femur 1.23/0.17, patella 0.44–0.47/0.18–0.19, chela 1.68–1.74/0.27–0.28, hand 0.61–0.66/0.27–0.28, movable finger length 1.06. Chelicera 0.64–0.65/0.27, movable finger length 0.34. Carapace 0.63/0.61–0.62. Leg I: trochanter 0.24–0.25/0.18, femur 0.73–0.75/0.10, patella 0.42–0.43/0.09, tibia 0.34–0.37/0.07, tarsus 0.77–0.78/0.06–0.07. Leg IV: trochanter 0.33–0.36/0.19–0.22, femoropatella 0.97–1.00/0.25–0.27, tibia 0.77–0.78/0.13, basitarsus 0.36/0.09, telotarsus 0.87–0.89/0.07–0.08.

Adult female (Figs 19B, 21C). Mostly same as males; tergal chaetotaxy I–XII: 2: 4: 6: 6: 6: 7: 8: 9: 7: 4: TT: 0; sternal chaetotaxy IV–XII: 10: 13: 11: 12: 12: 11: 8: 0: 2; anterior genital operculum with seven setae, posterior margin with 11 marginal setae, 18 in total; leg IV with a long tactile seta on both tarsal segments: basitarsus 3.60× longer than deep (TS = 0.25), telotarsus 11.63× longer than deep and 2.58× longer than basitarsus (TS = 0.24). Body length 1.93. Pedipalps: trochanter 0.32/0.19 (1.68×), femur

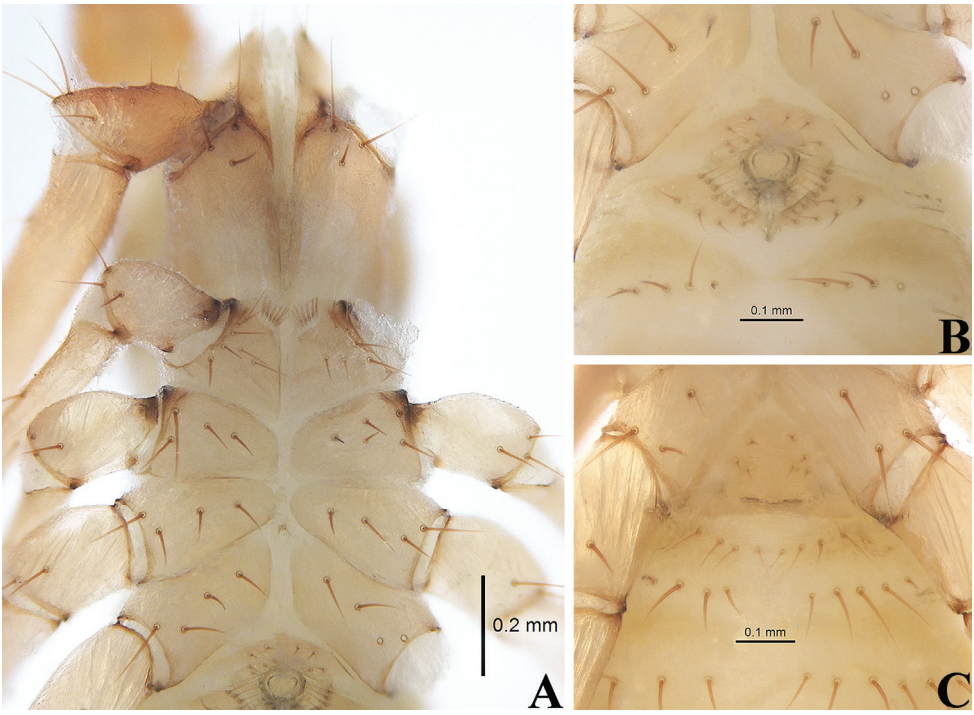

Figure 21. *Spelaeochthonius wulibeiensis* sp. nov., holotype male (**A, B**), paratype female (**C**) **A** coxae (ventral view) **B** male genital area (ventral view) **C** female genital area (ventral view). Scale bars: 0.20 mm (**A**); 0.10 mm (**B, C**).

1.28/0.20 (6.40×), patella 0.51/0.21 (2.43×), chela 1.76/0.31 (5.68×), hand 0.66/0.31 (2.13×), movable chelal finger length 1.11. Chelicera 0.70/0.30 (2.33×), movable finger length 0.38. Carapace 0.68/0.68 (1.00×). Leg I: trochanter 0.24/0.19 (1.26×), femur 0.77/0.12 (6.42×), patella 0.45/0.11 (4.09×), tibia 0.36/0.08 (4.50×), tarsus 0.83/0.08 (10.38×). Leg IV: trochanter 0.35/0.22 (1.59×), femoropatella 1.05/0.27 (3.89×), tibia 0.80/0.14 (5.71×), basitarsus 0.36/0.10 (3.60×), telotarsus 0.93/0.08 (11.63×).

Remarks. The new species shares similar characters with most species of *Centrochthonius* Beier, 1931, *Spelaeochthonius* and all species of "*Pseudotyrannochthonius*" Beier, 1930 from the western US by the presence of only 16 setae on the carapace. Schwarze et al. (2021) emphasized the importance of the number of carapaceal setae in Holarctic pseudotyrannochthoniids, thus, it indicates that the three "*Pseudotyrannochthonius*" species in the western US were misclassified in comparison with the twelve species from Australia and the three species from Chile (including the type species, the number of carapaceal setae is more than 18). It can be said that the genus *Pseudotyrannochthonius* is endemic to the southern hemisphere (Harvey and Harms 2022). Thus, it is inappropriate to place this new species in *Pseudotyrannochthonius*, even though the shape of this new species of coxal spines is similar to that of the three "*Pseudotyrannochthonius*" species.

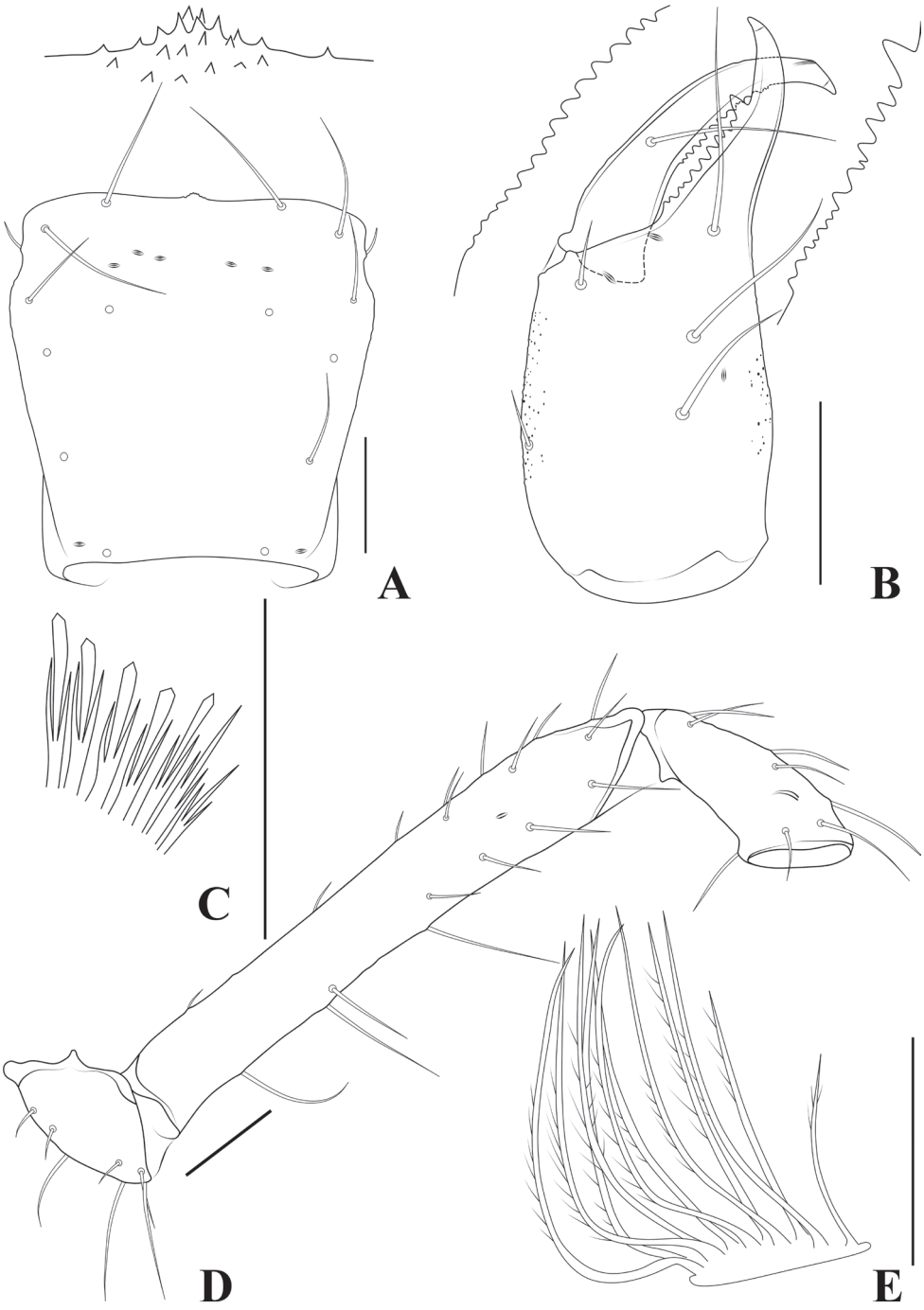

Figure 22. *Spelaeochthonius wulibeiensis* sp. nov., holotype male **A** carapace (dorsal view), with a detail of anterior margin **B** left chelicera (dorsal view), with details of teeth **C** coxal spines on coxae I (ventral view) **D** left pedipalp (minus chela, dorsal view) **E** rallum. Scale bars: 0.20 mm (**A, B, D**); 0.10 mm (**C, E**).

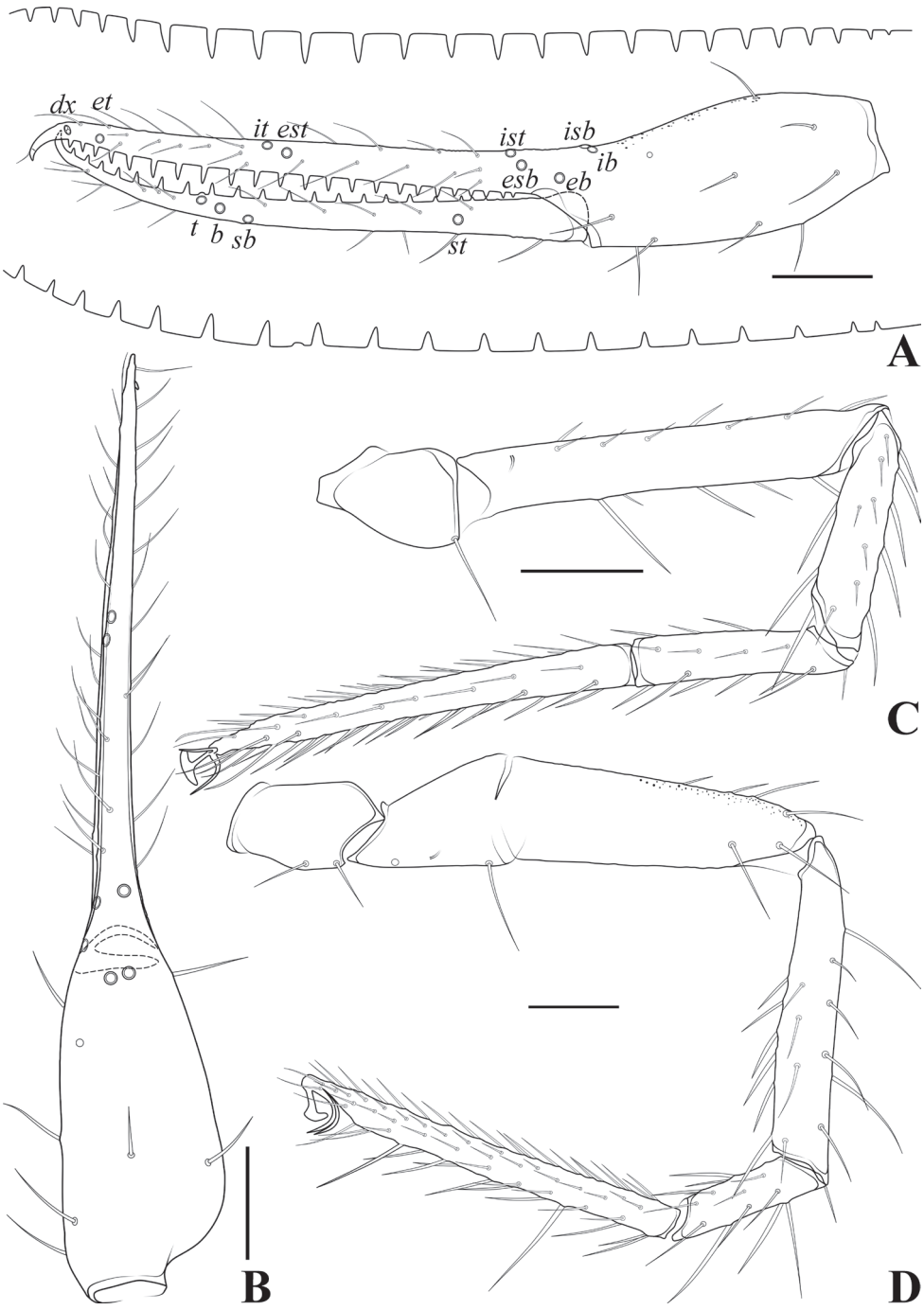

Figure 23. *Spelaeochthonius wulibeiensis* sp. nov., holotype male **A** left chela (lateral view), with details of teeth and trichobothrial pattern **B** left chela (dorsal view) **C** leg I (lateral view) **D** leg IV (lateral view). Scale bars: 0.20 mm.

The shape and number of the coxal spines are important distinguishing features between *Centrochthonius* and *Spelaeochthonius* (You et al. 2022). In our opinion, it is appropriate to place this new species to *Spelaeochthonius* rather than *Centrochthonius*, the reasons are as follows: for *Centrochthonius*, the number of carapaceal setae is not fixed (e.g., occasionally 18 are present in *C. anatonus* Harvey & Harms, 2022) and only four or five coxal spines blades; for *Spelaeochthonius*, the character of coxal spines is diverse (e.g., in *S. undecimclavatus* Morikawa, 1956, which is club-shaped, not distally plumose).

Spelaeochthonius wulibeiensis sp. nov. is similar to *S. cheonsooi* You, Yoo, Harvey & Harms, 2022, but differs by the number of setae on tergite I (2 vs. 4) and larger body size (body length 1.93 (♀) mm vs. 1.70 (♀) mm; chela 5.68 (♀) × vs. 5.32 (♀) × longer than board, length 1.76 (♀) mm vs. 1.49 (♀) mm).

Spelaeochthonius wulibeiensis sp. nov. can be distinguished from *S. seungsookae* You, Yoo, Harvey & Harms, 2022 by the number of setae on tergite I (2 vs. 4) and smaller body size (body length 1.93 (♀) mm vs. 2.05–2.36 (♀) mm; chela length 1.68–1.74 (♂), 1.76 (♀) mm vs. 1.90 (♂), 1.92 (♀) mm); from *S. undecimclavatus* and *S. dorogawaensis* by the number of setae on chelicera (6 vs. 7), a slender palp (palpal femur 7.24 (♂) × vs. 4.80–5.40 (♂) × longer than board; chela 6.21–6.22 (♂) × vs. 5.50–6.13 (♂) × longer than board) and lower number of blades of coxal spines (7–8 vs. 10–11); from *S. akiyoshiensis* Morikawa, 1956 and *S. kobayashii* Morikawa, 1956 by the number of setae on chelicera (6 vs. 7), lower number of movable chelal finger teeth (16–19 teeth vs. min. 26 teeth) and a slender palp (palpal femur 7.24 (♂) × vs. 5.00–5.60 (♂) × longer than board; chela 6.21–6.22 (♂) × vs. 5.13–5.74 (♂) × longer than board); from *S. dentifer* (Morikawa, 1970) by the number of setae on chelicera (6 vs. 7), lower number of movable chelal finger teeth (16–19 teeth vs. min. 36 teeth) and a shorter chela (chela 6.21–6.22 (♂), 5.68 (♀) × vs. 6.85 (♂), 7.12 (♀) × longer than board, length 1.68–1.74 (♂), 1.76 (♀) mm vs. 1.85 (♂♀) mm); from *S. kubotai* by the slightly smaller body size (body length 1.93 (♀) mm vs. 2.03 (♀) mm; chela 5.68 (♀) × vs. 5.70 (♀) × longer than board; movable chelal finger 1.68 (♀) × vs. 1.87 (♀) × longer than) and the number of setae of coxal spines (7 or 8 vs. 11); from *S. kishidai* (Morikawa, 1960) by a slender palp (palpal femur 7.24× vs. 4.90× longer than board; movable chelal finger 0.61–0.63× vs. 0.67–0.69× longer than board) (Morikawa 1954, 1956, 1960, 1970; You et al. 2022).

Distribution and habitat. This species is known only from the type locality, Wulibei Cave (Figs 1A, 18A–C), which is located ~ 1.2 km east of Yangguan Village (Weining County). This limestone cave has an elongated entrance (~ 2.5 m high and 8 m wide) with some corn stalks scattered nearby. Entrance of the cave has a large muddy cave hall, connected to a small hall through a narrow tunnel, which is a more enclosed, completely dark space, covered with gravel, with temperatures ~ 10 °C and humidity ~ 90%. The specimen was collected under a stone in a small cave hall.

Acknowledgements

We are grateful to Prof. Zhisheng Zhang, Dr. Huiming Chen, Dr. Luyu Wang, Zegang Feng, Zhaoyi Li, Chen Zhang, Hongru Xu, Lu Zhang, Jianzhou Sun and Wenlong Fan for their assistance in the field, to Ms Angela Xuanyu Lin for providing help in language editing of this manuscript, and to Dr. Jana Christophoryová, Dr. Mark S. Harvey, Dr. Nathalie Yonow, and other two anonymous reviewers for their helpful suggestions that greatly improved this paper. This work was supported by the National Natural Science Foundation of China (No. 31872198 & 32170468), the Natural Science Foundation of Hebei Province (No. C2021201030), and the Special Project of "1331 Project" to Wutai Mountain Cultural Ecological Collaborative Innovation Center in 2022 to Zhizhong Gao.

References

Chamberlin JC (1931) The arachnid order Chelonethida. Stanford University Publications, University Series, [Biol. Sci.] 7(1): 1–284.

Feng ZG, Wynne JJ, Zhang F (2019) Two new subterranean-adapted pseudoscorpions (Pseudoscorpiones: Neobisiidae: Parobisium) from Beijing, China. Zootaxa 4661(1): 145–160. https://doi.org/10.11646/zootaxa.4661.1.7

Feng ZG, Wynne JJ, Zhang F (2020) Cave-dwelling pseudoscorpions of China with descriptions of four new hypogean species of *Parobisium* (Pseudoscorpiones, Neobisiidae) from Guizhou Province. Subterranean Biology 34: 61–98. https://doi.org/10.3897/subtbiol.34.49586

Gao ZZ, Zhang YF, Zhang F (2016) Two new species of Pseudotyrannochthoniidae, including the first species of *Pseudotyrannochthonius* (Pseudoscorpiones) from China. Acta Zoologica Academiae Scientiarum Hungaricae 62(2): 117–131. https://doi.org/10.17109/AZH.62.2.117.2016

Gao ZZ, Chen HM, Zhang F (2017) Description of two new cave-dwelling *Bisetocreagris* species (Pseudoscorpiones: Neobisiidae) from China. Turkish Journal of Zoology 41: 615–623. https://doi.org/10.3906/zoo-1602-39

Gao ZZ, Wynne JJ, Zhang F (2018) Two new species of cave-adapted pseudoscorpions (Pseudoscorpiones: Neobisiidae, Chthoniidae) from Guangxi, China. The Journal of Arachnology 46(2): 345–354. https://doi.org/10.1636/JoA-S-17-063.1

Gao ZZ, Zhang F, Chen HM (2020) Two new cave-dwelling species of *Tyrannochthonius* Chamberlin, 1929 (Pseudoscorpiones: Chthoniidae) from the Guizhou karst, China. Zootaxa 4853(4): 572–580. https://doi.org/10.11646/zootaxa.4853.4.6

Harvey MS (1992) The phylogeny and classification of the Pseudoscorpionida (Chelicerata: Arachnida). Invertebrate Taxonomy 6(6): 1373–1435. https://doi.org/10.1071/IT9921373

Harvey MS, Harms D (2022) The pseudoscorpion genus *Centrochthonius* (Pseudoscorpiones: Pseudotyrannochthoniidae) from central Asia and description of a new species from Nepal. The Journal of Arachnology 50(2): 158–174. https://doi.org/10.1636/JoA-S-21-033

Hou YM, Gao ZZ, Zhang F (2022a) Two new species of cave-adapted pseudoscorpions (Pseudoscorpiones, Chthoniidae) from Yunnan, China. ZooKeys 1097: 65–83. https://doi.org/10.3897/zookeys.1097.82527

Hou YM, Gao ZZ, Zhang F (2022b) Diversity of cave-dwelling pseudoscorpions from eastern Yunnan in China, with the description of eleven new species of the genus *Lagynochthonius* (Pseudoscorpiones, Chthoniidae). Zootaxa 5198(1): 001–065. https://doi.org/10.11646/zootaxa.5198.1.1

Hu JF, Zhang F (2011) Description of three new species of the genus *Allochthonius* Chamberlin, 1929 (Pseudoscorpiones: Pseudotyrannochthoniidae) from China. Journal of Threatened Taxa 3(11): 2167–2176. https://doi.org/10.11609/JoTT.o2767.2167-76

Hu JF, Zhang F (2012) Two new species of the genus *Allochthonius* Chamberlin from China (Pseudoscorpiones: Pseudotyrannochthoniidae). Entomologica Fennica 22(4): 243–248. https://doi.org/10.33338/ef.5003

Judson MLI (2007) A new and endangered species of the pseudoscorpion genus *Lagynochthonius* from a cave in Vietnam, with notes on chelal morphology and the composition of the Tyrannochthoniini (Arachnida, Chelonethi, Chthoniidae). Zootaxa 1627(1): 53–68. https://doi.org/10.11646/zootaxa.1627.1.4

Latella L (2019) Biodiversity: China. In: White WB, Culver DC, Pipan T (Eds) Encyclopedia of Caves (3rd Edn). Academic Press, Amsterdam, 127–135. https://doi.org/10.1016/B978-0-12-814124-3.00016-9

Li YC (2022) Five new troglobitic species of *Tyrannochthonius* (Arachnida, Pseudoscorpiones, Chthoniidae) from the Yunnan, Guizhou and Sichuan Provinces, China. ZooKeys 1131: 173–195. https://doi.org/10.3897/zookeys.1131.91235

Li YC, Wang ML (2021) Description of a new cave-dwelling pseudoscorpion, *Anatemnus hemuensis* sp. nov. (Pseudoscorpiones, Atemnidae) from Gaoligong Mountain, China. Carsologica Sinica 40(6): 1058–1062.

Li YC, Shi AM, Liu H (2017) A new cave-dwelling species of *Bisetocreagris* Ćurčić (Arachnida, Pseudoscorpiones: Neobisiidae) from Yunnan Province, China. Entomologica Fennica 28(4): 212–218. https://doi.org/10.33338/ef.84688

Li YC, Liu H, Shi AM (2019) A new cave-dwelling species of *Lagynochthonius* (Arachnida: Pseudoscorpiones: Chthoniidae) from Yunnan Province, China. Zootaxa 4571(1): 28–34. https://doi.org/10.11646/zootaxa.4571.1.2

Lin JQ (2001) The distributed area and the features analysis of karst and non karst landscape in Guizhou. Journal of Guizhou Educational College 04: 43–46.

Mahnert V (2003) Four new species of pseudoscorpions (Arachnida, Pseudoscorpiones: Neobisiidae, Chernetidae) from caves in Yunnan Province, China. Revue Suisse de Zoologie 110: 739–748. https://doi.org/10.5962/bhl.part.80209

Mahnert V (2009) New species of pseudoscorpions (Arachnida, Pseudoscorpiones, Chthoniidae, Chernetidae) from caves in China. Revue Suisse de Zoologie 116(2): 185–201. https://doi.org/10.5962/bhl.part.79492

Mahnert V, Li YC (2016) Cave-inhabiting Neobisiidae (Arachnida: Pseudoscorpiones) from China, with description of four new species of Bisetocreagris Ćurčić. Revue Suisse de Zoologie 123: 259–268.

Morikawa K (1954) On some pseudoscorpions in Japanese lime-grottoes. Memoirs of Ehime University 2(2B): 79–87.

Morikawa K (1956) Cave pseudoscorpions of Japan (I). Memoirs of Ehime University 2(2B): 271–282.

Morikawa K (1960) Systematics studies of Japanese pseudoscorpions. Memoirs of Ehime University 2(2B): 85–172.

Morikawa K (1970) Results of the speleological survey in South Korea 1966. XX. New pseudoscorpions from South Korea. Bulletin of the National Science Museum, Tokyo 13: 141–148.

Schawaller W (1995) Review of the pseudoscorpion fauna of China (Arachnida: Pseudoscorpionida). Revue Suisse de Zoologie 102(4): 1045–1063. https://doi.org/10.5962/bhl.part.80489

Schwarze D, Harms D, Hammel J, Kotthoff U (2021) The first fossils of the most basal pseudoscorpion family (Arachnida: Pseudoscorpiones: Pseudotyrannochthoniidae): Evidence for major biogeographical shifts in the European paleofauna. PalZ 96(1): 11–27. https://doi.org/10.1007/s12542-021-00565-8

Viana ACM, Ferreira RL (2021) A new troglobitic species of *Allochthonius* (subgenus *Urochthonius*) (Pseudoscorpiones, Pseudotyrannochthoniidae) from Japan. Subterranean Biology 37: 47–55. https://doi.org/10.3897/subtbiol.37.58580

WPC (2022) World Pseudoscorpiones Catalog. Natural History Museum Bern. https://wac.nmbe.ch/order/pseudoscorpiones/3 [Accessed on 30 Nov. 2022]

Xu HR, Gao ZZ, Zhang F (2022) Two new species of the pseudoscorpion subfamily Lamprochernetinae Beier, 1932 from Guizhou, China (Pseudoscorpiones: Chernetidae). Zootaxa 5105(4): 581–592. https://doi.org/10.11646/zootaxa.5105.4.7

You J, Yoo JS, Harvey MS, Harms D (2022) Some cryptic Korean karst creatures: revalidation of the pseudoscorpion genus *Spelaeochthonius* (Pseudoscorpiones: Pseudotyrannochthoniidae) and description of two new species from Korea. The Journal of Arachnology 50(2): 135–157. https://doi.org/10.1636/JoA-S-21-025

Zhang FB, Zhang F (2014) A new species of the genus *Allochthonius* (Pseudoscorpiones: Pseudotyrannochthoniidae) from Liupan mountains, China, with description of the male of *Allochthonius brevitus*. Acta Zoologica Academiae Scientiarum Hungaricae 60(1): 45–56.

Zhang DF, Ouyang ZY, Wang SJ (2001) Population resources environment and sustainable development in the karst region of Southwest China. Zhongguo Renkou Ziyuan Yu Huanjing 11(1): 77–81. [In Chinese]

Zhang C, Feng ZG, Zhang F (2020) Two new cave-dwelling pseudoscorpions (Pseudoscorpiones: Neobisiidae: Parobisium) from Yunnan, China. Zootaxa 4834(1): 107–120. https://doi.org/10.11646/zootaxa.4834.1.7

ZooKeys 1139: 71–106 (2023)
doi: 10.3897/zookeys.1139.85270
https://zookeys.pensoft.net

RESEARCH ARTICLE

A peer-reviewed open-access journal
ZooKeys
Launched to accelerate biodiversity research

More than 80 years without new taxa: analysis of morphological variation among members of Mexican *Aeneolamia* Fennah (Hemiptera, Cercopidae) support a new species in the genus

Francisco Armendáriz-Toledano[1], Misael Adrián López-Posadas[2], Youssef Utrera-Vélez[3], Jesús Romero Nápoles[4], Ulises Castro-Valderrama[2]

1 *Colección Nacional de Insectos, Departamento de Zoología, Instituto de Biología, Universidad Nacional Autónoma de México, Cto. Zona Deportiva S/N, Ciudad Universitaria, Mexico City, CDMX 04510 Mexico* **2** *Universidad de Sonora, Departamento de Agricultura y Ganadería, Km 21 Carretera Hermosillo-Bahía Kino, C.P. 83000, Sonora, Mexico* **3** *Tecnológico de México-Campus Úrsulo Galván, Km 4.5 Carretera Cardel Chachalacas, Úrsulo Galván, Veracruz, Mexico* **4** *Colegio de Postgraduados, Postgrado en Fitosanidad-Entomología y Acarología, Km. 36.5 México-Texcoco, Montecillo, CP 56230, México State, Mexico*

Corresponding author: Ulises Castro-Valderrama (ulises.castro@unison.mx, ucastro.11@gmail.com)

Academic editor: Yalin Zhang | Received 12 April 2022 | Accepted 3 November 2022 | Published 9 January 2023

https://zoobank.org/ECA7E54D-E01D-4012-8282-5FDBB81D11A2

Citation: Armendáriz-Toledano F, López-Posadas MA, Utrera-Vélez Y, Romero Nápoles J, Castro-Valderrama U (2023) More than 80 years without new taxa: analysis of morphological variation among members of Mexican *Aeneolamia* Fennah (Hemiptera, Cercopidae) support a new species in the genus. ZooKeys 1139: 71–106. https://doi.org/10.3897/zookeys.1139.85270

Abstract

The genus *Aeneolamia* includes eight described species and 32 subspecies widely distributed in America. In Mexico, two species (*A. contigua* and *A. albofasciata*) and one subspecies (*A. contigua campecheana*) are recognized. In a recent study of Cercopidae in Mexico, a new species of *Aeneolamia* was noted from Oaxaca, Mexico based on body color and the ornamentation patterns of tegmen, without a formal taxonomic description. To test the hypothesis of an extant new taxon within the genus a comprehensive analysis of intraspecific morphological variation from 46 morphological features was performed, four related to tegmen color patterns in both sexes, six to male genitalia, and 36 continuous characters measured in specimens of both sexes of Mexican *Aeneolamia* from several geographical localities using traditional univariate, multivariate morphometric, and geometric morphometric methods. This is the first time that this approach has been used in Cercopidae. *Aeneolamia danpecki* Castro, Armendáriz & Utrera, **sp. nov.** from Oaxaca showed pronounced morphological differences in tegmen coloration patterns, the shape of different elements of the male genitalia, and body measurements compared to the other Mexican members of *Aeneolamia*; therefore, it is described as a new species.

Keywords
Aeneolamia aff. *albofasciata*, Cercopoidea, grasses pest, Spittlebug, sugarcane

Introduction

In the Neotropical region, 60 genera of Cercopidae are integrated into the subfamily Ischnorhininae (Carvalho and Webb 2005; Paladini et al. 2015; Armendáriz-Toledano et al. 2022). One of the most important taxa in this subfamily, due to its economic impact as pests in sugarcane and pastures, is the genus *Aeneolamia* Fennah, 1949, whose members promote considerable losses in crop yields in the countries they inhabit (Urich 1913; Williams 1921; Guagliumi 1962; Oomen 1975; De la Cruz-Llanas et al. 2005; Gómez 2007). The adults of *Aeneolamia* spp. suck the sap of the sugar cane, *Saccharum officinarum* L., promoting a decrease in the percentage of sucrose compared to canes not damaged by the insects, which causes the sugar extraction process to be less efficient (Williams 1921). Compared with other sugar cane pests in Cercopidae, species of the genus *Aeneolamia* have a shorter development time (Oomen 1975; Peck et al. 2002a; Rodríguez et al. 2002; Sendoya Corrales et al. 2011), which allows a greater number of generations per year and, therefore, increased potential to cause losses (Hernández et al. 2021a, b). For these reasons, *Aeneolamia* spp. have been extensively studied regarding biology (Urich 1913; Williams 1921; Guagliumi 1962; Fewkes1969a, b; Morales 1993; López et al. 2001; Peck et al. 2002a; Sendoya Corrales et al. 2011), taxonomy (Fennah 1949, 1953, 1968; Clark et al. 1976; Carvalho and Webb 2005; Thompson and León González 2005), population dynamics (Urich 1913; Oomen 1975; Jiménez 1978; Wiedijk 1982; Martin et al. 1995; Peck et al. 2002b), distribution (Urich 1913; Guagliumi 1962; Figueredo et al. 2021; Hernández et al. 2021a, b), natural enemies (Urich 1913; Medina et al. 1993; García et al. 2012; Matabanchoy Solarte et al. 2012; Moreno Salguero et al. 2012; Rosero-Guerrero et al. 2012; Obando et al. 2013; Hernández-Domínguez et al. 2016; Grifaldo-Alcántara et al. 2019), economic impact (Williams 1921; Guagliumi 1962; García-García et al. 2006), host plant resistance (Miles et al. 1995; Cardona et al. 2004, 2010; Sotelo-Cardona et al. 2008; Cuarán et al. 2012; Aguirre et al. 2013), and control strategies (Jiménez 1978; Martin et al. 1999; García-García et al. 2006).

Fennah (1949) created the genus *Aeneolamia* with six species, *A. varia semifascia* (Walker, 1851) as the type species and *A. varia* (Fabricius, 1787), *A. colon* (Germar, 1821), *A. contigua* (Walker, 1851), *A. flavilatera* (Urich, 1914), *A. lepidior* (Fowler, 1897), and *A. reducta* (Lallemand, 1924), defined by at least eight morphological features:

1) head with eyes two-thirds as wide as pronotum at widest part, anterolateral margins more or less straight, converging at 110°, width of head between eyes greater than length in middle line (approximately 1.2: 1);

2) fronto-vertex with two deeply impressed lines; ocelli nearer to one another than to eyes, situated on a common prominence;

3) antennae with second segment twice as long as broad, third segment sub globular, or broadly ovoid, both arista placed at same level, shorter arista scarcely longer than third segment;

4) postclypeus moderately inflated, not laterally compressed, distinctly wider across middle in anterior view than at base, in profile shallowly rounded to apex of well-developed median carina, then straight to anteclypeal suture, point of curvature subangulate (approx. 125°), smooth, shining, with setae along grooves;

5) rostrum moderately short, apical joint in anterior view 2.5 × as long as broad;

6) tegmina 2.5 × as long as broad, apical margin broadly rounded, Sc + R forked about level with the union of claval veins, M and Cu united for a short distance near the base, apical venation prominent above general surface, the distal area with very approximately 25 cells, dorsal surface of tegmen often markedly pubescent (2.5 × as long as broad, with apical reticulation);

7) shape of subgenital plates (never greatly elongated, relatively broad, distally transverse, obliquely truncate, or with apicomesal angle produced in a spine);

8) structure of aedeagus (tubular, with one pair of slender strongly deflexed spines attached anteriorly near middle).

In the compilation of Carvalho and Webb (2005), the six species considered by Fennah were reported together with two additional species, *A. albofasciata* (Lallemand, 1939) and *A. sanguiniplaga* (Lallemand, 1938), and more than 30 subspecies. Years later, a new species from Brazil, *A. bucca* Paladini & Cavichioli, 2013 was proposed within the genus (Paladini and Cavichioli 2013). However, it was later assigned by the same authors to the genus *Gervasiella* Paladini & Cavichioli, 2015, based on a cladistic analysis of morphological characters (Paladini and Cavichioli 2015). Currently, *Aeneolamia* includes eight species and 32 described subspecies widely distributed in Brazil, Colombia, Costa Rica, Guatemala, Guyana, Honduras, Mexico, Panama, Venezuela, and Trinidad and Tobago (Carvalho and Webb 2005; Armendáriz-Toledano et al. 2022). In a cladistics framework based on morphological characters, *Aeneolamia* is supported as a sister clade of *Isozulia* Fennah, 1953, and together as the sister group of *Prosapia* Fennah, 1949, within the tribe Tomaspidini (Paladini et al. 2015). The most recent molecular phylogenetic analysis of Ischnorhininae supports *Aeneolamia* and *Isozulia* as sister genera; however, its position within Tomaspidini was separated from *Prosapia* and associated with *Ferorhinella* Carvalho & Webb, 2004, *Aracamunia* Fennah, 1968, and *Tropidorhinella* Schmidt, 1910 (Paladini et al. 2018). Since the description of *A. albofasciata* Lallemand, 1939; *A. flavilatera belenensis* Guagliumi, 1956; and *A. flavilatera guarici* Guagliumi, 1956 no new species or subspecies have been added to the genus *Aeneolamia*.

In Mexico, *Aeneolamia* is represented by two species, *A. albofasciata* (Lallemand, 1939) and *A. contigua* (Walker, 1851). Both Mexican species of *Aeneolamia* are polyphagous on Poaceae and inhabit almost most regions from Mexican Republic (Martin et al. 1995; López-Collado and Pérez-Aguilar 2012), where they are reported as important damaging pests in sugar cane areas (De la Cruz-Llanas et al. 2005; López-Collado and Pérez-Aguilar 2012; Morales-Pérez et al. 2014; García-González et al. 2017) and

grasses (Oomen 1975; Martin et al. 1995; De la Cruz-Zapata et al. 2016). In *A. contigua*, three subspecies have been recognized, from southwestern Mexico: *A. contigua campecheana* Fennah, 1951 from Haltunchen, Campeche; *A. contigua postica* (Walker, 1858) from around Orizaba volcano, Veracruz; and *A. contigua sanctaerosae* (Fennah 1953) from Santa Rosa, Yucatan. These subspecies were proposed based on differences in coloration patterns of body and tegmina, without conspicuous differences in male genitalia morphology. In Arméndariz-Toledano et al. (2022), the type specimens of *A. contigua*, *A. contigua postica*, and *A. contigua sanctaerosae* were compared, leading to the conclusion that these subspecies corresponded only to variations of *A. contigua* in agreement with Clark et al. (1976). In a recent study of the taxonomy and diversity of Cercopidae in Mexico and based on body color and the ornamentation patterns of the tegmina, a new species of *Aeneolamia* was observed from the mountains and central valleys of Oaxaca State. This undescribed taxon was provisionally named *Aeneolamia* aff. *albofasciata* (handwritten label: "*Aeneolamia* aff. *albofasciata* nueva especie", UCV, deposited in CEAM) for its morphological similarities to *A. albofasciata* (Armendáriz-Toledano et al. 2022). Members of *Aeneolamia* display intra- and interspecific variation in tegmina color, both within and among localities, placing great importance on male genitalia characters as reliable species identifiers, because they are conservative within the species (Fennah 1949; Paladini and Cavichioli 2013). Thus, we tested the hypothesis that *A.* aff. *albofasciata* is a new taxon within the genus by analysis of the morphological variation of Mexican *Aeneolamia* species using traditional univariate and multivariate morphometrics of 46 discrete and continuous features of external morphology, tegmina color pattern, and male genitalia on 628 specimens from 59 localities representative of their entire distribution. In addition, we looked for new discrete characters, as well as assessed their usefulness in the identification of these taxa. Furthermore, we performed a geometric morphometric analysis to evaluate whether the variation in the shape of the aedeagus spine allows delimitation of these taxa. This is the first time that this approach has been used to support and define the taxonomic status of a new taxon of Cercopidae. Based on our results, we describe *A. danpecki* sp. nov. and provide a complete dichotomous key to the Mexican species of *Aeneolamia*, replacing the partial key of Armendáriz-Toledano et al. (2022).

Materials and methods

A total of 628 *Aeneolamia* adults from 59 Mexican localities corresponding to 260 females and 368 males were reviewed. From the total sample, 64 specimens (43 ♀, 21 ♂) correspond to *A. danpecki* sp. nov., 496 to *A. albofasciata* (178 ♀, 318 ♂), and 68 to *A. contigua* (39 ♀, 29 ♂). For the third species, we included specimens collected around the respective type localities of the previously recognized subspecies *A. contigua campecheana*, *A. contigua postica*, and *A. contigua sanctaerosae* because the type localities were not geographically detailed in the original descriptions or the habitat of the subspecies in the locality had disappeared (Table 1). The specimens reviewed were loaned by the following institutions:

CEAM Colección de Insectos del Colegio de Postgraduados, Montecillo, Texcoco, México;

CNIN Colección Nacional de Insectos del Instituto de Biología de la Universidad Nacional Autónoma de México, México City, Mexico.

Taxonomic identifications of the species were based on male genitalia. In addition, we included two specimens identified as *A. albofasciata* (= *A. albofasciata occidentalis*) from CEAM (Table 1) and determined by W. E. Clark in 1975, an authority on the identification of *Aeneolamia* species. *Aeneolamia danpecki* sp. nov. was recognized by a dark brown to light brown tegmen, with two incomplete and barely visible transverse bands, one of them oblique on the basal third and another straight on the distal third, or only the basal band visible, or both absent. Males and females were recognized by their genitalia.

To manipulate specimens and take photographs, we used the method of Valdez-Carrasco (Castro-Valderrama et al. 2018). The pygofer of some males of each taxon was

Table 1. Species, locality, date, and sample size of Mexican *Aeneolamia*. The number of specimens in parentheses refer to those included in the morphometric analysis. [a]*A. albofasciata* identified by Clark in 1975 and deposited in CEAM, [b]*A. contigua campecheana*, [c]*A. contigua postica*.

Species	Locality	Date	Total	Female	Male
A. albofasciata	Campeche, Colegio de Postgraduados	3/X/2016	199	79 (2)	120
	Campeche, Haltunchen, Km 159.5	2/X/2016	110	10 (1)	100 (2)
	Chiapas, Comunidad Providencia	6/VI/2011	1	–	1 (1)
	Chiapas, ECOSUR, Tapachula	18/VI/1999	1	1	–
	Chiapas, Ejido Rizo de Oro, Cintalapa	27/V/2011	2	–	2
	Guerrero, Acapulco	21/VIII/1938	1	1	–
	Guerrero, Petaquillas, 9 km W Chilpancingo	6/VI/1963	1	–	1
	Michoacán, Charapendo	18/VIII/2015	1	1 (1)	–
	Michoacán, Tangamandapio	14/IX/2017	119	56 (3)	63 (5)
	Michoacán, Taretan	13/IX/1963	2	2 (1)	–
	Michoacán, Uruapán	VII/1998	1	–	1 (1)
	Morelos, Cuatla	14/IX/1980	3	1 (1)	2
	Morelos, Cuautla, Cuautlixco	22/V/2002	1	–	1 (1)
	Morelos, Palo Bolero	7/X/1995	1	–	1 (1)
	Nuevo León, Apodaca	4/VIII/1979	20	6	14
	Quintana Roo, Tecnológico de Chetumal	15/X/2017	2	–	2
	San Luis Potosí, Sierra El Abra, Los Patos	8/IX/2017	1	1	–
	Sonora, Municipio de ímuris, ímuris	9/VIII/2013	1	–	1
	Sonora, Centro Invest. Pec. Est. Sonora, Carbó	X/1981	2	2	–
	Tabasco, Cárdenas	28/VI/1982	1	1 (1)	–
	Tabasco, Cárdenas	12/I/2012	1	1 (1)	–
	Tamaulipas, Cd. Mante	VI/1987	1	1 (1)	–
	Tamaulipas, Cd. Mante	7/X/1983	4	1 (1)	3 (1)
[a]	Veracruz, Cosamaloapan	20/VII/1962	1	1	–
[a]	Veracruz, Tecolutla	7/IX/1973	1	–	1
	Veracruz, Km 4.5 Carr Cardel-Salmoral	4/IX/2003	14	12 (1)	2
	Veracruz, Úrsulo Galván	23/VI/2021	4	1 (1)	3 (3)
	Total		496	178 (15)	318 (15)

Species	Locality	Date	Total	Female	Male
A. contigua	Quintana Roo, 2 km S Rancho El 24	20/XII/1984	1	–	1
	Chiapas, Calzada larga, Villaflores	27/X/2012	1	–	1
	Chiapas, Finca Cucalhuitz, 19 Km NE Bochil	28/XI/1961	1	1 (1)	–
	Chiapas, Llano La Lima, Tapachula	9/VI/2013	1	1	–
	Chiapas, Palenque	31/I/1985	1	1	
	Chihuahua, Chihuahua	12/VII/1938	1	–	1
	Guerrero, Almolonga	30/VII/1962	5	1 (1)	4 (3)
	Jalisco, Ameca	23/VII/1999	1	–	1
	Michoacán, Morelia	1/VI/1963	1	–	1 (1)
	Morelos, Cuatla	6/II/1996	2	1 (1)	1 (1)
	Morelos, Reserva de la Biosfera Huahutla	27/V/2000	15	13 (3)	2
	Nayarit, Guayabitos	2/X/1980	1	1 (1)	–
	Oaxaca, I. Bastida	12/IX/1981	1	–	1 (1)
	Oaxaca, Tehuantepec	10/VII/1966	1	1 (1)	–
[b]	Quintana Roo, Tecnológico de Chetumal	15/X/2017	1	–	1
	Tabasco, Cárdenas	14/VII/1994	1	–	1 (1)
[c]	Veracruz, Cd. Mendoza	15/IX/1994	2	1	1 (1)
[c]	Veracruz, Colegio de Postgraduados, Campus Córdoba	15/IX/1994	1	–	1 (1)
	Veracruz, Est. Los Tuxtlas, San Andrés	21/IX/2007	1	–	1 (1)
	Veracruz, Isla	13/VII/2002	2	2 (2)	–
	Veracruz, Km 14 Aut. Cárdenas-Minatitlán, Rancho La Majada	4/X/2016	15	10 (2)	5 (4)
[c]	Veracruz, La Antigua	28/VIII/1978	2	2 (2)	–
	Veracruz, Las Vigas	19/VI/1965	2	1	1 (1)
	Veracruz, Playa Escondida, Catemaco	13/VI/1979	1	1 (1)	–
	Veracruz, Playa Escondida, Catemaco	13/VI/1979	1	–	1
	Veracruz, Tinája	18/IX/1994	1	–	1
	Yucatán, Chichen Itza	20/VI/1985	2	1	1
	Yucatán, Ruta 295, Km 93 Rio Lagartos	18/VI/1985	2	–	2
[b]	Yucatán, Cuncunul	13/IX/1994	1	1	–
	Total		68	39 (15)	29 (15)
Aeneolamia danpecki	Oaxaca, 5 km San Martín Lochila	12/VII/2004	1	1 (1)	–
sp. nov.	Oaxaca, Sola de Vega	28/IX/2003	48	33 (5)	15 (9)
	Oaxaca, La Trinidad, Zaachila	28/VIII/2018	15	9 (9)	6 (6)
	Total		64	43 (15)	21 (15)
TOTAL			**628**	**260**	**368**

detached and clarified in 10% KOH solution for 12–24 h; after which the KOH was neutralized with acetic acid and washed with distilled water. Photographs of the genitalia were taken with a Leica MZ8 stereomicroscope, connected with Nikon E5700 camera and E5700 v. 1.1 software to capture images. Photographs of adult habitus were taken with a digital Olympus E-620 camera attached to an Olympus SZX7 stereoscope and images were captured with Olympus Studio 2.22 software. Images were stacked with COMBINE ZP free software and edited with GIMP 2.8.14 free software. Morphological terminology follows and is adapted from Fennah (1949, 1953, 1968), Nast (1950), Hamilton (1977), Paladini and Cavichioli (2015), and Le Cesne et al. (2021).

Discrete morphological characters. Because of high polymorphism in color patterns of wings recorded in some species of Auchenorrhyncha families, particularly in cercopids, and due to the male genitalia traits providing robust evidence to support *A. danpecki* sp. nov. (Paladini et al. 2015), a comparison of the variations of tegmina color patterns and male genitalia morphology was performed among *Aeneolamia* species. Tegmen color patterns were analyzed in the entire sample (n = 628), and male genitalia features from ten specimens of *A. danpecki* sp. nov., eleven specimens of *A. albofasciata*, and seven specimens of *A. contigua*. These characters are as follows:

1. Tegmen color (**TC**). Lateral and dorsal view. (1) Black (Fig. 1A, D), (2) dark brown (Fig. 1B, E), (3) light brown (Fig. 1C).
2. Color of internal clavus edge in the tegmen (**CIE**). Dorsal view. (1) Same color as tegmen (Fig. 1D), (2) a yellowish or white line (Fig. 1E), (3) an orange or red line (Fig. 1F).
3. Color pattern on the anterior third of tegmen (**CAT**). Lateral view. (1) Same color as tegmen (Fig. 1G), (2) an inconspicuous thin transversal line (Fig. 1H), (3) a conspicuous broad transversal yellowish or white line (Fig. 1I), (4) a conspicuous broad transversal orange or red line (Fig. 1J).
4. Color pattern on the distal third of tegmen (**CDT**). Lateral view. (1) The same color as tegmen (Fig. 1K), (2) an incomplete thin transversal line (Fig. 1L), (3) a complete broad transversal yellowish or white line (Fig. 1M), (4) a complete broad transversal orange or red line (Fig. 1N).
5. Elevation of the anal tube sclerites (**EAE**). (1) tenth and eleventh tergites at the same level on the horizontal (Fig. 2A), (2) tenth tergite higher than the eleventh, with respect to the horizontal (Fig. 2B).
6. Shape of subgenital plates (**SGP**). Ventral view. (1) Acute apex with straight lateral edges and rhomboidal to the apex (Fig. 2I, J), (2) apex obliquely truncate with lateral edges slightly concave (Fig. 2K).
7. Shape of internal edge of subgenital plate apex (**SEGP**). Ventral view. (1) Acuminate in a pointed lobe (Fig. 2I), (2) acuminate in a rounded lobe (Fig. 2J), (3) blunt (Fig. 2K).
8. Paramere, shape of primary apical spine (**ASP**). Lateral view. (1) Long and thin spine with a continuous curvature not angulated (Fig. 2F, G), and (2) short and wide spine with a pronounced angulated curvature (Fig. 2H).
9. Parameter, shape of secondary subapical spine (**SSP**). Lateral view. (1) Two rounded acute lobes similar in size and shape (Fig. 2L), (2) two acute lobes, the dorsal one conspicuously bigger than the ventral (Fig. 2M), (3) one big lobe (Fig. 2N).
10. Tip of aedeagus spines (**PRE**). (1) Lateral view, conspicuously curved upward and touching the superior margin of phallobase, bent to form an almost 90° angle (Figs 2O, 8A, B), and dorsal view, conspicuously sinuous (Fig. 2R); (2) lateral view, slightly curved upward (Figs 2P, 8C) and dorsal view, slightly sinuous (Fig. 2S); (3) lateral view, slightly curved downward (Figs 2Q, 8D) and dorsal view, conspicuously sinuous (Fig. 2T).

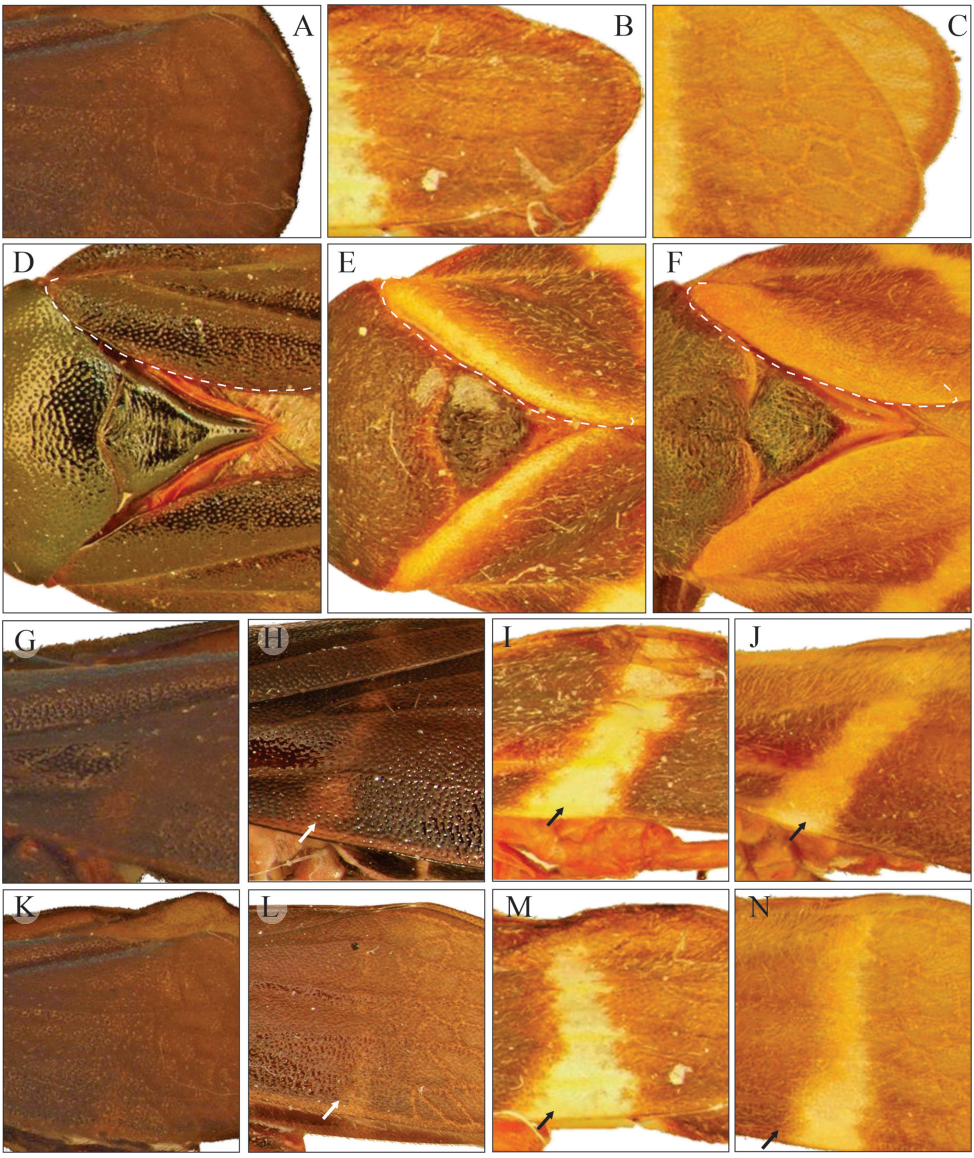

Figure 1. Character states to compare the variation of tegmen color patterns **A, D, G, H, K, L** *Aeneolamia danpecki* sp. nov. **B, E, I, M** *A. albofasciata* **C, F, J, N** *A. contigua* **D–F** dotted lines indicate the internal anterior region of tegmen. Arrows indicate the transversal lines on tegmen: **G–J** anterior region **K–N** posterior region.

Continuous quantitative morphological characters

Because the *Aeneolamia* species display apparent differences in body size, 90 adults from 31 Mexican localities were compared using measurements of the head, mouthparts, pronotum, tegmina, and legs (Fig. 3). Using these features, a comparison of the

morphological variation among *A. danpecki* sp. nov. (*n* = 15♂, 15♀), *A. albofasciata* (*n* = 15♂, 15♀), and *A. contigua* (*n* = 15♂, 15♀) could be performed. These characters are as follows:

11) Head width with eyes (**HWE_d**), 12) head length in dorsal view (**HL_d**), 13) pronotum width in dorsal view (**PW_d**), 14) pronotum length in dorsal view (**PL_d**), 15) scutellum width in dorsal view (**SW_d**), 16) scutellum length in dorsal view (**SL_d**), 17) postclypeus length in ventral view (**PcL_v**), 18) postclypeus width in ventral view (**PcW_v**), 19) anteclypeus length in ventral view (**Al_v**), 20) anteclypeus width in ventral view (**AW_v**), 21) stylet length in ventral view (**SL_v**), 22) stylet width in ventral view (**SW_v**), 23) posterior coxa width in ventral view (**PCW_v**), 24) posterior coxa length in ventral view (**PcL_v**), 25) body length without wings in ventral view (**BLW_v**), 26) postclypeus length in lateral view (**PCL_l**), 27) postclypeus width in lateral view (**PCW_l**), 28) eye length in lateral view (**EL_l**), 29) eye width in lateral view (**Ew_l**), 30) head length in lateral view (**HL_l**), 31) head width in lateral view (**HW_l**), 32) length of lateral margin pronotum in lateral view (**$LLMP_l$**), 33) body length including wings in lateral view (**BL_l**), 34) length of the anterior wing in lateral view (**LAW_l**), 35) width-length radio of head in dorsal view (**WLH_d**), 36) width-length ratio of pronotum in dorsal view (**WLP_d**), 37) width-lengh radio of scutellum in dorsal view (**WLS_d**), 38) width-length radio of clypeus (**WLC_v**), 39) postclypeus ratio in ventral view (width/length) (**PR_v**), 40) stylet ratio in ventral view (width/length) (**SR_v**), 41) coxa ratio (width/length) (**RCR_v**), 42) ratio between body length with wings and length without wings (**RBW_l**), 43) postclypeus radio in lateral view (width/length) (**RPC_l**), 44) eye ratio in lateral view (width/length) (**RE_l**), 45) head ratio in lateral view (width/length) (**$HRAL_l$**), 46) and ratio between the length of body with wings and forewing length in lateral view (**BLW_l**).

Data analyses

The frequency of character states for each feature was calculated for each taxon in the contingency tables (Tables 2, 3). To evaluate if the differences in frequency among character states are associated with different taxa, both Chi-square Test and the contingency coefficient were performed (e.g., Zar 2010). The normality of the distribution for the quantitative continuous features was independently tested by Shapiro and Wilkinson's test; these features were log-transformed to meet the criteria of normality. Basic descriptive statistics were calculated (mean and standard deviation) and the variation of each character was compared among species and between sexes. To determine whether each characteristic differed between sexes and putative species, we performed a two-way analysis of variance (ANOVA) with sex and species as factors, and multiple comparisons with a Tukey test (Zar 2010), but we only provide values that were significantly different at the 5% level (Tables 4, 5, 6).

Multivariate analyses

To explore if the variation of morphological characteristics together segregates the specimens of *A. danpecki* sp. nov. in a discrete group within multidimensional spaces, a series of ordination analyses were performed. A principal coordinate analysis (PCoA) was performed from a Gower pairwise matrix among 28 male specimens using the ten discrete (male tegmina color pattern and male genitalia) and 36 continuous features. Also, three principal components analyses (PCAs) were performed to explore the geographical patterns of morphological variation among specimens using pairwise covariance matrices of 36 continuous characters. Additionally, we include canonical variate analyses (CVAs) to determine to what extent these features explained the possible taxonomic segregation based on the 90 specimens in males, females, and both sexes together. Multivariate analyses were performed considering each specimen as an operational taxonomic unit (OTU). Lastly, we looked for multivariate statistical differences among taxonomic groups of *Aeneolamia* recovered in the ordination analyses, with an analysis of similarities (ANOSIM) and the respective pairwise Hotelling's T non-parametric tests among groups representing putative species. Groups recovered in the multivariate space were confirmed by the comparative morphological analysis of male genitalia.

Geometric morphometry of aedeagus

From the male genitalia images that show the aedeagus intact, shape variation in patterns of aedeagus spines were quantified among *A. danpecki* sp. nov. (n = 4), *A. albofasciata* (n = 6), and *A. contigua* (n = 7) specimens using potential homologous landmarks (lm) and semi-landmarks (sml) (Bookstein 1991; Zelditch et al. 2004). The aedeagus shape was defined by two type I lm, and 16 sml. Semi-landmarks were defined using digital curves of equidistant points on photographs of aedeagus spines in lateral view with TPS tpsDig 1.40 software (Rohlf 2004). Semi-landmarks were specific sites located along the digital curvatures representing the outline of the aedeagus spine. Form configurations were digitalized as two-dimensional coordinates with tpsDig 1.40 software (Rohlf 2004). To remove scale effects, position, and orientation from configurations, and obtain shape coordinates, a generalized Procrustes analysis (Zelditch et al. 2004) was performed with the CoordGen6 program of IMP (Sheets 2003). The tangential variation of curvatures of shape coordinates was minimized using the minimum Procrustes distance criterion (Pérez et al. 2006). The highest proportion of shape variation in the data set was quantified by means of a relative warps analysis from adjusted coordinates (Zelditch et al. 2004). Shape variation was analyzed with the first three RWs and shape changes were visualized with Thin-Plate Spline technique by means of deformation grids.

Geographical records

To illustrate the geographic distribution of *Aeneolamia* spp., the records of the analyzed specimens were projected onto a map of Mexican biogeographical provinces (Morrone et al. 2017).

Results

In total, 46 morphological characters were evaluated: four discrete characters focused on tegmen color patterns in both sexes, six discrete characters on male genitalia, and 36 continuous characters were measured in specimens of both sexes: Six continuous quantitative morphological were reported by Rodríguez et al. (2002, 2003), and 30 new ones are proposed in this study.

Discrete morphological characters

All tegmina and male genitalia features showed differences in character state frequencies among *A. danpecki* sp. nov., *A. albofasciata*, and *A. contigua* (Tables 2, 3). Two traits of the tegmen and four from the male genitalia exhibit exclusive character states for species: CAT, CDT, SGP, SEGP, SSP, and PRE.

Aeneolamia danpecki: dark brown (22%) to black (78%) tegmen (Fig. 1A), the color of the internal clavus edge of the same color as tegmen (100%; "without color lines") (Fig. 1D), the anterior third of the same color as tegmen (80%) (Fig. 1G) or with an inconspicuous, thin, transverse line (20%) (Fig. 1H), and the distal third of the same color (85%) (Fig. 1K) or with an incomplete transverse line (15%) (Fig. 1L) (Table 2); subgenital plates in ventral view: acute apex, acuminate in a pointed lobe

Table 2. Frequencies of multi-state or binary characters used to compare the variation of color patterns of tegmen among Mexican *Aeneolamia* species. Abbreviations: **TC** tegmen color **CIE** color of internal clavus edge in the tegmen **CAT** color pattern on the anterior third of tegmen **CDT** color pattern on the distal third of tegmen.

Attribute	Character states	*A. danpecki*	*A. albofasciata*	*A. contigua*	Chi²:	CC**
1.- **TC**	(1) Black.	50 (78%)	362 (73%)	0	180.5*	0.62
	(2) Dark brown.	14 (22%)	134 (27%)	48 (70%)		
	(3) Light brown.	0	0	20 (30%)		
2.- **CIE**	(1) Same color as tegmen.	64 (100%)	397 (80%)	0	300.94*	0.73
	(2) With a yellowish or white line.	0	99 (20%)	0		
	(3) With an orange line.	0	0	68 (100%)		
3.- **CAT**	(1) The same color as tegmen.	54 (85%)	0	0	500*	0.81
	(2) Incomplete thin transversal line.	10 (15%)	0	0		
	(3) Complete broad transversal yellowish or white line.	0	494 (100%)	0		
	(4) Complete broad transversal orange or red line.	0	0	68 (100%)		
4.- **CDT**	(1) The same color as tegmen.	54 (85%)	0	0	600*	0.81
	(2) With an incomplete thin transversal line.	10 (15%)	0	0		
	(3) With a complete broad transversal. yellowish or white line.	0	494 (100%)	0		
	(4) With a complete broad transversal orange or red line.	0	0	68 (100%)		
	n =	64	494	68		

** CC contingency coefficient: * $p \leq 0.001$ the significance of association of frequency among character states and taxa.

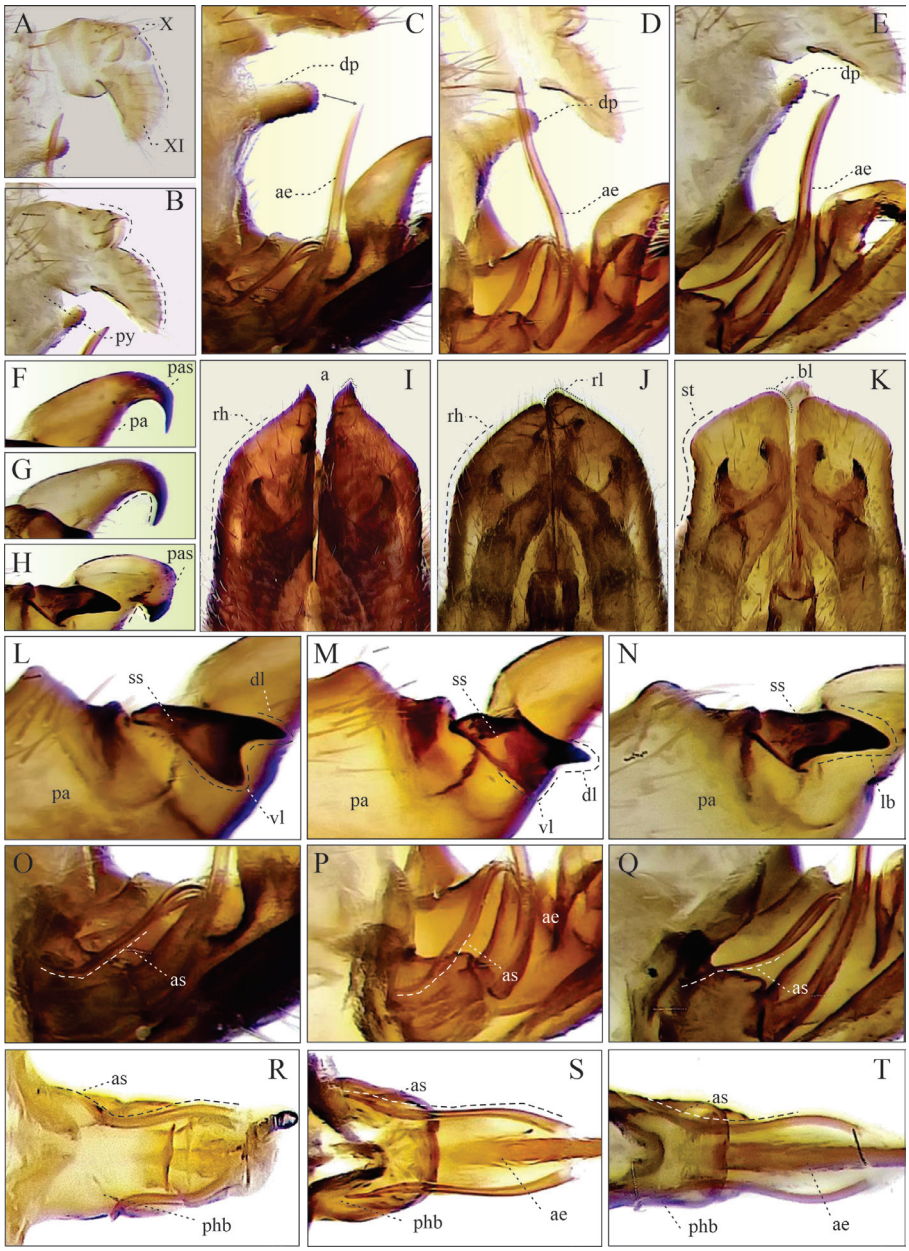

Figure 2. Character states to compare the variation of male genitalia **A, C, F, I, L, O, R** *Aeneolamia danpecki* sp. nov. **D, G, J, M, P, S** *A. albofasciata* **B, E, H, K, N, Q, T** *A. contigua* **A, B** anal tube, lateral view **C–E** aedeagus within pygofer, lateral view **F–H** distal region of parameres, lateral view **I–K** subgenital plates, ventral view **L–N** subapical spines of parameres, lateral view **O–Q** phallobase and aedeagus, lateral view **R–T** phallobase and aedeagus, anterodorsal view. Abbreviations: **ae** aedeagus, **a** acuminate, **as** aedeagus spine, **bl** blunt internal distal edge, **dl** dorsal lobe, **dp** digital process of pygofer, **lb** lobe, **pa** paramere, **pas** primary apical spine of parameres, **phb** phallobase, **py** pygofer, **rh** rhomboidal apex with lateral straight edge, **ss** secondary subapical spine of paramere, **st** slight concave lateral edge, **vl** ventral inferior lobe, **X** tenth segment of anal tube, **XI** eleventh segment of anal tube.

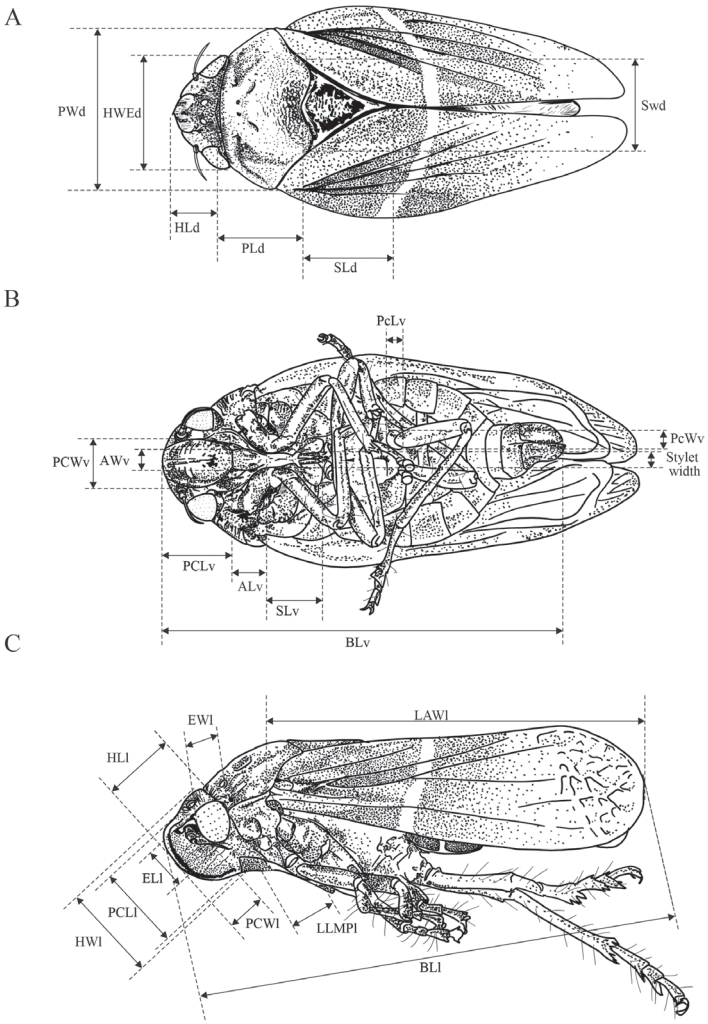

Figure 3. Distribution and details of the continuous features used to quantify the morphological variation of Mexican *Aeneolamia* spp. Habitus view: **A** dorsal **B** ventral **C** lateral. Features Abbreviations: $\mathbf{HWE_d}$ Head width with eyes $\mathbf{HL_d}$ head length in dorsal view, $\mathbf{PW_d}$ pronotum width in dorsal view $\mathbf{PL_d}$ pronotum length in dorsal view $\mathbf{SW_d}$ scutellum width in dorsal view $\mathbf{SL_d}$ scutellum length in dorsal view $\mathbf{PcL_v}$ postclypeus length in ventral view $\mathbf{PcW_v}$ postclypeus width in ventral view $\mathbf{Al_v}$ anteclypeus length in ventral view $\mathbf{AW_v}$ anteclypeus width in ventral view $\mathbf{SL_v}$ stylet length in ventral view $\mathbf{SW_v}$ stylet width in ventral view $\mathbf{PCW_v}$ posterior coxa width in ventral view $\mathbf{PcL_v}$ posterior coxa length in ventral view $\mathbf{BLW_v}$ body length without wings in ventral view $\mathbf{PCL_l}$ postclypeus length in lateral view $\mathbf{PCW_l}$ postclypeus width in lateral view $\mathbf{EL_l}$ eye length in lateral view $\mathbf{Ew_l}$ eye width in lateral view $\mathbf{HL_l}$ head length in lateral view $\mathbf{HW_l}$ head width in lateral view $\mathbf{LLMP_l}$ length of lateral margin pronotum in lateral view $\mathbf{BL_l}$ body length including wings in lateral view $\mathbf{LAW_l}$ length of the anterior wing in lateral view $\mathbf{WLH_d}$ width-length radio of head in dorsal view $\mathbf{WLP_d}$ width-length ratio of pronotum in dorsal view $\mathbf{WLS_d}$ width-lengh radio of scutellum in dorsal view $\mathbf{WLC_v}$ width-length radio of clypeus $\mathbf{PR_v}$ postclypeus ratio in ventral view (width/length) $\mathbf{SR_v}$ stylet ratio in ventral view (width/length) $\mathbf{RCR_v}$ coxa ratio (width/length) $\mathbf{RBW_l}$ ratio between body length with wings and length without wings $\mathbf{RPC_l}$ postclypeus radio in lateral view (width/length) $\mathbf{Re_l}$ eye ratio in lateral view (width/length) $\mathbf{HRAL_l}$ head ratio in lateral view (width/length) $\mathbf{BLW_l}$ ratio between the length of body with wings and forewing length in lateral view.

Table 3. Frequencies of multi-state or binary characters used to compare the variation male genitalia among Mexican *Aeneolamia* species. Abbreviations: **EAE** elevation of the anal tube sclerites **SGP** shape of subgenital plates **SEGP** shape of internal edge of subgenital plate apex **ASP** paramere, shape of primary apical spine **SSP** parameter, shape of secondary subapical spine **PRE** tip of aedeagus spines.

Attribute	Character state	*A. danpecki*	*A. albofasciata*	*A. contigua*	Chi2:	CC**
5.- **EAE**	(1) Tenth and eleventh tergites at the same level on the horizontal.	0	7 (58%)	0		
	(2) Tenth higher than the eleventh tergite, with respect to the horizontal.	10 (100%)	5 (42%)	7 (100%)	143.8*	0.56
6.- **SGP**	(1) Acute apex with straight lateral edges.	10 (100%)	12(100%)	0		
	(2) Apex obliquely truncate with lateral edges slightly concave.	0	0	7 (100%)		
7.- **SEGP**	(1) Acuminate in a pointed lobe.	10 (100%)	0	0		
	(2) Acuminate in a rounded lobe.	0	12 (100%)	0		
	(3) Blunt.	0	0	7 (100%)	300*	0.7
8.- **ASP**	(1) Long and thin spine with a continuous curvature not angulated.	10 (100%)	12 (100%)	0		
	(2) Short and wide spine with a pronounced angulated curvature.	0	0	7 (100%)	300*	0.7
9.- **SSP**	(1) With two rounded acute lobes similar in size and shape.	10 (100%)	0	0		
	(2) With two acute lobes, the dorsal one conspicuously bigger than the ventral.	0	12 (100%)	0		
	(3) With one big lobe.	0	0	7 (100%)	600*	0.81
10.- **PRE**	(1) Conspicuously curved upward.	10 (100%)	0	0		
	(2) Slightly curved upward.	0	12 (100%)	0		
	(3) Slightly curved downward.	0	0	7 (100%)	414*	0.81
	n =	10	11	7		

** CC contingency coefficient: * $p \leq 0.001$ the significance of association of frequency among character states and taxa.

and straight lateral edges (Fig. 2I); secondary subapical spine of parameres in lateral view: two rounded acute lobes similar in size and shape (Fig. 2L); aedeagus in lateral view: spines slightly sinuous, conspicuously curved upward and touching the superior margin of phallobase, tips bent to form an almost 90° angle (Figs 2O, 8A, B).

Aeneolamia albofasciata: dark brown (27%) to black (73%) tegmen (Fig. 1B), the color of internal clavus edge of the same color (85%) or with a yellowish or white line (15%) (Fig. 1E), the anterior third with a conspicuous broad transverse yellowish or white line (100%) (Fig. 1I), and the distal third with a complete broad transverse yellowish or white line (100%) (Fig. 1M) (Table 2); subgenital plates in ventral view: acute apex, acuminate in a rounded lobe and with straight lateral edges (Fig. 2J); secondary subapical spine of parameres lateral view: two acute lobes, the dorsal one conspicuously bigger than the ventral (Fig. 2M); aedeagus lateral view: spines slightly sinuous and tips slightly curved upward (Figs 2P, 8C).

Aeneolamia contigua: light brown (30%) to dark brown (70%) tegmen (Fig. 1C), with an orange or red line in the internal clavus (100%) (Fig. 1F), the anterior third of tegmen with a conspicuous broad transversal orange or red line (100%) (Fig. 1J), and the distal third with a complete broad transversal orange or red line (100%) (Fig. 1N)

(Table 2); subgenital plates in ventral view: obliquely truncate apex with a blunt distal edge and lateral edges slightly concave (Fig. 2K); secondary subapical of parameres in lateral view: with one prominent lobe (Fig. 2N); aedeagus in lateral view: spine sinuous and tips slightly curved downward (Figs 2Q, 8D).

Continuous quantitative morphological characters

Combining morphometric data of both sexes, *Aeneolamia danpecki* is smaller than both *A. albofasciata* and *A. contigua* in most features analyzed except SW_d, and $HRAL_l$ (Table 4). Two-way ANOVA supported significant statistical differences among the species in six features: SL_d ($F_{SLd} = 7.0$; $p_{SLd} \leq 0.001$), Al_v ($F_{Alv} = 4.3$; $p_{Alv} \leq 0.05$), SL_v ($F_{Slv} = 4.3$; $p_{slv} \leq 0.05$), SW_v ($F_{SWv} = 5.4$; $p_{SWv} \leq 0.05$), BLW_v ($F_{BLWv} = 3.9$; $p_{BLWv} \leq 0.05$), LLMPs ($F_{LLMPs} = 3.1$; $p_{LLMPs} \leq 0.05$) (Tables 4, 6); multiple comparisons support that these measurements were lower in *A. danpecki* than in *A. albofasciata* or *A. contigua* (Table 4).

Two-way ANOVA also supported significant statistical differences between sexes in more than 20 features (Tables 5, 6). The interaction of "species" and "sex" factors was considered only to evaluate which features differed between sexes within each species (Tables 5, 6). In *A. danpecki*, 17 features were larger in females than males (HWE_d, HL_d, PW_d, SW_d, SL_d, PL_d, PcW_v, AW_v, SL_v, PCW_v, BLW_v, PCL_l, PW_s, HL_s, HW_s, $LLMP_s$, SRv); in *A. albofasciata* three (AW_v, El_s, PW_s) were larger in females; and in *A. contigua* nine (HWE_d, HL_d, PcW_v, Al_v, AW_v, PCW_v, PcL_v, PCL_l, El_s) were larger in females (Table 5).

Multivariate analysis

The first two principal coordinates of PCoAs of continuous and discrete features of males explained 65% of variations (PCo1 = 39.99%, PCo2 = 15.01%) (Fig. 4A). Scatterplots of these principal coordinates (PCo1 vs. PCo2) showed that the specimens of *A. danpecki* and the other two *Aeneolamia* species fell into discrete phenotypic groups in the multivariate space analysis (Fig. 4A). The PCAs corresponding to the 36 characters combining both sexes ($PCA_{♂♀}$), males alone ($PCA_{♂}$), and females alone ($PCA_{♀}$) explained more than 80% of the total variation in the first two principal components: $PCA_{♂♀}$ = 99% ($PC1_{♂♀}$ = 62.0%, $PC2_{♂♀}$ = 37.0%); $PCA_{♀}$ = 88.5% ($PC1_{♀}$ = 72.5%, $PC2_{♀}$ = 16.0%); $PCA_{♂}$ = 98% ($PC1_{♂}$ = 68.0%, $PC2_{♂}$ = 30.0%). In the corresponding three-dimensional scatter plots, the specimens fell into three clusters in multivariate space corresponding to *A. albofasciata*, *A. contigua*, and *A. danpecki* (data not shown). The CVAs using 36 linear measurements explained more than 90% of the total variation in the first two canonical vectors in the three analyses performed; both sexes ($CVA_{♂♀}$): $CV1_{♂♀}$ = 64%, $CV2_{♂♀}$ = 33%; males alone ($CVA_{♂}$): $CV1_{♂}$ = 81%, $CV2_{♂}$ = 18%; and females alone ($CVA_{♀}$): $CV1_{♀}$ = 86% $CV2_{♀}$ = 13%. The scatter plot between these variables showed that the specimens in well-differentiated phenotypic clusters correspond to *A. albofasciata*, *A. contigua*, and *A. danpecki* (Fig. 4B). Separate analyses by sex ($CVA_{♂}$, $CVA_{♀}$) displayed the clearest segregations of operational taxonomic units in well-defined discrete clusters (Fig. 4C, D); in the multivariate space, the OTUs corresponding to *A. danpecki*

Table 4. Measurements of morphological characteristics of three Mexican *Aeneolamia* spp. as mean ± standard deviation (mm); * Features that display statistically significant differences among species supported by two way ANOVA; in these cases mean values with the same letter were not significantly different at the 5% level by the Tukey test. Abbreviations: **HWE_d** Head width with eyes **HL_d** head length in dorsal view, **PW_d** pronotum width in dorsal view **PL_d** pronotum length in dorsal view **SW_d** scutellum width in dorsal view **SL_d** scutellum length in dorsal view **PcL_v** postclypeus length in ventral view **PCW_v** postclypeus width in ventral view **Al_v** anteclypeus length in ventral view **AW_v** anteclypeus width in ventral view **SL_v** stylet length in ventral view **SW_v** stylet width in ventral view **PcW_v** posterior coxa width in ventral view **PcL_v** posterior coxa length in ventral view **BLW_v** body length without wings in ventral view **PCL_l** postclypeus length in lateral view **PCW_l** postclypeus width in lateral view **EL_l** eye length in lateral view **Ew_l** eye width in lateral view **HL_l** head length in lateral view **HW_l** head width in lateral view **$LLMP_l$** length of lateral margin pronotum in lateral view **BL_l** body length including wings in lateral view **LAW_l** length of the anterior wing in lateral view **WLH_d** width-length radio of head in dorsal view **WLP_d** width-length ratio of pronotum in dorsal view **WLS_d** width-lengh radio of scutellum in dorsal view **WLC_v** width-length radio of clypeus **PR_v** postclypeus ratio in ventral view (width/length) **SR_v** stylet ratio in ventral view (width/length) **RCR_v** coxa ratio (width/length) **RBW_l** ratio between body length with wings and length without wings **RPC_l** postclypeus radio in lateral view (width/length) **REl** eye ratio in lateral view (width/length) **$HRAL_l$** head ratio in lateral view (width/length) **BLW_l** ratio between the length of body with wings and forewing length in lateral view.

Attribute Abbreviation (mm)	*A. danpecki*	*A. albofasciata*	*A. contigua*
11.-**HWE_d**	1.90 ± 0.07	2.04 ± 0.03	1.96 ± 0.07
12.-**HL_d**	0.87 ± 0.03	0.94 ± 0.01	0.91 ± 0.04
13.-**PW_d**	2.73 ± 0.10	2.90 ± 0.04	2.81 ± 0.10
14.-**PL_d**	1.62 ± 0.06	1.75 ± 0.02	1.68 ± 0.06
15.-**SW_d**	1.24 ± 0.05	1.18 ± 0.01	1.14 ± 0.04
16.-**SL_d***	1.43^{c} ± 0.05	1.57^{b} ± 0.02	1.61^{a} ± 0.02
17.-**PcL_V**	1.24 ± 0.04	1.30 ± 0.02	1.22 ± 0.04
18.-**PCW_v**	0.83 ± 0.05	0.83 ± 0.02	0.77 ± 0.03
19.-**Al_v***	0.70^{b} ± 0.02	0.76^{a} ± 0.01	0.78^{a} ± 0.03
20.-**AW_v**	0.48 ± 0.02	0.53 ± 0.02	0.48 ± 0.02
21.-**SL_v***	0.76^{b} ± 0.03	0.77^{b} ± 0.01	0.82^{a} ± 0.01
22.-**SW_v***	0.19^{b} ± 0.00	0.22^{a} ± 0.01	0.21^{a} ± 0.01
23.-**PcW_v**	0.49 ± 0.02	0.54 ± 0.01	0.52 ± 0.02
24.-**PcL_v**	0.59 ± 0.02	0.62 ± 0.01	0.59 ± 0.02
25.-**BLW_v***	6.33^{c} ± 0.23	7.01^{a} ± 0.09	6.67^{b} ± 0.23
26.-**PCL_l**	0.73 ± 0.03	0.76 ± 0.02	0.71 ± 0.02
27.-**PCW_l**	1.17 ± 0.04	1.24 ± 0.03	1.18 ± 0.02
28.-**El_l**	0.47 ± 0.02	0.51 ± 0.01	0.49 ± 0.02
29.-**Ew_l**	0.63 ± 0.02	0.68 ± 0.01	0.67 ± 0.02
30.-**HL_l**	0.90 ± 0.03	0.92 ± 0.02	0.87 ± 0.03
31.-**HW_l**	1.34 ± 0.05	1.40 ± 0.02	1.38 ± 0.02
32.-**$LLMP_l$***	0.65^{c} ± 0.03	0.72^{a} ± 0.02	0.68^{b} ± 0.02
33.-**BL_l**	7.91 ± 0.27	8.21 ± 0.12	8.21 ± 0.28
34.-**LAW_l**	6.42 ± 0.22	6.57 ± 0.08	6.64 ± 0.22
35.-**WLH_d**	0.14 ± 0.00	0.14 ± 0.00	0.13 ± 0.01
36.-**WLP_d**	0.10 ± 0.00	0.11 ± 0.00	0.10± 0.00
37.-**WLS_d**	0.05 ± 0.00	0.05 ± 0.00	0.05 ± 0.00
38.-**WLC_v**	0.09 ± 0.00	0.10 ± 0.00	0.1 ± 0.00
39.-**PR_v**	0.09 ± 0.00	0.10 ± 0.00	0.1 ± 0.00

Attribute Abbreviation (mm)	*A. danpecki*	*A. albofasciata*	*A. contigua*
40.-SR_v	0.25 ± 0.01	0.24 ± 0.00	0.25 ± 0.01
41.-RCR_v	0.05 ± 0.00	0.06 ± 0.00	0.05 ± 0.00
42.-RBW_l	0.08 ± 0.00	0.08 ± 0.00	0.07 ± 0.00
43.-RPC_l	0.04 ± 0.00	0.04 ± 0.00	0.03 ± 0.00
44.-RE_l	0.05 ± 0.00	0.05 ± 0.00	0.04 ± 0.00
45.-$HRAL_l$	0.05 ± 0.00	0.04 ± 0.00	0.04 ± 0.00
46.-BLW_l	0.08 ± 0.00	0.08 ± 0.00	0.07 ± 0.00

Table 5. Measurements of morphological characteristics of three Mexican *Aeneolamia* spp. (Mean and standard deviation (mm)); * Features that display significant statistical differences among interaction species-sexes supported by two-way ANOVA, in each species, mean values with the same letter were not significantly different at the 5% level by Tukey test. Abbreviations: HWE_d Head width with eyes HL_d head length in dorsal view, PW_d pronotum width in dorsal view PL_d pronotum length in dorsal view SW_d scutellum width in dorsal view SL_d scutellum length in dorsal view PcL_v postclypeus length in ventral view PCW_v postclypeus width in ventral view Al_v anteclypeus length in ventral view AW_v anteclypeus width in ventral view SL_v stylet length in ventral view SW_v stylet width in ventral view PcW_v posterior coxa width in ventral view PcL_v posterior coxa length in ventral view BLW_v body length without wings in ventral view PCL_l postclypeus length in lateral view PCW_l postclypeus width in lateral view EL_l eye length in lateral view Ew_l eye width in lateral view HL_l head length in lateral view HW_l head width in lateral view $LLMP_l$ length of lateral margin pronotum in lateral view BL_l body length including wings in lateral view LAW_l length of the anterior wing in lateral view WLH_d width-length radio of head in dorsal view WLP_d width-length ratio of pronotum in dorsal view WLS_d width-lengh radio of scutellum in dorsal view WLC_v width-length radio of clypeus PR_v postclypeus ratio in ventral view (width/length) SR_v stylet ratio in ventral view (width/length) RCR_v coxa ratio (width/length) RBW_l ratio between body length with wings and length without wings RPC_l postclypeus radio in lateral view (width/length) RE_l eye ratio in lateral view (width/length) $HRAL_l$ head ratio in lateral view (width/length) BLW_l ratio between the length of body with wings and forewing length in lateral view.

Attribute	*A. danpecki*		*A. albofasciata*		*A. contigua*	
Acronym (mm)	♀	♂	♀	♂	♀	♂
11.-HWE_d*	2.06^a ± 0.01	1.75^b ± 0.12	2.13 ± 0.028	1.95 ± 0.04	2.11^a ± 0.02	1.81^b ± 0.12
12.-HL_d*	0.95^a ± 0.01	0.79^b ± 0.05	1.00 ± 0.014	0.89 ± 0.01	1.02^a ± 0.05	0.81^b ± 0.06
13.-PW_d*	2.95^a ± 0.03	2.50^b ± 0.17	3.01 ± 0.039	2.78 ± 0.05	3.00 ± 0.04	2.62 ± 0.18
14.-PL_d	1.74 ± 0.02	1.49 ± 0.10	1.82 ± 0.028	1.68 ± 0.03	1.80 ± 0.02	1.57 ± 0.11
15.-SW_d*	1.35^a ± 0.04	1.13^b ± 0.08	1.23 ± 0.015	1.13 ± 0.02	1.20 ± 0.02	1.09 ± 0.08
16.-SL_d*	1.58^a ± 0.03	1.28^b ± 0.09	1.64 ± 0.031	1.49 ± 0.02	1.61 ± 0.02	1.44 ± 0.11
17.-PcL_V*	1.35^a ± 0.01	1.13^b ± 0.08	1.37 ± 0.028	1.22 ± 0.02	1.29 ± 0.03	1.15 ± 0.08
18.-PCW_v*	0.97^a ± 0.06	0.69^b ± 0.05	0.91 ± 0.025	0.75 ± 0.02	0.85^a ± 0.03	0.70^b ± 0.05
19.-Al_v*	0.74 ± 0.01	0.66 ± 0.05	0.79 ± 0.019	0.73 ± 0.02	0.86^a ± 0.01	0.72^b ± 0.05
20.-AW_v*	0.54^a ± 0.01	0.42^b ± 0.03	0.58^a ± 0.025	0.47^b ± 0.01	0.55^a ± 0.01	0.43^b ± 0.03
21.-SL_v*	0.82^a ± 0.02	0.71^b ± 0.05	0.81 ± 0.021	0.73 ± 0.01	0.84 ± 0.02	0.75 ± 0.06
22.-SW_v	0.20 ± 0.00	0.20 ± 0.00	0.23 ± 0.009	0.21 ± 0.00	0.23 ± 0.01	0.19 ± 0.01
23.-PcW_v*	0.55^a ± 0.01	0.43^b ± 0.03	0.58 ± 0.011	0.50 ± 0.01	0.57^a ± 0.01	0.43^b ± 0.04
24.-PcL_v*	0.64 ± 0.01	0.55 ± 0.04	0.65 ± 0.013	0.59 ± 0.02	0.64^a ± 0.01	0.50^b ± 0.05
25.-BLW_v*	6.91^a ± 0.08	5.70^b ± 0.39	7.27 ± 0.115	6.74 ± 0.11	7.15 ± 0.10	6.21 ± 0.43
26.-PCL_l*	0.79^a ± 0.02	0.68^b ± 0.05	0.85^a ± 0.017	0.67^b ± 0.00	0.78^a ± 0.02	0.66^b ± 0.02
27.-PCW_l*	1.27^a ± 0.02	1.07^b ± 0.07	1.32^a ± 0.033	1.16^b ± 0.03	1.22 ± 0.02	1.14 ± 0.03
28.-El_l*	0.50 ± 0.01	0.44 ± 0.03	0.54 ± 0.008	0.48 ± 0.01	0.54^a ± 0.01	0.45^b ± 0.03

Attribute	*A. danpecki*		*A. albofasciata*		*A. contigua*	
Acronym (mm)	♀	♂	♀	♂	♀	♂
29.-Ew_l*	0.68 ± 0.01	0.61 ± 0.04	0.71^a ± 0.010	0.65^b ± 0.01	0.73 ± 0.01	0.63 ± 0.04
30.-HL_l*	0.98^a ± 0.02	0.83^b ± 0.06	0.98 ± 0.019	0.86 ± 0.01	0.95 ± 0.01	0.81 ± 0.06
31.-HW_l*	1.47^a ± 0.01	1.22^b ± 0.08	1.48 ± 0.033	1.33 ± 0.02	1.45 ± 0.02	1.32 ± 0.02
32.-$LLMP_l$*	0.72^a ± 0.02	0.58^b ± 0.04	0.76 ± 0.020	0.68 ± 0.02	0.73 ± 0.02	0.63 ± 0.04
33.-BL_l*	8.39^a ± 0.07	7.45^b ± 0.51	8.56 ± 0.125	7.85 ± 0.16	8.66^a ± 0.11	7.79^b ± 0.54
34.-LAW_l*	6.81^a ± 0.04	6.04^b ± 0.42	6.84 ± 0.075	6.31 ± 0.10	6.94 ± 0.06	6.35 ± 0.44
35.-WLH_d	0.14 ± 0.00	0.15 ± 0.00	0.14 ± 0.002	0.15 ± 0.00	0.14 ± 0.00	0.14 ± 0.01
36.-WLP_d	0.11 ± 0.00	0.11 ± 0.00	0.11 ± 0.001	0.11 ± 0.00	0.11 ± 0.00	0.10 ± 0.01
37.-WLS_d	0.06 ± 0.00	0.06 ± 0.00	0.05 ± 0.003	0.05 ± 0.00	0.05 ± 0.00	0.05 ± 0.00
38.-WLC_v	0.10 ± 0.00	0.10 ± 0.01	0.10 ± 0.002	0.11 ± 0.00	0.10 ± 0.00	0.11 ± 0.01
39.-PR_v	0.09 ± 0.00	0.10 ± 0.01	0.09 ± 0.003	0.10 ± 0.00	0.11 ± 0.00	0.10 ± 0.01
40.-SR_v	0.27^a ± 0.01	0.23^b ± 0.02	0.24 ± 0.007	0.24 ± 0.01	0.25 ± 0.01	0.25 ± 0.02
41.-RCR_v*	0.06^a ± 0.00	0.05^b ± 0.00	0.06 ± 0.001	0.06 ± 0.00	0.06^a ± 0.00	0.05^b ± 0.01
42.-RBW_l	0.08 ± 0.00	0.08 ± 0.01	0.08 ± 0.001	0.08 ± 0.00	0.08 ± 0.00	0.08 ± 0.01
43.-RPC_l	0.04 ± 0.00	0.04 ± 0.00	0.04 ± 0.001	0.04 ± 0.00	0.04 ± 0.00	0.04 ± 0.00
44.-RE_l	0.05 ± 0.00	0.04 ± 0.00	0.05 ± 0.001	0.05 ± 0.00	0.05 ± 0.00	0.05 ± 0.00
45.-$HRAL_l$	0.05 ± 0.00	0.05 ± 0.00	0.04 ± 0.001	0.04 ± 0.00	0.04 ± 0.00	0.04 ± 0.00
46.-BLW_l	0.08 ± 0.00	0.08 ± 0.00	0.08 ± 0.001	0.08 ± 0.00	0.08 ± 0.00	0.08 ± 0.01

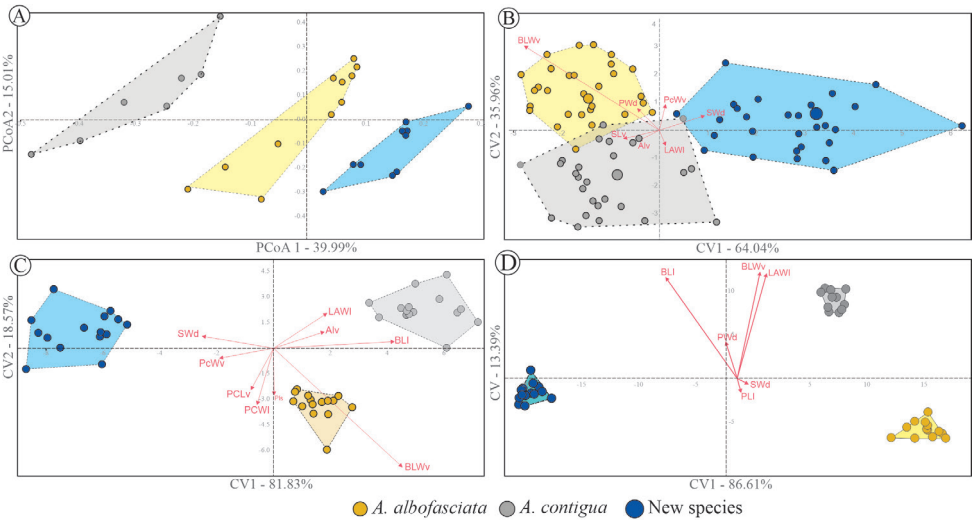

Figure 4. Scatter plots of ordination analyses to evaluate the morphological variation of Mexican *Aeneolamia* spp.: **A** principal coordinate analysis using the 10 discrete (male tegmina color pattern and male genitalia) and 36 continuous features of males **B** analysis of canonical variation with 36 morphological continuous features of both sexes **C** females **D** males. In the center of the scatter plot, vectors corresponding to the contribution of the traits in the multivariate space (**B, C, D**). The largest circles are the centroid of the polygons (B). Abbreviations: **Al_v** Anteclypeus length in ventral view **BL_s** body length without wings in ventral view **BLW_v** body length without wings in ventral view **LAW_l** length of the anterior wing in lateral view **PCW_v** postclypeus width in ventral view **PL_d** postclypeus length in dorsal view **PW_d** pronotum width in dorsal view **PcW_s** postclypeus width in lateral view **SW_d** scutellum width in dorsal view **SL_v** stylet length in ventral view.

were the most distant and therefore more morphologically distinct from *A. albofasciata* and *A. contigua* than they were from one another. PERMANOVA supported statistically significant differences among groups displayed in $CVA_{♂♀}$ ($R_{♂♀}$ = 0.094; $p \leq 0.001$), $CVA_{♂}$ ($R_{♂}$ = 0.094; $p \leq 0.001$), $CVA_{♀}$ ($R_{♀}$ = 0.094; $p_{♀} \leq 0.001$); pairwise comparisons supported differences among all constraints in the analyses of males and females alone: *A. danpecki* vs. *A. albofasciata* ($p_{♀} \leq 0.001$, $p_{♂} \leq 0.001$); *A. danpecki* vs. *A. contigua* ($p_{♀} \leq 0.05$, $p_{♂} \leq 0.001$), and *A. albofasciata* vs. *A. contigua* ($p_{♀} = 0.1$, $p_{♂} \leq 0.05$); meanwhile, in the analysis of males and females together, multiple comparisons did not support differences between *A. albofasciata* vs. *A. contigua* ($p_{♂♀} = 0.1$). In the $CVA_{♂♀}$ the discriminant function correctly classified 95.2% of OTUs according to the group to which they belong: one male of the new species was incorrectly classified as *A. contigua*, two males of *A. albofasciata* were classified as females of both *A. danpecki* and *A. contigua*, and one male of *A. contigua* was classified as *A. albofasciata*. Discriminant functions, analyzing the sexes separately, correctly classified 100% of the OTUs in both $CVA_{♂}$ and $CVA_{♀}$.

Geometric morphometry of aedeagus

The superimposition of 15 aedeagus spine configurations of *Aeneolamia* members (*A. albofasciata*, *n* = 5; *A. contigua*, *n* = 6; *A. danpecki*, *n* = 4) showed that shape variation is found on both proximal and medial regions (Fig. 5). The first three Rws explained 96.8% of total variation (Rw1 = 79.8%; Rw2 = 13.6%; Rw3 = 3.4%). The respective two-dimensional

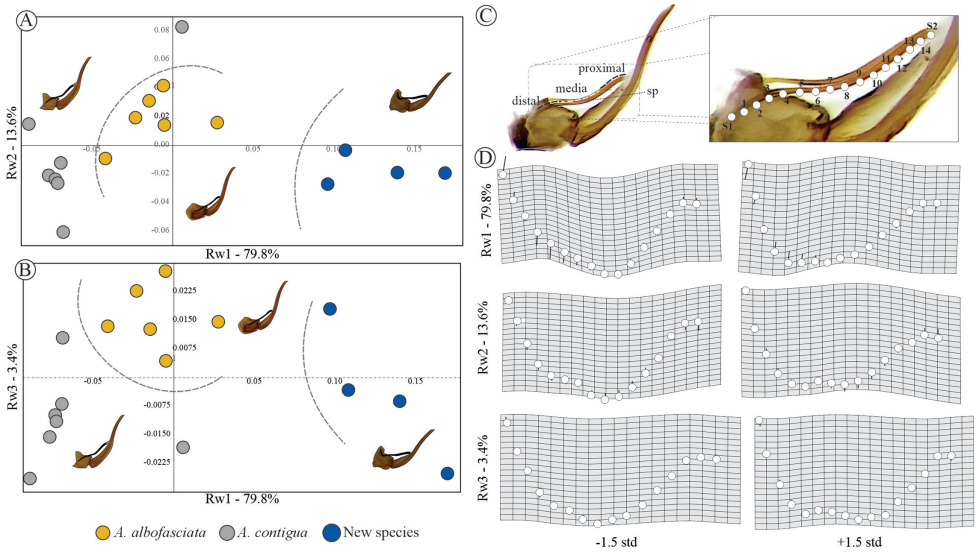

Figure 5. Scatter plots among the first three relative warps with its respective deformation grids ± 1.5 SD, corresponding to shape analysis of aedeagus spine (sp) of Mexican *Aeneolamia* spp. **A** Rw1 vs. Rw2 **B** Rw1 vs. Rw3 **C** position of landmarks (S1 and S2) and semi-landmarks (1–14) on aedeagus spine of *A. contigua* **D** deformation grids ± 1.5 SD.

Table 6. Results from two-way ANOVA to compare the variation of measurements of morphological characteristics of three Mexican *Aeneolamia* spp. Abbreviations: **HWE_d** Head width with eyes **HL_d** head length in dorsal view, **PW_d** pronotum width in dorsal view **PL_d** pronotum length in dorsal view **SW_d** scutellum width in dorsal view **SL_d** scutellum length in dorsal view **PcL_v** postclypeus length in ventral view **PCW_v** postclypeus width in ventral view **Al_v** anteclypeus length in ventral view **AW_v** anteclypeus width in ventral view **SL_v** stylet length in ventral view **SW_v** stylet width in ventral view **PcW_v** posterior coxa width in ventral view **PcL_v** posterior coxa length in ventral view **BLW_v** body length without wings in ventral view **PCL_l** postclypeus length in lateral view **PCW_l** postclypeus width in lateral view **EL_l** eye length in lateral view **Ew_l** eye width in lateral view **HL_l** head length in lateral view **HW_l** head width in lateral view **$LLMP_l$** length of lateral margin pronotum in lateral view **BL_l** body length including wings in lateral view **LAW_l** length of the anterior wing in lateral view **WLH_d** width-length radio of head in dorsal view **WLP_d** width-length ratio of pronotum in dorsal view **WLS_d** width-lengh radio of scutellum in dorsal view **WLC_v** width-length radio of clypeus **PR_v** postclypeus ratio in ventral view (width/length) **SR_v** stylet ratio in ventral view (width/length) **RCR_v** coxa ratio (width/length) **RBW_l** ratio between body length with wings and length without wings **RPC_l** postclypeus radio in lateral view (width/length) **REl** eye ratio in lateral view (width/length) **$HRAL_l$** head ratio in lateral view (width/length) **BLW_l** ratio between the length of body with wings and forewing length in lateral view.

Acronym	Species		Sex		Interaction	
	F	*P*	*F*	*P*	*F*	*P*
11.-**HWE_d**	1.744	0.181	18.75	4.09E-05	0.5288	0.5913
12.-**HL_d**	1.69	0.191	24.43	3.89E-06	0.7839	0.4599
13.-**PW_d**	1.261	0.289	16.7	9.95E-05	0.532	0.5894
14.-**PL_d**	2.074	0.132	15.43	0.0001752	0.4199	0.6585
15.-**SW_d**	2.127	0.126	12.87	0.0005607	0.9456	0.3925
16.-**SL_d**	7.015	0.002	24.03	4.64E-06	3.41	0.03773
17.-**PcL_V**	1.247	0.293	17.76	6.27E-05	0.3953	0.6747
18.-**PCW_v**	1.284	0.282	37.3	3.03E-08	1.751	0.1799
19.-**Al_v**	4.34	0.016	14.45	0.000272	0.8141	0.4465
20.-**AW_v**	2.79	0.067	41.35	7.38E-09	0.07588	0.927
21.-**SL_v**	3.333	0.041	14.03	0.0003309	0.9593	0.3874
22.-**SW_v**	5.43	0.006	10.72	0.001547	0.362	0.6974
23.-**PcW_v**	2.785	0.068	35.9	5.47E-08	0.5938	0.5546
24.-**PcL_v**	0.8573	0.428	16.48	0.0001129	0.5701	0.5677
25.-**BLW_v**	3.915	0.024	19.2	3.38E-05	0.923	0.4013
26.-**PCL_l**	1.625	0.203	40.45	1.01E-08	1.033	0.3603
27.-**PCW_l**	2.054	0.135	23.38	5.94E-06	1.596	0.2088
28.-**El_l**	2.106	0.128	18.46	4.65E-05	0.4292	0.6524
29.-**Ew_l**	1.037	0.359	12.17	0.0007772	0.2618	0.7703
30.-**HL_l**	0.7906	0.457	22.52	8.46E-06	0.06886	0.9335
31.-**HW_l**	1.068	0.348	30.43	3.75E-07	1.291	0.2803
32.-**$LLMP_l$**	3.131	0.049	22.86	7.33E-06	0.6679	0.5155
33.-**BL_l**	0.5747	0.565	10.47	0.001739	0.06293	0.939
34.-**LAW_l**	0.3988	0.672	9.184	0.003245	0.1178	0.889
35.-**WLH_d**	0.2057	0.815	0.1278	0.7216	0.4334	0.6498
36.-**WLP_d**	0.2475	0.781	2.128	0.1484	0.543	0.583
37.-**WLS_d**	1.834	0.166	1.272	0.2626	0.02747	0.9729
38.-**WLC_v**	0.7389	0.481	2.875	0.09368	0.02094	0.9793
39.-**PR_v**	2.144	0.124	2.638	0.1081	1.154	0.3202
40.-**SR_v**	2.506	0.088	1.278	0.2615	4.683	0.01183
41.-**RCR_v**	2.852	0.063	9.638	0.002617	0.9715	0.3828
42.-**RBW_l**	1.17	0.315	0.551	0.46	0.3265	0.7223

Acronym	Species		Sex		Interaction	
	F	***P***	***F***	***P***	***F***	***P***
43.-**RPC**$_1$	0.4304	0.652	2.741	0.1015	0.1586	0.8536
44.-**RE**$_1$	2.267	0.11	2.545	0.1144	1.71	0.1871
45.-**HRAL**$_1$	0.2143	0.808	0.381	0.5388	0.4524	0.6377
46.-**BLW**$_1$	0.8206	0.444	2.027	0.1582	0.6383	0.5307

scatterplot of these RWs displays three discrete groups corresponding to the three species (Fig. 5A, B). The deformations in the components Rw1, Rw2, and Rw3 were related to the curvature degree of proximal, medial, and distal areas of the spine, respectively (Fig. 5C, D). Specimens of *A. danpecki* showed a conspicuously curved proximal region upwardly bent to form an almost 90° angle, as was described in the character PRE.

Because our analyses support qualitative and quantitative discrete phenotypic variation among *Aeneolamia* species (two tegmina features characters and five genitalia ones) and the most pronounced morphological differences compared to the previously recognized species *A. albofasciata* and *A. contigua*, the specimens of the new species are grouped into a new taxon, *Aeneolamia danpecki* Castro, Armendáriz, Utrera, sp. nov., described below.

***Aeneolamia danpecki* Castro, Armendáriz & Utrera, sp. nov.**
https://zoobank.org/7F8549F1-109F-4DA1-871C-0D95B2E3FD39
Figures 6, 7

Type material. ***Holotype.*** HOM-TIP-166, 1 ♂ adult, coll. U. Castro-Valderrama and Youssef Utrera-Vélez leg., 28 September 2003, on *Paspalum* sp., Sola de Vega, 16°27'44.48"N, 97°1'25.73"W, 1715 m a.s.l., Oaxaca state, Mexico. Pinned adult deposited in CNIN (Fig. 6).

Paratypes. HOM-TIP-167, 1 ♀, same data as holotype; 1 ♀, coll. Cervantes, A. Delgado, C. Mayorga, S. Gámez leg.; 5 km W San Martín Lachila, Mpio Zimatlán, Oaxaca, México, 16°35'39.18"N, 96°52'14.16"W, 12 July 2004. Pinned specimens deposited in CNIN. HOM-TIP-167, 32 ♀, 14 ♂ same data as holotype; 9 ♀, 6 ♂, coll. J. Romero Nápoles leg., 28 August 2018, on *Pennisetum* sp., La Trinidad Zaachila, Oaxaca, México, 16°55'03.84"N, 96°46'07.02"W, 1507 m a.s.l. Pinned specimens deposited in CEAM.

Etymology. The epithet is a noun in the nominative singular standing in apposition to the genus *Aeneolamia*, in honor of Dr. Daniel C. Peck for his contributions to the knowledge of Cercopidae and his friendship with UC-V.

Diagnosis. *Aeneolamia danpecki* Castro, Armendáriz, Utrera, sp. nov. is assigned to the genus *Aeneolamia* by virtue of its tubular aedeagus with a single pair of slender spines attached anteriorly near the middle of the shaft. It can be distinguished from the other known Mexican species of *Aeneolamia* by the following combination of characters: tegmen dark brown to black, with two incomplete and barely visible transverse bands, one oblique band on the basal third, and another straight band on the distal

third or only basal band visible or both absent (Figs 6, 7); the apex of subgenital plates acute with an acuminate pointed lobe and straight lateral edges (Fig. 2I), the primary apical spine of parameres long and thin spine with a continuous curvature that is not angulated (Fig. 2F) and secondary subapical spine of parameres with two rounded acute lobes similar in size and shape (Fig. 2L); aedeagus spines slightly sinuous conspicuously curved upward and touching the superior margin of phallobase, tips bent to form an almost 90° angle (Figs 2O, 8A, B).

Description. Male measurements. Lateral view length (N = 15) 7.45 ± 0.51 mm; width of head in dorsal view (N = 15) 1.75 ± 0.12 mm.

Head. Dorsal view (Fig. 6A, D): black with brown setae; eyes black (discolored in figures); vertex black with median carina that originates in posterior margin of head and extends to tylus, a small depression between eye and median carina elongated and black,

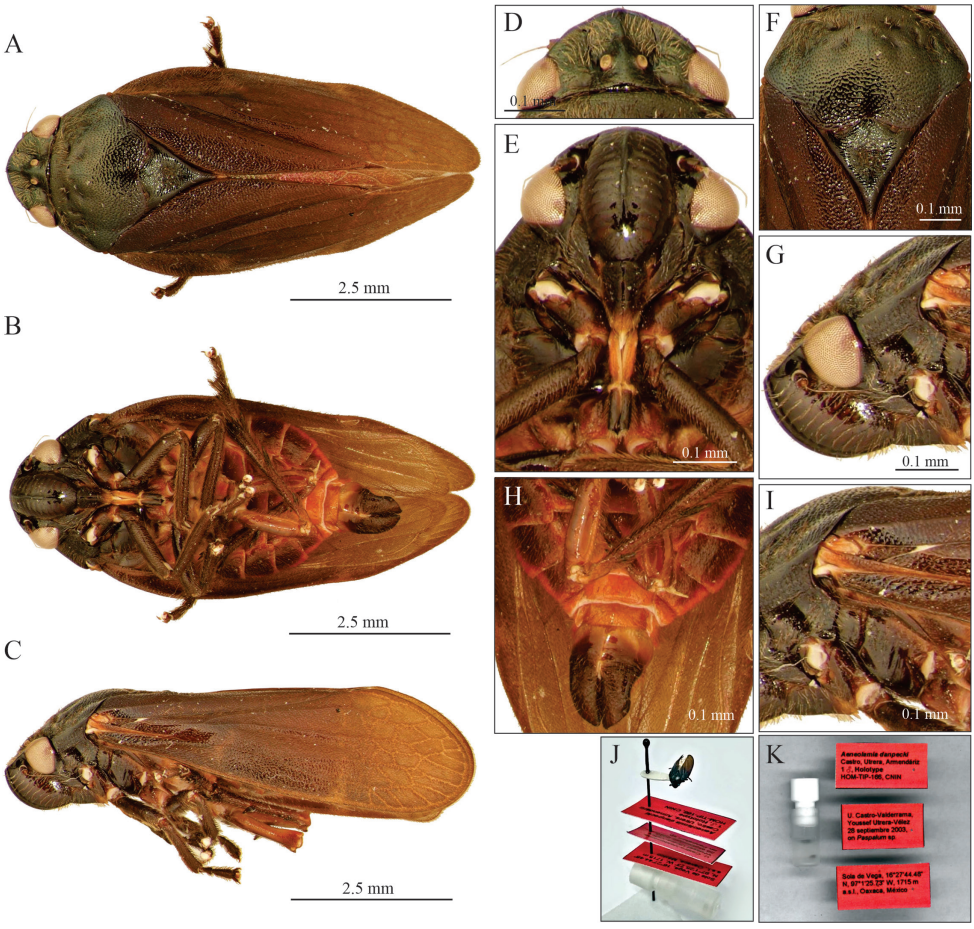

Figure 6. Male adult of *A. danpecki* (Holotype). Sola de Vega, Oaxaca **A** dorsal view **B** ventral view **C** lateral view **D** head in dorsal view **E** head in ventral view **F** prothorax in dorsal view **G** head in lateral view **H** abdomen in ventral view **I** anterior section of wing **J** mounted holotype **K** genital vial and labels of holotype.

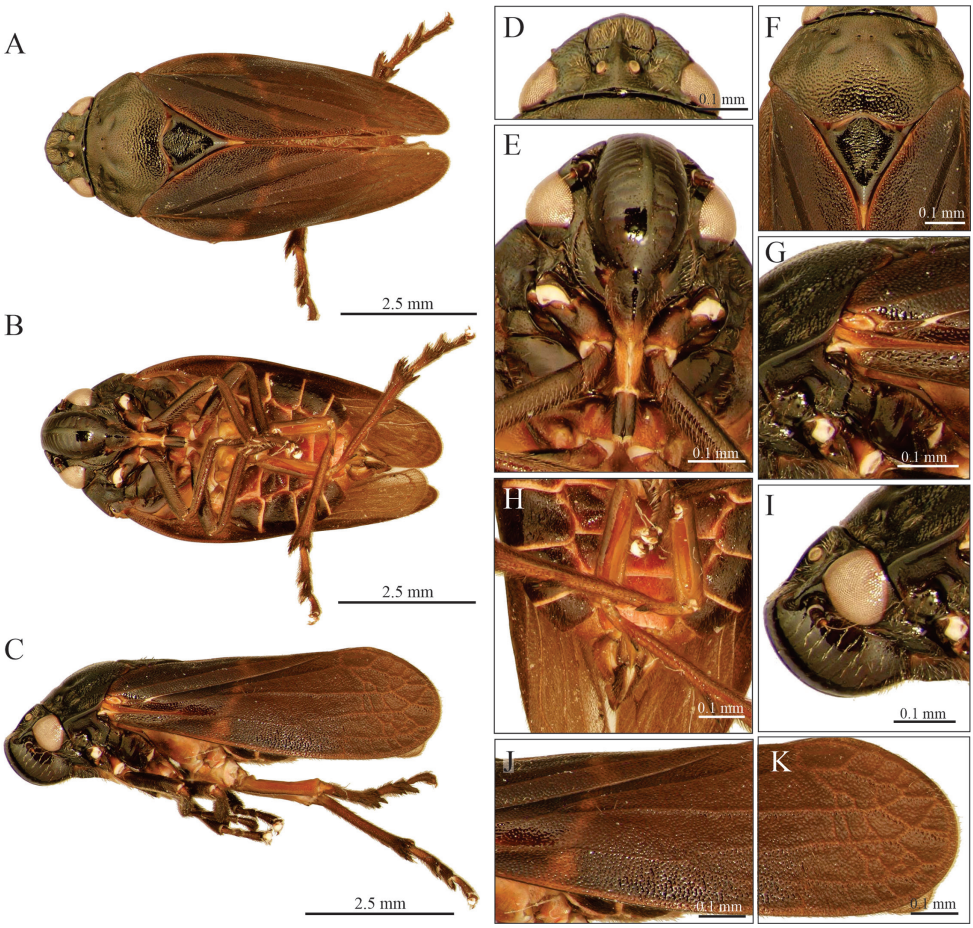

Figure 7. Female adult of *A. danpecki* (Paratype). Sola de Vega, Oaxaca **A** dorsal view **B** ventral view **C** lateral view **D** head in dorsal view **E** head in ventral view **F** prothorax in dorsal view **G** anterior section of wing **H** abdomen in ventral view **I** head in lateral view **J** median section of wing **K** distal section of wing.

without setae, ocelli as close to each other as width of an ocellus; tylus quadrangular and black, with median carina. Ventral view (Fig. 6B, E): postclypeus black, inflated, with median carina black; anteclypeus black; basal segment of rostrum light brown in middle with black sides, distal segment black, reaching mesocoxae; antennae with scape and pedicel black to light brown, basal body of flagellum light brown, setae on pedicel scarce, flagellum brown, basal body of flagellum subcylindrical, smaller than pedicel and with arista. Lateral view (Fig. 6C, G): postclypeus black, convex, lateral grooves slightly marked.

Thorax. Dorsal view (Fig. 6A, F): pronotum black with brown setae, punctate, hexagonal shape without carina, anterior zone with irregular depressed areas, one on each side, anterior margin straight, lateral anterior margin straight, lateral posterior margin slightly grooved, posterior margin grooved. Scutellum black, apex light brown in some specimens. Ventral view (Fig. 6B, E): with hind wing transparent light brown,

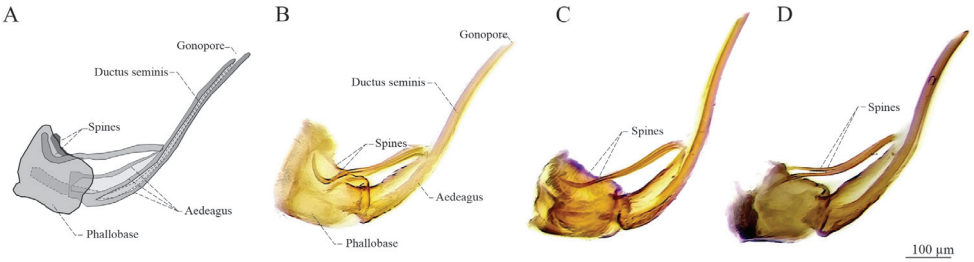

Figure 8. Lateral view of aedeagus of Mexicans *Aeneolamia* spp. **A, B** *A. danpecki* (paratype) **C** *A. albofasciata* **D** *A. contigua*.

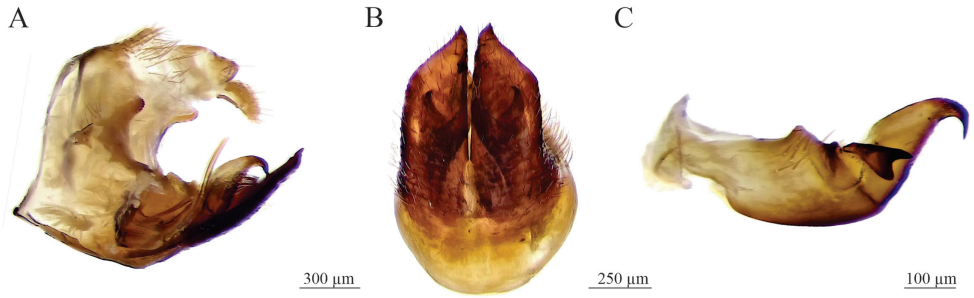

Figure 9. Genitalia of *A. danpecki* (paratype). Sola de Vega, Oaxaca **A** pygofer with phallobase, aedeagus and left paramere, lateral internal view **B** subgenital plates and parameres, ventral view **C** left paramere, lateral external view.

venation brown-reddish, setae on both faces light brown; prosternum black to light brown, mesosternum black to light brown, metasternum light brown to reddish; fore legs dark brown, and meddle legs dark brown, with trochanters dark brown to light brown; hind legs with coxae, trochanters, femurs light brown with reddish tints or reddish, tibiae and tarsi dark brown to black; tibiae with two lateral spines and an apical crown with two rows of spines, basal spine small, distal spine 2 × longer than basal one, basal spine same size as apical crown spines; basitarsus with two rows of spines covered with scarce setae. Lateral view (Fig. 6C, I): pronotum not curved; tegmen dark brown to black, with two incomplete and barely visible transverse bands, one oblique band on basal third and another straight band on distal third or only basal band visible or both absent, the junction between Cu and R brown.

Abdomen. Ventral view (Fig. 6B, H): black, except posterior and lateral edges of each sternite reddish, last sternite reddish and subgenital plates black or dark brown.

Genitalia. Pygofer in lateral view (Figs 2C, 9A): lateral digital process, superior and inferior margins subequal in length, at the level of the inferior margin of the anal tube with the apex directed forward to the anal tube; subgenital plates in ventral view (Figs 2I, 9B) with lateral edge straight, interior margins parallel, not touching distally, wide along almost entire length, but not truncated apex, with shape acute, and tip acuminate with small hook. Paramere in lateral view (Fig. 9A, C): resting on subgenital

plates, basal two-thirds broad and last third curved and tapered at tip to form a long hook, with two dorsal processes, one rounded mesal process with setae, another small process where the primary apical spine like-hook and the lateral secondary subapical spine converge, the primary apical spine long and slender with a continuous non-angulated curvature, sharp point and sclerotized; the lateral secondary subapical spine with two rounded lobes similar in size and shape, superior lobe sclerotized; inferior margin straight, distally curved to form a long spine like-hook. Aedeagus in antero-dorsal view (Fig. 2R): bottle-shape with a thin apex, two thin, sinuous spines touching phallobase, tips as small hooks and hugging phallobase. Aedeagus in lateral view (Figs 2C, O, 8A, B, 9A): tubular, wide at base, abruptly narrowed where two lateral spines join shaft, lateral slightly sinuous spines touching superior margin of phallobase, and tips bent to form an almost 90° angle, apex acute, gonopore apical.

Female measurements. Lateral view length (N = 15) 8.39 ± 0.07 mm; width of head in dorsal view (N = 15) 2.06 ± 0.01 mm. Same characteristics as the male, except larger and posterior and lateral edges of each sternite light brown or reddish (Fig. 7A–K).

Distribution. Oaxaca state, Mexico (Fig. 10).

Host. *Paspalum* sp. and *Pennisetum* sp.

Remarks. *Aeneolamia danpecki* has black or dark brown subgenital plates with an acute end. In the type of material, San Martín Lachila is a municipality and not part

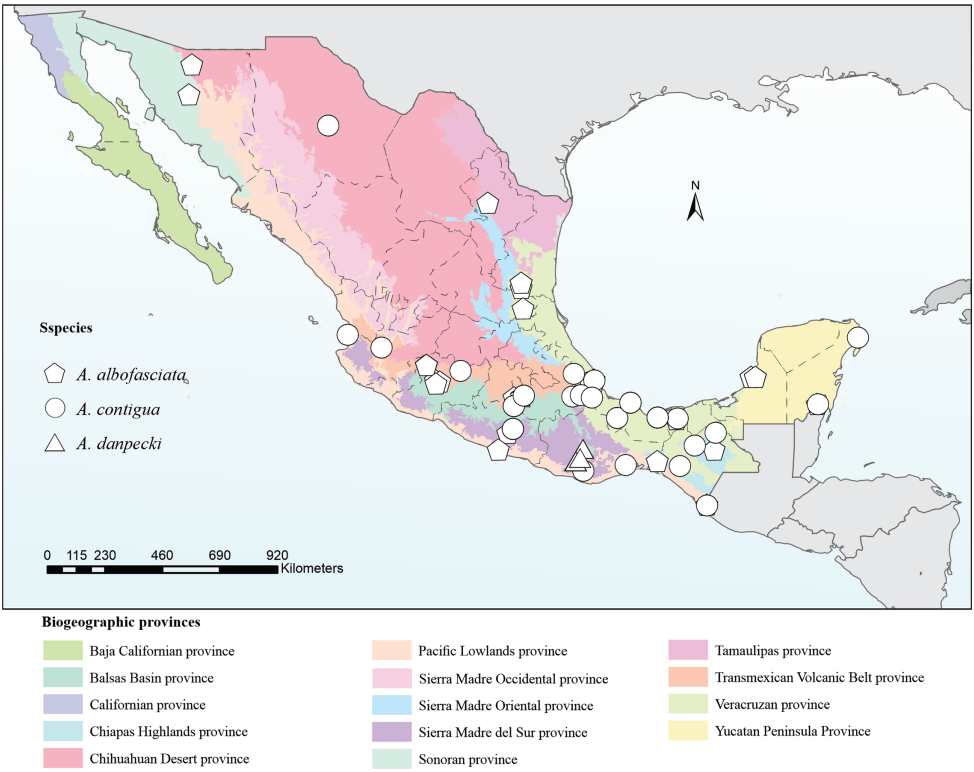

Figure 10. Geographical records of the three Mexican *Aeneolamia* species.

of the Municipality of Zimatlán. *Aeneolamia danpecki* was recognized as distinct for the first time as "*Aeneolamia* aff. *albofasciata* (Lallemand, 1939)" by López-Posadas (2021: 63).

Key to species and subspecies of *Aeneolamia* Fennah, 1949 from Mexico (based on Armendáriz-Toledano et al. 2022)

1 Apex of subgenital plates obliquely truncate (Fig. 2K)..... 2
– Apex of the subgenital plates acute (Fig. 2I, J)..... 3
2 Tegmen light brown to dark brown, with two orange transverse lines (Fig. 1J, N), with orange lines on claval edges V-shaped (Fig. 1F)..... .....***A. contigua*** **(Walker, 1851)**
– Tegmen black with narrow oblique transverse basal line interrupted at claval suture, a distal line straight, with lines on claval edges V-shaped (see Armendáriz-Toledano et al. 2022, fig. 13b); lines red in males, dark red in females..... .....***A. contigua campecheana*** **Fennah, 1951**
3 Tegmen dark brown to black, with one or two yellowish or white transverse lines (Fig. 1I, M), sometimes accompanied by lines on claval edges V-shaped (Fig. 1E), the secondary subapical spine of parameres with two acute lobes, the dorsal one conspicuously bigger than the ventral (Fig. 2M), aedeagus spines slightly sinuous and tips slightly curved upward (Figs 2P, 8C)..... .....***A. albofasciata*** **(Lallemand, 1939)**
– Tegmen dark brown to black, with two incomplete and barely visible transverse bands, one oblique band on basal third and another straight band on the distal third or only basal band visible or both absent (Figs 6, 7), the secondary subapical spine of parameres with two rounded acute lobes similar in size and shape (Figs 2L, 9C), aedeagus spines slightly sinuous, conspicuously curved upward and touching the superior margin of phallobase, tips bent to form an almost 90° angle (Figs 2O, 8A, B).....***A. danpecki*** **Castro, Armendáriz & Utrera, sp. nov.**

Geographic records

The distribution of *A. danpecki* was supported by three occurrence records from Sierra Madre del Sur province, in Oaxaca state (Fig. 10; Table 1). *Aeneolamia contigua* had 34 occurrence records in Chihuahuan Desert (ChD), TVP, V, Pacific Lowlands (PL), and Yucatan Peninsula (YP) provinces in Chiapas, Chihuahua, Guerrero, Morelos, Nayarit, Oaxaca, Quintana Roo, Veracruz, and Yucatán states; and *A. albofasciata* was supported by 31 records in ChD, Sonoran, Sierra Madre Oriental, V, TVP, PL, and YP biogeographic provinces in Campeche, Chiapas, Guerrero, Michoacán, Morelos, Nuevo León, San Luis Potosí, Sonora, Tabasco, Veracruz, and Quintana Roo states. *Aeneolamia danpecki* is sympatric with *A. contigua* and *A. albofasciata* in the Sierra Madre del Sur province. Meanwhile, *A. contigua* and *A. albofasciata* are distributed in almost all provinces except in the provinces of California and Baja California (Fig. 10).

Discussion

Discrete morphological characters

The evaluation of ten discrete characters of male tegmen and genitalia indicates that six of them (CAT, CDT, SGP, SEGP, SSP, and PRE) are useful to differentiate *A. danpecki*, and both sets of features together can differentiate this species from *A. albofasciata* and *A. contigua* as well as being diagnostic characters for *A. danpecki* (Tables 2, 3). The shape of subgenital plate apex, the shape of subapical spine of paramere, and the shape of the aedeagus spines of *A. danpecki* show unique character states (Figs 2I, L, O, 8A, B), and nothing similar was documented in the entire series of *A. albofasciata* and *A. contigua* examined. Additionally, the occurrence of diagnostic traits on the tegmen of both sexes allows reliable differentiation of both males and females of *A. danpecki* (Fig. 1A, D, G, H, K) from other species of the *Aeneolamia* (Fig. 1B, C, E, F, I, J, M, N). Regarding the tegmen, polymorphism is a common phenomenon in members of Cercopidae, with certain spittlebug species showing large variability in tegminal coloration patterns. Phenotypic variation in tegmen color among specimens within or among populations has been attributed to genetic causes (Aquino-Borges et al. 2020), resulting from differences in mating behavior, in attraction cues, or in geographic barriers (Hutchinson 1963; Farish and Scudder 1967). These factors have promoted highly diverse polymorphisms with dozens of morphotypes recognized throughout the species distribution in extreme cases (Farish 1972) and in others, only a few variants within and between localities (e.g., Paladini and Cavichioli 2015; Thompson and Carvalho 2016; Aquino-Borges et al. 2020). Members of the genus *Aeneolamia* are not exempt from this pattern, in which considerable color variation in tegmen has also been recognized in some species, within and among different spatially separated localities (Fennah 1949). For this reason, in a taxonomic sense, traits related to coloration patterns have been given less weight in defining taxa in this group than other body features (Paladini and Cavichioli 2013, 2015). As in other Cercopidae and *Aeneolamia* species, our analysis of discrete features in *A. danpecki*, *A. albofasciata*, and *A. contigua* allow us to recognize polymorphisms in the coloration patterns of the tegmen, reflected in that the species each presented traits with different character states (TC, CIE, CAT, CDT), and some of them were shared among the species (TC, CIE) (Table 2). However, the comparison of their frequencies supported the fact that the species have exclusive character states in two features, which constitute diagnostic features; in addition, they have different combinations of character states which together allow their recognition, at least in Mexico. The importance of the genital characters in Cercopidae studies was recognized by Fennah (1968) who stated that female and male genitalia characters can be used for grouping species. In comparison with the tegmen features of color, those characters of male genitalia have been shown to be conserved and therefore reliable for species identification and delimitation (Paladini and Cavichioli 2013, 2015; this study). In species with polymorphic tegminal color patterns, the specimens' series display consistent discrete morphological features in different elements of male

genitalia (Paladini and Cavichioli 2013; Paladini et al. 2018; Aquino-Borges et al. 2020). According to this pattern, our results show that elements of male genitalia easily discriminate males among the *Aeneolamia* analyzed (Figs 2, 8); despite the tegmen polymorphism found among them (Fig. 1), diagnostic characters of the genital plates, parameres, and aedeagus were found to be the same as in other *Aeneolamia* species (Paladini and Cavichioli 2013).

Continuous quantitative morphological characters

The statistical analysis of morphological variation of Mexican members of *Aeneolamia* supports the earlier suggestion that specimens identified previously as *A.* aff. *albofasciata* in Armendáriz-Toledano et al. (2022) represent a new species, described here as *Aeneolamia danpecki* Castro, Armendáriz, Utrera, sp. nov. Morphological differences in male genitalia (Fig. 2F–T) also support the species separation. *Aeneolamia danpecki* exhibited smaller mean measurements than both *A. albofasciata* and *A. contigua* in the 36 features analyzed. Among these features Al_v, BLW_v, LAW_l, PCW_v, PW_d, SW_d, and SL_v displayed the most pronounced differences (Table 4).

Multivariate analysis

From quantitative continuous and discrete characters (PCoA) of males and quantitative features of both sexes (PCA), permitted the recovery of discrete groups corresponding to the two previously recognized species, *A. albofasciata* and *A. contigua*, and the new species *A. danpecki* (Figs 4, 5), supporting that these cercopid species have strongly differentiated phenotypes. The robustness of the taxon clusters was demonstrated when the data set of characteristics was divided by sex, with *A. danpecki* being the most distant taxon in multivariate space and therefore morphologically distinct from *A. albofasciata* and *A. contigua*. In other hemipterans, quantitative measures and multivariate analysis have been used extensively to identify and delimit morphological variation within and between species (e.g., Blackman 1987; Gorla et al. 1993; Margaritopoulos et al. 2000; Jayasekera et al. 2010). This is the first time it has been utilized in Cercopidae. An outstanding result was that the multivariate analyses corresponding to each sex alone (CVA♂, CVA♀) displayed the clearest segregation of species (Fig. 4A, B). In the combined CVA of both sexes, one *A. contigua* female was grouped with *A. danpecki* and a male was grouped with *A. albofasciata* (Fig. 4B). This pattern can be explained by the sexual dimorphism of the three species studied. As in other cercopids, their females are usually equal to or somewhat larger than males of the same species (Paladini 2011), so most of the features measured in Mexican *Aeneolamia* females were larger than those of males. *Aeneolamia albofasciata* was the species with least pronounced sexual dimorphism in size, while *A. contigua* displays a greater difference between males and females (Fig. 4B). In other cercopids different sexually dimorphic traits have been recognized, such as ornamentation patterns in the tegmen (Peck et al. 2004; Paladini and Carvalho 2008), the profile of

the anteclypeus (Hamilton 1977; Liang 2020), the form of anteclypeus in ventral view (Liang 2020), the tibial glands in male adults (Liang 2003, 2020), and an elongated basal body of the antenna in males of some genera of Ischnorhinini (Fennah 1968; Carvalho and Sakakibara 1989). Also, in some species, size dimorphism goes in the other direction, where males are smaller than females (Peck et al. 2002a, 2004; Rodríguez et al. 2002, 2003).

Geometric morphometry of the aedeagus

Morphometric analyses have been poorly explored in Cercopidae and quantitative analyses of the shape of genital structures have not been performed previously in the family. However, in studies of other Cicadomorpha and other Cercopoidea, morphometric analyses have been used to recognize and delimit new species. In the genus *Cycloscytina* Martynov, 1926, shape analysis of the wing allowed to elucidate the species status of its members and support an extinct new species from the Triassic (Chen et al. 2022). In *Philaenus*, the species limits and distribution boundaries between *Philaenus spumarius* L., 1758 and *Philaenus tesselatus* Stål, 1864, were established based on a classical morphometric analysis of aedeagus (Seabra et al. 2019). Our results of geometric morphometric analysis indicate that the shape of the genital structures is quantitatively different among Mexican species of *Aeneolamia*. The lack of overlap in the shape configurations of the aedeagus spine confirms that this anatomical structure is a robust diagnostic character useful in their identification (Fig. 5A–D).

Geographical records

In this study, it is evident that, at the biogeographical level, *A. danpecki* sp. nov. is in sympatry with *A. contigua* and *A. albofasciata* in the Sierra Madre del Sur. However, the records of Mexican *Aeneolamia* species (Table 1) and some authors (López-Collado and Pérez-Aguilar 2012) do not support that *A. danpecki* coexists in the same localities with another congeneric species (Fig. 10). In addition, the distribution of *A. danpecki* is narrower than those of *A. contigua* or *A. albofasciata*, having been reported only within the eastern portion of the eastern Sierra Madre del Sur province, which corresponds to the central valleys and mountains between Sola de Vega and the city of Oaxaca, Oaxaca State (Fig. 10; Smith 1941; Arriaga et al. 1997; Santiago-Alvarado et al. 2016). This region is characterized by several endemic plants (Pinaceae, Bruceraceae, Cactaceae, Iridaceae, Poaceae), invertebrate animals (Amphypterigidae, Carabidae, Cordulidae, Curculionidae, Passalidae), and vertebrate taxa (Anguide, Cricetidae, Plethodontidae, Soricidae, Trochilidae) (Morrone et al. 2017). *Aeneolamia danpecki* specimens were collected on *Paspalum* sp. and *Pennisetum* sp. grasses and, like many other spittlebug species, probably makes use of other native and introduced grasses in Oaxaca. Its pest status, if any, was not established in *Paspalum* sp. or *Pennisetum* sp. The new species *A. danpecki* represents the first new species taxon in *Aeneolamia* since the description of *A. albofasciata* by Lallemand in 1939.

Acknowledgements

This research was supported by Programa para el Desarrollo Profesional Docente, Tipo Superior-2019 (PRODEP), project "Taxonomía y distribution de la familia Cercopidae (Hemiptera: Auchenorrhyncha) en México", granted to UC-V, and PAPIIT-UNAM IA201720, IA203122 and CONACyT Fronteras de la Ciencia (139030) granted to FA-T. Likewise, Grupo Papalotla S. A. de C. V. for supporting the trip to Oaxaca where *A. danpecki* was collected in 2003. We thank Cristina Mayorga Martínez (CNIN) for loaning entomological material. We appreciate Dr. Luis O. López Z. (North Carolina State University) and Dr. Gervasio S. Carvalho (Pontificia Universidade Católica do Rio Grande do Sul, Porto Alegre, Brazil) for sending literature relevant to this research, Jazmín García Roman for illustrations in Fig. 3 Tonatiuh Santos Neira for database management, Roman Emilio, brother of UC-V, for funding a visit to Dr. Daniel C. Peck at Cornell University in 2004. Maribel Cruz Gallego, Anuar Morales Rodríguez, and Vinton Thompson provided helpful comments on the manuscript.

References

Aguirre LM, Cardona C, Miles JW, Sotelo G (2013) Characterization of resistance to adult spittlebugs (Hemiptera: Cercopidae) in *Brachiaria* spp. Journal of Economic Entomology 106(4): 1871–1877. https://doi.org/10.1603/EC11189

Aquino-Borges R, Machado Auad A, Graças Fonseca MD, Vieira Borges CA, Sousa Azevedo AL, Teixeira De Resende T, Carvalho GS, Rodrigues De Oliveira F (2020) Coloration patterns of the tegmina of *Mahanarva spectabilis* (Hemiptera: Cercopidae): Biological, morphological and genetic bases. The Florida Entomologist 103: 376–383. https://doi.org/10.1653/024.103.0310

Armendáriz-Toledano F, López-Posadas MA, Romero Nápoles J, Utrera-Vélez Y, López-Córdova JP, Castro-Valderrama U (2022) Overview of spittlebugs of the family Cercopidae (Hemiptera: Auchenorrhyncha) from Mexico, with keys to genera and species. Revista Mexicana de Biodiversidad 93: e934030. https://doi.org/10.22201/ib.20078706e.2022.93.4030

Arriaga L, Aguilar C, Espinosa D, Jiménez R (1997) Regionalización ecológica y biogeográfica de México. Mexico City: Taller de la Comisión Nacional para el Conocimiento y Uso de la Biodiversidad.

Blackman RL (1987) Morphological discrimination of a tobacco-feeding form from *Myzus persicae* (Sulzer) (Hemiptera: Aphididae), and a key to New World *Myzus* (Nectarosiphori) species. Bulletin of Entomological Research 77(4): 713–730. https://doi.org/10.1017/S0007485300012219

Bookstein FL (1991) Morphometrics tools for landmark data: geometry and biology. Cambridge University Press, Cambridge, 435 pp. https://doi.org/10.1017/CBO9780511573064

Cardona C, Fory P, Sotelo G, Pabón A, Díaz G, Miles JW (2004) Antibiosis and tolerance to five species of spittlebug (Homoptera: Cercopidae) in *Brachiaria* spp.: implications for breeding for resistance. Journal of Economic Entomology 97(2): 635–645. https://doi.org/10.1603/0022-0493-97.2.635

Cardona C, Miles JW, Zuñiga E, Sotelo G (2010) Independence of resistance in *Brachiaria* spp. to nymphs or to adult spittlebugs (Hemiptera: Cercopidae): Implications for breeding for resistance. Journal of Economic Entomology 103(5): 1860–1865. https://doi.org/10.1603/EC10004

Carvalho GS, Sakakibara AM (1989) A new genus and species of Neotropical Cercopidae (Tomaspidinae, Tomaspidini). Revista Brasileira de Zoologia 6(1): 111–115. https://doi.org/10.1590/S0101-81751989000100012

Carvalho GS, Webb MD (2005) Cercopid Spittlebugs of the New World (Hemiptera: Auchenorrhyncha: Cercopidae). Pensoft, Sofía-Moscow, 271 pp.

Castro-Valderrama U, Carvalho GS, Peck DC, Valdez-Carrasco JM, Romero-Nápoles J (2018) Two new species of the spittlebug genus *Ocoaxo* Fennah (Hemiptera: Cercopidae) from Mexico, and keys for the groups, group three, and first subgroup. Neotropical Entomology 48(2): 260–268. https://doi.org/10.1007/s13744-018-0629-0

Chen J, Zhang Q, Hui J, Li Y, Zheng Y, Shuai Y, Wang X, Zhang H (2022) Geometric morphometric analysis for the systematic elucidation of new Hylicellidae from the Jurassic of China (Hemiptera: Cicadomorpha). Journal of Paleontology 96(5): 1119–1131. https://doi.org/10.1017/jpa.2022.20

Clark WE, Ibarra Diaz GE, van Cleave HW (1976) Taxonomy and biology of spittlebugs of the genera *Aeneolamia* Fennah and *Prosapia* Fennah (Cercopidae) in northeastern Mexico. Folia Entomologica Mexicana 34: 13–24.

Cuarán VL, Castro Valderrama U, Bustillo Pardey AE, Mesa Cobo NC, Ramírez Sánchez GD, Moreno Gil CA, Gómez Laverde LA (2012) Método para evaluar el daño de los salivazos (Hemiptera: Cercopidae) sobre caña de azúcar, *Saccharum* spp. Revista Colombiana de Entomologia 38(2): 171–176. https://doi.org/10.25100/socolen.v38i2.8986

De la Cruz-Llanas JJ, Vera-Graziano J, López-Collado J, Pinto VM, Garza-García R (2005) Una técnica sencilla para el desarrollo de ninfas de *Aeneolamia postica* (Homoptera: Cercopidae). Folia Entomologica Mexicana 44: 93–94.

De la Cruz-Zapata G, García-López E, Sánchez-Soto S, Bautista-Martínez N, Ortiz-Díaz JJ, Osorio-Osorio R (2016) Identidad de mosca pinta (Hemiptera: Cercopidae) y sus hospederas en cañaverales en Cárdenas, Tabasco, México. Southwester Entomologist 41(1): 145–151. https://doi.org/10.3958/059.041.0116

Farish DJ (1972) Balanced polymorphism in North American populations of the meadow spittlebug, *Philaenus spumarius* (Homoptera: Cercopidae). 1. North American Morphs 1.-. Annals of the Entomological Society of America 65(3): 710–719. https://doi.org/10.1093/aesa/65.3.710

Farish DJ, Scudder GGE (1967) The polymorphism in *Philaenus spumarius* (L.) (Hemiptera: Cercopidae) in British Columbia. Journal of the Entomological Society of British Columbia 64: 45–51.

Fennah RG (1949) New genera and species of Neotropical Cercopoidea (Homoptera). Annals & Magazine of Natural History 1(9): 605–620. https://doi.org/10.1080/00222934808653935

Fennah RG (1953) Revisionary notes on Neotropical monecphorene Cercopoidea (Homoptera). Annals & Magazine of Natural History 6(65): 337–360. https://doi.org/10.1080/00222935308654431

Fennah RG (1968) Revisionary notes on the new world genera of cercopid froghoppers (Homoptera: Cercopoidea). Bulletin of Entomological Research 58(1): 165–190. https://doi.org/10.1017/S0007485300055954

Fewkes DW (1969a) The biology of sugarcane froghoppers. In: Williams JR et al. (Ed.) Pests of Sugar Cane. Elsevier, Amsterdam, 283–307.

Fewkes DW (1969b) The control of froghoppers in sugarcane plantations. In: Williams JR et al. (Ed.) Pests of Sugar Cane. Elsevier, Amsterdam, 309–324.

Figueredo L, Villa-Murillo A, Colmenarez Y, Vásquez C (2021) A hybrid artificial intelligence model for *Aeneolamia varia* (Hemiptera: Cercopidae) populations in sugarcane crops. Journal of Insect Science 21(2): 1–6. https://doi.org/10.1093/jisesa/ieab017

García D AM, Bustillo P AE, Castro V U, Arenas B Y (2012) Selección de hongos entomopatógenos para controlar salivazos (Hemiptera: Cercopidae) de la caña de azúcar en Colombia. Revista Colombiana de Entomologia 38(2): 252–259. https://doi.org/10.25100/socolen.v38i2.9001

García-García C, López-Collado J, Nava-Tablada ME, Villanueva-Jiménez JA, Vera-Graziano J (2006) Modelo de predicción de riesgo de daño de la mosca pinta *Aeneolamia postica* (Walker) Fennah (Hemiptera: Cercopidae). Neotropical Entomology 35(5): 677–688. https://doi.org/10.1590/S1519-566X2006000500017

García-González JC, López-Collado J, García-García CG, Villanueva-Jiménez JA, Nava-Tablada ME (2017) Factores bióticos, abióticos y agronómicos que afectan las poblaciones de adultos de mosca pinta (Hemiptera: Cercopidae) en cultivos de caña de azúcar en Veracruz, México. Acta Zoológica Mexicana (n.s) 33: 508–517. https://doi.org/10.21829/azm.2017.3331152

Gómez L LA (2007) Manejo del salivazo *Aeneolamia varia* en cultivos de caña de azúcar en el valle del río Cauca. Carta Trimestral 29:10–17. https://www.cenicana.org/pdf_privado/carta_trimestral/ct2007/ct2y3_07/ct2y3_07_p10-17.pdf

Gorla DE, Jurberg J, Silva SC, Schofield CJ (1993) Systematics of *Triatoma sórdida*, *T. guasayana*, *T. patagónica* (Hemiptera: Reduviidae). Memorias do Instituto Oswaldo Cruz 88(3): 379–385. https://doi.org/10.1590/S0074-02761993000300006

Grifaldo-Alcántara PF, Alatorre-Rosas R, Villanueva-Jiménez JA, Hernández-Rosas F, Stock SP, Ramírez-Valverde G (2019) Evaluación de dos cepas de nematodos entomopatógenos (Steinernematidae, Heterorhabditidae) para el control del salivazo (Hemiptera Cercopidae) en caña de azúcar. Nematropica 49: 83–90. https://journals.flvc.org/nematropica/article/view/115628

Guagliumi P (1962) Las plagas de la caña de azúcar en Venezuela. Ministerio de Agricultura y Cria Centro de Investigaciones Agronómicas, Maracay, Venezuela, Vol. 1 y 2, 850 pp.

Hamilton KGA (1977) Review of the world species of *Prosapia* Fennah (Rhynchota: Homoptera: Cercopidae). Canadian Entomologist 109(4): 621–630. https://doi.org/10.4039/Ent109621-4

Hernández LM, Bonilla X, Espitia-Buitrago P (2021a) Primer registro de *Aeneolamia reducta* (Lallemand, 1924) (Hemiptera: Cercopidae) en el Valle del Cauca (Colombia). Boletin del Museo de Entomologia de la Universidad del Valle 20: 1–6.

Hernández LM, Espitia P, Florian D, Castiblanco V, Cardoso JA, Gómez-Jiménez MI (2021b) Geographic distribution of Colombian spittlebugs (Hemiptera: Cercopidae) via ecological

niche modeling: a prediction for the main tropical forages' pest in the Neotropics. Frontiers in Sustainable Food Systems 5: 725774. https://doi.org/10.3389/fsufs.2021.725774

Hernández-Domínguez AC, Guzmán-Franco W, Carrillo-Benítez MG, Alatorre-Rosas R, Rodríguez-Leyva E, Villanueva-Jiménez JA (2016) Specific diversity of *Metarhizium* isolates infecting *Aeneolamia* spp. (Hemiptera: Cercopidae) in sugarcane plantations. Neotropical Entomology 45(1): 80–87. https://doi.org/10.1007/s13744-015-0337-y

Hutchinson GE (1963) A note on the polymorphism of *Philaenus spumarius* (L.) (Homopt., Cercopidae) in Britain. Entomologist's Monthly Magazine 99: 175–178.

Jayasekera S, Thomas A, Kar A, Ramamurthy VV (2010) Host correlated morphometric variations in the populations of *Bemisia tabaci* (Gennadius) (Hemiptera: Aleyrodidae). Oriental Insects 44(1): 193–204. https://doi.org/10.1080/00305316.2010.10417613

Jiménez GJA (1978) Estudios tendientes a establecer el control integrado de las salivitas de los pastos. Revista Colombiana de Entomologia 4(1–2): 19–33. https://doi.org/10.25100/socolen.v4i1-2.10372

Lallemand V (1939) Cercopodes nouveaux de Musée National Hongrois (Budapest). Annales Historico-Naturales Musei Nationalis Hungarici 32: 58–64.

Le Cesne M, Crispolon Jr E, Soulier-Perkins A (2021) Male terminalia of Cercopidae (Hemiptera, Cicadomorpha): Toward a consensus terminology. Scientific Reports 11(1): 10412. https://doi.org/10.1038/s41598-021-89759-3

Liang A-P (2003) A new tibial gland in male spittlebugs with descriptions of two new species of *Augustohahnia* Schmidt (Hemiptera: Cercopidae) from New Guinea. Journal of Zoology 261(2): 173–180. https://doi.org/10.1017/S0952836903004072

Liang A-P (2020) A new structure on the front of male adults of the Asian rice spittlebug *Callitettix versicolor* (Hemiptera: Auchenorrhyncha: Cercopidae). Zootaxa 4801: 591–599. https://doi.org/10.11646/zootaxa.4801.3.12

López Machado F, Peck DC, Montoya Lerma J (2001) Importancia de la comunicación vibracional en el comportamiento reproductivo del salivazo de los pastos (Homoptera: Cercopidae). Revista Colombiana de Entomología 26: 24–31. https://cgspace.cgiar.org/bitstream/handle/10568/44342/2001-3.pdf?sequence%=%1&isAllowed%=%y

López-Collado J, Pérez-Aguilar WA (2012) Hoja técnica mosca pinta de la caña de azúcar. Colegio de Postgraduados. https://sites.google.com/site/moscapinta/hoja-tecnica [Accessed 11 Sept 2022]

López-Posadas MA (2021) Taxonomía y distribución de la familia Cercopidae (Hemiptera: Auchenorrhyncha) en México. Agronomy undergraduate thesis, University of Sonora, Mexico, 93 pp.

Margaritopoulos JT, Tsitsipis JA, Zintzaras E, Blackman RL (2000) Host-correlated morphological variation of *Myzus persicae* (Hemiptera: Aphididae) populations in Greece. Bulletin of Entomological Research 90(3): 233–244. https://doi.org/10.1017/S0007485300000353

Martin RM, Cox JR, Alston DG, Ibarra F (1995) Spittlebug (Homoptera: Cercopidae) life cycle on buffelgrass in Northwestern Mexico. Annals of the Entomological Society of America 88(4): 471–478. https://doi.org/10.1093/aesa/88.4.471

Martin RM, Cox JR, Ibarra F, Alston DG, Banner RE, Malecheck JC (1999) Spittlebug and buffelgrass responses to summer fires in Mexico. Journal of Range Management 52(6): 621–625. https://doi.org/10.2307/4003632

Matabanchoy Solarte JA, Bustillo Pardey AE, Castro Valderrama U, Mesa Cobo NC, Moreno Gil CA (2012) Eficacia de *Metarhizium anisopliae* para controlar *Aeneolamia varia* (Hemiptera: Cercopidae), en caña de azúcar. Revista Colombiana de Entomologia 38(2): 177–181. https://doi.org/10.25100/socolen.v38i2.8987

Medina CA, Lapointe SL, Chacón P (1993) Fauna de hormigas asociadas con forrajes tropicales y su implicación como depredadores de huevos y ninfas salivazo de los pastos, *Aeneolamia* spp. Revista Colombiana de Entomologia 19(4): 143–150. https://doi.org/10.25100/socolen.v19i4.10071

Miles JW, Lapointe SL, Escandon ML, Sotelo G (1995) Inheritance of resistance to spittlebug (Homoptera: Cercopidae) in interspecific *Brachiaria* spp. hybrids. Journal of Economic Entomology 88(5): 1477–1481. https://doi.org/10.1093/jee/88.5.1477

Morales J (1993) Egg diapause and pest management of *Aeneolamia varia* (Homoptera: Cercopidae) in Venezuela. Environmental Entomology 22(5): 1092–1095. https://doi.org/10.1093/ee/22.5.1092

Morales-Pérez A, Segura-León OL, Navarro-Martínez AK, Nuñez-Gaona O, Palacios-Torres RE (2014) Caracterización morfológica y molecular del salivazo *Prosapia simulans* (Hemiptera: Cercopidae) plaga de la caña de azúcar en Tuxtepec, Oaxaca, México. Entomología Mexicana 1: 1218–1222.

Moreno Salguero C, Bustillo-Pardey AE, López-Núñez JC, Castro Valderrama U, Ramírez Sánchez GD (2012) Virulencia de nematodos entomopatógenos para el control del salivazo *Aeneolamia varia* (Hemiptera: Cercopidae) en caña de azúcar. Revista Colombiana de Entomologia 38(2): 260–265. https://doi.org/10.25100/socolen.v38i2.9002

Morrone JJ, Escalante T, Rodríguez-Tapia G (2017) Mexican biogeographic provinces: Map and shapefiles. Zootaxa 4277(2): 277–279. https://doi.org/10.11646/zootaxa.4277.2.8

Nast J (1950) A revision of the genus *Sphenorhina* Am et Serv. (Homoptera, Cercopidae). Bulletin Entomologique de la Pologne 3–4: 114–148.

Obando B JA, Bustillo P AE, Castro V U, Mesa C NC (2013) Selección de cepas de *Metarhizium anisopliae* para el control de *Aeneolamia varia* (Hemiptera Cercopidae). Revista Colombiana de Entomologia 39: 26–33. http://www.scielo.org.co/pdf/rcen/v39n1/v39n1a05.pdf

Oomen PA (1975) A population study of the spittlebugs *Aeneolamia occidentalis* (Walk.) and *Prosapia simulans* (Walk.) (Homoptera: Cercopidae) in Mexican pangola pastures. Journal of Applied Entomology 79: 225–238. https://doi.org/10.1111/j.1439-0418.1975.tb02337.x

Paladini A (2011) A new species of *Ferorhinella* with an unusual pattern of sexual size dimorphism (Hemiptera, Cercopidae, Tomaspidinae). Zootaxa 2728(1): 57–60. https://doi.org/10.11646/zootaxa.2728.1.5

Paladini A, Carvalho GS (2008) Revisão taxonômica de *Kanaima* Distant (Hemiptera: Cercopidae: Ishnorhininae). Revista Brasileira de Entomologia 53(3): 311–325. https://doi.org/10.1590/S0085-56262008000300002

Paladini A, Cavichioli RR (2013) A new species of *Aeneolamia* (Hemiptera: Cercopidae: Tomaspidinae) from the Neotropical Region. Zoologia 30(3): 353–355. https://doi.org/10.1590/S1984-46702013000300016

Paladini A, Cavichioli RR (2015) A new genus and new species of spittlebug (Hemiptera: Cercopidae: Ischnorhininae) from Southern Brazil. Zoologia 32(1): 47–52. https://doi.org/10.1590/S1984-46702015000100007

Paladini A, Takiya DM, Cavichioli RR, Carvalho GS (2015) Phylogeny and biogeography of Neotropical spittlebugs (Hemiptera: Cercopidae: Ishnorhininae): revised tribal classification based on morphological data. Systematic Entomology 40(1): 82–108. https://doi.org/10.1111/syen.12091

Paladini A, Takiya DM, Urband JM, Cryan JR (2018) New World spittlebugs (Hemiptera: Cercopidae: Ischnorhininae): Dated molecular phylogeny, classification, and evolution of aposematic coloration. Molecular Phylogenetics and Evolution 120: 321–334. https://doi.org/10.1016/j.ympev.2017.12.020

Peck DC, Pérez AM, Medina JW (2002a) Biología y hábitos de *Aeneolamia reducta* y *A. lepidior* en la Costa Caribe de Colombia. Pasturas Tropicales 24: 16–26.

Peck DC, Pérez AM, Medina JW, Barrios M, Rojas J (2002b) Fenología de *Aeneolamia reducta* en la Costa Caribe de Colombia. Pasturas Tropicales 24: 39–55.

Peck DC, Rodríguez Ch J, Gómez LA (2004) Identity and first record of the spittlebug *Mahanarva bipars* (Hemiptera: Auchenorrhyncha: Cercopidae) on sugarcane in Colombia. The Florida Entomologist 87(1): 83–84. https://doi.org/10.1653/0015-4040(2004)087[0082:IAFROT]2.0.CO;2

Pérez SI, Bernal V, Gonzalez PN (2006) Differences between sliding semi-landmark methods in geometric morphometrics, with an application to human craniofacial and dental variation. Journal of Anatomy 208(6): 769–784. https://doi.org/10.1111/j.1469-7580.2006.00576.x

Rodríguez J, Peck DC, Canal NA (2002) Biología comparada de tres especies de salivazo de los pastos del género *Zulia* (Homoptera: Cercopidae). Revista Colombiana de Entomologia 28(1): 17–25. https://doi.org/10.25100/socolen.v28i1.9621

Rodríguez J, Castro U, Morales A, Peck D (2003) Biología de *Prosapia simulans* (Walker) (Homoptera: Cercopidae), nueva plaga de gramíneas cultivadas en Colombia. Revista Colombiana de Entomologia 29(2): 149–145. https://doi.org/10.25100/socolen.v29i2.9598

Rohlf FJ (2004) tpsDig version 1.40. Department of Ecology and Evolution, State University of New York, Stony Brook, NY.

Rosero-Guerrero M, Bustillo-Pardey AE, López Nuñez JC, Castro-Valderrama U, Gómez-López E (2012) Eficacia de entomonematodos para controlar estados de *Aeneolamia varia* (Hemiptera: Cercopidae) bajo condiciones de invernadero. Revista Colombiana de Entomologia 38(2): 266–273. https://doi.org/10.25100/socolen.v38i2.9003

Santiago-Alvarado M, Montaño-Arias G, Espinosa D (2016) Áreas de endemismo de la Sierra Madre del Sur. In: Luna-Vega I, Espinosa D, Contreras-Medina R (Eds) Biodiversidad de la Sierra Madre del Sur: Una síntesis preliminar. UNAM, Mexico City, 431–448.

Seabra SG, Neto AC, Rodrigues ASB, Streito J-C, Genson G, Pierre É, Silva SE, Popova G, Marabuto E, Figueiredo E, Mateus C, Wilson M, Rei FT, Quartau JA, Paulo OS, Rebelo MT (2019) Morphological and genomic assessment of divergence between closely related species of the genus *Philaeneus* (Hemipetera, Aphrophoridae). European Conference on *Xylella fastidiosa*: How research can support solutions. Ajaccio, France.

Sendoya Corrales CA, Ramírez Sánchez GD, García Díaz AM, Bustillo Pardey AE, Castro Valderrama U (2011) Parámetros reproductivos de *Aeneolamia varia* (F.) (Hemiptera: Cercopidae) en una cría masiva usando pasto braquiaria. In: Memorias de resumenes, XXXVIII Congreso de la Sociedad Colombiana de Entomología. Manizales, Colombia, 27–29 July 2011.

Sheets HD (2003). IMP-integrated morphometrics package. Department of Physics, Canisius Collegue, Buffalo, NY. https://www.sbmorphometrics.org/ [Accessed 11 Sept 2022]

Smith H (1941) Las provincias bióticas de México, según la distribución geográfica de las lagartijas del género *Sceloporus*. Anales. Escuela Nacional de Ciencias Biologicas (Mexico) 2: 103–110.

Sotelo PA, Miller MF, Cardona C, Miles JW, Sotelo G, Montoya J (2008) Sublethal effects of antibiosis resistance on the reproductive biology of two spittlebug (Hemiptera: Cercopidae) species affecting *Brachiaria* spp. Journal of Economic Entomology 1001(2): 564–568. https://doi.org/10.1093/jee/101.2.564

Thompson V, Carvalho GS (2016) Abrupt geographical transition between aposematic color forms in the spittlebug *Prosapia ignipectus* (Fitch) (Hemiptera: Cercopidae). Hindawi Publishing Corporation. Psyche: ID 3623092. https://doi.org/10.1155/2016/3623092

Thompson V, León González R (2005) La identificación y distribución de los salivazos de la caña de azúcar y los pastos (Homoptera: Cercopidae) en Costa Rica. Manejo integrado de plagas y agroecología (Costa Rica) 75: 43–51. http://www.sidalc.net/REPDOC/A1873E/A1873E.PDF

Urich FW (1913) The sugar cane froghopper and biological notes on some cercopids of Trinidad. Circular of the Board of Agriculture, Trinidad and Tobago (9): 7–47.

Wiedijk F (1982) Variability in the occurrence of the sugar cane froghopper, *Aeneolamia flavilatera* (Homoptera: Cercopidae), on sugar estates in Guyana and Surinam. Mededelingen Landbouwhogeschool Wageningen 7: 1–55.

Williams CB (1921) Report on the froghopper-blight of sugarcane in Trinidad. Memoirs of the Department of Agriculture, Trinidad and Tobago, 170 pp. https://doi.org/10.5962/bhl.title.15427

Zar JH (2010) Biostatistical Analysis. Prentice-Hall, NJ, 994 pp.

Zelditch LM, Swiderski DL, Sheets HD, Fink WL (2004) Geometric morphometrics for biologist: A primer. Maple Vail, New York, 443 pp.

ZooKeys 1139: 107–126 (2023)
doi: 10.3897/zookeys.1139.96508
https://zookeys.pensoft.net

RESEARCH ARTICLE

A peer-reviewed open-access journal
ZooKeys
Launched to accelerate biodiversity research

Scratching the surface: a new species of Bent-toed gecko (Squamata, Gekkonidae, *Cyrtodactylus*) from Timor-Leste of the *darmandvillei* group marks the potential for future discoveries

Kin Onn Chan[1], L. Lee Grismer[2,3], Fernando Santana[4], Pedro Pinto[4], Frances W. Loke[5], Nathan Conaboy[6]

1 *Lee Kong Chian Natural History Museum, National University of Singapore, 2 Conservatory Drive, 117377 Singapore, Singapore* **2** *Herpetology Laboratory, Department of Biology, La Sierra University, 4500 Riverwalk Parkway, Riverside, San Diego, California 92505, USA* **3** *Department of Herpetology, San Diego Natural History Museum, PO Box 121390, San Diego, California, 92112, USA* **4** *Department of Protected Areas and National Parks, Ministry of Agriculture and Fisheries, Dili, Timor-Leste* **5** *Conservation International Singapore, 42B Boat Quay, Singapore 049831, Singapore* **6** *Conservation International Timor-Leste, Rua Dom Aleixo Corte Real, Mandarin, Dili, P.O. BOX 006, Timor-Leste*

Corresponding author: Kin Onn Chan (cko@nus.edu.sg)

Academic editor: Thomas Ziegler | Received 28 October 2022 | Accepted 13 December 2022 | Published 11 January 2023

https://zoobank.org/9C1A97F0-4039-4789-AA07-6AD25712B5CB

Citation: Chan KO, Grismer LL, Santana F, Pinto P, Loke FW, Conaboy N (2023) Scratching the surface: a new species of Bent-toed gecko (Squamata, Gekkonidae, *Cyrtodactylus*) from Timor-Leste of the *darmandvillei* group marks the potential for future discoveries. ZooKeys 1139: 107–126. https://doi.org/10.3897/zookeys.1139.96508

Abstract

A new species of limestone-dwelling Bent-toed gecko (genus *Cyrtodactylus*) is described from Nino Konis Santana National Park in the far-east region of Timor-Leste. Both genetic and morphological data strongly support the evolutionary distinctness of the new species, which we describe herein as *Cyrtodactylus santana* **sp. nov.** Phylogenetic analysis based on the ND2 mitochondrial gene inferred the new species as part of the *C. darmandvillei* group with close genetic affinities to *C. batucolus*, *C. seribuatensis*, *C. petani*, *C. sadleiri*, and two undescribed lineages from the Moluccas in Indonesia. The new species represents the first species of *Cyrtodactylus* identified at the species level from Timor-Leste and fills an important gap in our understanding of the biogeography and evolutionary history of *Cyrtodactylus* especially in the Wallacean region. Our results strongly suggest that the diversity of *Cyrtodactylus* in Wallacea is still underestimated and many more unnamed species remain to be described.

Keywords
Biogeography, Gekkota, lizards, phylogenetics, systematics, taxonomy, Wallacea

Introduction

The Southeast Asian island of Timor is the largest of the Lesser Sunda Islands and is located within the biogeographical region of Wallacea, bounded by Wallace's Line in the west and Lydekker's Line in the east. The Democratic Republic of Timor-Leste (hereafter referred to as Timor-Leste) is a sovereign country occupying the eastern half of the island of Timor and includes the islands of Ataúro, Jaco, and the semi-enclave of Oecusse, a Special Administrative Region located in the western part of Timor. The western half of Timor is part of the Indonesian province of East Nusa Tenggara (Fig. 1). The terrain of Timor-Leste is mostly rugged and mountainous, with a central mountain range stretching east to west, reaching an elevation of 2,986 m at Mount Ramelau, the highest mountain on the island of Timor. The steep terrain slopes towards the north and the south, forming coastal versants dissected by alluvial outwashes, riverine plains, and wetland areas. Timor-Leste has a dry tropical climate with a pronounced dry season that lasts longer in the northern portion of the island, typically from May to November. Consequently, forest habitats are generally semi-deciduous and drought-adapted in the north and evergreen in the south. Other major habitat types include coral reefs, seagrass meadows, tropical montane forest, beach forest, coastal scrub, savannah woodland, open eucalyptus forest, swamps, mangroves, and a variety of agricultural lands such as coffee plantations and paddy fields. A more comprehensive review of Timor-Leste's geography and environment can be obtained from Trainor et al. (2007) and Kaiser et al. (2011).

The herpetofaunal diversity of Timor-Leste is relatively poorly known, largely due to centuries of conflict and political instability that have hampered biological research. The first comprehensive report on the herpetofauna of Timor-Leste was published by Kaiser et al. (2011) followed by several complementary surveys throughout various parts of the country (Sanchez et al. 2012; Kaiser et al. 2013; O'Shea et al. 2015). These initial reports documented several undescribed species of *Cyrtodactylus* indicating that the diversity of this group of lizards in Timor-Leste is still underestimated and lack a formal scientific description. In August 2022, we surveyed the eastern region of Timor-Leste including Nino Konis Santana National Park (NKS) in the municipality of Lautém. Established in 2007, NKS is the first national park in Timor-Leste and encompasses the entire eastern tip of Timor, including Jaco Island (Fig. 1). It is mostly characterised by lowland tropical forest and includes several limestone caves that are of archaeological importance (García-Diez et al. 2020; O'Connor et al. 2021). It was during a survey of two of these caves that we discovered a population of *Cyrtodactylus* that is morphologically and genetically distinct from all other described congeners. In this study, we present evidence supporting the recognition of the *Cyrtodactylus* from NKS as a distinct evolutionary lineage followed by its description as a new species.

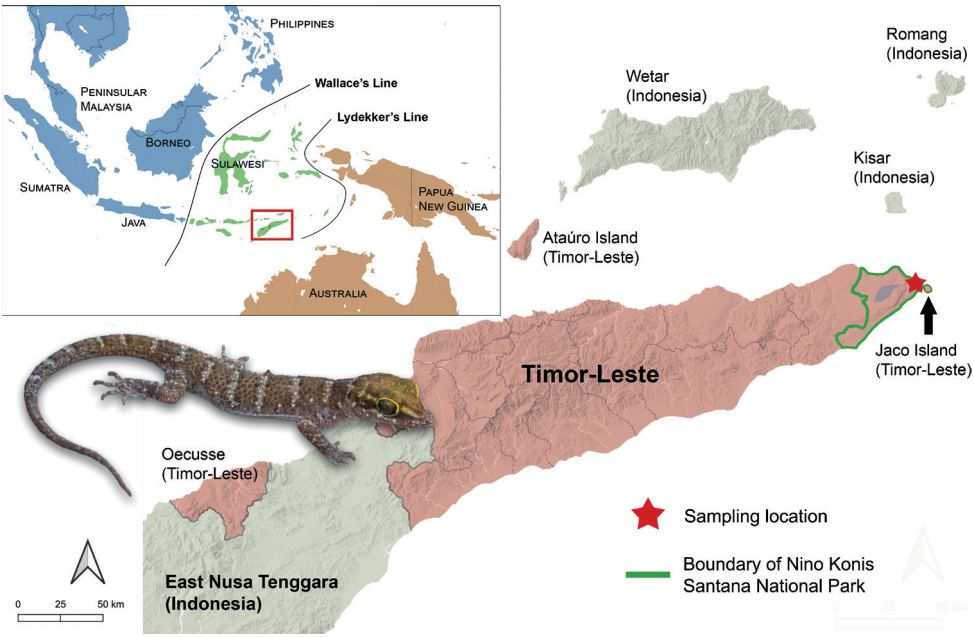

Figure 1. Upper left inset: Map of Sundaland (blue), Wallacea (green), and the Australo-Papuan region (orange) including Wallace's and Lydekker's lines that demarcates the boundaries of the three biogeographic regions. The red box denotes Timor and the surrounding islands. Right: An expanded map of Timor-Leste and the surrounding islands. Territories belonging to Timor-Leste are shaded in red. The red star indicates the location of the field site in the northeastern sector of the Nino Konis Santana National Park.

Materials and methods

Sampling and phylogenetic analysis

Fieldwork was conducted at the adjacent caves of Lene Hara and Napana Wei (8.411758°S, 127.293321°E; 152 m a.s.l.) in the northeastern sector of Nino Konis Santana National Park (**NKS**) on 30 August 2022. Specimens were euthanised using MS-222, fixed in 10% formalin, and transferred to 70% ethanol for long-term preservation. Liver samples were dissected and stored in 95% ethanol before fixation. All specimens are deposited at the Zoological Reference Collection (**ZRC**) of the Lee Kong Chian Natural History Museum, Singapore (**LKCNHM**).

We selected three (of the ten collected) specimens for DNA sequencing. The NADH dehydrogenase subunit 2 (ND2) mitochondrial gene was sequenced using the primers L4437 (AAGCTTTCGGGCCCATACC) and H5934 (AGRGTGCCAATGTCTTTGTGRTT) (Macey et al. 1997). The following PCR thermal protocol was used: initial denaturation at 95 °C for 5 min, followed by 35 cycles of a second denaturation at 94 °C for 60 s, annealing at 58 °C for 60 s, and cycle extension at 72 °C for 60 s. The newly generated sequences are accessioned at GenBank under the numbers OP650033–OP650035. An additional 350 sequences were obtained from GenBank representing six outgroup taxa and 344 ingroup taxa comprising all published ND2 sequences of

described and undescribed *Cyrtodactylus* (Suppl. material 1: table S1). Sequences were assembled and aligned (MUSCLE algorithm) using Geneious v. 5.6.7 (Kearse et al. 2012). A partitioned maximum likelihood phylogenetic analysis was performed using IQTREE 2 (Minh et al. 2020). The sequence alignment was divided into four partitions comprising the 1st, 2nd, and 3rd codon positions of the ND2 gene, and all tRNAs combined. The TEST function was implemented to determine the best-fit partition model using ModelFinder (Kalyaanamoorthy et al. 2017). Branch support was assessed via 1000 ultrafast bootstrap replicates (Hoang et al. 2017). Uncorrected *p*-distances were calculated using the complete deletion option in MEGA-X (Kumar et al. 2018). A Bayesian phylogeny was also inferred using BEAST2 v. 2.7.0 (Bouckaert et al. 2014) following the same partition scheme. Substitution models were averaged using the BEAST plugin bModelTest (Bouckaert and Drummond 2017). Two separate MCMC chains were executed (30,000,000 generations per chain) and subsequently assessed for convergence using Tracer v. 1.7 (Rambaut et al. 2018). Converged MCMC runs (ESS > 200) were combined and the first 10% of sampled trees were discarded as burn-in. The BEAST module TreeAnnotator was used to generate a Maximum Clade Credibility tree. The BEAST2 analysis was performed through the CIPRES Science Gateway portal (Miller et al. 2010).

Morphology

The following morphological data were collected following Grismer et al. (2022): Snout-vent-length (**SVL**) = tip of snout to vent; axila-groin length (**AG**) = posterior margin of forelimb at its insertion point on the body to anterior margin of hind limb at its insertion point on the body; humeral length (**HumL**) = proximal end of humerus at its insertion point in the glenoid fossa to distal margin of elbow while flexed 90°; forearm length (**ForL**) = posterior margin of elbow while flexed 90° to inflection of the flexed wrist on the ventral side; femur length (**FemL**) = proximal end of femur at insertion point in the acetabulum to distal margin of knee while flexed 90°; tibial length (**TibL**) = posterior margin of knee while flexed 90° to base of heel on the ventral side; head length (**HL**) = posterior margin of retroarticular process of lower jaw to tip of snout; head width (**HW**) = distance across angle of jaws; head depth (**HD**) = maximum height of head from occiput to base of lower jaw posterior to eyes; eye diameter (**ED**) = greatest horizontal diameter of eye-ball; eye-to-ear distance (**EE**) = anterior edge of ear opening to posterior edge of the bony orbit; eye-to-snout distance (**ES**) = anteriormost margin of the bony orbit to tip of snout; eye-to-nostril distance (**EN**) = anterior margin of the bony orbit to posterior margin of the external nares; interorbital distance (**IO**) = distance between dorsomedial-most edges of the bony orbits; ear length (**EL**) = greatest oblique length across the auditory meatus; internarial distance (**IN**) = distance between the external nares across the rostrum; supralabials (**SL**) = largest scale at the corner of mouth or posterior to eye, to rostral scale; infralabials (**IL**) = from termination of enlarged scales at the corner of mouth to mental scale; paravertebral tubercles (**PVT**) = number of tubercles between limb insertions counted in a straight line immediately left of vertebral column; total subdigital lamellae beneath 4th toe (**TL4T**); total subdigital lamellae beneath 4th finger (**TL4T**); ventral scales (**VS**) = number of ventral scales across midbody between ventrolateral folds; enlarged femoral scales (**FS**) = number of

enlarged scales from each thigh combined as a single metric; total precloaco-femoral pores in males (**PFP**) = total number of continuous pores on the femur and precloacal region.

To eliminate bias stemming from ontogenetic variation (Chan and Grismer 2021), we performed allometric body-size correction using the Thorpe method (Thorpe 1983) implemented in the GroupStruct R package (Chan and Grismer 2022). We then used principal components analysis (PCA) to find the best low-dimensional representation of variation in the data to determine whether morphological variation could form the basis of detectable group structure. The PCA only included closely related species for which published morphometric data are available. These were *Cyrtodactylus petani* Riyanto, Grismer & Wood, 2015, *C. batucolus* Grismer, Chan, Grismer, Wood & Belabut, 2008, and *C. seribuatensis* Youmans & Grismer, 2006. Only males were included in the analysis because the sample size for females was too low. Using the size-corrected dataset, we performed an ANOVA followed by a TukeyHSD posthoc test to determine whether the means of assessed characters were significantly different among all species pairs. All morphological analyses were performed and visualised in R (R Core Team 2014).

Supplementary material

All supplementary material associated with this study can be obtained from the online version of this manuscript and the Figshare repository (https://doi.org/10.6084/m9.figshare.21359970.v1).

Results

Genetic analyses

The final sequence alignment comprised 1566 base pairs, 1297 variable sites, 1141 parsimony informative sites, and 23.2% missing data. The best substitution model scheme for the IQ-TREE analysis was TVM + F + I + G4 for the 1st codon position of ND4 and tRNAs, TIM + F + I + G4 for the 2nd codon position, and GTR + F + I + G4 for the 3rd codon position. The phylogenetic analysis recovered the new population within the *darmandvillei* group (sensu Grismer et al. 2021) with strong support (Ultrafast bootstrap/Bayesian posterior probability, UFB/BPP = 100/1.0; Fig. 2). Within this group, the new population was inferred as the sister lineage to a clade comprising *Cyrtodactylus batucolus*, *C. petani*, *C. seribuatensis*, *C. sadleiri* Wells & Wellington, 1985, *C.* cf. *jatnai* from Bali and two undescribed lineages from Yamdena Island, Indonesia (*C.* sp. 1) and the Kai Islands (*C.* sp. 2) (Fig. 2). Both maximum likelihood and Bayesian phylogenies inferred identical topologies for the *darmandvillei* group with strong support across all taxa except for one branch that received moderate support (UFB/BPP = 91/0.7). Fully annotated and genus-wide phylogenies are included in the Suppl. material 1. Genetic divergence (uncorrected *p*-distance) between the new population and all other taxa in the *darmandvillei* group is high (range = 9.8–20.2%, mean = 13.3%) and consistent with the species-level divergences of other taxa within the *darmandvillei* group (Fig. 3A).

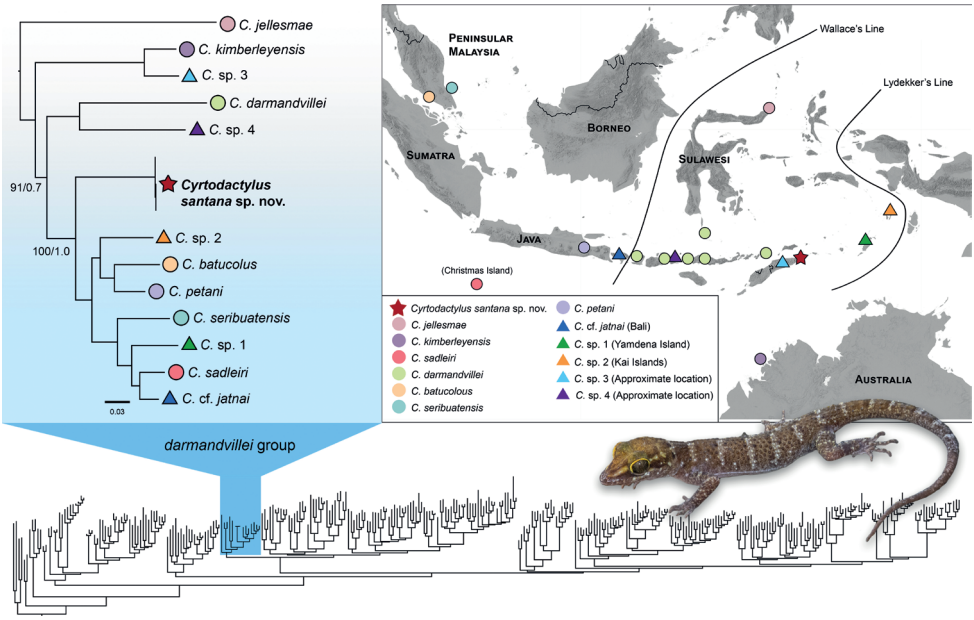

Figure 2. Lower: Genus-wide phylogeny based on all published sequences of described and undescribed lineages of *Cyrtodactylus* (see Suppl. material 1 for the fully annotated phylogeny). The *C. darmandvillei* group is highlighted in blue. Upper left: Maximum-likelihood phylogeny of the *C. darmandvillei* group (Bayesian phylogeny has identical topologies). All nodes are highly supported in the maximum likelihood and Bayesian analysis (UFB/BPP ≥ 99/0.95) except for one node that was moderately supported in the Bayesian analysis (BPP = 0.8). Coloured symbols correspond to the distribution map on the right; Circles = nominal species, Triangles = undescribed/uncertain species, and Star = new species described in this study. Upper right: Distribution of nominal and undescribed lineages in the *C. darmandvillei* group. The specific localities of *C.* sp. 3 (East-Timor) and *C.* sp. 4 (East Nusa Tenggara) are not known, thus, their placements on the map are approximated.

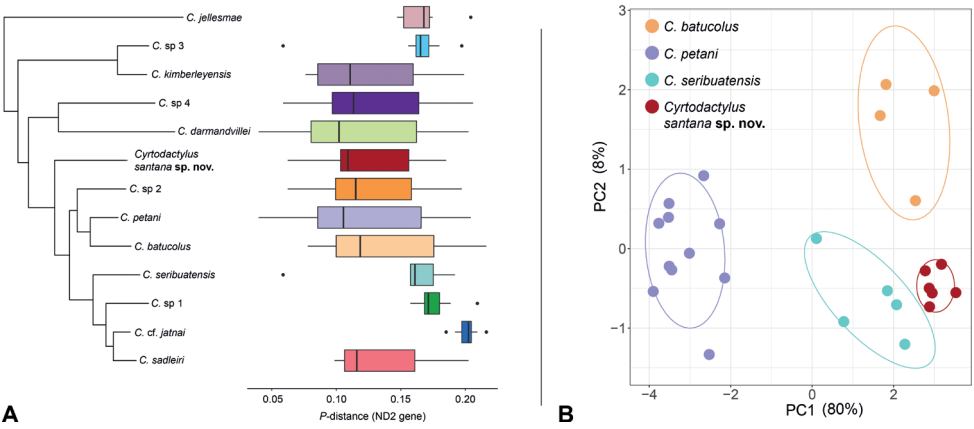

Figure 3. A Maximum-likelihood phylogeny of the *Cyrtodactylus darmandvillei* group with boxplots showing the distribution of pairwise uncorrected *p*-distances (ND2 gene) between each corresponding taxon and all other taxa within the *C. darmandvillei* group **B** plot of PCA scores based on a subset of ten continuous characters.

Morphological analyses

For the PCA analysis, only PC1 had eigenvalues above 1.0 indicating that most variation (80%) is captured along the first axis (Table 1). Along the first axis (PC1), *Cyrtodactylus petani* is distinctly separated from the other species and there is a slight separation between *C. seribuatensis* and the new population (Fig. 3B). The second axis (PC2) captured 8% of the variation and further separates *C. batucolus* from *C. seribuatensis* and the new species. PCA loadings for PC1 are relatively consistent (0.27–0.34) indicating that all assessed characters contributed to the overall variation with slightly heavier loadings on ForL, TibL, and HL (Table 1). The fact that *Cyrtodactylus santana* sp. nov., *C. batucolus*, and *C. seribuatensis* overlap along the heavily loaded first PC and all are well-separated from *C. petani* is likely due to the fact that the former are rock-dwellers, and the latter is more of a habitat generalist. Similar results have been observed in *Cyrtodactylus* from Vietnam (Grismer and Grismer 2017) and Peninsular Malaysia (Kaatz et al. 2021).

The ANOVA and TukeyHSD posthoc test showed that the new population is significantly different from *C petani* in all assessed characters; from *C. batucolus* for the characters TibL and IOD; and from *C. seribuatensis* for the characters ForL and EN (Table 2). The morphological analyses of continuous characters indicate that the new population is morphometrically more similar to *C. batucolus* and *C. seribuatensis* than it is to *C. petani*. Comparisons of discrete and meristic characters provide additional distinguishing characters between the new population and other species within the *darmandvillei* group (Table 3).

Systematics

Taken together, the results from our analyses demonstrate that the new population from Timor-Leste is a strongly supported, distinct evolutionary lineage (Fig. 2) that is both genetically (Figs 2, 3A) and morphometrically (Fig. 3B) divergent from its congeners. Therefore, we describe it as a new species below.

Table 1. Summary statistics and loadings for the PCA analysis. Character abbreviations are defined in Materials and methods.

	PC1	PC2	PC3	PC4	PC5	PC6	PC7	PC8	PC9	PC10
Standard deviation	2.84	0.89	0.57	0.49	0.44	0.41	0.28	0.26	0.22	0.18
Proportion of Variance	0.80	0.08	0.03	0.02	0.02	0.02	0.01	0.01	0.01	0.00
Cumulative Proportion	0.80	0.88	0.92	0.94	0.96	0.98	0.99	0.99	1.00	1.00
Eigenvalue	8.05	0.79	0.33	0.24	0.20	0.17	0.08	0.07	0.05	0.03
SVL	0.31	0.23	0.55	0.28	-0.65	0.11	-0.12	-0.02	0.06	0.09
ForL	0.34	0.13	0.04	-0.23	0.23	-0.37	-0.51	0.04	-0.21	0.57
TibL	0.34	-0.18	-0.14	-0.02	-0.07	-0.11	-0.20	0.78	0.20	-0.36
AG	0.32	0.20	0.45	0.03	0.56	0.03	-0.08	-0.21	-0.07	-0.54
HL	0.34	0.08	-0.05	-0.33	-0.10	0.30	0.44	0.19	-0.66	0.03
HD	0.30	0.33	-0.61	0.43	-0.16	-0.27	-0.02	-0.27	-0.18	-0.22
ED	0.29	-0.51	0.08	0.62	0.29	0.03	0.27	0.05	-0.04	0.33
EE	0.33	-0.02	-0.31	-0.10	0.07	0.74	-0.28	-0.20	0.33	0.12
EN	0.33	0.26	-0.01	-0.26	0.06	-0.26	0.57	-0.04	0.57	0.18
IOD	0.27	-0.64	0.01	-0.34	-0.29	-0.25	-0.05	-0.45	-0.01	-0.21

Table 2. Results of the Tukey posthoc test showing the *p*-values for all pairwise comparisons. Values highlighted in green represent $p < 0.05$, whereas those in red represent $p > 0.05$.

	SVL	ForL	TibL	AG	HL	HD	ED	EE	EN	IOD
petani-batucolus	0.00	0.00	0.00	0.00	0.00	0.00	0.06	0.00	0.00	0.53
santana-batucolus	0.32	0.92	0.04	0.15	0.81	0.78	0.11	0.26	0.69	0.00
seribuatensis-batucolus	0.46	0.03	0.94	0.02	0.97	0.02	0.40	0.95	0.00	0.00
santana-petani	0.00	0.00	0.00	0.00	0.00	0.00	0.00	0.00	0.00	0.00
seribuatensis-petani	0.00	0.00	0.00	0.00	0.00	0.02	0.00	0.00	0.00	0.00
seribuatensis-santana	1.00	0.00	0.09	0.58	0.50	0.08	0.86	0.07	0.00	0.48

Table 3. Comparisons of discrete and meristic characters among species of the *Cyrtodactylus darmandvillei* group. NA = not applicable; ? = unknown or not assessable.

	Cyrtodactylus santana sp. nov.	*C. batucolus*	*C. darmandvillei*	*C. jellesmae*	*C. kimberleyensis*	*C. petani*	*C. sadleiri*	*C. seribuatensis*
Max SVL	74	75.2	75	63	45	57.2	88	75
Tuberculation moderate to strong	yes	yes	yes	yes	no	yes	yes	yes
Tubercules on forelimbs	yes	yes	yes	yes	no	yes	yes	yes
Tubercules on hindlimbs	yes	yes	yes	yes	no	yes	yes	yes
Tubercules on head and/or occiput	yes	yes	yes	yes	no	yes	yes	yes
Paravertebral tubercles	23–27	30–35	17–20	?	16–18	20–25	22–25	27–35
Proximal subdigital lamellae broad	yes	yes	yes	yes	yes	yes	yes	yes
Subdigital lamellae on 4th toe	15–19	17–19	?	?	16	17–18	19–24	19–22
Ventral scales	42–48	38–42	36–40	40–45	36	30–35	34–42	32–39
Deep precloacal groove	no	no	no	no	no	no	yes	no
Enlarged precloacal scales	yes	yes	?	no	no	yes	yes	yes
Enlarged femoral scales	yes	yes	?	no	no	yes	yes	yes
Precloacal and femoral pores continuous	yes	yes	?	NA	NA	yes	NA	yes
Precloaco-femoral pores	43–45	43–46	?	NA	NA	31–35	NA	42–45
Enlarged median subcaudals	no	no	yes	no	no	no	no	no

Cyrtodactylus santana sp. nov.

https://zoobank.org/4D481F41-F6F5-4A6E-ABCD-FEFFA8868D2F
Figs 4, 5
(Nino Konis Santana Bent-toed Gecko)

Material examined. ***Holotype.*** ZRC 2.7672 (Fig. 4), adult male collected by Chan Kin Onn, Iffah Iesa, Fernando Santana, and Pedro Pinto on 30 August 2022 at 2230 hrs from Napana Wei cave (8.411758°S, 127.293321°E; 152 m a.s.l.) in the northeastern sector of NKS. ***Paratypes.*** ZRC 2.7673–77 (adult males) and ZRC 2.7678–81 (adult females) with the same collection information as the holotype.

Diagnosis. The new species is a distinct evolutionary lineage that is closely related to *C. batucolus*, *C. seribuatensis*, *C. petani*, and *C. sadleiri*. It can be differentiated from other congeners by the following combination of characters: strong dorsal

tuberculation present, 23–27 paravertebral tubercles, 15–19 subdigital lamellae on 4th toe, 42–48 ventral scales across midbody, deep precloacal groove absent, enlarged femoral and precloacal scales present, distinct blotches on top of the head absent, dorsal bands faint, whitish, lightly counter-shaded with dark brown.

Description of holotype. Adult male SVL 68.6 mm; head moderate in length (HL/SVL 0.30), wide (HW/HL 0.65), somewhat flattened (HD/HL 0.40), distinct from neck, triangular in dorsal profile; lores weakly inflated, prefrontal region concave, canthus rostralis smoothly rounded; snout elongate (ES/HL 0.43) rounded in dorsal profile; eye large (ED/HL 0.23); ear opening elliptical, moderate in size (EL/HL 0.11), obliquely oriented; eye to ear distance greater than diameter of eye; rostral wider than high, concave, partially divided dorsally, bordered posteriorly by left and right supranasals and smaller medial postrostral (= internasal), bordered laterally by first supralabials; external nares bordered anteriorly by rostral, dorsally by a large, anterior supranasal and small, posterior supranasal, posteriorly by two postnasals, ventrally by first supralabial; 10 (R) 10 (L) squarish supralabials extending to just beyond dorsal inflection of labial margins tapering in size abruptly below midpoint of eye, first supralabial largest; nine (R) and eight (L) infralabials tapering smoothly posteriorly slightly beyond last supralabial posteriorly; scales of rostrum and lores raised, larger than granular scales on top of head and occiput; scales of occiput intermixed with slightly enlarged tubercles; dorsal superciliaries elongate, keeled; mental triangular, bordered laterally by first infralabials and posteriorly by left and right rectangular postmentals which contact medially; one row of slightly enlarged, elongate sublabials extending posteriorly to 6th infralabial; gular scales small, granular, grading posteriorly into slightly larger, flatter, throat scales which grade into larger, flat, smooth, imbricate, pectoral and ventral scales.

Body relatively short (AG/SVL 0.43) with well-defined ventrolateral folds; dorsal scales small, granular, interspersed with moderately sized, conical, semi-regularly arranged, keeled tubercles; tubercles extend from occiput to anterior one-third of tail; tubercles on occiput and nape relatively small, increases in size and density posteriorly; tubercles on pelvic region and hindlimbs largest and densest; approximately 15 longitudinal rows of tubercles at midbody; 27 paravertebral tubercles on body; 44 flat, imbricate, ventral scales between ventrolateral body folds, ventral scales much larger than dorsal scales; precloacal scales large, seven scales across base of precloacal region; precloacal depression weak (Fig. 4E).

Forelimbs moderate in stature, relatively short (ForL/SVL 0.17); granular scales of forearm slightly larger than those of body, interspersed with large, keeled tubercles; palmar scales slightly raised; digits well-developed, inflected at basal, interphalangeal joints; subdigital lamellae transversely expanded throughout its length; digits slightly more narrow distal to inflection; claws well-developed, sheathed by a dorsal and ventral scale; hind limbs more robust than forelimbs, moderate in length (TibL/SVL 0.18), covered dorsally by granular scales interspersed with larger, keeled tubercles and covered anteriorly by flat, slightly larger scales; ventral scales of thigh flat, imbricate, larger than dorsals; ventral tibial scales flat, imbricate; two rows of enlarged, flat, imbricate,

femoral scales extend from knee to knee through the precloacal region where they are continuous with enlarged, precloacal scales; posterior row of enlarged femoral scales contains 41 contiguous pore-bearing scales extending from knee to knee forming a V-shape bordering the precloacal depression; postfemoral scales immediately posterior to the row of pore-bearing scales nearly one-half their size, forming an abrupt union on posteroventral margin of thigh; plantar scales low, slightly rounded; digits well-developed, inflected at basal, interphalangeal joints; subdigital lamellae transversely expanded throughout length of digit; digits more narrow distal to joints; 17 subdigital lamellae on right 4th toe, 16 on left; claws well-developed, sheathed by a dorsal and ventral scale.

Tail robust, original, tip broken; dorsal scales at base of tail granular becoming flatter posteriorly; no median row of transversely enlarged, subcaudal scales; subcaudal scales much larger than dorsal caudal scales; one pair of paravertebral and dorsolateral tubercle rows on either side of midline; distance between paravertebral tubercle rows much greater than distance between paravertebral and adjacent dorsolateral rows; caudal tubercles decrease in size posteriorly, extending approximately 40% length of tail; four enlarged, postcloacal tubercles at base of tail on hemipenial swelling; all postcloacal scales flat, imbricate.

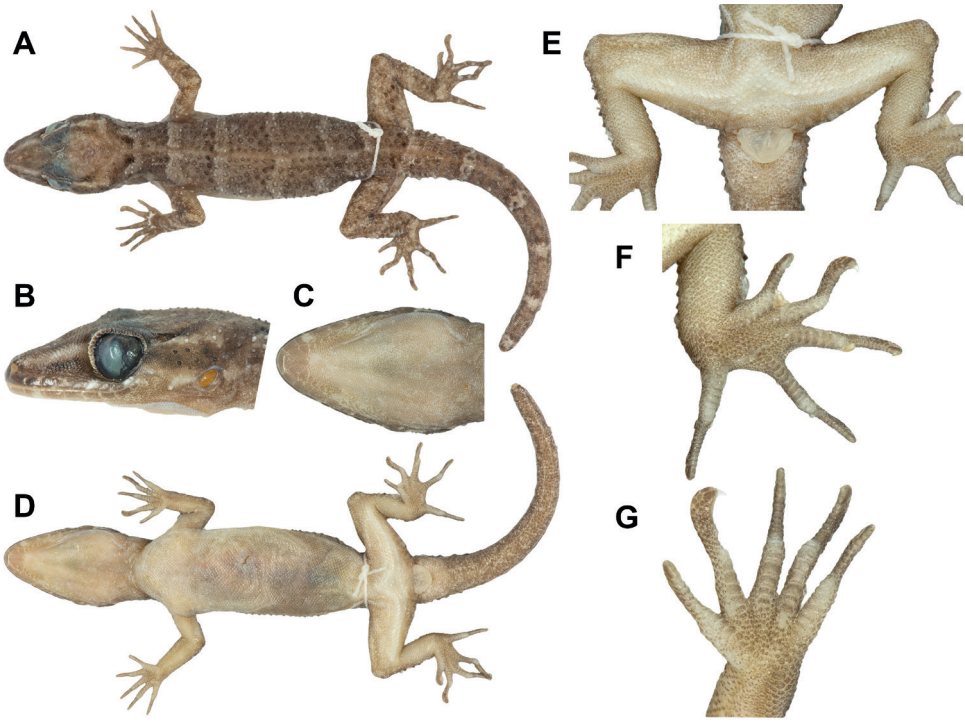

Figure 4. Holotype of *Cyrtodactylus santana* sp. nov. (ZRC 2.7672) **A** dorsal view of entire specimen **B** closeup of side of head **C** closeup of underside of head **D** ventral view of entire specimen **E** ventral view of pelvic region **F** ventral view of right foot **G** ventral view of right hand.

Figure 5. Live images of *Cyrtodactylus santana* sp. nov. paratype female (ZRC 2.7679) (top), *C. batucolus* from Pulau Besar, Malacca, Peninsular Malaysia (middle), and *C. seribuatensis* from Pulau Mentigi, Johor, Peninsular Malaysia (lower).

Colouration in life. Dorsal ground colour of head yellowish; neck, trunk, limbs, and tail brown; no distinct markings on top of head; pale loreal stripe extend from nostril to eye and continuing as a postorbital stripe that forms a faint forked pattern on occiput; area dorsal and ventral to the loreal and postorbital stripe counter-shaded with dark brown; six pale, faint, thin, irregular bands from nape to base of tail faintly counter-shaded anteriorly and posteriorly with dark brown; dark speckling and faint, cream-coloured blotches on limbs; pale body banding extend onto tail but not encircling tail (Fig. 5). Ventral surfaces of head, body and limbs lightly stippled with grey; subcaudal region darkened with fine mottling; iris greenish brown.

Variation. ZRC 2.7674–76, ZRC 2.7678, and ZRC 2.7680–81 have broken tails. Some specimens have more distinct dorsal markings than others (Fig. 6). The level of yellowness of the head also varies and does not appear to be a sexually dimorphic character. Meristic differences are listed in Table 4.

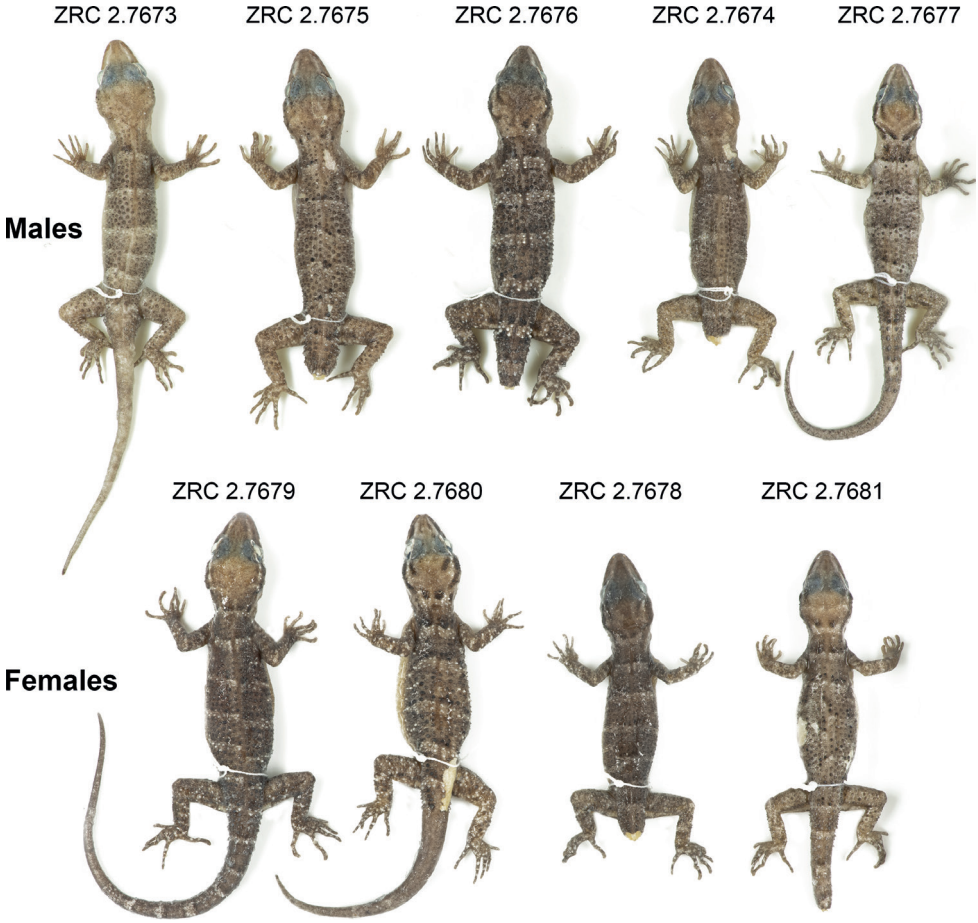

Figure 6. Paratypes of *Cyrtodactylus santana* sp. nov. and their corresponding voucher numbers.

Table 4. Raw morphological data for the type series. Character abbreviations are defined in Materials and methods.

	ZRC 2.7672	**ZRC 2.7673**	**ZRC 2.7674**	**ZRC 2.7675**	**ZRC 2.7676**	**ZRC 2.7677**	**ZRC 2.7678**	**ZRC 2.7679**	**ZRC 2.7680**	**ZRC 2.7681**
Type	Holotype	Paratype	Paratype	Paratype	Paratype	Paratype	Paratype	Paratype	Paratype	Paratype
Sex	male	male	male	male	male	male	female	female	female	female
SVL	68.6	70	64.6	74	70.6	59.1	62.2	70	64.2	60.6
AG	29.6	28.7	25.8	32.3	28	24.3	27.5	31.6	27.5	27.2
HumL	7.7	8.3	7.8	8.8	9	6.9	7.6	8.6	7.9	6.7
ForL	11.5	11.2	10	12	11.8	10	9.8	10.8	10	9.5
FemL	17.6	17	14.8	17.1	16.3	14.4	15	17.2	16.6	14
TibL	12.1	12	11.8	13.7	13.5	11	11.8	12.9	12	11.6
HL	20.5	20.7	19.2	22.7	21.5	17.1	18.4	20.7	19.2	17.9
HW	13.5	14	12.4	14.7	14.9	11.9	11.6	13.6	13.3	12
HD	8.2	9.3	8	9.1	9.8	7.3	7.4	8.6	8.5	7.4
ED	4.8	5.2	4.2	4.8	5.1	4.2	4.3	5.2	5.2	4
EE	5.8	5.7	5.9	6.4	6.3	5	5.4	5.7	5.3	4.7
ES	8.9	8.7	8	9.8	8.8	7.8	7.5	9.2	8.2	7.7
EN	6.4	6.7	6.5	7.1	6.8	5.7	6	6.7	6.2	5.7
IO	6.2	6.1	5.7	6.8	6.3	5.2	5.4	6	6	5.6
EL	2.3	2.2	1.5	2.3	1.7	1.4	1.9	1.8	2	1.2
IN	2.4	2.8	2.2	2.3	2.3	2	2	2.4	1.9	1.8
SL (R/L)	10/10	10/11	11/11	11/12	12/11	10/10	11/11	11/11	10/11	12/11
IL (R/L)	9/8	8/8	9/9	9/9	10/9	9/9	10/9	9/9	9/9	9/9
PVT	27	25	27	27	25	23	26	27	24	24
TL4T	17	15	16	18	19	15	15	15	15	16
TL4F	17	17	17	17	18	15	18	18	18	18
VS	44	45	48	42	48	45	47	47	42	42
FS	28	28	28	26	27	25	27	27	26	26
PFP	44	45	43	45	45	?	NA	NA	NA	NA

Comparisons. Due to the large number of *Cyrtodactylus* species, we restrict our comparison to species within the *darmandvillei* group. The new species differs from *C. batucolus* by having fewer paravertebral tubercles (23–27 vs. 30–35), more ventral scales (42–48 vs. 38–42), lacking distinct blotches on top of a yellowish head, lacking dark paravertebral dorsal blotches on the body and tail, and having less distinct but well-defined pale-coloured dorsal bands (Fig. 5). From *C. darmandvillei* Weber, 1890, it differs by having more paravertebral tubercles (23–27 vs. 17–20), more ventral scales (42–48 vs. 36–40), and lacking enlarged median subcaudals. From *C. jellesmae* Boulenger, 1897 it differs by being larger in size (max SVL 74 mm vs. 63 mm) and having as opposed to lacking enlarged femoral and precloacal scales. From *C. kimberleyensis* Bauer & Doughty, 2012, it differs by being larger in size (max SVL 74 mm vs. 45 mm), having moderate to strong dorsal tubercles (vs. weak to absent), more paravertebral tubercles (23–27 vs. 16–18), more ventral scales (42–48 vs. 36), and having as opposed to lacking enlarged femoral and precloacal scales. From *C. petani*, it differs by being larger in size (max SVL 74 mm vs. 57.2 mm), having more ventral scales (42–48 vs. 30–35), and more precloaco-femoral pores in males (43–45 vs. 31–35). From *C. sadleiri*, it differs by being smaller in size (max SVL 74 mm vs. 88 mm), having less subdigital lamellae on 4th toe (15–19 vs. 19–24), more ventral scales (42–48 vs. 34–42), and lacking a deep precloacal groove. From *C. seribuatensis*, it differs by having fewer subdigital lamellae on 4th toe

(15–19 vs. 19–22), more ventral scales (42–48 vs. 32–39), and lacking distinct blotches on top of a yellowish head, lacking dark paravertebral dorsal blotches on the body and tail, and having less distinct but well-defined pale-coloured dorsal bands (Fig. 5).

Distribution. *Cyrtodactylus santana* sp. nov. occurs in Lene Hara and Napana Wei caves within NKS. The nearest village is Tutuala in the municipality of Lautém. The larger distribution of this species is not yet known but it likely occurs in other limestone caves within NKS. There is a report of a similar-looking and unidentified *Cyrtodactylus* on Ataúro island (Kaiser et al. 2013: fig. 3B). However, the specific identity of the Ataúro *Cyrtodactylus* cannot be ascertained at this point due to the lack of comparative material. As such, we consider the distribution of *Cyrtodactylus santana* sp. nov. to be restricted to NKS until new data suggest otherwise (see Discussion for more information about the *Cyrtodactylus* from Ataúro).

Natural history. Lizards were considerably more abundant in Napana Wei cave compared to Lene Hara cave (Fig. 7) even though the two caves are adjacent to each other and are less than 500 m apart but not connected by contiguous limestone. This disparity could be associated with the differences in the geomorphology of both caves. Lene Hara cave is cavernous and dome-like with a high ceiling (Fig. 7), whereas Napana Wei is low and narrow. In Lene Hara, a small number of lizards were observed under small rocks and on columnar formations but in Napana Wei, lizards were found in abundance on the underside and exterior surface of the cave wall. No lizards were observed on surrounding vegetation, suggesting that they could be limestone specialists. The caves are located less than 1 km from the coast. *Cyrtodactylus santana* sp. nov. is nocturnal and is found in sympatry with *Gehyra* sp.

Figure 7. Type locality of *Cyrtodactylus santana* sp. nov. at Lene Hara cava as viewed from the exterior (left) and interior (right). Photographs by Tan Heok Hui.

Etymology. Nino Konis Santana was a freedom fighter who led the Falintil militia against the Indonesian occupation of Timor-Leste. He was not only a fearless leader of the armed wing of the Resistance but also played a key role in peace initiatives, earning him a reputation as a peacemaker, diplomat, and statesman. The Nino Konis Santana National Park was named in honor of this national hero who was born in the suco (village in Tetum) of Tutuala, located within the boundaries of the park. The specific epithet *santana* is used as a noun in apposition referring to Nino Konis Santana National Park, which is the type locality of the new species.

Discussion

Members of the *darmandvillei* group comprise lineages from Wallacea (*Cyrtodactylus santana* sp. nov., *C. jellesmae*, *C. darmandvillei*, *C.* sp. 1, *C.* sp. 2, *C.* sp. 3, and *C.* sp. 4), Sundaland (*C. batucolus*, *C. petani*, *C. seribuatensis*, *C. sadleiri*, *C.* cf. *jatnai*), and an island off the northern tip of Western Australia (*C. kimberleyensis*; Fig. 2). However, the most recent common ancestors of the non-Wallacean lineages are younger than the Wallacean lineages suggesting that the ancestor of the *darmandvillei* group likely originated in Wallacea with more recent dispersals into Sundaland and Australia (Grismer et al. 2022). It is interesting to note that members of the *darmandvillei* group are absent in the greater Sunda islands of Borneo and Sumatra but are present on islands off the eastern and western coast of southern Peninsular Malaysia (*C. batucolus* and *C. seribuatensis*). Stranger still are the phylogenetic placements of *C. batucolus* and *C. seribuatensis* from Peninsular Malaysia, which are more closely related to lineages from Java and the Moluccas, respectively, than they are to each other (Fig. 2). This anomalous pattern could be attributed to missing taxa that have yet to be discovered or taxa that lack genetic representation, particularly from Sulawesi and the Moluccas. There are numerous species of *Cyrtodactylus* described from Wallacea that have not yet been sequenced including *C. batik* Iskandar, Rachmansah & Umilaela, 2011, *C. celatus* Kathriner, Bauer, O'Shea, Sanchez & Kaiser, 2014, *C. fumosus* (Müller, 1895), *C. halmahericus* (Mertens, 1929), *C. deveti* (Brongersma 1948), *C. hitchi* (Riyanto et al. 2016), *C. nuaulu* (Oliver et al. 2009), *C. tahuna* (Riyanto et al. 2018b), *C. tanahjampea* Riyanto, Kurniati & Engilis, 2018, *C. tambora* Riyanto, Mulyadi, McGuire, Kusrini, Febylasmia, Basyir & Kaiser, 2017, *C. wetariensis* (Dunn 1927), and *C. wallacei* Hayden, Brown, Gillespie, Setiadi, Linkem, Iskandar, Umilaela, Bickford, Riyanto, Mumpuni & McGuire, 2008. Although most Wallacean taxa belong to the *darmandvillei* group, there is one known exception, *C. papeda* Riyanto, Faz, Amarasinghe, Munir, Fitriana, Hamidy, Kusrini & Oliver, 2022 from Obi Island in the Moluccas that is part of the *marmoratus* group. This is a relatively small group comprising species that are distributed in Java, Sumatra, the Moluccas, and New Guinea (Grismer et al. 2021); and are notably absent in the intervening regions of the Lesser Sunda Islands and Sulawesi. Nevertheless, we expect that most Wallacean taxa will fall within the *darmandvillei* group barring a few exceptions. We anticipate that the eventual inclusion of sequences from missing taxa in a comprehensive phylogenetic

analysis will reveal new insights and improve our understanding of the biogeography and evolutionary history of *Cyrtodactylus* in the Southeast Asian region and beyond.

Our phylogenetic analysis also included several lineages of uncertain identities. Riyanto et al. (2015) published a phylogeny that included two lineages of *Cyrtodactylus* from Bali, one of which we consider to be conspecific with *C. seribuatensis* based on low genetic differentiation. Subsequently, *Cyrtodactylus jatnai* Amarasinghe, Riyanto, Mumpuni & Grismer, 2020 was described from Bali solely based on morphology and was demonstrated to be distinct from *C. seribuatensis*. We hypothesise that the unidentified sequence from Bali (GenBank KU232624) could represent *C. jatnai* and therefore we refer to that sequence as *C.* cf. *jatnai* pending confirmation from additional data. There is also an unidentified lineage from Timor-Leste (*C.* sp. 3) that is more closely related to *C. kimberleyensis* from Australia than it is to *Cyrtodactylus santana* sp. nov. indicating that *Cyrtodactylus* on Timor-Leste is not monophyletic. Based on the general colour pattern and small size of *C. kimberleyensis* (Bauer and Doughty 2012), we believe that *C.* sp. 3 could be one of the unidentified species shown in O'Shea et al. (2015), all of which are relatively small in size and bear broad morphological resemblance to *C. kimberleyensis*.

Based on currently available data, *Cyrtodactylus santana* sp. nov. is a nocturnal species occurring in limestone caves in the lowland tropical forest of NKS. We did not observe any lizards on the vegetation surrounding the caves. However, our observations are based on one night's sampling effort and our supposition that this species occurs exclusively on limestone could be overturned with more extensive and intensive surveys. There is also a report of a similar-looking and unidentified *Cyrtodactylus* on Ataúro Island that is referred to as *C.* sp. 'Ataúro coast' in O'Shea et al. (2015). In that report, the authors noted that the lizard was superficially similar to *C. darmandvillei* and was found in a variety of habitats including a limestone cliff, coconut groves, rock piles, and a tropical dry forest. Unfortunately, due to the lack of comparative material, the specific identity of *C.* sp. 'Ataúro coast' cannot be determined at this point. We hypothesise that the population from Ataúro could either be conspecific with *Cyrtodactylus santana* sp. nov. or represent a closely related but distinct lineage that is yet to be described. It is worth noting that *Cyrtodactylus santana* sp. nov. is the first *Cyrtodactylus* with a specific identity in Timor-Leste as all previous reports of the genus were not identified at the species level (Kaiser et al. 2011, 2013; O'Shea et al. 2015), a clear indication that the diversity of *Cyrtodactylus* in Timor-Leste is still underestimated and poorly understood.

Acknowledgements

We thank the following people and institutions who made this research possible:

Raimundo Mau (Director-General for Forests, Coffee, and Industrial Plant) for permits and logistical support; Manuel Mendes, Natalino Martins (Conservation International), Tan Heok Hui, Iffah Binte Iesa (LKCNHM), and Daniel Thomas (Singapore Botanic Gardens) for planning, logistical support, and field assistance.

References

Amarasinghe AAT, Riyanto A, Mumpuni M, Grismer LL (2020) A new bent-toed gecko species of the genus *Cyrtodactylus* Gray, 1827 (Squamata: Gekkonidae) from the West Bali National Park, Bali, Indonesia. Taprobanica 9(1): 59–70. https://doi.org/10.47605/tapro.v9i1.222

Bauer AM, Doughty P (2012) A new bent-toed gecko (Squamata: Gekkonidae: *Cyrtodactylus*) from the Kimberley region, Western Australia. Zootaxa 3187(1): 32–42. https://doi.org/10.11646/zootaxa.3187.1.2

Bouckaert R, Drummond A (2017) bModelTest: Bayesian phylogenetic site model averaging and model comparison. BMC Evolutionary Biology 17(1): 1–11. https://doi.org/10.1186/s12862-017-0890-6

Bouckaert R, Heled J, Kühnert D, Vaughan T, Wu CH, Xie D, Suchard MA, Rambaut A, Drummond AJ (2014) BEAST 2: A software platform for Bayesian evolutionary analysis. PLoS Computational Biology 10(4): e1003537. https://doi.org/10.1371/journal.pcbi.1003537

Brongersma LD (1948) Lizards from the island of Morotai (Moluccas). Proceedings of the Koninklijke Nederlandse Akademie van Wetenschappen 51(C): 486–495.

Chan KO, Grismer LL (2021) A standardized and statistically defensible framework for quantitative morphological analyses in taxonomic studies. Zootaxa 5023(2): 293–300. https://doi.org/10.11646/zootaxa.5023.2.9

Chan KO, Grismer LL (2022) GroupStruct: An R package for allometric size correction. Zootaxa 5124(4): 471–482. https://doi.org/10.11646/zootaxa.5124.4.4

Dunn ER (1927) Results of the Douglas Burden Expedition to the Island of Komodo. III.- Lizards from the East Indies. American Museum Novitates 288: 1–13.

García-Diez M, Standish CD, Oliveira NV, O'Connor S (2020) Lene Kici cave art: Possible symbolic evidence associated with palaeolithic human occupation in Timor-Leste. Asian Perspective 60(1): 197–212. https://doi.org/10.1353/asi.2020.0042

Grismer LL, Grismer JL (2017) A re-evaluation of the phylogenetic relationships of the *Cyrtodactylus condorensis* group (Squamata; Gekkonidae) and a suggested protocol for the characterization of rock-dwelling ecomorphology in *Cyrtodactylus*. Zootaxa 4300(4): 486–504. https://doi.org/10.11646/zootaxa.4300.4.2

Grismer LL, Wood PL, Poyarkov NA, Le MD, Kraus F, Agarwal I, Oliver PM, Nguyen SN, Nguyen TQ, Welton LJ, Stuart BL, Luu VQ, Bauer AM, Kyle A, Quah ESH, Chan KO, Ziegler T, Ngo H, Roman A, Aowphol A, Chomdej S, Suwannapoom C, Siler CD, Anuar S, Tri NV, Grismer JL (2021) Phylogenetic partitioning of the third-largest vertebrate genus in the world, *Cyrtodactylus* Gray, 1827 (Reptilia; Squamata; Gekkonidae) and its relevance to taxonomy and conservation. Vertebrate Zoology 71: 101–154. https://doi.org/10.3897/vertebrate-zoology.71.e59307

Grismer LL, Poyarkov NA, Quah ESH, Grismer JL, Wood Jr PL (2022) The biogeography of bent-toed geckos, *Cyrtodactylus* (Squamata: Gekkonidae). PeerJ 10: e13153. https://doi.org/10.7717/peerj.13153

Hayden CJ, Brown RM, Gillespie G, Setiadi MI, Linkem CW, Iskandar DT (2008) A new species of bent-toed gecko *Cyrtodactylus* Gray, 1827, (Squamata: Gekkonidae) from the Island of Sulawesi, Indonesia. Herpetologica 64(1): 109–120. https://doi.org/10.1655/07-026.1

Hoang DT, Chernomor O, von Haeseler A, Minh BQ, Le SV (2017) UFBoot2: Improving the ultrafast bootstrap approximation. Molecular Biology and Evolution 35(2): 518–522. https://doi.org/10.1093/molbev/msx281

Iskandar DT, Rachmansah A, Umilaela (2011) A new bent-toed gecko of the genus *Cyrtodactylus* Gray, 1827 (Reptilia, Gekkonidae) from Mount Tompotika, eastern peninsula of Sulawesi, Indonesia. Zootaxa 2838(1): 65–78. https://doi.org/10.11646/zootaxa.2838.1.4

Kaatz A, Grismer JL, Grismer LL (2021) Convergent evolution of karst habitat preference and its ecomorphological correlation in three species of Bent-toed Geckos (*Cyrtodactylus*) from Peninsular Malaysia. Vertebrate Zoology 71: 367–386. https://doi.org/10.3897/vz.71.e66871

Kaiser H, Carvalho VL, Ceballos J, Freed P, Heacox S, Lester B, Richards SJ, Trainor CR, Sanchez C, O'Shea M (2011) The herpetofauna of Timor-Leste: A first report. ZooKeys 109: 19–86. https://doi.org/10.3897/zookeys.109.1439

Kaiser H, Sanchez C, Heacox S, Kathriner A, Varela Ribeiro A, Afranio Soares Z, de Araujo LL, Mecke S, O'Shea M (2013) First Report on the Herpetofauna of Ataúro Island, Timor-Leste. Check List 9(4): 752–762. https://doi.org/10.15560/9.4.752

Kalyaanamoorthy S, Minh BQ, Wong TKF, von Haeseler A, Jermiin LS (2017) ModelFinder: Fast model selection for accurate phylogenetic estimates. Nature Methods 14(6): 587–589. https://doi.org/10.1038/nmeth.4285

Kathriner A, Bauer AM, O'Shea M, Sanchez C, Kaiser H (2014) Hiding in plain sight: A new species of bent-toed gecko (Squamata: Gekkonidae: Cyrtodactylus) from West Timor, collected by Malcolm Smith in 1924. Zootaxa 3900(4): 555–568. https://doi.org/10.11646/zootaxa.3900.4.6

Kearse M, Moir R, Wilson A, Stones-Havas S, Cheung M, Sturrock S, Buxton S, Cooper A, Markowitz S, Duran C, Thierer T, Ashton B, Meintjes P, Drummond A (2012) Geneious Basic: An integrated and extendable desktop software platform for the organization and analysis of sequence data. Bioinformatics 28(12): 1647–1649. https://doi.org/10.1093/bioinformatics/bts199

Kumar S, Stecher G, Li M, Knyaz C, Tamura K (2018) MEGA X: Molecular evolutionary genetics analysis across computing platforms. Molecular Biology and Evolution 35(6): 1547–1549. https://doi.org/10.1093/molbev/msy096

Macey RJ, Larson A, Ananjeva NB, Fang Z, Papenfuss TJ (1997) Two Novel Gene Orders and the Role of Light-Strand Replication in Rearrangement of the Vertebrate Mitochondrial Genome. Molecular Biology and Evolution 14(1): 91–104. https://doi.org/10.1093/oxfordjournals.molbev.a025706

Mertens R (1929) Zwei neue Haftzeher aus dem Indo—Australischen Archipel (Rept.). Senckenbergiana 11: 237–241.

Miller MA, Pfeiffer W, Schwartz T (2010) Creating the CIPRES Science Gateway for inference of large phylogenetic trees. 2010 Gateway Computing Environments Workshop, GCE 2010: 1–8. https://doi.org/10.1109/GCE.2010.5676129

Minh BQ, Schmidt HA, Chernomor O, Schrempf D, Woodhams MD, Von Haeseler A, Lanfear R, Teeling E (2020) IQ-TREE 2: New models and efficient methods for phylogenetic inference in the genomic era. Molecular Biology and Evolution 37(5): 1530–1534. https://doi.org/10.1093/molbev/msaa015

Müller F (1895) Reptilien und Amphibien aus Celebes. Verhandlungen der Naturforschenden Gesellschaft in Basel 10: 825–843.

O'Connor S, Oliveira NV, Standish CD, Garciá-Diez M, Kealy S, Shipton C (2021) Faces in the stone: Further finds of anthropomorphic engravings suggest a discrete artistic tradition flourished in Timor-Leste in the Terminal Pleistocene. Cambridge Archaeological Journal 31(1): 129–142. https://doi.org/10.1017/S0959774320000323

O'Shea M, Sanchez C, Kathriner A, Mecke S, Carvalho L, Ribeiro AV, Soares ZA, Araujo LDE, Kaiser H (2015) Herpetological diversity of Timor-Leste: Updates and a review of species distributions. Asian Herpetological Research 6: 73–131. https://doi.org/10.16373/j.cnki.ahr.140066

Oliver P, Edgar P, Mumpuni, Iskandar DT, Lilley R (2009) A new species of bent-toed gecko (*Cyrtodactylus*: Gekkonidae) from Seram Island, Indonesia. Zootaxa 2115(1): 47–55. https://doi.org/10.11646/zootaxa.2115.1.4

R Core Team (2014) A language and environment for statistical computing. R Foundation for Statistical Computing, Vienna.

Rambaut A, Drummond AJ, Xie D, Baele G, Suchard MA (2018) Posterior summarization in Bayesian phylogenetics using Tracer 1.7. Systematic Biology 67(5): 901–904. https://doi.org/10.1093/sysbio/syy032

Riyanto A, Wood PL, Grismer LL (2015) The fourth Bent-toed gecko of the genus *Cyrtodactylus* (Squamata: Gekkonidae) from Java, Indonesia. Zootaxa 4059(2): 351–363. https://doi.org/10.11646/zootaxa.4059.2.6

Riyanto A, Kurniati H, Engilis Jr A (2016) A new Bent-toed gecko (Squamata: Gekkonidae) from the Mekongga Mountains, South East Sulawesi, Indonesia. Zootaxa 4109(1): 59–72. https://doi.org/10.11646/zootaxa.4109.1.5

Riyanto A, Mulyadi M, McGuire JA, Kusrini MD, Febylasmia F, Basyir IH, Kaiser H (2017) A new small bent-toed gecko of the genus *Cyrtodactylus* (Squamata: Gekkonidae) from the lower slopes of Mount Tambora, Sumbawa Island, Indonesia. Zootaxa 4242(3): 517–528. https://doi.org/10.11646/zootaxa.4242.3.5

Riyanto A, Hamidy A, McGuire JA (2018a) A new bent-toed gecko (*Cyrtodactylus*: Squamata: Gekkonidae) from the island of Tanahjampea, south Sulawesi, Indonesia. Zootaxa 4442(1): 122–136. https://doi.org/10.11646/zootaxa.4442.1.6

Riyanto A, Arida E, Koch A (2018b) *Cyrtodactylus tahuna* sp. nov., a new bent-toed gecko (Reptilia: Squamata: Gekkonidae) from Sangihe Island, North Sulawesi, Indonesia. Zootaxa 4399(2): 220–232. https://doi.org/10.11646/zootaxa.4399.2.6

Riyanto A, Faz FH, Amarasinghe AAT, Munir M, Fitriana YS, Hamidy A, Kusrini MD, Oliver PM (2022) A new bent-toed gecko of the *Cyrtodactylus marmoratus* Group (Reptilia: Gekkonidae) from Obi Island, Indonesia. Herpetologica 78(1): 30–39. https://doi.org/10.1655/Herpetologica-D-21-00028.1

Sanchez C, Carvalho VL, Kathriner A, O'Shea M, Kaiser H (2012) First report on the herpetofauna of the Oecusse District, an enclave of Timor-Leste. Herpetology Notes 5: 137–149.

Thorpe RS (1983) A review of the numerical methods for recognising and analysing racial differentiation. In: Felsenstein J (Ed.) Numerical Taxonomy. Springer Verlag, Berlin, Heidelberg, 404–423. https://doi.org/10.1007/978-3-642-69024-2_43

Trainor CR, Santana F, Xavier AF, Crosby MJ (2007) Important bird areas in Timor-Leste. Key sites for conservation, 90 pp.

Supplementary material 1

Supplementary information

Authors: Kin Onn Chan, L. Lee Grismer, Fernando Santana, Pedro Pinto, Frances W. Loke, Nathan Conaboy

Data type: zip file

Explanation note: Maximum Clade Credibility Bayesian tree inferred using BEAST. Maximum Likelihood consensus tree inferred using IQ-TREE. Raw (not size corrected) measurements in mm used in the morphological analyses. Information on all sequences used in this study and their associated GenBank accession numbers (Suppl. material 1: table S1).

Link: https://doi.org/10.3897/zookeys.1139.96508.suppl1

ZooKeys 1139: 127–136 (2023)
doi: 10.3897/zookeys.1139.94972
https://zookeys.pensoft.net

RESEARCH ARTICLE

A peer-reviewed open-access journal
ZooKeys
Launched to accelerate biodiversity research

Chasitermes pax, a new genus and species of soldierless termite (Termitidae, Apicotermitinae) from the island of Trinidad

Rudolf H. Scheffrahn[1], Tiago F. Carrijo[2]

1 *Fort Lauderdale Research and Education Center, Institute for Food and Agricultural Sciences, University of Florida, 3205 College Avenue, Davie, Florida 33314, USA* **2** *Centro de Ciências Naturais e Humanas, Universidade Federal do ABC, Rua Arcturus 03, Jardim Antares, 09606-070, São Bernardo do Campo, SP, Brazil*

Corresponding author: Rudolf H. Scheffrahn (rhsc@ufl.edu)

Academic editor: Eliana Cancello | Received 16 September 2022 | Accepted 28 November 2022 | Published 11 January 2023

https://zoobank.org/DEE0DCAA-0348-4B4A-9990-A989D913651E

Citation: Scheffrahn RH, Carrijo TF (2023) *Chasitermes pax*, a new genus and species of soldierless termite (Termitidae, Apicotermitinae) from the island of Trinidad. ZooKeys 1139: 127–136. https://doi.org/10.3897/zookeys.1139.94972

Abstract

Chasitermes pax Scheffrahn & Carrijo **gen. et sp. nov.** is described from workers collected from a single colony in the Northern Range of Trinidad. The shape and texture of the unsclerotized enteric valve, tubular shape of the enteric valve seating, and prominent spherical mesenteric tongue of *C. pax* are the diagnostic characters for both the genus and species. A Bayesian phylogenetic analysis using the COI gene and including all neotropical Apicotermitinae genera described to date supports the new genus as a distinct terminal.

Keywords

Anoplotermes-group, enteric valve, Isoptera, Neotropics, new species, taxonomy

Introduction

The soldierless termites of the New World form a monophyletic clade (Romero Arias et al. 2021) that comprises 16–47% of the termite diversity in Amazonian ecosystems (Bourguignon et al. 2016b). Although the richness of soldierless taxa is recognized, most have not yet been described (Bourguignon et al. 2016b). Originally, all neotropical soldierless termites were placed in the genus *Anoplotermes* Müller, 1873. Recognition

of much greater taxonomic diversity began with Mathews (1977) who described *Grigiotermes* and *Ruptitermes*, and Fontes (1986) who described *Aparatermes* and *Tetimatermes*. Fontes (1992) provided the first identification key for workers of these five genera. The descriptions of *Longustitermes* (Bourguignon et al. 2010), *Compositermes* (Scheffrahn 2013), *Amplucrutermes*, *Humutermes*, *Hydrecotermes*, *Patawatermes*, and *Rubeotermes* (Bourguignon et al. 2016a), *Disjunctitermes* (Scheffrahn et al. 2017), *Echinotermes* and *Rustitermes* (Castro et al. 2018, 2020, respectively) and, for now, *Tonsuritermes* and *Dissimulitermes* (Constantini et al. 2018, 2020, respectively) have expanded the defined diversity of neotropical soldierless taxa.

Trinidad and Tobago are continental islands that separated from Venezuela during the Holocene (Comeau 1992; Mychajliw et al. 2020). As such, they have a rich diversity of Amazonian flora and fauna. The University of Florida Termite Collection (UFTC) database shows that 24 described and undescribed genera of Apicotermitinae occur on the islands (Scheffrahn 2019); about the same number as northern Venezuela (Scheffrahn 2019) and possibly somewhat more in French Guiana (Davies 2002; Bourguignon et al. 2013).

In this paper we describe *Chasitermes pax* gen. et sp. nov. based on the morphology of the worker caste and molecular data.

Materials and methods

Workers were collected and preserved in 85% ethanol. External and internal dissections were suspended in Purell Instant Hand Sanitizer in a plastic Petri dish and photographed using a Leica M205C stereomicroscope controlled by Leica Application Suite ver. 3.0 montage software. The enteric valve (EV) was prepared by removing the entire worker proctodeal segment (P2) section in ethanol. Food particles were expelled from the P2 tube by pressure manipulation. The tube was quickly submerged in a droplet of PVA medium (BioQuip Products Inc.) which, by further manipulation, eased muscle detachment. The remaining EV cuticle was left intact or longitudinally cut, splayed open, and mounted on a microscope slide using the PVA medium. The EV was photographed with a Leica CTR 5500 compound microscope with phase-contrast optics using the same montage software. Terminology of the worker gut follows that of Sands (1972) and Noirot (2001). Mandible terminology as in Sands (1972) except for the left subsidiary fourth marginal tooth which was clarified and redefined as the "premolar process" (Constantini et al. 2020).

The barcode region of the mitochondrial gene cytochrome c Oxidase subunit I (COI) of *Chasitermes pax* was obtained by DNA extraction and PCR performed by the Canadian Centre for DNA Barcoding (BOLD systems) following standard high-throughput protocols (deWaard et al. 2008). The PCR employed the primers *LepF1* and *LepR1* (Hebert et al. 2003) which generated 658bp. A gene tree was created under Bayesian Inference (BI) using the COI. In addition to the sequence of *C. pax*, a total of 56 GenBank or BOLD sequences were used: 36 sequences of neotropical

Apicotermitinae (23 species, 15 genera), eight Old World Apicotermitinae genera, five non-Apicotermitinae Termitidae, and one Rhinotermitidae, [*Heterotermes crinitus* (Emerson)] as the outgroup. Sequences were aligned under MUSCLE algorithm implemented in Geneious ver. 9.1.8 (Biomatters Ltd., Auckland, New Zealand). Substitution model used (GTR+I+G) was selected through the Akaike Information Criterion (AIC) with the software jModelTest2 (Darriba et al. 2012). The XML input files were generated with BEAUti ver. 1.8.0, and the BI was performed with BEAST ver. 1.8.0 (Drummond et al. 2012). A Yule speciation process was used as the tree prior. Three Markov chain Monte Carlo (MCMC) searches were conducted independently, each one for 20,000,000 generations, and they were combined to search the most probable tree. Convergence and stationarity were assessed with Tracer ver. 1.5 (Rambaut et al. 2014) and the first 100 trees were discarded as burn-in with TreeAnnotator ver. 1.8.0 and visualized using FigTree ver. 1.3.1.

Taxonomy

***Chasitermes* Scheffrahn & Carrijo, gen. nov.**
https://zoobank.org/84F91A07-5829-4250-84EB-305E9BCFE300

Type-species. *Chasitermes pax* Scheffrahn & Carrijo, sp. nov.

Diagnosis. The combination of unsclerotized rectangular EVA cushions, a tubular extension of EVS, and a prominent spherical mesenteric tongue make *C. pax* unique among all Apicotermitinae genera.

Description. Imago unknown. Worker. (Figs 1–4). Monomorphic. Head capsule and antennae light yellowish. Head covered with ca 50 longer (0.1 mm) setae and a few shorter ones (Fig. 1). In lateral view, dorsal surface of the head capsule slightly convex; postclypeus is moderately inflated. Antennae with 14 articles (formula 2>3≈4<5). Pronotum with about 20 long setae concentrated mainly at the borders and a few shorter ones. Mandibles with apical teeth very prominent; left mandible with M1 triangulate, shorter than apical; premolar process longer than M3 (Fig. 2A). Apical tooth of right mandible as long as that of left but narrower; M1 as long as M2. Fore tibia moderately inflated (Fig. 2C) with about a dozen thick posterior setae concentrated at the distal half; lateral and anterior surfaces with thinner long and shorter setae. Digestive tube (Fig. 3 with abbreviations) with voluminous crop; mesenteron forming half circle; mixed segment with prominent spherical mesenteric tongue. First proctodeal segment (P1) widens to maximum diameter before P2, enteric valve seating (EVS) slightly trilobed. Third proctodeal segment (P3) with long tubular extension of the EVS seating to main reservoir (Fig. 4C) then narrowing again toward P4 (Fig. 3D). Cuticle of EVA without sclerotization (Fig. 4A, B) forming six rectangular cushions with about 100 scales each (Fig. 4A). Scales proximal to P1 subrectangular, each with 5–10 creases; scales in distal one-third lacking creases, more scale-like with long fringes (Fig. 4B). Measurements are provided in Table 1.

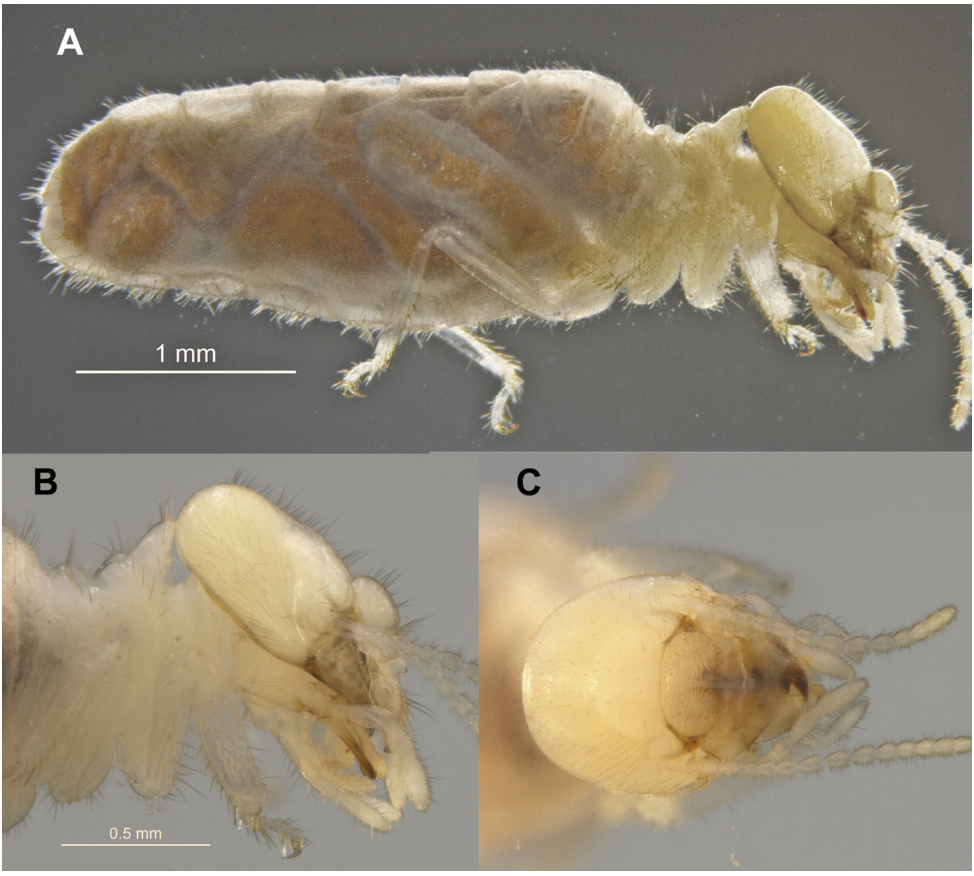

Figure 1. *Chasitermes pax* gen. et sp. nov. **A** right lateral habitus of worker **B** lateral and **C** dorsal views of head.

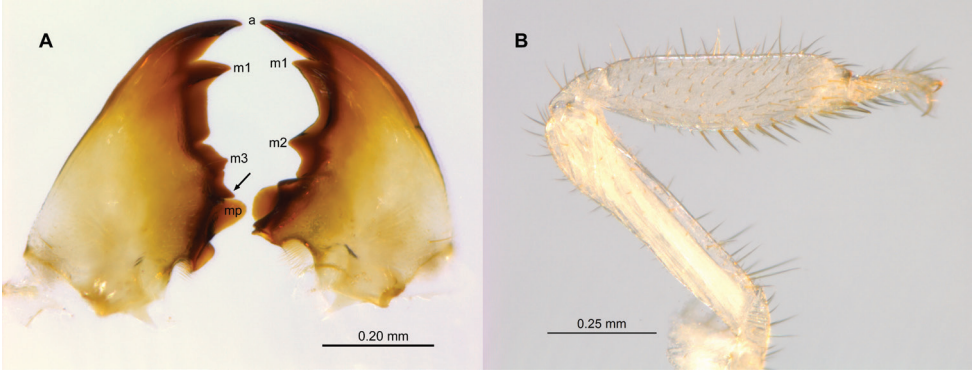

Figure 2. *Chasitermes pax* gen. et sp. nov. **A** mandibles (abbreviations: a = apical, m1-m3 = marginal teeth, mp = molar process, arrow = premolar process (Constantini *et al.* 2020) **B** right fore tibia.

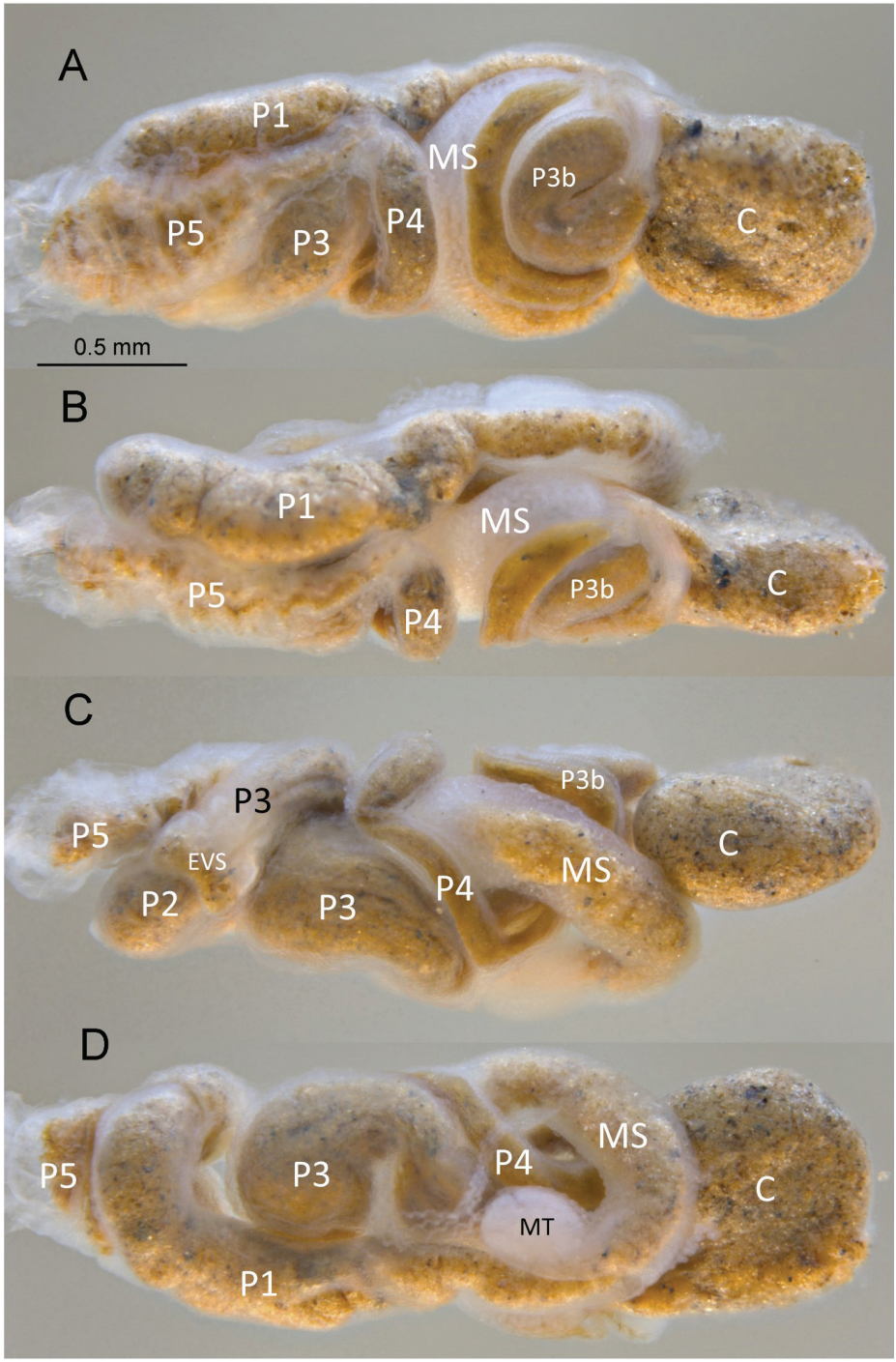

Figure 3. *Chasitermes pax* gen. et sp. nov. digestive tube **A** dorsal **B** right **C** left, and **D** ventral (abbreviations: C = crop, EVS = enteric valve seating, MS = mesenteron, MT = mesenteric tongue, P1–P5 = proctodeal segments).

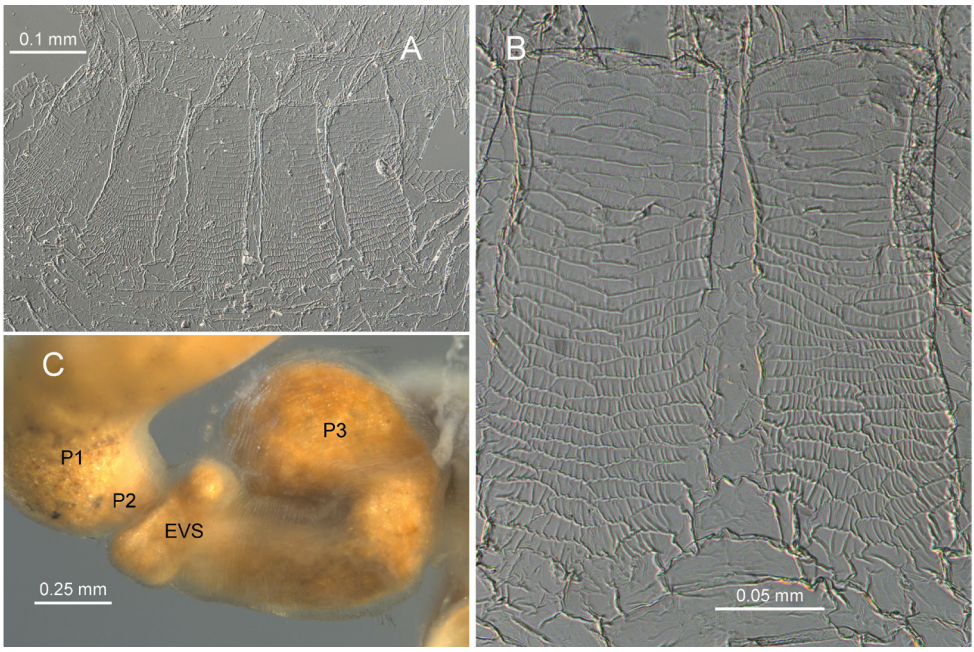

Figure 4. *Chasitermes pax* gen. et sp. nov. **A** spliced whole mount of enteric valve armature (rightmost cushion torn) **B** close-up of two cushions **C** region encompassing EVS (abbreviations as in Fig. 3).

Table 1. Measurements (mm, *N* = 10) of *Chasitermes pax* gen. et sp. nov. workers.

	Max.	Min.	Mean
Length of head to lateral base of mandibles	0.77	0.70	0.73
Maximum head width	0.93	0.82	0.85
Length of hind tibia	0.77	0.67	0.72
Length of postclypeus	0.25	0.18	0.21
Width of postclypeus	0.44	0.39	0.40
Length of fore tibia	0.67	0.53	0.60
Width of fore tibia	0.18	0.12	0.15
Fore tibia width:length ratio	0.30	0.21	0.25

Remarks. The single most diagnostic character of the *C. pax* worker is the enteric valve armature which has unsclerotized rectangular cushions composed of creased or fringed scales. The tubular extension of the EVS in *C. pax* is closest to *Patawatermes nigripunctatus* (Emerson, 1925) but is much longer in the former and *P. nigripunctatus* lacks a trilobed enteric valve seating. The left mandible of *C. pax* has prominent premolar process closest to *Patawatermes turricola* (Silvestri, 1901) but it is narrower and longer in the former.

Etymology. Named in honor of the collector, James A. Chase.

***Chasitermes pax* Scheffrahn & Carrijo, sp. nov.**
https://zoobank.org/3458C43A-3215-49A1-BE7F-A27761032D7D

Type locality. Tunapuna, island of Trinidad.

Material examined. Republic of Trinidad and Tobago, Tunapuna (10.667, -61.396), elev. 248 m, 4JAN2012, J. Chase, UFTC no. TT2188 holotype worker and about 75 additional workers.

Diagnosis and description. As described for the genus.

Etymology. The species is named for the Pax Guest House where we stayed during our expeditions to Trinidad. It is on the tranquil and inspirational property of the Mount Saint Benedict Abby which encompasses the type locality of *C. pax*. "Pax" is latin for "peace", and represents a noun in apposition.

Ecology and distribution. The *C. pax* workers were collected under a stone. Gut contents confirm that *C. pax* feeds on soil organic matter. So far, this species is only known from the Northern Range on the island of Trinidad.

Molecular analysis. The gene tree recovered *Chasitermes pax* as sister group to *Rubeotermes*, but with very low posterior probability. The low branch support for most major clades in the neotropical Apicotermitinae should be interpreted as a polytomy (Fig. 5).

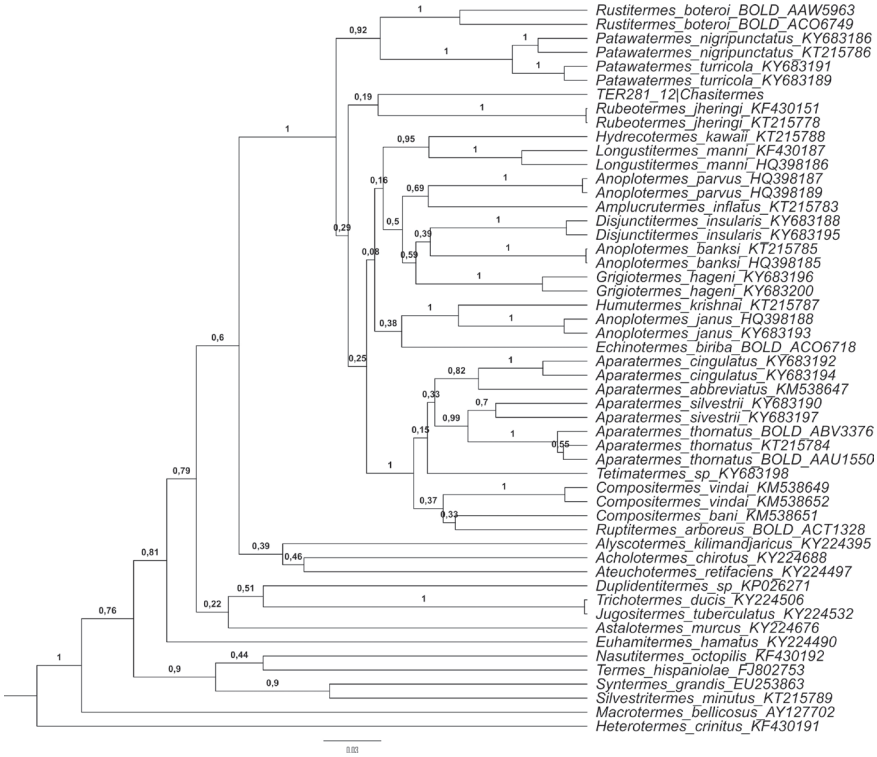

Figure 5. Bayesian phylogenetic tree of the Apicotermitinae subfamily using the COI region. *Chasitermes pax* gen. et sp. nov. is shown in red. Branch support is posterior probability.

Discussion

Advances in the taxonomy, phylogeny, biogeography, ecology of the Apicotermitinae are ongoing (Bourguignon et al. 2016b, Romero Arias et al. 2021). One area of study that remains poorly understood is the physiology, especially, digestive physiology and its relationship with the gut morphology of these mostly soil-feeding insects. Work by Andres Brune and colleagues (e.g., Schmitt-Wagner and Brune 1999; Brune and Friedrich 2000) provided some insight into the digestive process of the soil-feeding Cubitermitinae. Are there similarities with the Apicotermitinae? What role does such different EVAs, like those of *Chasitermes* gen. nov. and *Patawatermes*, have in the inoculation of the food bolus (Scheffrahn 2013) by the myriad of bacteria (Bourguignon et al. 2018) occurring in the enteric valve seating (suggestively called a "bacterial pouch" by Noirot (2001)? Finally, is the singular P3 shape of *Chasitermes pax* related to a different diet or bacterial biota? The present work does not directly contribute to the advances in this particular field, but we hope to instigate terminologists to seek the answers linking the morphology, such as those described here, to the function and biology of the groups.

Acknowledgements

The authors thank Jim Chase for his uncompromising, energetic, and enthusiastic attitude toward termite collection over a span of more than 25 years. TFC was funded through a grant from São Paulo Research Foundation (FAPESP, #2020/06041-4).

References

Bourguignon T, Scheffrahn RH, Křeček J, Nagy ZT, Sonet G, Roisin Y (2010) Towards a revision of the Neotropical soldierless termites (Isoptera: Termitidae): redescription of the genus *Anoplotermes* and description of *Longustitermes*, gen. nov. Invertebrate Systematics 24(4): 357–370. https://doi.org/10.1071/IS10012

Bourguignon T, Šobotník J, Hanus R, Krasulov J, Vrkoslav V, Cvačka J, Roisin Y (2013) Delineating species boundaries using an iterative taxonomic approach: The case of soldierless termites (Isoptera, Termitidae, Apicotermitinae). Molecular Phylogenetics and Evolution 69(3): 694–703. https://doi.org/10.1016/j.ympev.2013.07.007

Bourguignon T, Scheffrahn RH, Nagy ZT, Sonet G, Host B, Roisin Y (2016a) Towards a revision of the Neotropical soldierless termites (Isoptera: Termitidae): redescription of the genus *Grigiotermes* Mathews and description of five new genera. Zoological Journal of the Linnean Society 176(1): 15–35. https://doi.org/10.1111/zoj.12305

Bourguignon T, Šobotník J, Dahlsjö CA, Roisin Y (2016b) The soldierless Apicotermitinae: Insights into a poorly known and ecologically dominant tropical taxon. Insectes Sociaux 63(1): 39–50. https://doi.org/10.1007/s00040-015-0446-y

Bourguignon T, Lo N, Dietrich C, Šobotník J, Sidek S, Roisin Y, Brun A, Evans TA (2018) Rampant host switching shaped the termite gut microbiome. Current Biology 28(4): 649–654. https://doi.org/10.1016/j.cub.2018.01.035

Brune A, Friedrich M (2000) Microecology of the termite gut: Structure and function on a microscale. Current Opinion in Microbiology 3(3): 263–269. https://doi.org/10.1016/S1369-5274(00)00087-4

Castro D, Scheffrahn RH, Carrijo TF (2018) *Echinotermes biriba*, a new genus and species of soldierless termite from the Colombian and Peruvian Amazon (Termitidae, Apicotermitinae). ZooKeys 748: 21–30. https://doi.org/10.3897/zookeys.748.24253

Castro D, Constantini JP, Scheffrahn RH, Carrijo TF, Cancello EM (2020) *Rustitermes boteroi*, a new genus and species of soldierless termites (Blattodea, Isoptera, Apicotermitinae) from South America. ZooKeys 922: 35–49. https://doi.org/10.3897/zookeys.922.47347

Comeau PL (1992) Geological events influencing natural vegetation in Trinidad. Living World, Journal of the Trinidad and Tobago Field Naturalists' Club, 1991–1992: 29–38.

Constantini JP, Carrijo TF, Palma-Onett V, Scheffrahn R, Carnohan LP, Šobotník J, Cancello EM (2018) *Tonsuritermes*, a new soldierless termite genus and two new species from South America (Blattaria: Isoptera: Termitidae: Apicotermitinae). Zootaxa 4531(3): 383–394. https://doi.org/10.11646/zootaxa.4531.3.4

Constantini J, Janei V, Costa-Leonardo AM, Cancello EM (2020) *Dissimulitermes*, a new soldierless termite genus (Blattaria: Isoptera: Termitidae: Apicotermitinae) from the Neotropics and the histology of its dehiscent organ. Insect Systematics & Evolution 52(4): 412–427. https://doi.org/10.1163/1876312X-bja10014

Darriba D, Taboada GL, Doallo R, Posada D (2012) jModelTest 2: More models, new heuristicsand parallel computing. Nature Methods 9(8): 772–772. https://doi.org/10.1038/nmeth.2109

Davies RG (2002) Feeding group responses of a Neotropical termite assemblage to rain forest fragmentation. Oecologia 133(2): 233–242. https://doi.org/10.1007/s00442-002-1011-8

deWaard JR, Ivanova NV, Hajibabaei M, Hebert PD (2008) Assembling DNA barcodes: analytical protocols. In: Martin C (Ed.) Methods in Molecular Biology: Environmental Genetics, Humana Press Inc., Totowa USA, 275–293. https://doi.org/10.1007/978-1-59745-548-0_15

Drummond AJ, Suchard MA, Xie D, Rambaut A (2012) Bayesian Phylogenetics with BEAUti and the BEAST 1.7. Molecular Biology and Evolution 29(8): 1969–1973. https://doi.org/10.1093/molbev/mss075

Fontes LR (1986) Two new genera of soldierless Apicotermitinae from the Neotropical region (Isoptera, Termitidae). Sociobiology 12: 285–297.

Fontes LR (1992) Key to the genera of New World Apicotermitinae (Isoptera: Termitidae). In: Quintero DA, Aiello A (Eds) Insects of Panama and Mesoamerica. Oxford University Press, New York, 242–248.

Hebert PD, Cywinska A, Ball S, deWaard J (2003) Biological identifications through DNA barcodes. Proceedings of the Royal Society of London: Series B, Biological Sciences 270(1512): 313–321. https://doi.org/10.1098/rspb.2002.2218

Mathews AGA (1977) Studies on Termites from the Mato Grosso State, Brazil. Academia Brasileira de Ciências, Rio de Janeiro, 267 pp.

Mychajliw AM, Mohammed RS, Rice KA, Farrell AB, Rincón AD, McAfee R, McDonald HG, Lindsey EL (2020) The biogeography of "breas": Contextualizing the taphonomy, ecology, and diversity of Trinidad's asphaltic fossil record. Quaternary Science Reviews 232: 106–179. https://doi.org/10.1016/j.quascirev.2020.106179

Noirot C (2001) The gut of termites (Isoptera). Comparative anatomy, systematics, phylogeny. II. Higher termites (Termitidae). Annales de la Société Entomologique de France 37: 431–471.

Rambaut A, Suchard MA, Xie D, Drummond AJ (2014) Tracer v1.6. http://tree.bio.ed.ac.uk/software/tracer/ [23/01/2018]

Romero Arias J, Boom A, Wang M, Clitheroe C, Šobotník J, Stiblik P, Bourguignon T, Roisin Y (2021) Molecular phylogeny and historical biogeography of Apicotermitinae (Blattodea: Termitidae). Systematic Entomology 46(3): 741–756. https://doi.org/10.1111/syen.12486

Sands WA (1972) The soldierless termites of Africa (Isoptera: Termitidae). Bulletin of the British Museum (Natural History). Entomology 18: 1–244. https://doi.org/10.5962/p.192782

Scheffrahn RH (2013) *Compositermes vindai* (Isoptera: Termitidae: Apicotermitinae), a new genus and species of soldierless termite from the Neotropics. Zootaxa 3652(3): 381–391. https://doi.org/10.11646/zootaxa.3652.3.6

Scheffrahn RH (2019) University of Florida Termite Collection (UFTC). https://www.termitediversity.org/ [Accessed Aug. 2022]

Scheffrahn RH, Carrijo TF, Postle AC, Tonini F (2017) *Disjunctitermes insularis*, a new soldierless termite genus and species (Isoptera, Termitidae, Apicotermitinae) from Guadeloupe and Peru. ZooKeys 665: 71–84. https://doi.org/10.3897/zookeys.665.11599

Schmitt-Wagner D, Brune A (1999) Hydrogen profiles and localization of methanogenic activities in the highly compartmentalized hindgut of soil-feeding higher termites (*Cubitermes* spp.). Applied and Environmental Microbiology 65(10): 4490–4496. https://doi.org/10.1128/AEM.65.10.4490-4496.1999

ZooKeys 1139: 137–163 (2023)
doi: 10.3897/zookeys.1139.94586
https://zookeys.pensoft.net

RESEARCH ARTICLE

A peer-reviewed open-access journal
ZooKeys
Launched to accelerate biodiversity research

Baetidae (Baetidae, Ephemeroptera) in the Maghreb: state of the art, key, and perspectives

Jean-Luc Gattolliat[1,2], Boudjéma Samraoui[3,4], Nadhira Benhadji[5,6], Lina Kechemir[7], Sonia Zrelli[8,9], Sara El Yaagoubi[10], Majida El Alami El Moutaouakil[10], Michel Sartori[1,2]

1 *Museum of Zoology, Palais de Rumine, Place Riponne 6, CH-1014 Lausanne, Switzerland* **2** *Department of Ecology and Evolution, Biophore, University of Lausanne, CH-1015 Lausanne, Switzerland* **3** *Laboratoire de Conservation des Zones Humides, University 8 mai 1945, Guelma, Algeria* **4** *Department of Biology, University Badji Mokhtar Annaba, Annaba, Algeria* **5** *Laboratoire de Recherche Valorisation des Actions de L'homme Pour la Protection de L'environnement et Application en Santé Publique, University of Tlemcen, BP 119, 13000 Tlemcen, Algeria* **6** *Department of Hydrobiology, Institute of Biology, University of Szczecin, Felczaka street 3 c, 71- 412 Szczecin, Poland* **7** *Faculté des Sciences agronomiques et des sciences biologiques, University of Mouloud Mammeri, Tizi-Ouzou, Algeria* **8** *Unit of Hydrobiology, Laboratory of Environment Biomonitoring (LBE), Faculty of Sciences of Bizerta, University of Bizerta, 7021 Jarzouna, Tunisia* **9** *Honoris United Universities, Ecole Polytechnique Centrale, Avenue Mohamed V, 1002 Tunis, Tunisia* **10** *Laboratory of Ecology, Systematics and Conservation of the Biodiversity, department of Biology, Faculty of Science, University of Abdelmalek Essaadi, Avenue Sebta, 93002 Tetouan, Morocco*

Corresponding author: Jean-Luc Gattolliat (jean-luc.gattolliat@vd.ch)

Academic editor: L. P.-da-Conceicoa | Received 8 September 2022 | Accepted 30 November 2022 | Published 13 January 2023

https://zoobank.org/57CDA884-15C5-42A3-9CF7-89DBC60150C4

Citation: Gattolliat J-L, Samraoui B, Benhadji N, Kechemir L, Zrelli S, El Yaagoubi S, El Moutaouakil MEA, Sartori M (2023) Baetidae (Baetidae, Ephemeroptera) in the Maghreb: state of the art, key, and perspectives. ZooKeys 1139: 137–163. https://doi.org/10.3897/zookeys.1139.94586

Abstract

Among mayflies, Baetidae are often considered as easy to recognise at the family level, but difficult to identify at lower level. In several faunistic or ecological studies, the identification remains at the family level; Baetidae are generally considered as widespread and ubiquitous, therefore as poorly informative for ecological studies or bioassessments. Here, a straightforward identification key is offered to larvae of the ten genera of Baetidae reported from Maghreb based on easily observable and understandable characters. The diversity, ecology, and distribution of each taxonomic unit (genera or subgenera) are discussed and the main difficulties for deeper identification are pointed out. Future challenges and remaining taxonomic riddles for Maghrebian Baetidae are detailed.

Keywords
Algeria, aquatic insects, identification key, mayflies, Morocco, Tunisia

Introduction

Ephemeroptera (mayflies) is a small order of insects with approximately 3700 species. Baetidae are the most diversified family as they encompass approximately one third of generic and specific mayfly diversity (Jacobus et al. 2019). The family is almost worldwide distributed but is mostly diversified in the tropics (Gattolliat and Nieto 2009). Mayflies are merolimnic insects, the larval stage is strictly linked to freshwater habitats while the winged stages are aerial. Imaginal stages are extremely brief and have no functional mouthparts and digestive system. Mayflies are the only insects having an intermediate winged stage between larva and imago, called subimago (Barber-James et al. 2008; Sartori and Brittain 2015).

Mayflies are widely used to assess freshwater quality and global changes in hydrosystems. They are generally very abundant, sensitive to environmental alterations, sufficiently diversified and can be considered as efficient bioindicators if identified at a relevant systematic level (Jacobus et al. 2019). Most Mediterranean rivers and streams, and especially Maghrebian ones, suffer from several threats directly or indirectly linked to human activities. Water abstraction for agriculture and domestic use, water pollution and eutrophication, dam construction and other water regulation, in addition to climate change, have direct severe negative impact on the river ecosystem and on aquatic community composition (Hafiane et al. 2016; Morghad et al. 2019; Zerrouk et al. 2021).

The term Maghreb (Arabic for "the west") refers to the countries of western North Africa. In its traditional sense, the Maghreb includes Morocco, Algeria, and Tunisia. The Maghreb, a biogeographic unit, is distinct from the "Greater Maghreb" or "Great Maghreb", a political and historical entity that additionally includes Libya and Mauritania. As no data and materials are available for Libya, and data is limited to a single short checklist for Mauritania (Fraser 1952), we refrain from including these countries in our study. However, we can assume that they have a very impoverished fauna, mainly covered by our study. Despite important improvements in the last decades, the knowledge of the mayfly fauna of the Maghreb is still incomplete. Historically, Eaton (1899) was the first to establish a list of mayflies for a Maghrebian country. He reported thirteen species from Algeria, including six species of Baetidae, one of them being new to science (Eaton 1899). For one century, little attention was paid to this fauna (Lestage 1925; Navás 1929; Kimmins 1938; Grandi 1951; Verrier 1952), till Thomas and collaborators gave a new impulse to the study of this fauna. They described new species and provided new reports in almost all families. In addition, Thomas (1998) provided a provisional checklist of the mayflies from the Maghreb including 69 species: 41 from Morocco, 50 from Algeria, and 29 from Tunisia. He listed 17 species of Baetidae and considered the report of nine additional species as needing to be confirmed. The checklist was updated by various subsequent contributions including description of new taxa and new reports (see below for the complete reference per country).

The Moroccan mayflies remained practically unknown until the 1970s, since only a few reports were available: five species inventoried by Lestage (1925), then seven other species listed by Navás (1929) and Kimmins (1938). The first faunistic inventory dedicated to this group was carried out by Dakki and El Agbani (1983) who were able to identify 26 species of Ephemeroptera, distributed in the different Moroccan regions. This list was greatly enriched subsequently through hydrobiological studies carried out on various Moroccan streams and rivers (Dakki 1986, 1987; Ouahsine and Lavandier 1988a, b; Qninba et al. 1988; El Agbani et al. 1992; El Alami and Dakki 1998; El Alami et al. 2000; El Bazi et al. 2017; Khadri et al. 2017; Mabrouki al. 2017; Guellaf et al. 2021). Species new for science were also described (Dakki and Giudicelli 1980; Peters 1980; Thomas and Mohati 1985; Dakki and Thomas 1986; Sartori and Thomas 1986; Thomas and Bouzidi 1986; Thomas et al. 1987, 1992; Thomas and Vitte 1988; Vitte and Thomas 1988a, b; Vitte 1991), but only a few of them were on Baetidae (Thomas and Bouzidi 1986; Thomas et al. 1992). Thus, after the synthesis of these works, Thomas (1998) was able to list 41 species distributed in the different Moroccan massifs. Subsequent studies enabled the discovery of nine additional new species or new reports for Morocco; the specific richness for this country reaches 50 species, half of them being Baetidae (Alba-Tercedor and El Alami 1999; El Alami et al. 2000; Mabrouki et al. 2017; Zerrouk et al. 2021). A complete checklist including the diversity and distribution of all Moroccan mayflies was recently published (El Alami et al. 2022a). In order to assess the impact of climate change, human disturbances and pollution on aquatic macroinvertebrates, studies have been carried out over the different geographical Moroccan areas; the main goal was to evaluate the evolution of the mayfly community between the 1980s and the present days by prospecting selected stations in Haut Sebou (Zerrouk et al. 2021), Moulouya (Mabrouki et al. 2017), Ourika (Zuedzang Abessolo et al. 2021) and Rifian watersheds (El Bazi et al. 2017; Khadri et al. 2017; Guellaf et al. 2021).These recent studies of the main Moroccan watersheds confirms the presence of some species never reported since their original descriptions and increase the known distribution of others. Moreover, the specific diversity could increase with the verification of some doubtful identifications through genetic analysis, and the discovery of new species such as the recent description of *Prosopistoma maroccanum* (El Alami et al. 2022b).

In Algeria, the largest African country, it took decades after the pioneering investigations of Eaton (1899) and Lestage (1925), before significant taxonomical progress was made on mayfly knowledge (Soldán and Thomas 1983a; Gagneur and Thomas 1988; Thomas and Vitte 1988; Thomas 1998). Thomas (1998) provisionally listed 50 species of mayflies from Algeria. This checklist is undeniably valuable, despite confirmatory work remains needed as it likely contained some synonymies and misidentifications. In the last few years, a renewed interest in the taxonomy and ecological determinants of mayfly distribution is noted (Mebarki et al. 2017; Benhadji et al. 2018, 2019, 2020; Kechemir et al. 2020; Samraoui et al. 2021a–d). Systematic surveys by the Laboratoire de Conservation des Zones Humides in Algeria are covering eight regions or river basins (Seybouse River, Rhummel, Wadi El Kebir-East, Collo, Aures, Djurdjura, Tiaret, and the Sahara). Collected data have improved knowledge of the distribution and status of Algerian mayflies and led to the discovery of undescribed species

(Samraoui et al. 2021c). In addition, collected data have allowed the elucidation of several mayfly life cycles (Bouhala et al. 2020a, b; Samraoui et al. 2021a, d). Further west, investigations of the mayflies from the Tafna River Basin are still proceeding (Benhadji et al. 2020). With 19 reported species, Baetidae is by far the most diversified but also the most problematic family in Algeria. Recent studies allowed the discovery of several potentially new species of Baetidae, as well as species not previously reported from this country (Benhadji et al. 2020; Samraoui et al. 2021b, c; Kaltenbach et al. 2022).

Mayflies from Tunisia encompass 25 species, 12 of them belonging to Baetidae (Zrelli et al. 2016). Boumaiza and Thomas (1986, 1994, 1995) studied and detailed the distribution and ecology of the different species. *Baetis punicus* was originally described from northern Tunisia (Thomas et al. 1983), but it is now reported from the whole Maghreb (Thomas 1998). More recently, a long-term survey was carried out in northern Tunisia, allowing the report of five additional species for this country (including three species of Baetidae) and the description a new species of *Rhithrogena* (Heptageniidae) (Zrelli et al. 2011a, b, 2012, 2016). The most important streams are in northern Tunisia where all the species occur. Despite corresponding to the 4/5 of the territory, the arid southern area only harbours three species. The Tunisian fauna can be considered as relatively well known; recent surveys did not reveal any new taxon or report (Bennas et al. 2018). As in Algeria and Morocco, the main challenges concern the identification of specimens assigned to widely distributed Western European species. Affinities and biogeographical patterns are discussed (Zrelli et al. 2016), but, here again, they need to be updated in the light of new molecular data. As far as we know, after two decades of important surveys, less attentions are paid nowadays on the mayfly systematics, ecology or monitoring in Tunisia (Bennas et al. 2018).

In Baetidae, imaginal stages remain difficult to identify to the species level. Larvae are easier to determine at a finest taxonomic level. Moreover, they are generally present all-year-round while emergence can be more sporadic. Therefore, collecting larvae generally remains the most efficient method to correctly assess the local fauna. Our main aim is to provide a key as easy to use as possible to allow a secure identification of baetid larvae to the most efficient level. The circled alphanumeric codes (1a, 1b, ...) indicated in the dichotomous key refer to the different illustrations of Figs 1, 2. We also summarize the main difficulties and gaps in knowledge.

Materials and methods

Mayfly larvae can be sampled using a Surber net or a dipnet, then stored in alcohol ideally at 80% to 95%. To preserve DNA, they must not be fixed in 5% formaldehyde. Adults can be collected with handnets or attracted by light traps. For the association of the ontogenic stages or just obtaining imagoes, rearing can be made in the field (following detailed instructions presented in http://www.insecta.bio.spbu.ru/z/rearing.htm). Rearing larvae in the laboratory until emergence generally requests equipment for water oxygenation. Association of the different stages can be also securely made by using molecular barcodes (Gattolliat and Monaghan 2010; Gattolliat et al. 2012, 2018).

Identification at the family or generic levels can be generally made under an efficient stereo microscope. In most cases, specific identification request slide mounting and observation under a compound microscope. Dissection can be made in alcohol or in Cellosolve (2-Ethoxyethanol), in adequation with subsequent mounting liquid (Canada balsam or Euparal). Identification to the species level based on mesoscopic characters such as abdominal pattern, shape and setation on legs, relative length of cerci and paracercus or tergite ornamentation should be restricted to the case of well-known fauna of a restricted watershed with examiners possessing important skills and training.

DNA can be extracted from the whole specimens or just from a small part, such as leg or thorax; specimens must be stored in alcohol at high concentration, without denaturant. Long term storage under inappropriate conditions (high temperature or temperature variations) may fragment DNA and inhibit the gene amplification. Non-destructive methods allowing subsequent morphological analysis should be preferentially used (see Vuataz et al. (2011) for details). For routine procedure, most effective results are obtained by amplifying the 658 bp fragment of the mitochondrial gene cytochrome oxidase subunit 1 (COI) using the primers LCO 1490 and HCO 2198 (Folmer et al. 1994, see Kaltenbach et al. (2020) for details).

Results

Key

Figs 1, 2

Synopses of genera

1. *Acentrella* Bengtsson, 1912

Diagnosis. 1) Very reduced paracercus; 2) stocky mouthparts; 3) head compressed dorsoventrally; 4) presence of a complete row of long thin setae on the dorsal margin of tibia; 5) villopore present on the ventral margin of fore femora.

Remarks. In the past, *Acentrella* was considered as a subgenus of *Baetis* (Müller-Liebenau 1969). Confusions with species with reduced paracercus (*Baetis pavidus* or the subgenus *Patites*) can be avoided by the examination of the mouthparts, especially of the mandibles as well as the distal margin of the tergites. The abdominal tergites also present a characteristic dark brown pattern (Fig. 3A).

Two species of *Acentrella* are reported in the Maghreb: *Acentrella* cf. *sinaica* Bogoescu, 1931 and *Acentrella almohades* Alba-Tercedor & El-Alami, 1999. *Acentrella sinaica* was originally described from Romania, then reported from several countries from Central and South Europe. This species is not abundant but widely distributed in North Algeria and North-West Tunisia. Maghrebian populations seem morphologically very similar to those from central Europe. However, molecular preliminary results suggest that the Maghreb populations most probably belong to a new undescribed

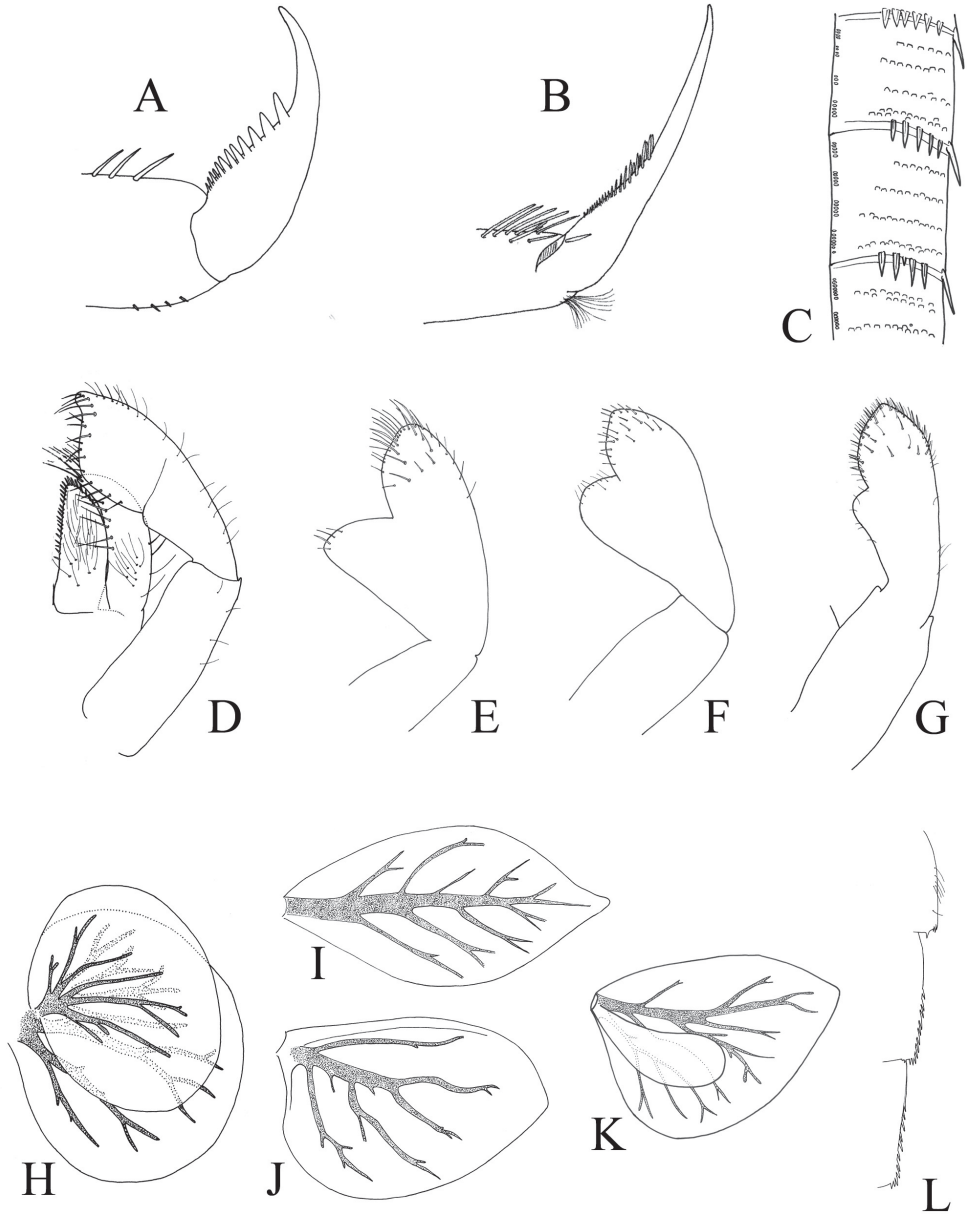

Figure 1. Baetidae: larval characters **A** claw: *Baetis* sp. **B** claw: *Cloeon* sp. **C** lateral margin of cercus: *Procloeon* sp. **D** labial palp: *Cloeon peregrinator* **E** labial palp: *Cheleocloeon dimorphicum* **F** labial palp: *Labiobaetis* cf. *neglectus* **G** labial palp: *Baetis (Rhodobaetis)* sp. **H** abdominal gill IV: *Cloeon peregrinator* **I** abdominal gill IV: *Centroptilum* sp. **J** abdominal gill IV: *Procloeon* sp. **K** abdominal gill IV: *Similicloeon simile* **L** lateral margin of abdominal segments VII to IX: *Cloeon peregrinator*.

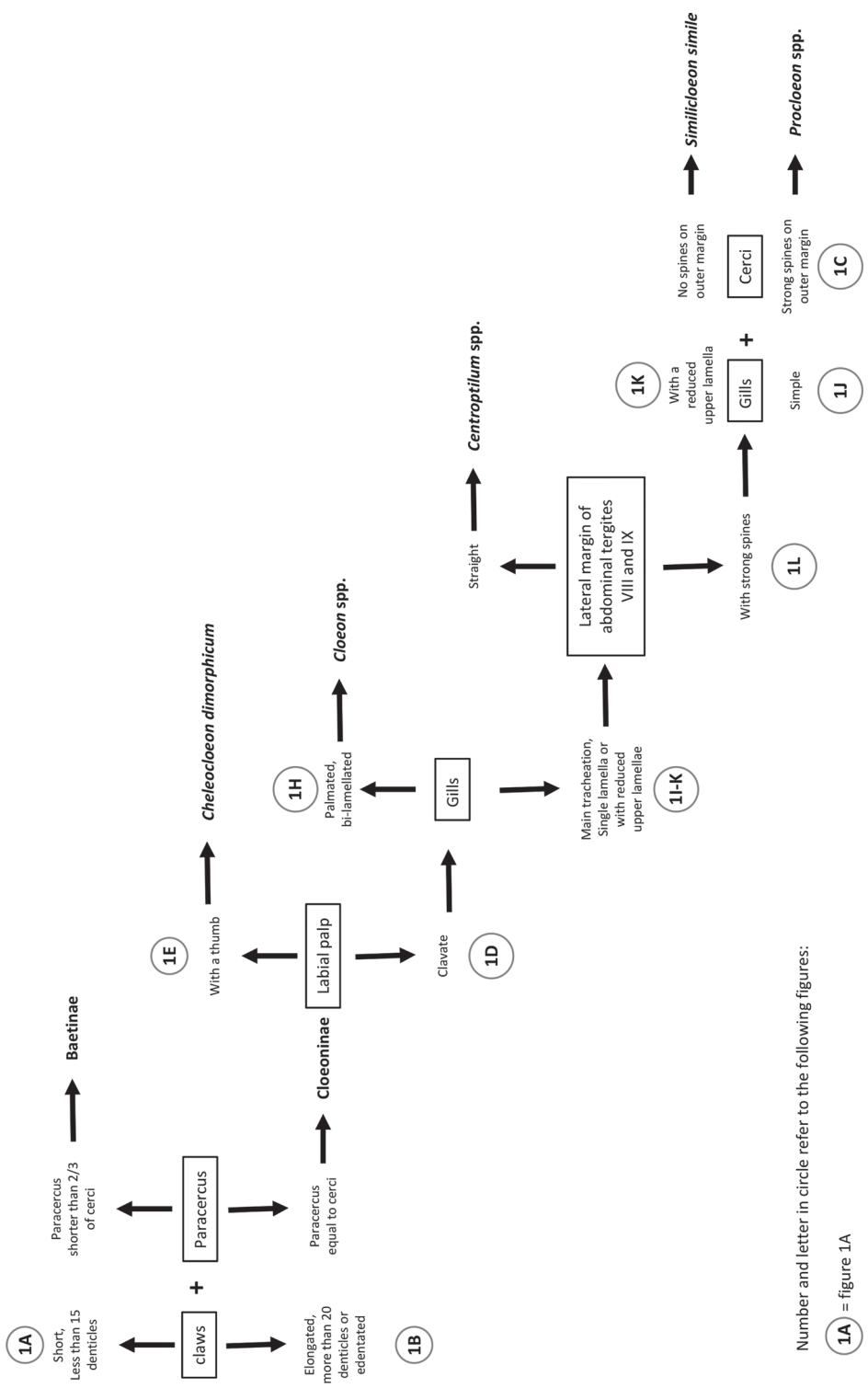

Number and letter in circle refer to the following figures:

1A = figure 1A

Figure 1. Continued.

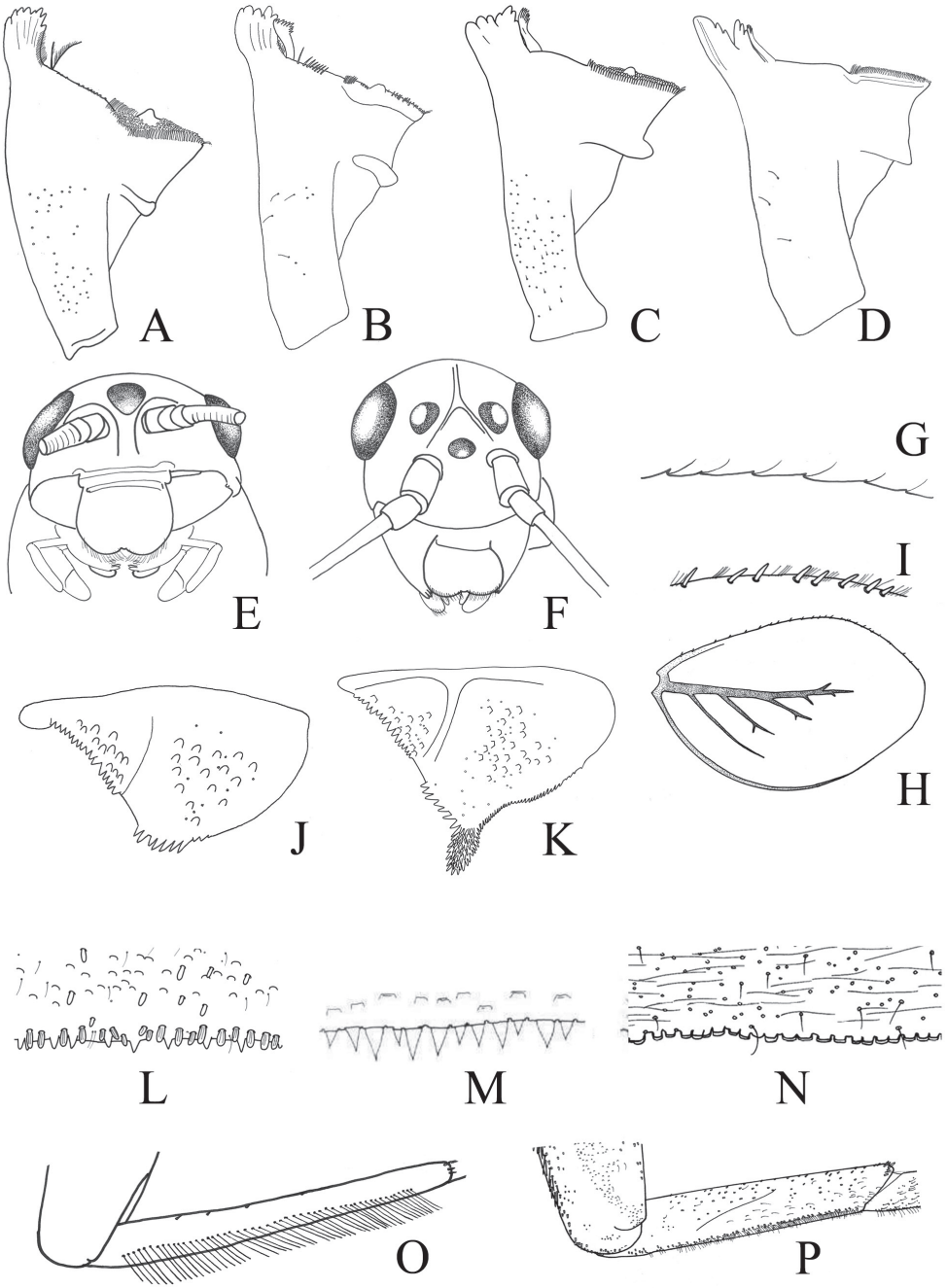

Figure 2. Baetidae: larval characters **A** right mandible: *Alainites sadati* **B** right mandible: *Nigrobaetis rhithralis* **C** right mandible: *Baetis (Rhodobaetis)* sp. **D** right mandible: *Baetis* (*Patites*) sp. **E** head frontal view: *Alainites* sp. **F** head frontal view: *Baetis* sp. **G** costal margin of gill IV: *Baetis (Baetis)* sp. **H** gill IV: *Baetis (Rhodobaetis)* sp. **I** costal margin of gill IV: *Baetis (Rhodobaetis)* sp. **J** paraproct: *Nigrobaetis rhithralis* **K** paraproct: *Alainites sadati* **L** distal margin tergite IV: *Baetis (Rhodobaetis)* sp. **M** distal margin tergite IV: *Baetis (Patites)* sp. **N** distal margin tergite IV: *Baetis (Baetis)* pavidus **O** foretibia: *Acentrella* cf. *sinaica* **P** foretibia: *Baetis (Rhodobaetis)* sp.

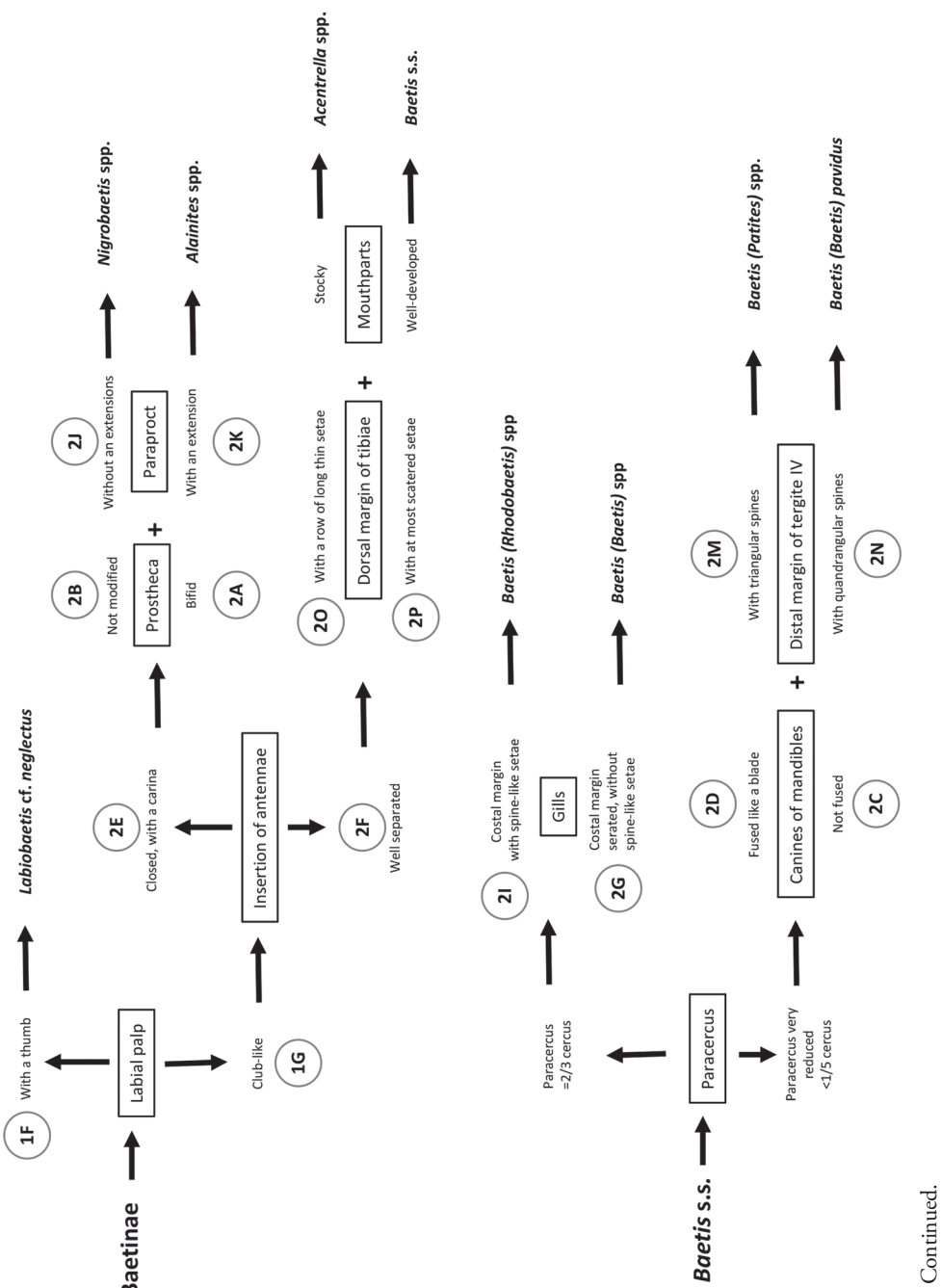

Figure 2. Continued.

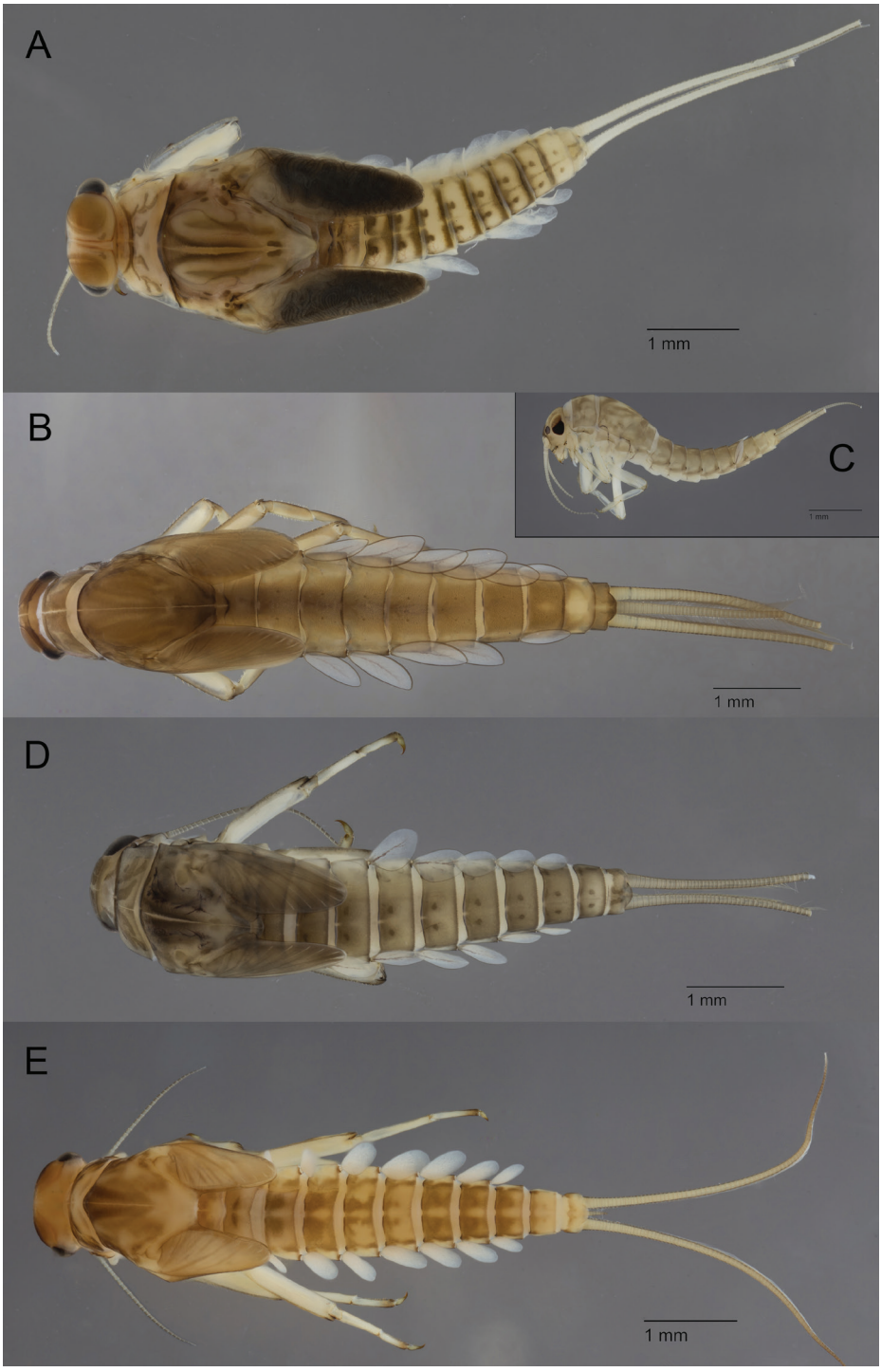

Figure 3. Baetidae: larvae in toto in dorsal view (except 3C lateral view) **A** *Acentrella* cf. *sinaica* **B** *Alainites oukaimeden* **C** *Alainites sadati* **D** *Baetis* (*Patites*) sp. **E** *Baetis* (*Baetis*) *pavidus*.

species (Benhadji et al. 2020). *Acentrella almohades* is originally described from the Rif mountains and middle Atlas as well as from south-west of Spain. The two species do not seem to co-occur. They can be separated by the length of the setae of the dorsal margin of femora (longer in *A.* cf. *sinaica* than in *A. almohades*) and the number of regular rows of stout setae at apex of paraglossa (three rows in *A.* cf. *sinaica*, four rows in *A. almohades*) (Alba-Tercedor and El-Alami 1999).

2. *Alainites* Waltz & McCafferty, 1994

Diagnosis. 1) Antennae located close together with a well-developed carina in between; 2) paraproct with unique elongate prolongation on distal margin; 3) mouthparts in a hypognathous position giving to the body a characteristic curved posture in lateral view; 4) right mandible with a bifid prostheca.

Remarks. The position of the antenna and the general posture in lateral view (Fig. 3C) easily separate *Alainites* and *Nigrobaetis* from other genera in the Maghreb. The prolongation of the distal margin of paraproct (Fig. 2K) and the bifid prostheca (Fig. 2A) unambiguously separate *Alainites* from all the other Maghreb genera including *Nigrobaetis*.

Three species of *Alainites* are reported in the Maghreb: *Alainites* cf. *muticus* (Linnaeus, 1758), *Alainites oukaimeden* (Thomas & Sartori, 1992) (Fig. 3B) and *Alainites sadati* Thomas, 1994 (Fig. 3C). *Alainites oukaimeden* and *A. sadati* are endemic to the Maghreb and present allopatric distribution: *A. sadati* is widely distributed in north Algeria and north Tunisia (Zrelli et al. 2012), while *A. oukaimeden* is only reported from the High Atlas, Morocco (Thomas et al. 1992; El Alami et al. 2022a). The two endemic species have six pairs of gills; they can be only separated by intricate characters such as the reticulation of the surface of tergites and mandibles, the shape of the spines of distal margin of tergite IV and the number of strong setae on the dorsal margin of fore femora. A still undescribed new species, closely related to the West Palaearctic species *Alainites muticus*, with seven pairs of gills, is present in Maghreb but with a restricted distribution limited to northern Morocco (El Alami et al. 2022a).

3. *Baetis* Leach, 1815

Diagnosis. 1) Claw short generally with a single row of restricted number of denticles (exception *B. maurus* with two rows of denticles); 2) paracercus reduced or at most equal to 2/3 of the cerci; 3) presence of a villopore on the ventral margin of fore femora; 4) mouthparts normally developed.

Remarks. Except for the presence of the villopore (which is also present in *Acentrella* and *Labiobaetis*), the genus *Baetis* is mainly defined by the absence of characters. The genus encompasses three subgenera in the Maghreb. These subgenera are relatively easy to recognize and must be considered as the suitable identification level to reach. Except for a few cases, species identification is rather difficult and requires expertise.

3.1 *Baetis* (*Baetis*)

Diagnosis. 1) Canines of the right and left mandibles not fused and not forming a blade-like tooth; 2) costal margin of gills serrated but without spine-like setae; 3) distal margin of tergites with triangular or quadrangular spines but without spatulas.

Remarks. As for the genus, the nominal subgenus *Baetis* is mostly defined by the absence of unique characters (mouthparts and legs not modified). *Baetis* (*Baetis*) *pavidus* Grandi, 1949 (Fig. 3E), described from Italy, is by far the most common species of Baetidae in lower and middle section of streams and rivers. The Maghreb populations are morphologically extremely close to European ones. Moreover, from a genetic point of view, they belong to the same species as populations from Spain and South of France (Benhadji et al. 2020). No sequences are, for the moment, available from continental Italy. This species seems to be rare and restricted in Italy and South of France, while it is the most successful species in the Maghreb. It can be recognised by the very short paracercus and the distal margin of the tergites with quadrangular spines. Presence of other species of the subgenus *Baetis* is certain at least in Morocco, but the species identification remains problematic. *Baetis* (*Baetis*) *fuscatus* (Linnaeus, 1760), *Baetis* (*Baetis*) *meridionalis* Ikonomov, 1954, and *Baetis* (*Baetis*) *nigrescens* Navás, 1932 were reported from Morocco (Thomas 1998; El Alami et al. 2000); but it remains unclear if they really occur in this region or if these reports represent in fact either new species or more recently described species.

3.2 *Baetis* (*Patites*) Thomas & Dia, 2000

Diagnosis. 1) paracercus reduced to a few segments; 2) labrum rectangular with a row of numerous setae parallel to the distal margin; 3) canines of the right and left mandibles fused to form a blade-like tooth; 4) distal margin of tergite IV with triangular spines.

Remarks. The subgenus *Patites* was initially established for *Baetis melanonyx* and related species (Thomas and Dia 2000). The present concept of the subgenus encompasses all the species previously assigned to the *alpinus* species group (sensu Müller-Liebenau 1969), despite most of the species were never formally transferred to this subgenus. This subgenus encompasses at least three species in the Maghreb: *Baetis* (*Patites*) *berberus* Thomas, 1986, *Baetis* (*Patites*) *maurus* Kimmins, 1938, and *Baetis* (*Patites*) *punicus* Thomas, Boumaiza & Soldán, 1983. All of them have two dark spots on each abdominal tergite (Fig. 3D). *Baetis* (*Patites*) *maurus* is the only species of *Baetis* s. l. with two rows of denticles on all claws (Soldán and Thomas 1983a; Thomas et al. 1983). This character allows an easy and unambiguous identification of the species in the Maghreb. *Baetis* (*Patites*) *berberus* and *Baetis* (*Patites*) *punicus* are much more difficult to identify with confidence; especially as the preliminary molecular results indicate that *Patites* is much more diversified than expected and new sibling species are expected (Murria et al. 2017; Benhadji et al. 2020).

3.3 *Baetis* (*Rhodobaetis*) Jacob, 2003

Diagnosis. 1) Gills with spine-like setae along the costal margin; 2) Distal margin of tergites with spatulas in addition to triangular spines; 3) paracercus length 2/3 of cerci.

Remarks. The subgenus *Rhodobaetis* is widely distributed in the Maghreb where it colonizes all types of running waters. Colouration, size, setation of legs and degree of development of the spine-like setae on the gills are highly variable, but may also represent plasticity and intraspecific variations. Three species of *Rhodobaetis* are reported from Maghreb with certainty: *Baetis* (*Rhodobaetis*) *atlanticus* Soldán & Godunko, 2006 (Fig. 4A), *Baetis* (*Rhodobaetis*) *chelif* Soldán, Godunko & Thomas, 2005 and *Baetis* (*Rhodobaetis*) *sinespinosus* Soldán & Thomas, 1983. Reports of *Baetis* (*Rhodobaetis*) *rhodani* (Pictet, 1843) in Maghreb probably concern misidentification of one of the three species mentioned above. In most cases, *B.* (*R.*) *rhodani* must be considered sensu lato and by consequence as equivalent to *Rhodobaetis*. Distinction of the three species is rather difficult as important intraspecific variations have been found at least in *B.* (*R.*) *atlanticus*. Only two reliable characters allow the separation of the three species: *B.* (*R.*) *sinespinosus* has no scale at the tip of maxillary palp and four rows of setae at apex of paraglossae; *B.* (*R.*) *atlanticus* and *B.* (*R.*) *chelif* have one scale at the tip of maxillary palp and differ by number of rows at the apex of paraglossae (three in *B.* (*R.*) *atlanticus* and four in *B.* (*R.*) *chelif*) (Soldán and Thomas 1983a; Soldán et al. 2005; Soldán and Godunko 2006). The three species are at least partially sympatric and can be collected in the same site. Specific identification is therefore very difficult. It requires high expertise and slides preparation; it should be also corroborated by molecular analysis.

4. *Centroptilum* Eaton, 1869

Diagnosis. 1) Both mandibles with a row of abundant setae between prostheca and mola; 2) gills present on segment I to VII, all simple and elongated; 3) absence of spines on the lateral margin of abdominal segments; 4) paracercus subequal in length to cerci.

Remarks. All the specimens we checked from the North-East of Algeria and North Morocco belong to the two recently described species *Centroptilum alamiae* Kaltenbach, Vuataz & Gattolliat, 2022 (Fig. 4B) and *Centroptilum samraouii* Kaltenbach, Vuataz & Gattolliat, 2022. Both species are closely related to *Centroptilum luteolum* (Müller, 1776) but clearly different both morphologically and genetically (Kaltenbach et al. 2022). The description of the species *Centroptilum algiricum* Eaton, 1899 was based on male and female imagoes collected close to Tizi-Ouzou (Algeria) (Eaton 1899). According to the shape of the hindwing, especially of its apex, this species should be assigned to *Procloeon* rather than to *Centroptilum* and therefore cannot be considered as the winged stage of one of the two new species of *Centroptilum* (Samraoui et al. 2021c).

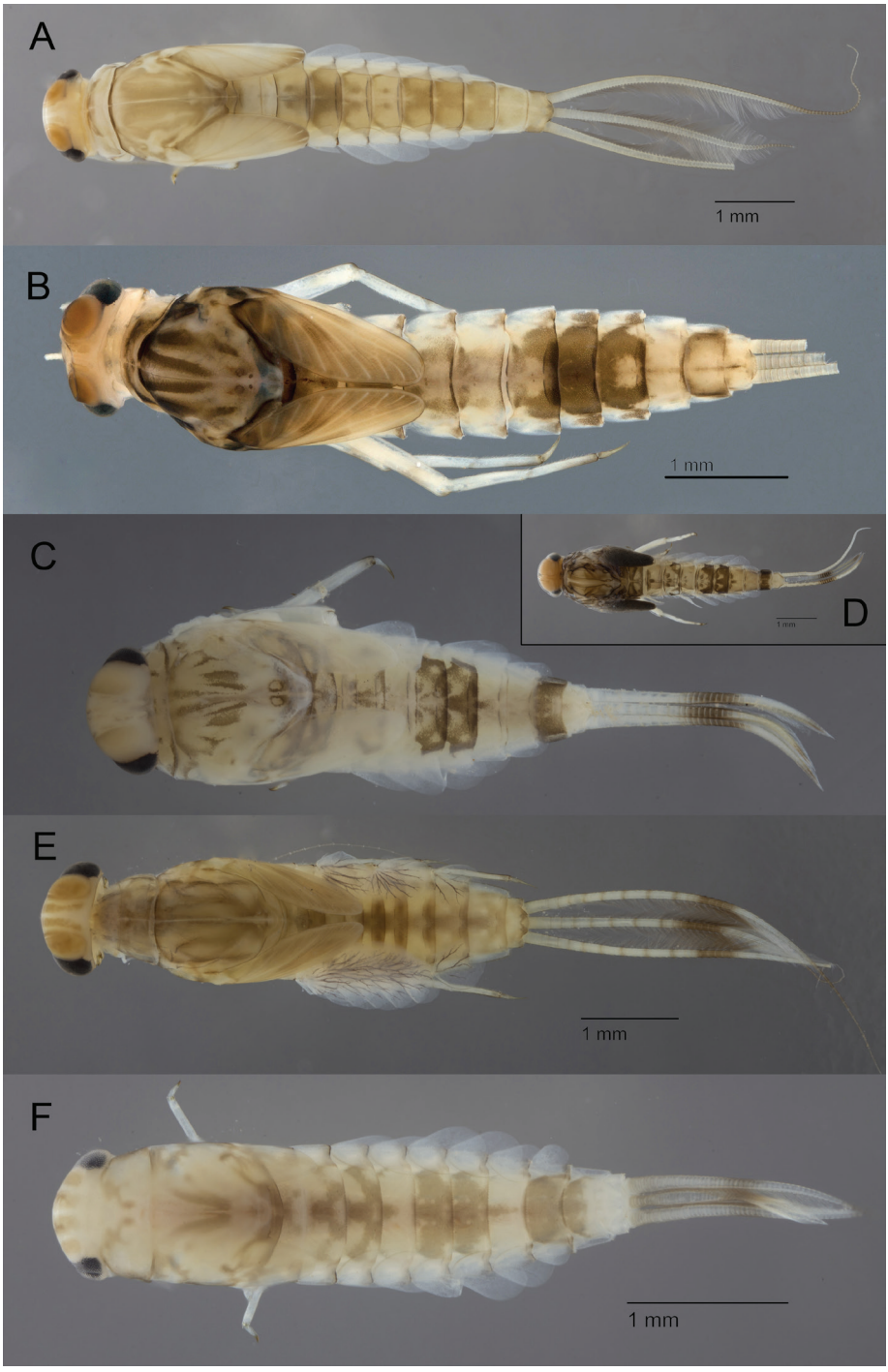

Figure 4. Baetidae: larvae in toto in dorsal view **A** *Baetis* (*Rhodobaetis*) *atlanticus* **B** *Centroptilum alamiae* **C** *Cheleocloeon dimorphicum* **D** *Cheleocloeon dimorphicum* (ready to molt specimen) **E** *Cloeon peregrinator* **F** *Labiobaetis* cf. *neglectus.*

5. *Cheleocloeon* Wuillot & Gillies, 1993

Diagnosis. 1) Claws elongate with two rows of minute denticles; 2) Second segment of the labial palp with a thumb-like process; 3) paracercus subequal to cerci; 4) male with hindwing pads and female without.

Remarks. The genus *Cheleocloeon* is mostly diversified in the Afrotropical region and reaches in the Maghreb its north-western limit. *Cheleocloeon dimorphicum* (Soldán & Thomas, 1985) is the single species of the genus reported from Maghreb (Fig. 4C, D). This endemic species is widespread through this area but seems nowhere abundant (Soldán and Thomas 1985; Boumaiza and Thomas 1995; Mabrouki et al. 2017; El Alami et al. 2022a).

6. *Cloeon* Leach, 1815

Diagnosis. 1) Gills I-VI with double lamellae, upper lamellae similar in shape to lower ones and only slightly smaller; 2) legs elongated, claw elongated with two rows of abundant small to medium denticles; 3) labial palp conical and truncated; 4) maxillary palp 3-segmented; 5) paracercus subequal in length to cerci.

Remarks. *Cloeon* is the most common and most abundant mayfly genus in still and standing waters all over the world (except in America). It can survive in conditions with high temperature and very low oxygen level. *Cloeon* gr. *dipterum* is a complex of very similar species. In Maghrebian ecological and faunistic surveys, it is generally referred as *Cloeon dipterum* (Linneaus, 1761) or *Cloeon cognatum* Stephens, 1835 (Boumaiza and Thomas 1995; Thomas 1998; Mabrouki et al. 2017; El Alami et al. 2022a). Recent molecular studies support the presence of six lineages in the West Palearctic and at least one of them is present in the Maghreb (Rutschmann et al. 2014, 2017). This lineage corresponds to *Cloeon peregrinator* Gattolliat & Sartori, 2008 (Fig. 4E), a species originally thought to be endemic to Macaronesian archipelago but reported later from Algeria (Gattolliat et al. 2008; Benhadji et al. 2020). *Cloeon* gr. *dipterum* is known to present high plasticity; for example the size of the gills is directly adapted to the concentration of dissolved oxygen (Sweeney et al. 2018). Therefore, for the moment, identification to the species level can only be securely made based on molecular evidence (CO1 barcoding).

Besides *Cloeon* gr *dipterum*, another species, *Cloeon saharense* Soldán & Thomas, 1983, was reported from different localities in intermittent brooks and pools in arid and subarid zones of Algeria (Soldán and Thomas 1983a). This species should be easily separated from *C.* gr. *dipterum* by the absence of spines on the lateral side of abdominal segments, a character which is unique among *Cloeon*. Forewing of female imagoes are hyaline while those of *C.* gr. *dipterum* have costal and subcostal areas with dark brown pattern (Soldán and Thomas 1983a). Although this species is supposed to be morphologically easily recognisable, *C. saharense* has never been reported from the Maghreb since its original description.

7. *Labiobaetis* Novikova & Kluge, 1987

Diagnosis. 1) Claws hooked with one row of well-developed denticles; 2) second segment of the labial palp with a thumb-like process; 3) paracercus 2/3 of cerci.

Remarks. All the Maghreb specimens of *Labiobaetis* were assigned to the Iberian species *Labiobaetis neglectus* (Navàs, 1913) (Fig. 4F). Originally the species was only described at the imaginal stage. The type material is lost, and the original description is very succinct. The specific attribution of the specimens from Algeria to *L. neglectus* was based on rather obscure criteria (Soldán and Thomas 1983a). In the same publication, the authors provided the first description of the larval stage based on material from Algeria. Subsequent reports of the species only concerned larvae (Zrelli et al. 2016; Mabrouki et al. 2017; Samraoui et al. 2021c; El Alami et al. 2022a), and were only based on the characters depicted by Soldán and Thomas (1983a). Examination of larvae from the type locality in Spain is a crucial point to confirm or refute the conspecificity of Maghrebian and Iberian populations.

8. *Nigrobaetis* Novikova & Kluge, 1987

Diagnosis. 1) Antennae located close together with a well-developed carina in between; 2) mouthparts in a hypognathous position giving to the body a curved posture in lateral view; 3) right mandible with a simple robust prostheca; 4) paraproct without protuberance.

Remarks. The position of the antenna and the general posture in lateral view easily separate *Alainites* and *Nigrobaetis* from other genera in Maghreb. Contrary to *Alainites*, *Nigrobaetis* presents unmodified paraproct (Fig. 2J) and prostheca (Fig. 2B).

Two species of *Nigrobaetis* are reported in the Maghreb: *Nigrobaetis numidicus* (Soldán & Thomas, 1983) (Fig. 5A) and *Nigrobaetis rhithralis* (Soldán & Thomas, 1983) (Fig. 5B). *Nigrobaetis rhithralis* is widely distributed through the Maghreb from Tunisia to Morocco but is rather restricted and never abundant (El Alami et al. 2000; Godunko et al. 2018).

Nigrobaetis numidicus was originally described from Oued Chiffa, close to Alger at an altitude of 200m. It was most certainly a very rare species there, as only four specimens were collected (Soldán and Thomas 1983b). Despite being easily recognizable by the smooth distal margin of abdominal tergites and its peculiar tergal pattern (Fig. 5A), this species was never reported from Algeria since its original description; in Morocco it seems to only occur in a few localities of the Middle Atlas and Rif (Zerrouk et al. 2021; El Alami et al. 2022a).

9. *Procloeon* Bengtsson, 1915

Diagnosis. 1) Gills I-VI with simple or double lamellae, if double, the upper lamella much smaller than lower lamella; 2) legs elongated, claw elongated with two rows of small to minute denticles; 3) labial palp conical and truncated; 4) lateral margin of abdominal segments VII–IX with strong spines; 5) paracercus subequal in length to cerci; 6) cerci with strong spines on the outer margin.

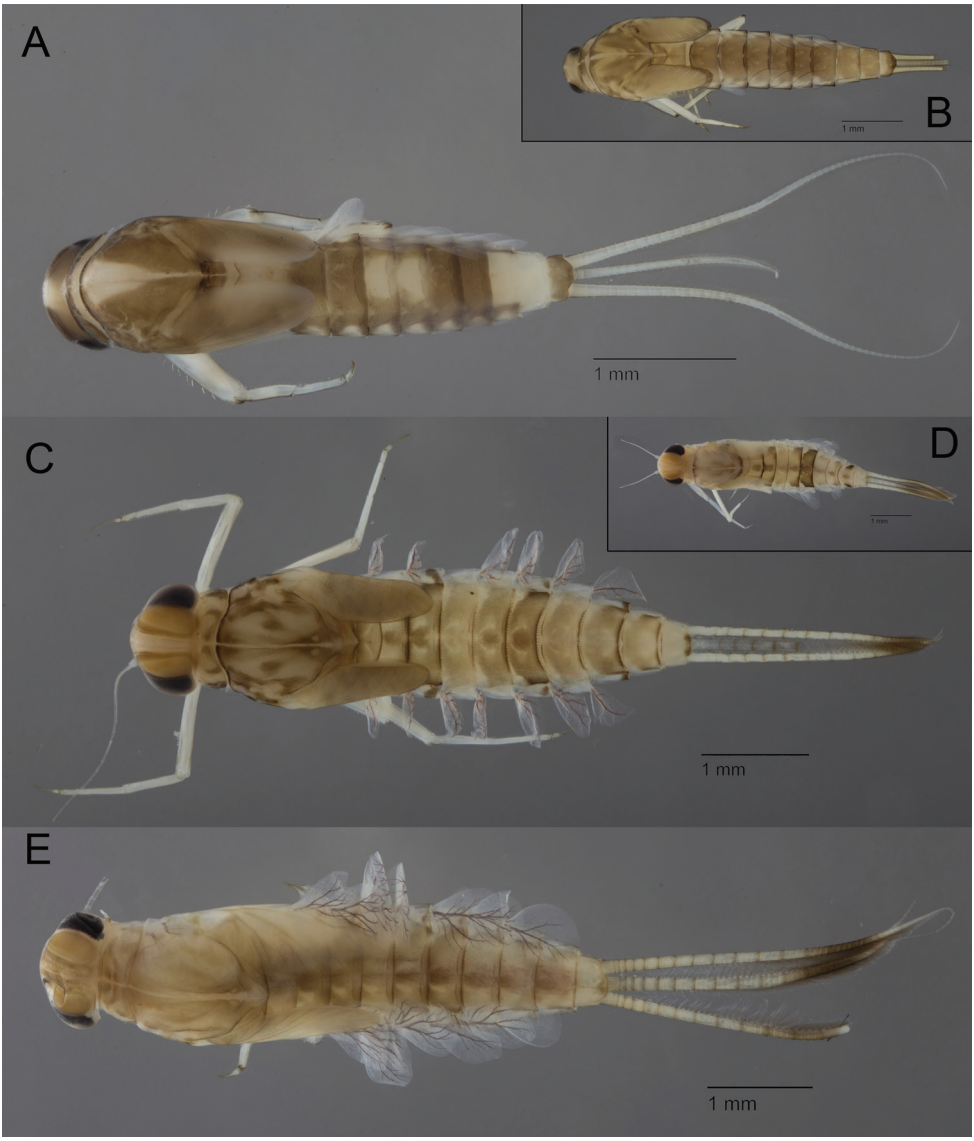

Figure 5. Baetidae: larvae in toto in dorsal view **A** *Nigrobaetis numidicus* **B** *Nigrobaetis rhithralis* **C** *Procloeon stagnicola* **D** *Procloeon* cf. *pennulatum* **E** *Similicloeon simile*.

Remarks. *Procloeon stagnicola* Soldán & Thomas, 1983 (Fig. 5C) is rather similar to the European species *Procloeon bifidum* (Bengtsson, 1912). Old reports of *P. bifidum* most certainly refer to *P. stagnicola*. This species possesses gills with single lamellae (Soldán and Thomas 1983a). It is widely distributed in the Maghreb. Besides this endemic species, reports of other species of the genus are more problematic. Reports of *Procloeon pennulatum* (Eaton, 1870) are limited to Morocco (Fig. 5D). Within this species, morphological comparison between Maghrebian and Central European specimens was still not performed, and no molecular analyses are available. The conspecificity needs to

be confirmed by morphological and molecular evidence; the identification is probably mostly based on presence of hindwings and very long claws. *Procloeon concinnum* (Eaton, 1885) was originally described from Portugal and is only known at the imaginal stage: eggs, larvae and subimagoes remain unknown (Bauernfeind and Soldán 2012). It is unclear which characters allow a reliable assignment of specimens from Morocco to this species, especially at the larval stage (El Bazi et al. 2017; Khadri et al. 2017; Mabrouki et al. 2017; Guellaf et al. 2021). As mentioned above, *Centroptilum algiricum* Eaton, 1899 should be assigned to *Procloeon* based to the shape of the hindwing, and may be the imaginal stage of one of the known species of *Procloeon* (Samraoui et al. 2021c).

10. *Similicloeon* Kluge & Novikova, 1992

Diagnosis. 1) Gills I–VI with double lamellae, upper lamella much smaller than lower lamella; 2) legs elongated, claw elongated with two rows of small to minute denticles; 3) labial palp conical and truncated; 4) maxillary palp 2-segmented; 5) paracercus subequal in length to cerci; 6) lateral margin of abdominal segments VII to IX with strong spines; 6) cerci without spines on the outer lateral margin.

Remarks. *Similicloeon* present intermediate characters between *Cloeon* and *Procloeon*; it may be confused with either of them. It was first considered as a subgenus of *Cloeon* and was only recently raised to the generic level (Kluge and Novikova 1992; Kluge 2016). *Similicloeon simile* (Eaton, 1870) is the single species of the genus known from the Maghreb (Fig. 5E). No morphological differences or genetic distances were observed between Maghrebian and Central European populations (unpublished data). A restricted part of the reports of *Cloeon* sp. may represent misidentification of *S. simile* (as in most previous keys, *Similicloeon* is not separated from *Cloeon*). This species is rarely reported but seems rather widespread across the region (Boumaiza and Thomas 1995; Khadri et al. 2017; Mabrouki et al. 2017). This species is considered as highly euryhaline (Boumaiza and Thomas 1995). Based on the variety of colonized habitats, Mabrouki et al. (2017) suggested that the genus is probably not monospecific in Morocco; we have no evidence to confirm or refute this hypothesis.

Checklist of valid species

Acentrella almohades Alba-Tercedor & El-Alami, 1999
Acentrella cf. *sinaica* Bogoescu, 1931
Alainites cf. *muticus* (Linnaeus, 1758)
Alainites oukaimeden (Thomas & Sartori, 1992)
Alainites sadati Thomas, 1994
Baetis (*Baetis*) cf. *fuscatus* (Linnaeus, 1760)
Baetis (*Baetis*) *pavidus* Grandi, 1949
Baetis (*Patites*) *berberus* Thomas, 1986
Baetis (*Patites*) *maurus* Kimmins, 1938

Baetis (*Patites*) *punicus* Thomas, Boumaiza & Soldán, 1983
Baetis (*Rhodobaetis*) *atlanticus* Soldán & Godunko, 2006
Baetis (*Rhodobaetis*) *chelif* Soldán, Godunko & Thomas, 2005
Baetis (*Rhodobaetis*) *sinespinosus* Soldán & Thomas, 1983
Centroptilum alamiae Kaltenbach, Vuataz & Gattolliat, 2022
Centroptilum samraouii Kaltenbach, Vuataz & Gattolliat, 2022
Cheleocloeon dimorphicum (Soldán & Thomas, 1985)
Cloeon peregrinator Gattolliat & Sartori, 2008
Cloeon saharense Soldán & Thomas, 1983
Labiobaetis cf. *neglectus* (Navàs, 1913)
Nigrobaetis numidicus (Soldán & Thomas, 1983)
Nigrobaetis rhithralis (Soldán & Thomas, 1983)
Procloeon algiricum (Eaton, 1899)
Procloeon cf. *pennulatum* (Eaton, 1870)
Procloeon stagnicola Soldán & Thomas, 1983
Similicloeon simile (Eaton, 1870)

Reported species with uncertain status

Baetis (*Rhodobaetis*) *rhodani* (Pictet, 1843)
Baetis (*Baetis*) *meridionalis* Ikonomov, 1954
Baetis (*Baetis*) *nigrescens* Navás, 1932
Cloeon dipterum (Linneaus, 1761)
Cloeon cognatum Stephens, 1835
Procloeon bifidum (Bengtsson, 1912)
Procloeon concinnum (Eaton, 1885)

Discussion

In the Maghreb, Baetidae are the most diversified family of mayflies; they encompass ten genera, and three subgenera. We offer a straightforward dichotomic key to separate this family in twelve taxonomic units corresponding either to genera or subgenera. In the future, these taxonomic units should represent the standard identification level for environmental studies and water quality assessment. Among the 25 species of Baetidae reported from Maghreb, at least fourteen species are endemic to this area, underlying the diversity and uniqueness of this fauna. With eight species, *Baetis* is by far the most species-rich genus; other genera only contain one or two species. Links between European and Maghrebian faunas exist (Thomas 1998; Zrelli et al. 2016) but are less important than previously thought (Benhadji et al. 2020). Only six species unambiguously occur in the Maghreb and in Central Europe. *Similicloeon simile* is widely distributed in West Palearctic and in the Maghreb; *Cloeon peregrinator* is reported from Macaronesia and the Maghreb; *Baetis atlanticus* was originally described from Madeira, it is now reported from the Maghreb to Sweden including the British Islands; *Baetis pavidus* is

extremely common in the whole Maghreb but seems rare in South of France and Italy; *Acentrella almohades* and *Baetis maurus* occur in the Maghreb and the Iberian Peninsula (Alba-Tercedor and El Alami 1999; Gattolliat et al. 2008; Benhadji et al. 2020; Samraoui et al. 2021b; El Alami et al. 2022a). Five taxa are tentatively attributed to Central European species (indicated as cf. in the list). Preliminary studies indicated that *Acentrella* cf. *sinaica*, *Alainites* cf. *muticus* and *Labiobaetis* cf. *neglectus* morphologically and/or genetically differ between these two regions (Benhadji et al. 2020; Samraoui et al. 2021c). These three taxa may represent endemic species to the Maghreb, closely related to their European sister species. The case of *Cloeon* cf. *dipterum* is more problematic as the species concept itself remains unclear. This complex of species encompasses at least six different lineages in the West Palearctic based on molecular evidence only, representing the same number of potential species (Rutschmann et al. 2014, 2017). According to our present knowledge, it remains impossible to decide which lineage corresponds to *Cloeon dipterum sensu stricto*. For the moment, only one lineage is reported with certainty from the Maghreb and it corresponds to *Cloeon peregrinator* (Benhadji et al. 2020). According to the diversity of habitats colonized by the larvae and the important morphological differences observed between populations, we could assume that more than one species occurs in the Maghreb. Species identification within *Cloeon* remains impossible without a broad scale study based on an integrative approach.

We consider as dubious, or at least requiring confirmation, the reports of seven species in the Maghreb, all of them having a European distribution. *Baetis rhodani*, *Cloeon dipterum*, and *Cloeon cognatum* belong to complexes of very close species; other species from these complexes are already reported from the Maghreb. However, the presence of these three species cannot be completely excluded. At least an important part of their reports corresponds to old identifications and are based on inappropriate concepts. According to preliminary results (El Alami et al. 2022a), some specimens of *Baetis* from Morocco cannot be assigned to any reported species. They clearly belong to the subgenus *Baetis*, their paracercus is not reduced and they do not exhibit spines on the margin of gills. They cannot be assigned to any species of the checklist; they are reported either as *Baetis* gr *fuscatus* or *Baetis* gr *lutheri* in El Alami et al. (2022a). As mentioned above, beside *P. stagnicola*, other species of *Procloeon* need a complete revision and extensive morphological and molecular comparisons with Iberian and Central European populations.

All these problematic cases clearly indicate the need of an extensive taxonomic revision in some taxa including specimens from Maghrebian, Mediterranean and Central European populations. Only an integrative approach involving at least morphology and molecular evidence can solve these taxonomic riddles.

In conclusion, Baetidae is the most diverse family of mayflies in the Maghreb. This family encompasses on the one hand common species with large ecological valence (e.g., *Baetis pavidus*, *Baetis atlanticus*, *Cloeon peregrinator*) and, on the other hand, rare species with very specific ecological requirements (e.g., *Nigrobaetis rhithralis*, *Nigrobaetis numidicus*, *Alainites sadati*). Therefore, identification to the family level may completely hide important environmental information as key conservation values. By offering a reasonably simple key to generic or subgeneric level, the main goal is to open the identifica-

tion of this family to a wide range of scientists, and not only to a restricted set of experts. We hope that further ecological or environmental studies will confirm the high potential of this group for bioindication when working at lower taxonomic level. A better understanding of the distribution and ecology of the members of this family is an essential step for the conservation of these species and of the endangered freshwater habitat in general.

Acknowledgements

We want to thank Marion Podolak (MZL: Museum of Zoology, Lausanne) for the pictures of the different genera. The molecular study of Maghrebian Baetidae is still in progress; we want to express our gratitude to Céline Stoffel (MZL) and Marion Podolak for their dedicated work with the molecular lab. Further, we are thankful to Thomas Kaltenbach and Laurent Vuataz (MZL) for their constant interest and support for our projects in link with the study of Maghrebian mayflies. Lastly, the authors are grateful to the reviewers, Pavel Sroka and Zohar Yanai, for their valuable recommendations and comments on the manuscript.

References

Alba-Tercedor J, El Alami M (1999) Description of the Nymphs and Eggs of *Acentrella almohades* sp.n. from Morocco and Southern Spain (Ephemeroptera, Baetidae). Aquatic Insects 21(4): 241–247. https://doi.org/10.1076/aqin.21.4.241.4509

Barber-James HM, Gattolliat J-L, Sartori M, Hubbard MD (2008) Global diversity of mayflies (Ephemeroptera, Insecta) in freshwater. Hydrobiologia 595(1): 339–350. https://doi.org/10.1007/s10750-007-9028-y

Bauernfeind E, Soldán T (2012) The Mayflies of Europe (Ephemeroptera). Apollo Books, Ollerup, Denmark, 781 pp. https://doi.org/10.1163/9789004260887

Benhadji N, Hassaine KA, Sartori M (2018) *Habrophlebia hassainae*, a new mayfly species (Ephemeroptera: Leptophlebiidae) from North Africa. Zootaxa 4403(3): 557–569. https://doi.org/10.11646/zootaxa.4403.3.8

Benhadji N, Hassaine KA, Gattolliat J-L, Sartori M (2019) Thirty years after: An update to the mayflies composition in the Tafna basin (Algeria). Zoosymposia 16: 22–35.

Benhadji N, Sartori M, Hassaine KA, Gattolliat J-L (2020) Reports of Baetidae (Ephemeroptera) species from Tafna Basin, Algeria and biogeographic affinities revealed by DNA barcoding. Biodiversity Data Journal 8: 1–23. https://doi.org/10.3897/BDJ.8.e55596

Bennas N, L'mohdi O, El-Haissoufi M, Charfi F, Ghlala A, El-Alami M (2018) New Data on the Aquatic Insect Fauna of Tunisia. Transactions of the American Entomological Society 144(3): 575–592. https://doi.org/10.3157/061.144.0309

Bouhala Z, Márquez-Rodríguez J, Chakri K, Samraoui F, El-Serehy HA, Ferreras-Romero M, Samraoui B (2020a) The life history of the Ibero-Maghrebian endemic *Oligoneuriopsis skhounate* Dakki and Guidicelli (Ephemeroptera: Oligoneuriidae). Limnologica 81: 125761. https://doi.org/10.1016/j.limno.2020.125761

Bouhala Z, Márquez-Rodríguez J, Chakri K, Samraoui F, El-Serehy HA, Ferreras-Romero M, Samraoui B (2020b) The life cycle of the Maghrebian endemic *Ecdyonurus rothschildi* Navás, 1929 (Ephemeroptera: Heptageniidae) and its potential importance for environmental monitoring. Limnology 22(1): 17–26. https://doi.org/10.1007/s10201-020-00625-z

Boumaiza M, Thomas A (1986) Répartition et écologie des Ephéméroptères de Tunisie (1ère partie) (Insecta, Ephemeroptera). Archives de l'Institut Pasteur de Tunis 63(4): 567–599.

Boumaiza M, Thomas A (1994) Premier inventaire faunistique et biogéographique des Baetidae (Insecta, Ephemeroptera) de Tunisie. Bulletin de la Société des Sciences Naturelles de Tunisie 23: 26–31.

Boumaiza M, Thomas A (1995) Distribution and ecological limits of Baetidae vs the other mayfly families in Tunisia: A first evaluation (Insecta, Ephemeroptera). Bulletin de la Société d`Histoire Naturelle de Toulouse 131: 27–33.

Dakki M (1986) Biotypologie et gradient thermique spatio-temporels, étude sur un cours d`eau du Moyen Atlas (Maroc). Bulletin d'Ecologie 17(2): 79–85.

Dakki M (1987) Ecosystèmes d'eau courante du haut Sebou (Moyen Atlas): études typologiques et analyses écologique et biogéographique des principaux peuplements entomologiques. Travaux de l'Institut scientifique, Rabat 42: 1–99.

Dakki M, El Agbani MA (1983) Ephéméroptères d`Afrique du Nord 3. Eléments pour la connaissance de la faune marocaine. Bulletin de l'Institut Scientifique, Rabat 7: 115–126.

Dakki M, Giudicelli J (1980) Ephémeroptères d`Afrique du Nord 2. Description d`*Oligoneuriella skoura* n. sp. et d'*Oligoneuriopsis skhounate* n. sp., avec notes sur leur écologie (Ephem., Oligoneuriidae). Bulletin de l'Institut Scientifique, Rabat 4: 13–28.

Dakki M, Thomas AGB (1986) *Rhithrogena ayadi* n. sp., Ephéméroptère nouveau du Moyen Atlas marocain (Heptageniidae). Annales de Limnologie 22(1): 27–29. https://doi.org/10.1051/limn/1986002

Eaton AE (1899) List of Ephemeridae hitherto observed in Algeria, with localities. Entomologist's Monthly Magazine 35: 4–5.

El Agbani MA, Dakki M, Bournaud M (1992) Etude typologique du Bou Regreg (Maroc): Les milieux aquatiques et leurs peuplements en macroinvertébrés. Bulletin d'Ecologie 23: 103–113.

El Alami M, Dakki M (1998) Peuplements d'Ephéméroptères et de Trichoptères de l'Oued Laou (Rif Occidentale, Maroc): distribution longitudinale et biotypologie. Bulletin de l'institut Scientifique, Rabat 21: 51–70.

El Alami M, Dakki M, Errami M, Alba-Tercedor J (2000) Nouvelles données sur les Baetidae du Maroc (Insecta: Ephemeroptera). Zoologica Baetica 11: 105–113.

El Alami M, El Yaagoubi S, Gattolliat JL, Sartori M, Dakki M (2022a) Diversity and Distribution of Mayflies from Morocco (Ephemeroptera, Insecta). Diversity 14(6): 498. https://doi.org/10.3390/d14060498

El Alami M, Benlasri M, Sartori M, Vuataz L, Ghamizi M (2022b) A new species of *Prosopistoma* Latreille, 1833 (Ephemeroptera, Prosopistomatidae) from Morocco. ZooKeys 1117: 203–218. https://doi.org/10.3897/zookeys.1117.83539

El Bazi R, El Alami M, Khadri O, Errochdi S, Slimani M, Bennas N (2017) Projet du parc naturel de Bouhachem (Nord-Ouest du Maroc) II: Ephemeroptera, Plecoptera, Trichoptera. Boletin de la SEA 61: 55–66.

Folmer O, Black M, Hoeh W, Lutz R, Vrijenhoek R (1994) DNA primers for amplification of mitochondrial cytochrome c oxidase subunit I from diverse metazoan invertebrates. Molecular Marine Biology and Biotechnology 3: 294–299. http://www.mbari.org/staff/vrijen/PDFS/Folmer_94MMBB.pdf

Fraser FC (1952) Contribution à l'étude du peuplement de la Mauritanie. Odonata, Neuroptera, Nemoptera et Ephemeroptera. Bulletin de l'Institut français d'Afrique noire 14(A): 479-484.

Gagneur J, Thomas A (1988) Contribution à la connaissance des Ephéméroptères d`Algérie I. Répartition et écologie (1ère partie) (Insecta, Ephemeroptera). Bulletin de la Société d`Histoire Naturelle de Toulouse 124: 213–223.

Gattolliat J-L, Monaghan MT (2010) DNA-based association of adults and larvae in Baetidae (Ephemeroptera) with the description of a new genus *Adnoptilum* in Madagascar. Journal of the North American Benthological Society 29(3): 1042–1057. https://doi.org/10.1899/09-119.1

Gattolliat J-L, Nieto C (2009) The family Baetidae (Insecta: Ephemeroptera): synthesis and future challenges. Aquatic Insects 31(Suppl. 1): 41–62. https://doi.org/10.1080/01650420902812214

Gattolliat J-L, Hughes SJ, Monaghan MT, Sartori M (2008) Revision of Madeiran mayflies (Insecta, Ephemeroptera). Zootaxa (1957): 52–68. https://doi.org/10.11646/zootaxa.1957.1.2

Gattolliat J-L, Vuataz L, Sartori M (2012) First contribution to the mayflies of Jordan. Zoology in the Middle East 56(1): 91–110. https://doi.org/10.1080/09397140.2012.10648945

Gattolliat J-L, Kondratieff BC, Kaltenbach T, Al Dhafer HM (2018) *Labiobaetis* from the Kingdom of Saudi Arabia (Insecta: Ephemeroptera: Baetidae). ZooKeys 774: 77–104. https://doi.org/10.3897/zookeys.774.25273

Godunko RJ, Martynov AV, Gattolliat J-L (2018) Redescription of *Nigrobaetis rhithralis* (Soldán & Thomas, 1983) (Ephemeroptera: Baetidae). Zootaxa 4462(1): 41–72. https://doi.org/10.11646/zootaxa.4462.1.2

Grandi M (1951) Contributi allo studio degli Efemeroideiesotici I. Un nuovo Cenide africano: *Caenis hoggariensis* sp.n. Bolletino del l'Istituto di Entomologia del l'Universita di Bologna 18: 173–180.

Guellaf A, El Alami M, Kassout J, Errochdi S, Khadri O, Kettani K (2021) Diversity and ecology of aquatic insects (Ephemeroptera, Plecoptera and Trichoptera) in the Martil basin (Northwestern Morocco). Community Ecology 22(3): 331–350. https://doi.org/10.1007/s42974-021-00058-3

Hafiane M, Hamzaoui D, Attou F, Bouchelouche D, Arab A, Alfarhan AH, Samraoui B (2016) Anthropogenic impacts and their influence on the spatial distribution of the Odonata of Wadi El Harrach (north-central Algeria). Revue d`Écologie 71(3): 239–249. https://doi.org/10.3406/revec.2016.1848 [la Terre et la Vie]

Jacobus LM, Macadam CR, Sartori M (2019) Mayflies (Ephemeroptera) and their contributions to ecosystem services. Insects 10: 170. https://doi.org/10.3390/insects10060170

Kaltenbach T, Garces JM, Gattolliat J-L (2020) The success story of *Labiobaetis* Novikova & Kluge in the Philippines (Ephemeroptera, Baetidae), with description of 18 new species. ZooKeys 1002: 1–114. https://doi.org/10.3897/zookeys.1002.58017

Kaltenbach T, Vuataz L, Samraoui B, El Yaagoubi S, El Alami M, Gattolliat JL (2022) Two new species of *Centroptilum* Eaton, 1869 from North Africa (Ephemeroptera, Baetidae). ZooKeys 1131: 71–97. https://doi.org/10.3897/zookeys.1131.91017

Kechemir LH, Sartori M, Lounaci A (2020) An unexpected new species of *Habrophlebia* from Algeria (Ephemeroptera, Leptophlebiidae). ZooKeys 953: 31–47. https://doi.org/10.3897/zookeys.953.51244

Khadri O, Alami M, El Bazi R, Slimani M (2017) Ephemeroptera's diversity and ecology in streams of the ultramafic massif of Beni Bousera and in the adjacent non-ultramafic sites (NW, Morocco). Journal of Materials & Environmental Sciences 8: 3508–3523.

Kimmins DE (1938) A new Moroccan Ephemeropteron. Annals & Magazine of Natural History 11(1): 302–305. https://doi.org/10.1080/00222933808526771

Kluge N (2016) A new subgenus *Oculogaster* subgen. n. for viviparous representatives of *Procloeon* s.l., with discussion about status of the generic name *Austrocloeon* Barnard, 1932 and the species name *africanum* Esben-Petersen, 1913 *Cloeon* (Ephemeroptera, Baetidae). Zootaxa 4107(4): 491–516. https://doi.org/10.11646/zootaxa.4107.4.2

Kluge N, Novikova EA (1992) Revision of Palearctic genera and subgenera of Mayflies in the subfamily Cloeoninae (Ephemeroptera, Baetidae) with description of new species from the USSR. Entomological Review 71(9): 29–54.

Lestage JA (1925) Ephéméroptères, Plécoptères et Trichoptères recueillis en Algérie par M. H. Gauthier et liste des espèces connues actuellement de l`Afrique du Nord. Bulletin de la Société d`Histoire Naturelle de l`Afrique du Nord 16: 8–18.

Mabrouki Y, Taybi AF, El Alami M, Berrahou A (2017) New and interesting data on distribution and ecology of mayflies from Eastern Morocco (Ephemeroptera). Journal of Materials and Environmental Sciences and Engineering 8(8): 2839–2859.

Mebarki M, Taleb A, Arab A (2017) Environmental factors influencing the composition and distribution of mayfly larvae in northern Algerian wadis (regional scale). Revue d`Écologie 72(3): 303–313. https://doi.org/10.3406/revec.2017.1893 [la Terre et la Vie]

Morghad F, Samraoui F, Touati L, Samraoui B (2019) The times they are a changin': Impact of land-use shift and climate warming on the odonate community of a Mediterranean stream over a 25-year period. Vie et Milieu 69: 25–33.

Müller-Liebenau I (1969) Revision der europäischen Arten der Gattung *Baetis* Leach, 1815 (Insecta, Ephemeroptera). Gewässer und Abwässer 48/49: 1–214.

Murria C, Bonada N, Vellend M, Zamora-Munoz C, Alba-Tercedor J, Sainz-Cantero CE, Garrido J, Acosta R, El Alami M, Barquin J, Derka T, Alvarez-Cabria M, Sainz-Bariain M, Filipe AF, Vogler AP (2017) Local environment rather than past climate determines community composition of mountain stream macroinvertebrates across Europe. Molecular Ecology 26(21): 6085–6099. https://doi.org/10.1111/mec.14346

Navás L (1929) Insectes Névroptères et voisins de Barbarie. Bulletin de la Société d`Histoire Naturelle de l`Afrique du Nord 20: 57–60.

Ouahsine H, Lavandier P (1988a) Développement larvaire de *Baetis rhodani* (Ephemeroptera) dans un torrent du Haut-Atlas de Marrakech (Maroc). Bulletin de la Société d`Histoire Naturelle de Toulouse 124: 69–72. https://doi.org/10.1051/limn/1988014

Ouahsine H, Lavandier P (1988b) Dynamique des populations larvaires de *Baetis navasi* M.-L. (Ephemeroptera) dans un torrent du Haut-Atlas de Marrakech, Maroc. Annales de Limnologie 24(2): 167–171. https://doi.org/10.1051/limn/1988014

Peters WL (1980) *Choroterpes* (*Choroterpes*) *lindrothi*, a new species of Mayfly from Morocco (Ephemeroptera: Leptophlebiidae). Entomologia Generalis 6(2–4): 371–373. https://doi.org/10.1127/entom.gen/6/1980/371

Qninba AJ, El Agbani MA, Dakki M, Benhoussa A (1988) Evolution saisonnière de quelques peuplements d`invertébrés benthiques de l`Oued Bou Regreg (Maroc). Bulletin de l'Institut Scientifique, Rabat 12: 149–156.

Rutschmann S, Gattolliat J-L, Hughes SJ, Baez M, Sartori M, Monaghan MT (2014) Evolution and island endemism of morphologically cryptic *Baetis* and *Cloeon* species (Ephemeroptera, Baetidae) on the Canary Islands and Madeira. Freshwater Biology 59(12): 2516–2527. https://doi.org/10.1111/fwb.12450

Rutschmann S, Detering H, Simon S, Funk DH, Gattolliat J-L, Hughes SJ, Raposeiro PM, DeSalle R, Sartori M, Monaghan MT (2017) Colonization and diversification of aquatic insects on three Macaronesian archipelagos using 59 nuclear loci derived from a draft genome. Molecular Phylogenetics and Evolution 107: 27–38. https://doi.org/10.1016/j.ympev.2016.10.007

Samraoui B, Vuataz L, Sartori M, Gattolliat J-L, Al-Misned FA, El-Serehy HA, Samraoui F (2021a) Taxonomy, Distribution and Life Cycle of the Maghrebian Endemic *Rhithrogena sartorii* (Ephemeroptera: Heptageniidae) in Algeria. Diversity 13(11): 547. https://doi.org/10.3390/d13110547

Samraoui B, Bouhala Z, Chakri K, Marquez-Rodriguez J, Ferreras-Romero M, El-Serehy HA, Samraoui F, Sartori M, Gattolliat J-L (2021b) Environmental determinants of mayfly assemblages in the Seybouse River, north-eastern Algeria (Insecta: Ephemeroptera). Biologia 76(8): 2277–2289. https://doi.org/10.1007/s11756-021-00726-9

Samraoui B, Márquez-Rodríguez J, Ferreras-Romero M, El-Serehy HA, Samraoui F, Sartori M, Gattolliat J-L (2021c) Biogeography, ecology, and conservation of mayfly communities of relict mountain streams, north-eastern Algeria. Aquatic Conservation 31(12): 3357–3369. https://doi.org/10.1002/aqc.3719

Samraoui B, Marquez-Rodríguez J, Ferreras-Romero M, Sartori M, Gattolliat J-L, Samraoui F (2021d) Life history and ecology of the Maghrebian endemic *Choroterpes atlas* Soldán & Thomas, 1983 (Ephemeroptera: Leptophlebiidae). Limnologica 89: 125887. https://doi.org/10.1016/j.limno.2021.125887

Sartori M, Brittain JE (2015) Order Ephemeroptera. Ecology and General Biology, Vol I: Thorp and Covich's Freshwater Invertebrates, 4th edn. J. H. Thorp and D. C. Rogers, New York, 873–891. https://doi.org/10.1016/B978-0-12-385026-3.00034-6

Sartori M, Thomas AGB (1986) Révision taxonomique du genre *Habroleptoides* Schönemund, 1929 (Ephemeroptera, Leptophlebiidae). I. *Habroleptoides assefae*, n. sp. du Haut-Atlas marocain. Revue Suisse de Zoologie 93(2): 417–422. https://doi.org/10.5962/bhl.part.79703

Soldán T, Godunko RJ (2006) *Baetis atlanticus* n. sp., a new species of the subgenus *Rhodobaetis* Jacob, 2003 from Madeira, Portugal (Ephemeroptera: Baetidae). Genus 17(1): 5–17.

Soldán T, Thomas AGB (1983a) New and little-known species of mayflies (Ephemeroptera) from Algeria. Acta Entomologica Bohemoslovaca 80: 356–376.

Soldán T, Thomas AGB (1983b) *Baetis numidicus* n.sp., Ephéméroptère nouveau d`Algérie (Baetidae). Annales de Limnologie 19(3): 207–211. https://doi.org/10.1051/limn/1983024

Soldán T, Thomas AG (1985) *Centroptilum dimorphicum* sp. n., a new species of mayfly (Ephemeroptera, Baetidae) from Algeria. Acta Entomologica Bohemoslovaca 82: 180–186.

Soldán T, Godunko RJ, Thomas AG (2005) *Baetis chelif* n. sp., a new mayfly from Algeria with notes on *B. sinespinosus* Soldán & Thomas, 1983, n. stat. (Ephemeroptera: Baetidae). Genus 16(2): 155–165.

Sweeney BW, Funk DH, Camp AA, Buchwalter DB, Jackson JK (2018) Why adult mayflies of *Cloeon dipterum* (Ephemeroptera: Baetidae) become smaller as temperature warms. Freshwater Science 37(1): 64–81. https://doi.org/10.1086/696611

Thomas AGB (1998) A provisional checklist of the mayflies of North Africa (Ephemeroptera). Bulletin de la Société d`Histoire Naturelle de Toulouse 134: 13–20.

Thomas AGB, Bouzidi A (1986) Trois Ephéméroptères nouveaux du Haut Atlas marocain (Heptageniidae, Baetidae, Leptophlebiidae). Bulletin de la Société d`Histoire Naturelle de Toulouse 122: 7–10.

Thomas AGB, Dia A (2000) Compléments et corrections à la faune des Ephéméroptères du Proche Orient: 4. Description de l'imago mâle de *Baetis baroukianus* Thomas & Dia, 1984 et érection de *Patites* n. subgen. (Ephemeroptera, Baetidae). Ephemera 1(2): 105–109 [1999].

Thomas AGB, Mohati A (1985) *Rhithrogena ourika* n.sp., Ephéméroptère nouveau du Haut Atlas marocain (Heptageniidae). Annales de Limnologie 21(2): 145–148. https://doi.org/10.1051/limn/1985014

Thomas AGB, Vitte B (1988) Compléments et corrections à la faune des Ephéméroptères d`Afrique du Nord. 1. Le genre *Choroterpes* Eaton, sensu stricto (Ephemeroptera). Annales de Limnologie 24(1): 61–65. https://doi.org/10.1051/limn/1988006

Thomas AGB, Boumaiza M, Soldán T (1983) *Baetis punicus* n.sp., Ephéméroptère nouveau de Tunisie (Baetidae). Annales de Limnologie 19(2): 107–111. https://doi.org/10.1051/limn/1983010

Thomas AGB, Vitte B, Soldán T (1987) *Rhithrogena ryszardi* n. sp., Ephéméroptère nouveau du Moyen Atlas (Maroc) et redescription de *Rh. soteria* Navás, 1917 (Heptageniidae). Annales de Limnologie 23(3): 169–177. https://doi.org/10.1051/limn/1987015

Thomas AGB, Bouzidi A, Sartori M, Assef S, Ajakane A (1992) Complément et corrections à la faune des Ephéméroptères d`Afrique du Nord. 5. *Baetis oukaimeden* n. sp. du Haut Atlas marocain: Description et écologie (Ephemeroptera, Baetidae). Mitteilungen der Schweizerische Entomologische Gesellschaft 65: 369–377.

Verrier M-L (1952) Ephéméroptères récoltés par M. Paul Rémy au Hoggar et au Tidikelt. Bulletin de la Société Zoologique de France 77(5–6): 292–304.

Vitte B (1991) *Rhithrogena mariae* n.sp., Ephéméroptère nouveau du Rif marocain (Ephemeroptera, Heptageniidae). Nouvelle Revue d'Entomologie 8(1): 89–96.

Vitte B, Thomas AGB (1988a) Complément et corrections à la faune des Ephéméroptères d`Afrique du Nord. 2. Le genre *Choroterpes* Eaton, sous-genre *Euthraulus* Barnard

(Ephemeroptera). Annales de Limnologie 24(2): 160–165. https://doi.org/10.1051/limn/1988013

Vitte B, Thomas AGB (1988b) Compléments et corrections à la faune des Ephéméroptères d`Afrique du Nord. 3. *Ecdyonurus ifranensis* n. sp. du Moyen Atlas marocain (Ephemeroptera). Annales de Limnologie 24(3): 269–273. https://doi.org/10.1051/limn/1988023

Vuataz L, Sartori M, Wagner A, Monaghan MT (2011) Toward a DNA taxonomy of Alpine *Rhithrogena* (Ephemeroptera: Heptagenidae) using a mixed Yule-Coalescent Analysis of mitochondrial and nuclear DNA. PLoS ONE 6(5): 1–11. https://doi.org/10.1371/journal.pone.0019728

Zerrouk M, Dakki M, El Agbani MA, El Alami M, Bennas N, Qninba A, Himmi O (2021) Evolution of the benthic communities in a north-African river, the upper Sebou (Middle Atlas-Morocco) between 1981 and 2017: Effects of global changes. Biologia 76(10): 2973–2989. https://doi.org/10.1007/s11756-021-00787-w

Zrelli S, Boumaïza M, Béjaoui M, Gattolliat J-L, Sartori M (2011a) New reports of mayflies (Insecta: Ephemeroptera) from Tunisia. Revue Suisse de Zoologie 118(1): 3–11.

Zrelli S, Sartori M, Bejaoui M, Boumaïza M (2011b) *Rhithrogena sartorii*, a new mayfly species (Ephemeroptera: Heptageniidae) from North Africa. Zootaxa 3139(1): 63–68. https://doi.org/10.11646/zootaxa.3139.1.4

Zrelli S, Gattolliat J-L, Boumaïza M, Thomas A (2012) First record of *Alainites sadati* Thomas, 1994 (Ephemeroptera: Baetidae) in Tunisia, description of the larval stage and ecology. Zootaxa 3497(1): 60–68. https://doi.org/10.11646/zootaxa.3497.1.6

Zrelli S, Boumaïza M, Béjaoui M, Gattolliat J-L, Sartori M (2016) New data and revision of the Ephemeroptera of Tunisia. Biology of Inland Waters (Supplement No. 3): 99–106.

Zuedzang Abessolo JR, Yacoubi Khebiza M, Messouli M (2021) Réponse des macroinvertébrés benthiques (éphéméroptères, plécoptères, trichoptères) aux pressions anthropiques dans un contexte de changement climatique sur le bassin versant de l`Ourika (Haut-Atlas du Maroc). Hydroécologie Appliquée 21: 115–155. https://doi.org/10.1051/hydro/2021001

ZooKeys 1139: 165–182 (2023)
doi: 10.3897/zookeys.1139.96216
https://zookeys.pensoft.net

RESEARCH ARTICLE

A peer-reviewed open-access journal
ZooKeys
Launched to accelerate biodiversity research

First mitochondrial genome of subfamily Julodinae (Coleoptera, Buprestidae) with its phylogenetic implications

Zhonghua Wei[1], Xuyan Huang[2], Aimin Shi[1]

1 *The Key Laboratory of Southwest China Wildlife Resources Conservation of the Ministry of Education, College of Life Sciences, China West Normal University, 637009, Nanchong, Sichuan Province, China* **2** *College of Life Sciences, China West Normal University, 637009, Nanchong, Sichuan Province, China*

Corresponding author: Zhonghua Wei (wzh1164@126.com)

Academic editor: Natalia Golub | Received 12 October 2022 | Accepted 28 December 2022 | Published 13 January 2023

https://zoobank.org/4B68DA72-5A94-4697-8BC2-85D604821FAF

Citation: Wei Z, Huang X, Shi A (2023) First mitochondrial genome of subfamily Julodinae (Coleoptera, Buprestidae) with its phylogenetic implications. ZooKeys 1139: 165–182. https://doi.org/10.3897/zookeys.1139.96216

Abstract

Complete mitochondrial genomes of three species of the family Buprestidae were sequenced, annotated, and analyzed in this study. To explore the mitogenome features of the subfamily Julodinae and verify its phylogenetic position, the complete mitogenome of *Julodis variolaris* was sequenced and annotated. The complete mitogenomes of *Ptosima chinensis* and *Chalcophora japonica* were also provided for the phylogenetic analyses within Buprestidae. Compared to the known mitogenomes of Buprestidae species varied from 15,499 bp to 16,771 bp in length, three newly sequenced mitogenomes were medium length (15,759–16,227 bp). These mitogenomes were encoded 37 typical mitochondrial genes. Among the three studied mitogenomes, Leu2 (L2), Ser2 (S2), and Pro (P) were the three most frequently encoded amino acids. Within the Buprestidae, the heterogeneity in sequence divergences of Agrilinae was highest, whereas the sequence homogeneity of Chrysochroinae was highest. Moreover, phylogenetic analyses were performed based on nucleotide matrix (13 PCGs + 2 rRNAs) among the available sequenced species of Buprestidae using Bayesian Inference and Maximum Likelihood methods. The results showed that the Julodinae was closely related to the subfamily Polycestinae. Meanwhile, the genera *Melanophila*, *Dicerca*, and *Coomaniella* were included in Buprestinae, which was inconsistent with the current classification system of Buprestidae. These results could contribute to further studies on genetic diversity and phylogeny of Buprestidae.

Keywords

Jewel beetles, Julodinae, mitogenome, phylogenetics

Introduction

The family Buprestidae is one of the largest families in Coleoptera, including six subfamilies, 521 genera, and more than 15,000 species distributed worldwide (Bellamy 2008; Kubáň et al. 2016). In this family, all species are phytophagous. The adults are feeders on flowers, leaves and stems, whereas the larvae are internal feeders in roots and stems, or feed on the foliage of woody and herbaceous plants, the larvae of Julodinae are soil habitants feeding externally by the roots (Bellamy and Volkovitsh 2016). Different groups have different functions covered ecological, social and economic functions, such as: most larvae of Buprestinae and Chrysochroinae are important decomposers of woody plants; with most species being ornamental beetles with attractive metallic luster; many species of Agrilinae are forest and agricultural pests; and some species of the tribes Stigmoderini, Acmaeoderini, and Anthaxiini are pollinator taxa. Although some buprestid taxonomists have made important contributions to the classification based on morphological analyses (Cobos 1980, 1986; Tôyama 1987; Hołyński 1988, 1993, 2009; Kolibáè 2000; Bellamy 2003), the problems of the overall classification of Buprestidae remain.

In the past two decades, the mitochondrial genome emerged as important molecular data for higher-level phylogenetic analyses (Saccone et al. 1999; Timmermans et al. 2010, 2016; Cameron 2014; Li et al. 2015; Qin et al. 2015; Nie et al. 2020, 2021; Motyka et al. 2022; Zheng et al. 2022), evolutionary strategies (Krzywinski et al. 2011; Nie et al. 2019; Motyka et al. 2022; Zhang et al. 2022), and genetic diversity analyses (Lim et al. 2021). The buprestid mitogenome also caught the attention of taxonomists. In Buprestidae, the first complete mitogenome of *Chrysochroa fulgidissima* (Schönherr, 1817) was reported by Hong et al. (2009). In the same year, the mitogenome of *Acmaeodera* sp. was used to analyze the nonstationary evolution and compositional heterogeneity of Coleoptera. To date, only 22 buprestid mitogenomes (Table 1) have been reported worldwide, including three newly generated in this study.

To date, the mitogenome of the subfamily Julodinae has not been reported. The lack of the data on complete mitogenome of Julodinae species has limited our understanding of the real phylogenetic relationships within jewel beetles. The single molecular phylogenetic analysis, including Julodinae, showed that Julodinae is monophyletic group and close to Polycestinae (Evans et al. 2015). The subfamily Julodinae includes one tribe and six genera (Hołyński 2014). The described Julodinae species are mainly distributed in the arid and semiarid zones of the Ethiopian and Palaearctic regions, except for the species of the genus *Sternocera* Eschscholtz, 1829 distributed in humid tropical zones of Asia and Africa (Bellamy 2008; Hołyński 2014).

In the present study, three complete mitogenomes are sequenced and annotated, of which that of *Julodis variolaris* (Pallas, 1771) is the first complete mitogenome sequence to be reported in the subfamily Julodinae. In China, this species is widely distributed in Xinjiang Uygur Autonomous Region. The adults, appearing in May and June, feeder on the leaves of *Haloxylon ammodendron* (Meyer, 1829) and the larvae feeder on the roots of this plant. Additionally, the complete mitogenomes of *Chalcophora japonica* (Gory, 1840) (Chrysochroinae: Chalcophorini) and *Ptosima*

Table 1. Information on the mitogenomes of Buprestidae and outgroup taxa used for phylogenetic analysis.

Subfamily	Taxa	Accession No.	Genome size (bp)	A+T%	AT-skew	Reference
Agrilinae	*Coraebus diminutus* Gebhardt, 1928	OK189521	15,499	68.42	0.12	Wei 2022
	Coraebus cloueti Théry, 1895	OK189520	15,514	69.27	0.11	Wei 2022
	Coraebus cavifrons Descarpentries & Villiers, 1967	MK913589	15,686	69.79	0.12	Cao and Wang 2019a
	Meliboeus sinae Obenberger, 1935	OK189522	16,108	72.42	0.11	Wei 2022
	Sambus femoralis Kerremans, 1892	OK349489	15,367	73.23	0.12	Wei 2022
	Agrilus sichuanus Jendek, 2011	OK189519	16,521	71.73	0.12	Wei 2022
	Agrilus planipennis Fairmaire, 1888	KT363854	15,942	71.90	0.12	Duan et al. 2017
	Agrilus mali Matsumura, 1924	MN894890	16,204	74.46	0.08	Sun et al. 2020
	Trachys auricollis Saunders, 1873	MH638286	16,429	71.05	0.10	Xiao et al. 2019
	Trachys troglodytiformis Obenberger, 1918	KX087357	16,316	74.62	0.10	Unpublished
	Trachys variolaris Saunders, 1873	MN178497	16,771	72.11	0.11	Cao and Wang 2019b
Buprestinae	*Melanophila acuminata* (De Geer, 1774)	MW287594	15,853	75.66	0.02	Peng et al. 2021
	Anthaxia chinensis Kerremans, 1898	MW929326	15,881	73.61	0.09	Chen et al. 2021
	Coomaniella copipes Jendek & Pham, 2013	OL694145	16,196	74.47	0.03	Huang et al. 2022
	Coomaniella dentata Song, 2021	OL694144	16,179	76.59	0.01	Huang et al. 2022
Chrysochroinae	*Chrysochroa fulgidissima* (Schönherr, 1817)	EU826485	15,592	69.92	0.15	Hong et al. 2009
	Chalcophora japonica (Gory, 1840)	OP388437	15,759	67.97	0.13	In this study
	Chalcophora japonica (Gory, 1840)	OM161962	15,759	67.94	0.13	Weng et al. 2022
	Dicerca corrugata Fairmaire, 1902	OL753086	16,276	71.76	0.09	Huang et al. 2022
Polycestinae	*Acmaeodera* sp.	FJ613420	16,217	68.41	0.11	Sheffield et al. 2009
	Ptosima chinensis Marseul, 1867	OP388449	16,115	67.00	0.13	In this study
Julodinae	*Julodis variolaris* (Pallas, 1771)	OP390084	16,227	70.43	0.12	In this study
outgroup	*Heterocerus parallelus* Gebler, 1830	KX087297	15,845	74.03	0.13	Unpublished
	Dryops ernesti Gozis, 1886	KX035147	15,672	72.98	0.07	Unpublished

chinensis Marseul, 1867 (Polycestinae: Ptosimini) are provided for phylogenetic analyses, which are also enriching the diversity of mitogenomes studied in Buprestidae. The total length of the mitogenome in *C. japonica* was consistent with the results of Weng et al. (2022). In order to explore the phylogenetic position of the subfamily Julodinae, phylogenetic analyses of the family Buprestidae were performed based on a nucleotide matrix (13 PCGs + 2 rRNAs) among buprestid species using Bayesian Inference (BI) and Maximum Likelihood (ML) methods.

Materials and methods

Sampling and DNA extraction

Specimens of *J. variolaris* were collected on *H. ammodendron* in the vicinities of Turpan City, Xinjiang Uygur Autonomous Region, China, on 14 May 2022. Specimens of *P. chinensis* were collected from Dayaoshan Mountains in Guangxi Zhuang Autonomous Region, China, on 20 March 2021. Specimens of *C. japonica* were collected from Quanzhou City, Fujian Province, China, on 23 February 2021. The above specimens are preserved in 95% alcohol at -24 °C in specimen collection at China West Normal University, Nanchong, China. Next-generation sequencing and assembly were performed by Beijing Aoweisen Gene Technology Co. Ltd. (Beijing, China) to obtain the complete mitogenome sequences.

Sequence assembly, annotation, and analysis

The raw data were processed using Trimmomatic v. 0.35 (Bolger et al. 2014) to remove low-quality reads and obtain a high-quality clean data. Finally, 4.8 Gb, 5.28 Gb, and 6.8 Gb clean data were obtained to assemble complete mitogenome of *J. variolaris*, *P. chinensis*, and *C. japonica*, respectively. Three mitogenome sequences were annotated using Geneious 11.0.2 (Kearse et al. 2012) based on the invertebrate mitochondrial genetic code. All tRNA genes were reconfirmed using the online tool MITOS Web Server (Bernt et al. 2013) and the second structures were further predicted using tRNAscan-SE server v. 1.21 (Lowe and Chan 2016). Two rRNA genes were identified by alignment with other buprestid rRNA sequences. Three mitogenome maps were drawn using Organellar Genome Draw v. 1.3.1 (Greiner et al. 2019). Strand asymmetry of mitogenome sequence was calculated using the formulae reported by Perna and Kocher (1995): AT-skew = (A – T)/(A + T), and GC-skew = (G – C)/(G + C). The base composition and relative synonymous codon usage (RSCU) values of three mitogenome sequences were determined using MEGA v. 12.0.0 (Kumar et al. 2016). The non-synonymous substitutions (Ka) and synonymous substitutions (Ks) of all PCG genes were calculated using DnaSP v. 5 (Librado and Rozas 2009). The tandem repeat elements of control region (CR, also known as A + T-rich region) were detected by the online tool Tandem Repeats Finder (Benson 1999). The heterogeneous analysis of nucleotide matrix (13 PCGs + 2 tRNAs) was performed using AliGROOVE v. 1.06 (Kück et al. 2014).

Phylogenetic analysis

To investigate mitogenome arrangement patterns in Buprestidae, the gene orders of all known buprestid mitogenomes were compared with that of closely related taxa. A total of 22 buprestid mitogenomes (Table 1), including three newly generated sequences in this study, were subjected for phylogenetic analyses, using *Heterocerus parallelus* Gebler, 1830 (Heteroceridae) and *Dryops ernesti* Gozis, 1886 (Dryopidae) as outgroups (Xiao et al. 2019; Huang et al. 2022; Wei 2022). The test of substitution saturation for the dataset (13 PCGs + 2 rRNAs) was performed with DAMBE to test whether the sequence is suitable for constructing a phylogenetic tree (Xia 2017). Then, the phylogenetic trees were reconstructed using nucleotide matrix 13 PCGs + 2 rRNAs based on ML and BI methods. The nucleotide matrix was aligned using ClustalW (Thompson et al. 1994) and trimmed by trimAl v. 1.2 (Capella-Gutiérrez et al. 2009). In BI and ML analyses, the best-fit models were deduced by ModelFinder (Kalyaanamoorthy et al. 2017). The phylogenetic trees were reconstructed using IQ-tree v. 1.6.8 (Guindon et al. 2010) and MrBayes v. 3.2.6 (Ronquist et al. 2012) integrated into PhyloSuite v. 1.2.2 (Zhang et al. 2020). During this analyzing process, PhyloSuite was run with previous parameters (Wei 2022).

Results

Genome organization and base composition

We sequenced and annotated the complete mitogenome of *J. variolaris* (GenBank No. OP390084), *P. chinensis* (No. OP388449), and *C. japonica* (No. OP388437). Overall, these mitogenome sequences were 15,759 to 16,227 bp in length, which are medium length in Buprestidae (Table 1). It is a circular, double-stranded ring that includes 37 insect mitochondrial genes (13 PCGs, 22 tRNAs, and 2 rRNAs) and an A + T-rich region (control region, CR).

In these three mitogenome, the N-strand encoded the sense-strand of 14 genes (*nad1*, *nad4L*, *nad4*, *nad5*, *trnQ*, *trnV*, *trnL1*, *trnP*, *trnH*, *trnF*, *trnY*, *trnC*, *rrnL*, and *rrnS*), while the J-strand encoded the sense-strand of the remaining 23 genes (Table 2), which was consistent with the known buprestid species (Cao and Wang 2019a, b; Xiao et al. 2019; Chen et al. 2021; Peng et al. 2021; Huang et al. 2022; Wei 2022; Weng et al. 2022).

These three mitogenome sequences had a high A + T content, with an average of 68.47%, showing a strong AT bias (Suppl. material 1: table S1). Among them, the A + T content of *J. variolaris* (70.43%) was higher than of both *C. japonica* (67.97%) and *P. chinensis* (67.00%). These three mitogenome sequences showed a positive AT skew (0.12–0.13) and negative GC skew (-0.22), which is consistent with the known buprestid species. In this study, there were 21 gaps in three mitogenome sequences, which varied from 1 bp to 57 bp. The longest intergenic spacer (bp) was located between *trnD* and *atp8* genes in *C. japonica*. There were 41 overlapping gene regions in total, ranging from 1 bp to 27 bp in length.

Protein-coding genes, codon usage, and nucleotide diversity

In Julodinae, the concatenated length of 13 PCGs of *J. variolaris* (Julodinae) was 11,170 bp, which encoded 3715 amino acid residues. In *P. chinensis* (Polycestinae), the total length of 13 PCGs was 11,162 bp, which encoded 3710 amino acid residues. In *C. japonica* (Chrysochroinae), the total length of 13 PCGs was 11,161 bp, which encoded 3710 amino acid residues. Compared with the other known buprestid species (Chen et al. 2021; Peng et al. 2021; Huang et al. 2022; Wei 2022; Weng et al. 2022), the concatenated length of 13 PCGs and the number of amino acid-coding codons of Julodinae is slightly higher than in other subfamilies.

The majority of PCGs directly used ATN as the start codon, but the exceptions were *nad1* (*J. variolaris*, *P. chinensis*, and *C. japonica*), *nad4L* (*C. japonica*), and *nad5* (*C. japonica*) genes which started with TTG, GTG, and GTG, respectively. The unusual start codon TTG was also reported in Agrilinae (Wei 2022) and Buprestinae (Huang et al. 2022). The start codon of the *cox1* gene in these three mitogenomes was not determined, which may use non-canonical start codons (Friedrich and Muquim

Table 2. The three newly annotated Buprestidae mitogenomes. The order of the three species in the table is as follows: *Julodis variolaris*, *Ptosima chinensis*, and *Chalcophora japonica*. – not determined.

Gene	Strand	Position From	To	Start codons	Stop codons	Intergenic nucleotides
trnI	J	1/1/1	66/64/67			0/0/0
trnQ	N	64/65/65	134/133/133			-3/0/-3
trnM	J	134/133/133	202/201/201			-1/-1/-1
nad2	J	203/202/202	1228/1221/1224	ATT/ATT/ATC	TAA/TAA/TAA	0/0/0
trnW	J	1241/1220/1223	1306/1285/1291			12/-2/-2
trnC	N	1299/1278/1284	1360/1341/1345			-7/-7/-7
trnY	N	1361/1343/1346	1426/1406/1409			0/1/0
cox1	J	1428/1408/1411	2958/2941/2943	–/–/–	T(AA)/T(AA)/TAA	1/1/1
trnL2	J	2959/2942/2944	3024/3006/3009			0/0/0
cox2	J	3025/3007/3010	3709/3691/3697	ATA/ATA/ATA	T(AA)/T(AA)/T(AA)	0/0/0
trnK	J	3710/3692/3698	3780/3761/3767			0/0/0
trnD	J	3780/3762/3768	3845/3824/3829			-1/0/0
atp8	J	3846/3825/3887	4004/3983/4042	ATT/ATT/ATT	TAA/TAA/TAA	0/0/57
atp6	J	3998/3977/4036	4672/4651/4710	ATG/ATG/ATG	TAA/TAA/TAA	-6/-7/-7
cox3	J	4672/4651/4710	5458/5439/5496	ATG/ATG/ATG	T(AA)/TAA/T(AA)	-1/-1/-1
trnG	J	5459/5447/5497	5522/5512/5558			0/7/0
nad3	J	5523/5513/5559	5876/5866/5912	ATT/ATT/ATT	TAG/TAG/TAG	0/0/0
trnA	J	5875/5865/5911	5940/5929/5974			-2/-2/-2
trnR	J	5940/5934/5975	6006/5998/6035/			-1/4/0
trnN	J	6006/6002/6035	6070/6066/6099			-1/3/-1
trnS1	J	6071/6067/6100	6137/6131/6166			0/0/0
trnE	J	6138/6132/6168	6201/6197/6229			0/0/1
trnF	N	6201/6196/6229	6265/6260/6292			-1/-2/-1
nad5	N	6265/6260/6293	7983/7978/8012	ATA/ATC/GTG	TAA/TAA/T(AA)	-1/-1/0
trnH	N	7984/7979/8013	8047/8042/8075			0/0/0
nad4	N	8048/8042/8076	9380/9379/9411	ATG/ATG/ATG	T(AA)/TAA/T(AA)	0/-1/0
nad4L	N	9374/9373/9405	9664/9666/9695	ATG/ATG/GTG	TAA/TAA/TAA	-7/-7/-7
trnT	J	9667/9669/9698	9731/9733/9762			2/2/2
trnP	N	9731/9733/9763	9795/9798/9827			-1/-1/0
nad6	J	9797/9800/9829	10,303/10,306/10,335	ATA/ATA/ATC	TAA/TAA/TAA	1/1/1
cytb	J	10,303/10,306/10,335	11,454/11,448/11,474	ATG/ATG/ATG	TAG/TAA/TAG	-1/-1/-1
trnS2	J	11,453/11,447/11,473	11,519/11,512/11,539			-2/-2/-2
nad1	N	11,539/11,536/11559	12,489/12,480/12,509	TTG/TTG/TTG	TAA/TAA/TAG	39/33/19
trnL1	N	12,491/12,482/12,511	12,554/12,546/12,574			1/1/1
rrnL	N	12,555/12,547/12,575	13,855/13,845/13,873			0/0/0
trnV	N	13,856/13,846/13,847	13,925/13,915/13,943			0/0/-27
rrnS	N	13,926/13,916/13,944	147,17/14,664/14,679			0/0/0
A+T-rich region		14,718/14,665/14,680	16,227/16,115/15,759			0/0/0

2003; Fenn et al. 2007; Yang et al. 2013; Wang et al. 2021; Wu et al. 2022). There were three types of stop codons, TAA, TAG, and an incomplete stop codon T, which was completed by the addition of 3' A residues to the mRNA.

To investigate further, the frequency of synonymous codon usage and relative synonymous codon usage (RSCU) values were calculated and presented. Taken together, the three most frequently used amino acids were L2, S2, and P (Fig. 1A, B), and the most frequently used codons were TTA (L2), TCT (S2), and CCT (P) (Fig. 2).

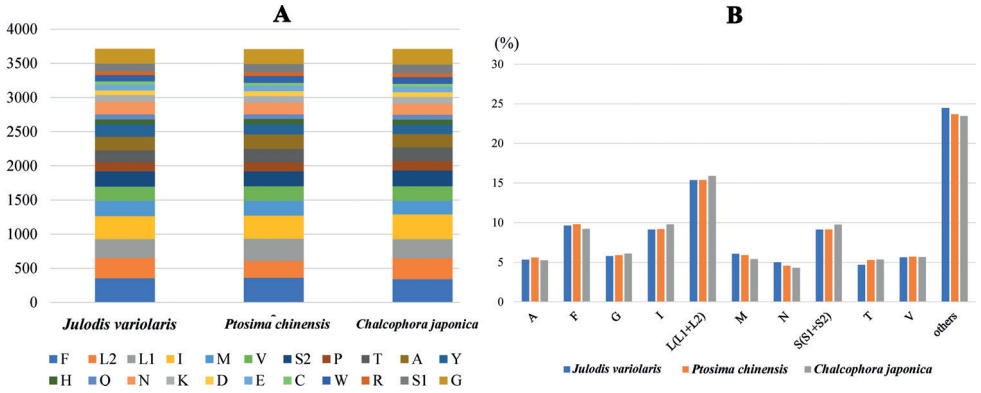

Figure 1. Numbers of different amino acids in the three new mitogenome sequences **A** and the percentages of the top ten amino acids **B** the stop codon is not included in these graphs.

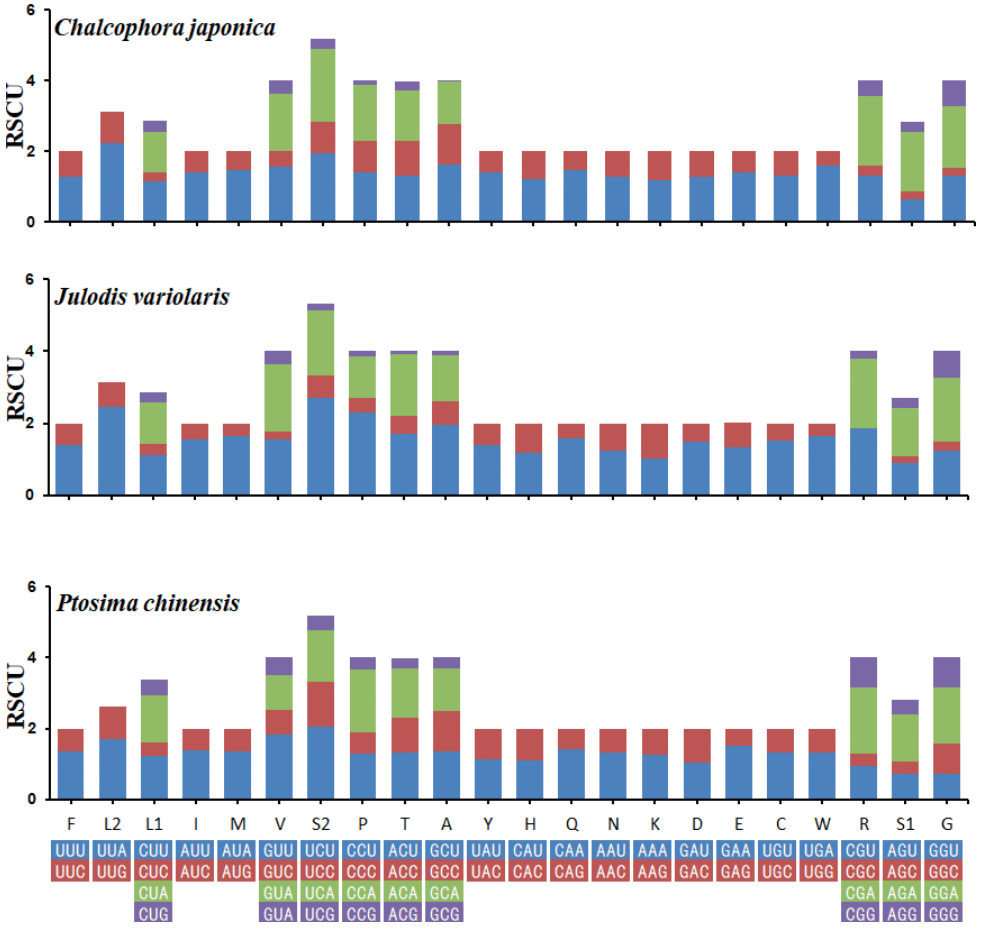

Figure 2. Relative synonymous codon usage (RSCU) of the three newly sequenced mitogenomes.

The Ka/Ks ratio can be used to estimate whether a sequence is undergoing negative, neutral, or positive selection (Hurst 2002; Mori and Matsunami 2018). The ratio of Ka/Ks for each mitogenome sequence was calculated using *Anthaxia chinensis* Kerremans, 1898 as the reference sequence (Fig. 3A). In three mitogenome sequences, values of Ka, Ks, and Ka/Ks were all less than 1, suggesting the presence of purifying selection in these three species.

Ribosomal and transfer RNA genes, and heterogeneity

The rRNA genes were located between the A + T-rich region and *trnL1*, and separated by *trnV*, which is consistent with previous studies (Duan et al. 2017; Cao and Wang 2019a, b; Xiao et al. 2019; Sun et al. 2020; Chen et al. 2021; Peng et al. 2021; Huang et al. 2022; Wei 2022; Weng et al. 2022). The total length of rRNA genes ranged from 2035 bp (*C. japonica*) to 2093 bp (*J. variolaris*), of which the length of *16S* gene ranged from 1299 bp (*C. japonica* and *P. chinensis*) to 1301 bp (*J. variolaris*). The A + T content of rRNA genes ranged from 71.50% (*C. japonica*) to 74.30% (*J. variolaris*).

The concatenated lengths of all tRNA genes ranged from 1437 bp (*C. japonica*) to 1456 bp (*J. variolaris*), whereas individual tRNA genes ranged from 61 bp (*trnR*) to 71 bp (*trnK*), of which eight tRNA genes were encoded on the N-strand and the remaining 14 genes encoded on the J-strand. The predicted secondary structure of tRNAs showed a standard clover-leaf structure (Suppl. material 1: figs S2–S4), except for *trnS1* (Fig. 4A), which lacked the dihydrouridine arm, and formed a loop commonly found in other insects (Xiao et al. 2011; Park et al. 2012; Yu et al. 2016; Yan et al. 2017; Yu and Liang 2018; Li et al. 2019). The UG mismatches were detected in some tRNAs (Suppl. material 1: figs S2–S4), which also appeared in other buprestid species (Sun et al. 2020; Chen et al. 2021; Huang et al. 2022; Wei 2022; Weng et al. 2022).

The degree of heterogeneity of the PCGs + RNAs dataset was higher than that of the PCGs dataset (Fig. 3B). Additionally, the heterogeneity in sequence divergences was slightly stronger for Agrilinae than for other families (Fig. 3B). The heterogeneity in sequence homogeneity was higher for Chrysochroinae than other families.

A + T-rich region and gene arrangement

The A + T-rich region was the largest non-coding region in mitogenome, located between *trnI* and *rrnS*. This region, containing regulatory elements correlated with the regulation of replication and transcription (Zhang et al. 1995), plays a very important role in molecular evolution (Zhang and Hewitt 1997). The length of A + T-rich region ranged from 1080 bp (*C. japonica*) to 1510 bp (*J. variolaris*), which are of medium length in the Buprestidae (Sun et al. 2020; Huang et al. 2022; Wei 2022). The A + T content of the A + T-rich region of *C. japonica* (75.93%) and *P. chinensis* (78.38%) was found to be higher than that of the whole genome (67.97%, 67.00%), PCGs (66.46%, 64.55%), rRNAs (71.50%, 72.51%), and tRNAs (68.82%, 71.46%),

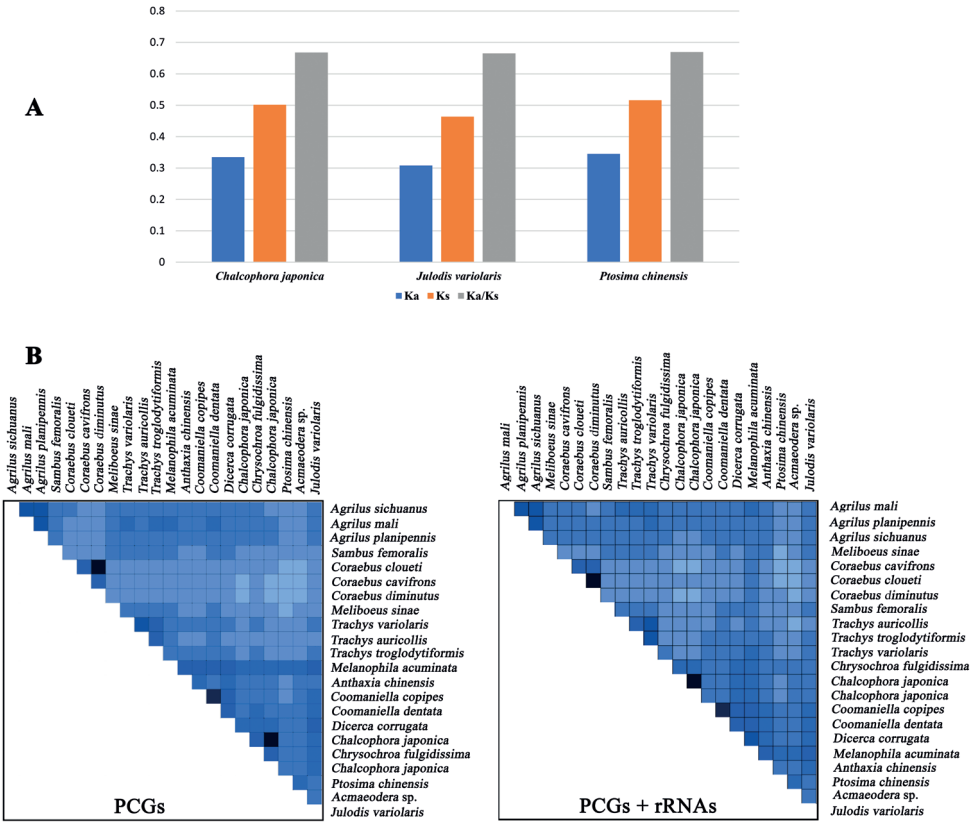

Figure 3. Evolutionary rates of mitochondrial genomes in three new mitogenome sequence (**A**) and the heterogeneity of two dataset in Buprestidae (**B**).

whereas the A + T content of *J. variolaris* (72.85%) was lower than that of whole genome (70.43%), PCGs (68.82%), rRNAs (74.30%), and tRNAs (74.79%).

The tandem repeat regions of three species were detected in this study. The repeat regions in each of the three new mitogenomes differ from each other in length and copy number of tandem repeat units. The repeat region of *J. variolaris* was 43 bp in length, comprising a 17 bp and a 26 bp tandem repeat element. In contrast, in *P. chinensis*, the total length of the repeat sequence was 111 bp, consisting of three incomplete repeat units. These tandem repeat elements are slightly shorter than those of Agrilinae (Wei 2022).

The gene rearrangements were regarded as important molecular markers for exploring the evolution and phylogeny of insects (Dowton et al. 2002; Cameron 2014). All the buprestid mitogenomes released in GenBank were compared and analyzed, with one mitogenome arrangement pattern exhibited in Buprestidae (Fig. 4B). The mitochondrial gene order of these three species was consistent with other known buprestid mitogenomes.

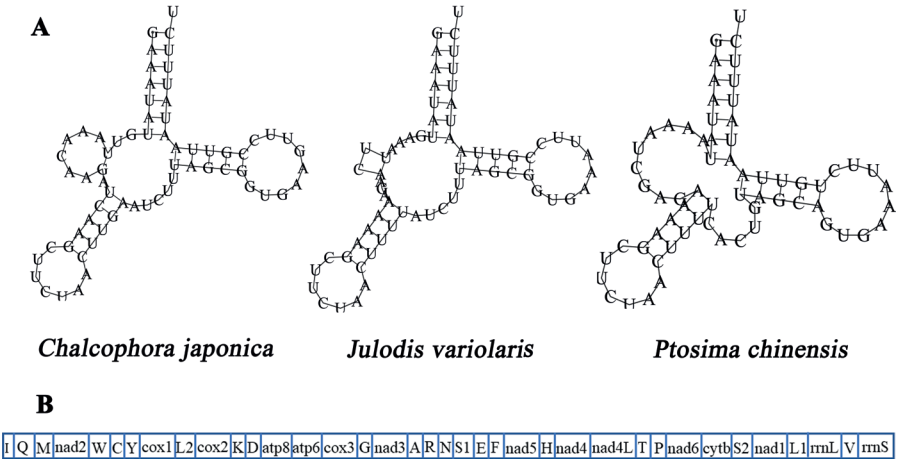

Figure 4. The predicted secondary cloverleaf structure for the *trnS1* of three new mitogenomes (**A**) and the gene order of known buprestid mitogenomes (**B**).

Phylogenetic analysis

For the concatenated sequences, the test of substitution saturation showed that the value of I_{ss} = 0.3910 was significantly smaller than $I_{ss.c}$ = 0.8537 and $p(0.0000) < 0.01$, suggesting the sequences suitable for phylogenetic analysis. In the present study, both ML and BI trees using a nucleotide matrix (13 PCGs + 2 rRNAs) produced identical topologies (Fig. 5, Suppl. material 1: fig. S5), (Chrysochroniae + ((Julodinae + Polycestinae) + Buprestinae) + Agrilinae), in terms of subfamily-level relationship.

The target species *J. variolaris*, representing Julodinae, formed an independent clade close to Polycestinae with high support values (BI: 1; ML: 94), which supported the results of a previous study (Evans et al. 2015). The target species *P. chinensis* and *Acmaeodera* sp. are grouped together as an independent clade with high support values (BI: 1; ML: 100), representing Polycestinae. The Julodinae and Polycestinae formed a clade which was sister to Buprestinae with high support values (BI: 1; ML: 84). The target species *C. japonica* was clustered with other chrysochroine species as a clade, representing Chrysochroinae, with high support values (BI: 1; ML: 100). All the species of Agrilinae were clustered on one branch with high support values (BI: 1; ML: 100) and close to other buprestid clades, while the Coraebini was polyphyletic.

Discussion

The gene composition and arrangement of these three mitogenomes are the same as other known buprestid mitogenomes (Cao and Wang 2019a, b; Xiao et al. 2019; Chen et al. 2021; Peng et al. 2021; Huang et al. 2022; Wei 2022; Weng et al. 2022). These three mitogenome had a positive AT skew, which was similar to most known buprestid

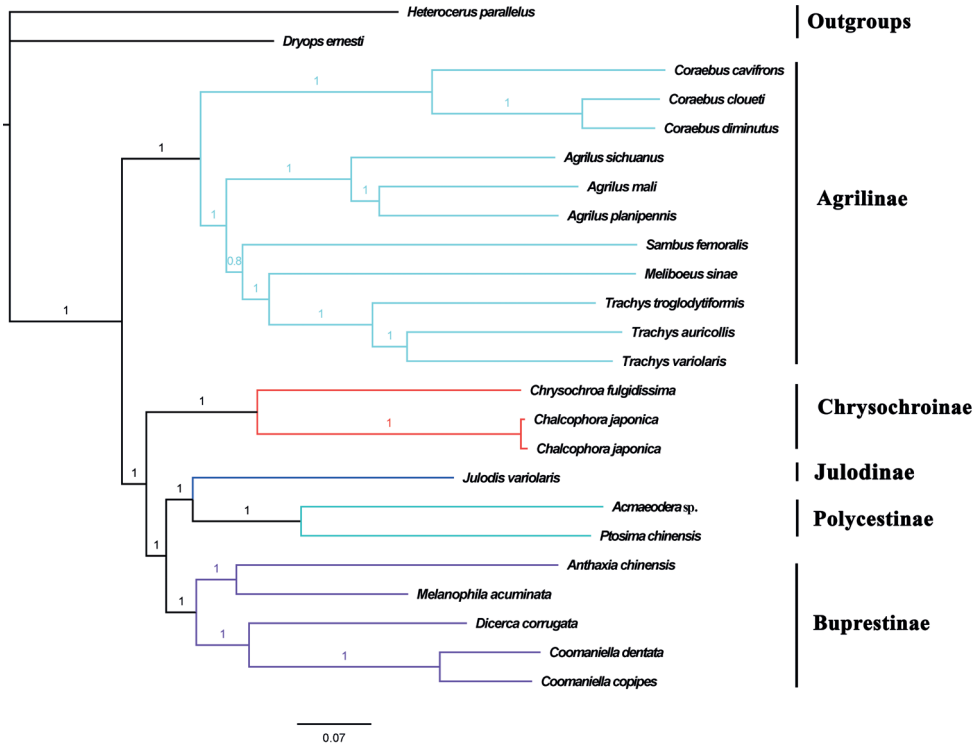

Figure 5. Phylogenetic relationships of studied species of Buprestidae using BI analyses based on 13 PCGs + 2 rRNAs of mitogenomes. The numbers on the branches show posterior probabilities.

mitogenomes (Duan et al. 2017; Cao and Wang 2019a, b; Xiao et al. 2019; Sun et al. 2020; Chen et al. 2021; Peng et al. 2021; Huang et al. 2022; Wei 2022; Weng et al. 2022). The genes *nad1* (*J. variolaris*, *P. chinensis*, and *C. japonica*), *nad4L*, and *nad5* (*C. japonica*) which started with TTG, GTG, and GTG, respectively, was also reported by previous studies in Buprestidae (Huang et al. 2022; Wei 2022). The Julodinae are closest to Polycestinae with high support values, which is consistent with the results of a previous study (Evans et al. 2015). The monophyly of Buprestidae has been corroborated once more, as all the buprestid species converge together as an independent clade (Evans et al. 2015; Huang et al. 2022; Wei 2022). In this study, the Coraebini was also found to be polyphyletic with the genera *Meliboeus* Deyrolle, 1864 and *Coraebus* Gory & Laporte, 1839 in different clades, also consistent with the previous studies (Evans et al. 2015; Huang et al. 2022; Wei 2022). Compared to Melanophilini, Coomaniellini is more closely related to Dicercini, which is in line with previous studies (Volkovitsh 2001; Evans et al. 2015; Huang et al. 2022).

In the present study, the sampling might be too limited to address the comprehensive phylogeny of Buprestidae. In the future, classification problems could be solved when enough mitogenomes are accumulated for more buprestid species, which requires the cooperation of taxonomists around the world.

Conclusions

In this study, the complete mitogenomes of *Julodis variolaris*, *Chalcophora japonica*, and *Ptosima chinensis* were annotated and analyzed, of which the mitogenome of *J. variolaris* was the first complete mitogenome representative of the subfamily Julodinae. The three mitogenome sequences were of medium length (15,759–16,227 bp) in Buprestidae. These three mitogenomes shared the same gene order, which was consistent with those of known buprestid species. These three mitogenome sequences all had a high A + T content, and strong AT bias. All PCGs of the three species began with the typical ATN codon except *nad1* (*J. variolaris*, *P. chinensis*, and *C. japonica*), *nad4L* (*C. japonica*), and *nad5* (*C. japonica*) which were initiated with TTG, GTG, and GTG, respectively. In the present study, the BI and ML trees had exact same topologies with high-value support. The results of phylogenetic analyses also show that Julodinae is close to Polycestinae, the clade composed of Julodinae and Polycestinae is close to that of Buprestinae, and the Agrilinae clade is sister to that of (Chrysochroniae + ((Julodinae + Polycestinae) + Buprestinae)), and all the subfamilies are grouped in a monophyletic group with high support.

Acknowledgements

We thank Dr. Mark Volkovitsh (Russian Academy of Sciences, Moscow, Russia) and Dr. Zhao Pan (Hebei University, Baoding, China) for revising the manuscript. This work was supported by Natural Science Foundation of Sichuan Province (2022NSFSC1707) and the Doctoral Scientific Research Foundation of China West Normal University (20E054).

References

Bellamy CL (2003) An illustrated summary of the higher classification of the superfamily Buprestoidea (Coleoptera). Folia Heyrovskyana, Supplementum 10: 1–197.

Bellamy CL (2008) A world catalogue and bibliography of the jewel beetles (Coleoptera: Buprestoidea), Volumes 1–4. Pensoft Series Faunistica No. 76–79, Sofia/Moscow, 2684 pp.

Bellamy CL, Volkovitsh M (2016) 18 Buprestoidea Crowson, 1955. In: Beutel RG, Leschen RAB (Eds) Handbook of Zoology, Arthropoda: Insecta, Morphology and Systematics (Archostemata, Adephaga, Myxophaga, Polyphaga partim) (2nd edn.). Walter de Gruyter, Berlin/Boston, 543–552. https://doi.org/10.1515/9783110373929-021

Benson G (1999) Tandem repeats finder: A program to analyze DNA sequences. Nucleic Acids Research 27(2): 573–580. https://doi.org/10.1093/nar/27.2.573

Bernt M, Donath A, Jühling F, Externbrink F, Florentz C, Fritzsch G, Pütz J, Middendorf M, Stadler PF (2013) MITOS: Improved de novo metazoan mitochondrial genome annotation. Molecular Phylogenetics and Evolution 69(2): 313–319. https://doi.org/10.1016/j.ympev.2012.08.023

Bolger AM, Lohse M, Usadel B (2014) Trimmomatic: A flexible trimmer for Illumina sequence data. Bioinformatics 30(15): 2114–2120. https://doi.org/10.1093/bioinformatics/btu170

Cameron SL (2014) Insect mitochondrial genomics: Implications for evolution and phylogeny. Annual Review of Entomology 59(1): 95–117. https://doi.org/10.1146/annurev-ento-011613-162007

Cao LM, Wang XY (2019a) The complete mitochondrial genome of the jewel beetle *Coraebus cavifrons* (Coleoptera: Buprestidae). Mitochondrial DNA Part B Resources 4(2): 2407–2408. https://doi.org/10.1080/23802359.2019.1636730

Cao LM, Wang XY (2019b) The complete mitochondrial genome of the jewel beetle *Trachys variolaris* (Coleoptera: Buprestidae). Mitochondrial DNA Part B Resources 4(2): 3042–3043. https://doi.org/10.1080/23802359.2019.1666053

Capella-Gutiérrez S, Silla-Martínez JM, Gabaldón T (2009) TrimAl: A tool for automated alignment trimming in large-scale phylogenetic analyses. Bioinformatics 25(15): 1972–1973. https://doi.org/10.1093/bioinformatics/btp348

Chen B, Wei ZH, Shi AM (2021) The complete mitochondrial genome of the jewel beetle, *Anthaxia chinensis* (Coleoptera: Buprestidae). Mitochondrial DNA Part B Resources 6(10): 2962–2963. https://doi.org/10.1080/23802359.2021.1973920

Cobos A (1980) Ensayo sobre los géneros de la subfamilia Polycestinae (Coleoptera, Buprestidae) (Parte I). EOS Revista Española de Entomologia 54(1–4): 15–94.

Cobos A (1986) Fauna Iberica de Coleopteros Buprestidae. Consejo Superior de Invertigaciones Cientifificas, Madrid, 364 pp.

Dowton M, Castro LR, Austin AD (2002) Mitochondrial gene rearrangements as phylogenetic characters in the invertebrates: The examination of genome 'morphology'. Invertebrate Systematics 16(3): 345–356. https://doi.org/10.1071/IS02003

Duan J, Quan GX, Mittapalli O, Cusson M, Krell PJ, Doucet D (2017) The complete mitogenome of the Emerald Ash Borer (EAB), *Agrilus planipennis* (Insecta: Coleoptera: Buprestidae). Mitochondrial DNA Part B Resources 2(1): 134–135. https://doi.org/10.1080/23802359.2017.1292476

Evans AM, Mckenna DD, Bellamy CL, Farrell BD (2015) Large-scale molecular phylogeny of metallic wood-boring beetles (Coleoptera: Buprestoidea) provides new insights into relationships and reveals multiple evolutionary origins of the larval leaf-mining habit. Systematic Entomology 40(2): 385–400. https://doi.org/10.1111/syen.12108

Fenn JD, Cameron SL, Whiting RLF (2007) The complete mitochondrial genome sequence of the Mormon cricket (*Anabrus* simplex: Tetdgonildae: Orthoptera) and an analysis of control region variability. Insect Molecular Biology 16(2): 239–252. https://doi.org/10.1111/j.1365-2583.2006.00721.x

Friedrich M, Muquim N (2003) Sequence and phylogenetic analysis of the complete mitochondrial genome of the flour beetle *Tribolium castanaeum*. Molecular Phylogenetics and Evolution 26(3): 502–512. https://doi.org/10.1016/S1055-7903(02)00335-4

Greiner S, Lehwark P, Bock R (2019) OrganellarGenomeDRAW (OGDRAW) version 1.3.1: Expanded toolkit for the graphical visualization of organellar genomes. Nucleic Acids Research 47(W1): W59–W64. https://doi.org/10.1093/nar/gkz238

Guindon S, Dufayard J, Lefort V, Anisimova M, Hordijk W, Gascuel O (2010) New algorithms and methods to estimate maximum-likelihood phylogenies: Assessing the per-

formance of PhyML 3.0. Systematic Biology 59(3): 307–321. https://doi.org/10.1093/sysbio/syq010

Hołyński RB (1988) Remarks on the general classification of Buprestidae Leach as applied to Maoraxiina. Folia Entomologica Hungarica 49(1): 49–54.

Hołyński RB (1993) A reassessment of the internal classification of the Buprestidae Leach (Coleoptera). Crystal. Series Zoologica [Göd] 1: 1–42.

Hołyński RB (2009) Taxonomic Structure of the Subtribe Chrysochroina Cast. with Review of the Genus *Chrysochroa* Dej. Gondwana, Warszawa, 391 pp.

Hołyński RB (2014) Review of the Indo-Pacific Buprestidae Leach (Coleoptera) I: Julodinae Lac. Gondwana, Warszawa, 85 pp.

Hong MY, Jeong HC, Kim MJ, Jeong HU, Lee SH, Kim I (2009) Complete mitogenome sequence of the jewel beetle, *Chrysochroa fulgidissima* (Coleoptera: Buprestidae). Mitochondrial DNA Mapping, Sequencing, and Analysis 20(2–3): 46–60. https://doi.org/10.1080/19401730802644978

Huang XY, Chen B, Wei ZH, Shi AM (2022) First report of complete mitochondrial genome in the tribes Coomaniellini and Dicercini (Coleoptera: Buprestidae) and phylogenetic implications. Genes 13(6): e1074. https://doi.org/10.3390/genes13061074

Hurst LD (2002) The Ka/Ks ratio: Diagnosing the form of sequence evolution. Trends Genetics 18(9): 486–487. https://doi.org/10.1016/S0168-9525(02)02722-1

Kalyaanamoorthy S, Minh BQ, Wong TKF, von Haeseler A, Jermiin LS (2017) ModelFinder: Fast model selection for accurate phylogenetic estimates. Nature Methods 14(6): 587–589. https://doi.org/10.1038/nmeth.4285

Kearse M, Moir R, Wilson A, Stones-Havas S, Cheung M, Sturrock S, Buxton S, Cooper A, Markowitz S, Duran C, Thierer T, Ashton B, Meintjes P, Drummond A (2012) Geneious Basic: An integrated and extendable desktop software platform for the organization and analysis of sequence data. Bioinformatics 28(12): 1647–1649. https://doi.org/10.1093/bioinformatics/bts199

Kolibáè J (2000) Classification and phylogeny of the Buprestoidea (Insecta: Coleoptera). Acta Musei Moraviae, Scientiae biologicae [Brno] 85: 113–184.

Krzywinski J, Li C, Morris M, Conn JE, Lima JB, Povoa MM, Wilkerson RC (2011) Analysis of the evolutionary forces shaping mitochondrial genomes of a Neotropical malaria vector complex. Molecular Phylogenetics and Evolution 58(3): 469–477. https://doi.org/10.1016/j.ympev.2011.01.003

Kubáň V, Volkovitsh MG, Kalashian MJ, Jendek E (2016) Family Buprestidae Leach, 1815. In: Löbl I, Löbl D (Eds) Catalogue of Palaearctic Coleoptera. Scarabaeoidea, Scirtoidea, Dascilloidea, Buprestoidea, Byrrhoidea. Revised and Updated Edition. Apollo Books, Stenstrup, 432–574.

Kück P, Meid SA, Groß C, Wägele JW, Misof B (2014) AliGROOVE–visualization of heterogeneous sequence divergence within multiple sequence alignments and detection of inflated branch support. Bioinformatics 15(1): e294. https://doi.org/10.1186/1471-2105-15-294

Kumar S, Stecher G, Tamura K (2016) MEGA7: Molecular Evolutionary Genetics Analysis version 7.0 for bigger datasets. Molecular Biology and Evolution 33(7): 1870–1874. https://doi.org/10.1093/molbev/msw054

Li H, Shao RF, Song N, Song F, Jiang P, Li ZH, Cai WZ (2015) Higher-level phylogeny of paraneopteran insects inferred from mitochondrial genome sequences. Scientific Reports 5(1): e8527. https://doi.org/10.1038/srep08527

Li R, Shu XH, Li XD, Meng L, Li BP (2019) Comparative mitogenome analysis of three species and monophyletic inference of Catantopinae (Orthoptera: Acridoidea). Genomics 111(6): 1728–1735. https://doi.org/10.1016/j.ygeno.2018.11.027

Librado P, Rozas J (2009) DnaSP v5: A software for comprehensive analysis of DNA polymorphism data. Bioinformatics 25(11): 1451–1452. https://doi.org/10.1093/bioinformatics/btp187

Lim LWK, Chung HH, Lau MMLL, Aziz F, Gan HM (2021) Improving the phylogenetic resolution of Malaysian and Javan mahseer (Cyprinidae), *Tor tambroides* and *Tor tambra*: Whole mitogenomes sequencing, phylogeny and potential mitogenome markers. Gene 791: e145708. https://doi.org/10.1016/j.gene.2021.145708

Lowe TM, Chan PP (2016) tRNAscan-SE On-line: Integrating search and context for analysis of transfer RNA genes. Nucleic Acids Research 44(W1): W54–W57. https://doi.org/10.1093/nar/gkw413

Mori S, Matsunami M (2018) Signature of positive selection in mitochondrial DNA in Cetartiodactyla. Genes & Genetic Systems 93(2): 65–73. https://doi.org/10.1266/ggs.17-00015

Motyka M, Kusy D, Háva J, Jahodářová E, Bílková R, Vogler AP, Bocak L (2022) Mitogenomic data elucidate the phylogeny and evolution of life strategies in Dermestidae (Coleoptera). Systematic Entomology 47(1): 82–93. https://doi.org/10.1111/syen.12520

Nie RE, Wei J, Zhang SK, Vogler AP, Wu L, Konstantinov AS, Li WZ, Yang XK, Xue HJ (2019) Diversification of mitogenomes in three sympatric *Altica* flea beetles (Insecta, Chrysomelidae). Zoologica Scripta 48(5): 657–666. https://doi.org/10.1111/zsc.12371

Nie RE, Andújar C, Gómez-Rodríguez C, Bai M, Xue HJ, Tang M, Yang CT, Tang P, Kang XK, Vogler AP (2020) The phylogeny of leaf beetles (Chrysomelidae) inferred from mitochondrial genomes. Systematic Entomology 45(1): 188–204. https://doi.org/10.1111/syen.12387

Nie R, Vogler AP, Yang XK, Lin MY (2021) Higher-level phylogeny of longhorn beetles (Coleoptera: Chrysomeloidea) inferred from mitochondrial genomes. Systematic Entomology 46(1): 56–70. https://doi.org/10.1111/syen.12447

Park JS, Cho Y, Kim MJ, Nam SH, Kim I (2012) Description of complete mitochondrial genome of the black-veined white, *Aporia crataegi* (Lepidoptera: Papilionoidea), and comparison to papilionoid species. Journal of Asia-Pacific Entomology 15(3): 331–341. https://doi.org/10.1016/j.aspen.2012.01.002

Peng XJ, Liu J, Wang Z, Zhan QZ (2021) The complete mitochondrial genome of the pyrophilous jewel beetle *Melanophila acuminata* (Coleoptera: Buprestidae). Mitochondrial DNA Part B Resources 6(3): 1059–1060. https://doi.org/10.1080/23802359.2021.1899079

Perna NT, Kocher TD (1995) Patterns of nucleotide composition at fourfold degenerate sites of animal mitochondrial genomes. Journal of Molecular Evolution 41(3): 353–358. https://doi.org/10.1007/BF01215182

Qin J, Zhang YZ, Zhou X, Kong XB, Wei SJ, Ward RD, Zhang AB (2015) Mitochondrial phylogenomics and genetic relationships of closely related pine moth (Lasiocampidae:

Dendrolimus) species in China, using whole mitochondrial genomes. Genomics 16(1): 428. https://doi.org/10.1186/s12864-015-1566-5

Ronquist F, Teslenko M, Der Mark PV, Ayres DL, Darling AE, Hohna S, Huelsenbeck JP (2012) MrBayes 3.2: Efficient Bayesian Phylogenetic Inference and Model Choice across a Large Model Space. Systematic Biology 61(3): 539–542. https://doi.org/10.1093/sysbio/sys029

Saccone C, De Giorgi C, Gissi C, Pesole G, Reyes A (1999) Evolutionary genomics in Metazoa: The mitochondrial DNA as a model system. Gene 238(1): 195–209. https://doi.org/10.1016/S0378-1119(99)00270-X

Sheffield NC, Song H, Cameron SL, Whiting MF (2009) Nonstationary evolution and compositional heterogeneity in beetle mitochondrial phylogenomics. Systematic Biology 58(4): 381–394. https://doi.org/10.1093/sysbio/syp037

Sun HQ, Zhao WX, Lin RZ, Zhou ZF, Huai WX, Yao YX (2020) The conserved mitochondrial genome of the jewel beetle (Coleoptera: Buprestidae) and its phylogenetic implications for the suborder Polyphaga. Genomics 112(5): 3713–3721. https://doi.org/10.1016/j.ygeno.2020.04.026

Thompson JD, Higgins DG, Gibson TJ (1994) Clustal W: Improving the sensitivity of progressive multiple sequence alignment through sequence weight, position-specific gap penalties and weight matrix choice. Nucleic Acids Research 22(22): 4673–4680. https://doi.org/10.1093/nar/22.22.4673

Timmermans MJTN, Dodsworth S, Culverwell CL, Bocak L, Ahrens D, Littlewood DTJ, Pons J, Vogler AP (2010) Why barcode? High-throughput multiplex sequencing of mitochondrial genomes for molecular systematics. Nucleic Acids Research 38(21): e197. https://doi.org/10.1093/nar/gkq807

Timmermans MJTN, Barton C, Haran J, Ahrens D, Culverwell CL, Ollikainen A, Dodsworth S, Foster PG, Bocak L, Vogler AP (2016) Family-level sampling of mitochondrial genomes in Coleoptera: Compositional heterogeneity and phylogenetics. Genome Biology and Evolution 8(1): 161–175. https://doi.org/10.1093/gbe/evv241

Tôyama M (1987) The systematic positions of some buprestid genera (Coleoptera, Buprestidae). Elytra 15: 1–11.

Volkovitsh MG (2001) The comparative morphology of antennal structures in Buprestidae (Coleoptera): evolutionary trends, taxonomic and phylogenetic implications. Part 1. Acta Musei Moraviae, Scientiae Biologicae [Bron] 86: 43–169.

Wang X, Zhang H, Kitching I, Xu ZB, Huang YX (2021) First mitogenome of subfamily Langiinae (Lepidoptera: Sphingidae) with its phylogenetic implications. Gene 789: e145667. https://doi.org/10.1016/j.gene.2021.145667

Wei ZH (2022) The complete mitochondrial genomes of five Agrilinae (Coleoptera, Buprestidae) species and phylogenetic implications. ZooKeys 1092: 195–212. https://doi.org/10.3897/zookeys.1092.80993

Weng MQ, Wang Y, Huang J, Huang LL, Lin YQ, Zheng QL, Wu YZ, Wu SQ (2022) The complete mitochondrial genome of *Chalcophora japonica chinensis* Schaufuss, 1879 (Coleoptera: Buprestidae). Mitochondrial DNA Part B Resources 7(8): 1571–1573. https://doi.org/10.1080/23802359.2022.2113750

Wu C, Zhou Y, Tian T, Li TJ, Chen B (2022) First report of complete mitochondrial genome in the subfamily Alleculinae and mitochondrial genome-based phylogenetics in Tenebrionidae (Coleoptera: Tenebrionoidea). Insect Science 29(4): 1226–1238. https://doi.org/10.1111/1744-7917.12983

Xia XH (2017) DAMBE6: New tools for microbial genomics, phylogenetics and molecular evolution. The Journal of Heredity 108(4): 431–437. https://doi.org/10.1093/jhered/esx033

Xiao JH, Jia JG, Murphy RW, Huang DW (2011) Rapid evolution of the mitochondrial genome in chalcidoid wasps (Hymenoptera: Chalcidoidea) driven by parasitic lifestyles. PLoS ONE 6(11): e26645. https://doi.org/10.1371/journal.pone.0026645

Xiao LF, Zhang SD, Long CP, Guo QY, Xu JS, Dai XH, Wang JG (2019) Complete mitogenome of a leaf-Mining buprestid Beetle, *Trachys auricollis*, and its phylogenetic implications. Genes 10(12): e992. https://doi.org/10.3390/genes10120992

Yan L, Zhang M, Gao Y, Pape T, Zhang D (2017) First mitogenome for the subfamily Miltogramminae (Diptera: Sarcophagidae) and its phylogenetic implications. European Journal of Entomology 114(1): 422–429. https://doi.org/10.14411/eje.2017.054

Yang F, Du Y, Cao J, Huang F (2013) Analysis of three leafminers' complete mitochondrial genomes. Gene 529(1): 1–6. https://doi.org/10.1016/j.gene.2013.08.010

Yu F, Liang AP (2018) The complete mitochondrial genome of *Ugyops* sp. (Hemiptera: Delphacidae). Journal of Insect Science 18(3): e25. https://doi.org/10.1093/jisesa/iey063

Yu P, Cheng X, Ma Y, Yu D, Zhang J (2016) The complete mitochondrial genome of *Brachythemis contaminata* (Odonata: Libellulidae). Mitochondrial DNA A DNA Mapping. Seqencing, and Analysis 27(3): 2272–2273. https://doi.org/10.3109/19401736.2014.984176

Zhang DX, Hewitt GM (1997) Insect mitochondrial control region: A review of its structure, evolution and usefulness in evolutionary studies. Biochemical Systematics and Ecology 25(2): 99–120. https://doi.org/10.1016/S0305-1978(96)00042-7

Zhang DX, Szymura JM, Hewitt GM (1995) Evolution and structural conservation of the control region of insect mitochondrial DNA. Journal of Molecular Evolution 40(4): 382–391. https://doi.org/10.1007/BF00164024

Zhang D, Gao F, Jakovlić I, Zou H, Zhang J, Li WX, Wang GT (2020) PhyloSuite: An integrated and scalable desktop platform for streamlined molecular sequence data management and evolutionary phylogenetics studies. Molecular Ecology Resources 20(1): 348–355. https://doi.org/10.1111/1755-0998.13096

Zhang H, Lu CC, Liu Q, Zou TM, Qiao GX, Huang XL (2022) Insights into the evolution of aphid mitogenome features from new data and comparative analysis. Animals 12(5): e1970. https://doi.org/10.3390/ani12151970

Zheng BY, Han YY, Yuan RZ, Liu JX, Achterberg C, Tang P, Chen XX (2022) Comparative mitochondrial genomics of 104 Darwin wasps (Hymenoptera: Ichneumonidae) and its implication for phylogeny. Insects 13(2): e124. https://doi.org/10.3390/insects13020124

Supplementary material 1

First mitochondrial genome of subfamily Julodinae (Coleoptera, Buprestidae) with its phylogenetic implications

Authors: Zhonghua Wei, Xuyan Huang, Aimin Shi

Data type: table, images (word document)

Explanation note: Nucleotide composition of three newly generated mitogenomes. Circular maps of mitogenomes for *Julodis variolaris*, *Ptosima chinensis*, and *Chalcophora japonica*. The predicted secondary cloverleaf structure for the tRNAs of *Julodis variolaris* (image S2), *Ptosima chinensis* (image S3) and *Chalcophora japonica* (image S4). Phylogenetic relationships of Buprestidae using ML analyses based on 13 PCGs + 2 rRNAs of mitogenomes; the values one branches are bootstrap.

Link: https://doi.org/10.3897/zookeys.1139.96216.suppl1